Chemical State and Luminescence Imaging of Natural and Synthetic Diamond

THESIS

Submitted to

Prifysgol Aberystwyth University

by

Geraint Owen Jones

MPhys (Hons)

In candidature for the degree of

Philosophiae Doctor

September 2010

DECLARATION

This work has not previously been accepted in substance for any degree and is not being concurrently submitted in candidature for any degree.

Signed……(candidate)

Date……

STATEMENT 1

This thesis is the result of my own investigations, except where otherwise stated. Where correction services have been used, the extent and nature of the correction is clearly marked in a footnote(s).

Other sources are acknowledged by footnotes giving explicit references. A bibliography is appended.

Signed……(candidate)

Date……

STATEMENT 2

I hereby give consent to my thesis, if accepted, to be made available for photocopying and for inter-library loan, and for the title and summary to be made available to outside organisations.

Signed……(candidate)

Date……

Acknowledgements

I would like to take this opportunity to express my heartfelt thanks to my supervisor Prof. Andrew Evans. His provision of the opportunity to study this field and his continued support and enthusiasm throughout my period at Aberystwyth has been greatly appreciated as well as his advice, discussions and guidance. I must also give thanks to Dr. Nigel Poolton who provided assistance and expertise at the Synchrotron Radiation Source (SRS), Daresbury. His discussions and advice are also appreciated.

Successful data collection on beam-times at the SRS would not have been possible without the aid of my fellow PhD researchers past and present with whom I have shared many an hour gathering data for the purpose of this research as well as their own. The long hours and long days would most certainly have been longer still without their company and their approach to the work required. Indeed, the same is to be said at Aberystwyth – providing an excellent working environment and making the research a much more enjoyable experience, so I thank you Andy (Andrew McGlynn), Ows (Owain Rhys Roberts) and Gruff (Gruffudd Trefor Williams).

Dave Francis and John Parry are to be acknowledged for their high quality work in the mechanical workshop, providing high quality bespoke parts along with valuable discussion. Les Dean, David Lewis, and Matt Gunn are also to be thanked for their technical support.

In addition, I am grateful for the financial support provided by the EPSRC and a CASE award from the DTC (Diamond Trading Company). My thanks also go to Philip Martineau, Simon Lawson, David Fisher and Riz Khan for their discussions and provision of samples.

Lastly, but by no means least, my greatest thanks go to my family for their unreserved support and encouragement over the years. *Felly diolch i Mam, Dad a Ler.* I also thank Elen for her support as well as her patience over the years!

My fore-fathers and relations would have undoubtedly succeeded academically, but they never had the means or the opportunities to do so, I am extremely aware of this and how fortunate I have been to have this opportunity. This has been the catalyst and drive during my research and I therefore dedicate this thesis and research to them.

Geraint Owen Jones,
Aberystwyth.
2010

Abstract

This thesis presents work undertaken using Synchrotron and Laboratory based techniques in parallel on the Chemical State and Luminescence Imaging of Natural and Synthetic Diamond. X-ray absorption spectroscopy (XAS) techniques have revealed information on the chemical structure and bonding within brown and variegated type Ia, IIa, CVD and high-pressure, high-temperature (HPHT) treated diamonds.

XAS, Raman, X-ray Excited Optical Luminescence (XEOL) and Photoluminescence (PL) are some of the techniques that have been applied to characterise and investigate the cause of the brown colouration.

The XAS measurements have been undertaken in imaging mode with the capabilities of correlating the luminescence image with the brown regions in partial luminescence yield (PLY) and total luminescence yield (TLY). OD-XAS spectrums have been obtained at non-brown and brown regions and have revealed a higher concentration of sp^2-bonded carbon present at the brown sites. Raman spectroscopy utilized in imaging mode also supports this discovery.

Publications

"Non-resonant X-ray/laser interaction spectroscopy as a method for assessing charge competition, trapping and luminescence efficiency in wide band-gap materials" – N.R.J. Poolton, A.J.J. Bos, J. Wallinga, J.T.M. de Haas, P. Dorenbos, L. de Vries, R.H. Kars, **G.O. Jones**, W. Drozdowski – Journal of Luminescence **130** (2010) 1404-1414

"Probing electron transfer processes in YPO4 :Ce,Sm by combined synchrotron-laser excitation spectroscopy" – N.R.J. Poolton, A.J.J. Bos, **G.O. Jones**, P. Dorenbos – Journal of Physics: Condensed Matter **22** (2010) 185403

"Correlating local bonding and light emission in brown diamonds: a combined luminescence, Raman and x-ray absorption approach" - **G. O. Jones**, D. A. Evans, A. R. Vearey-Roberts, A. G. McGlynn, O. R. Roberts, N. R. J. Poolton, D. Twitchen, P. Martineau, S. Lawson, D Fisher. (*Submitted*)

I

Deulu Blaenau Ffestiniog a Llandrillo,

Dad, Mam a Ler.

Table of Contents

Chapter 2

Chapter 3

Chapter 4

Part II

Results – Foreword

Chapter 5

Chapter 6

Chapter 7

Chapter 8

Part I

Chapter

1

"Crystals are like people; it is only the defects that make them interesting."

F. C. Frank.

(Materials Scientist)

1.0 Diamond, an Introduction

1.1 Introduction

Material science plays a significant role in day-to-day life whether in tool or electrical applications in implements ranging from solar panels, to space exploration. Engineers are constantly attempting to further develop and improve concepts involved in applications and in order to do so, an understanding of the physical and chemical properties of the materials is required. A fine example is Diamond.

Diamond is a material that can be applied to a wide range of applications ranging from electronics to medicine and in order to fully implement its highly desirable properties, the material firstly needs to be characterised and dynamically understood. Studies on the optical and electronic properties of diamond have been inclined to focus on high purity, high quality material. Brown coloured diamond as a result has received very little interest, possibly due to its low commercial value.

The main topic of this thesis is one aspect that is significantly important in the study of Diamond and has posed questions that are still not fully understood. The cause of brown colouration.

Studies on the cause of brown colouration in diamond has been widely reviewed and explored recently by a wide range of techniques as will be discussed later in this thesis.

Presented in this thesis are studies that have been carried out specifically on brown diamond. The types of brown diamond samples used range from uniformly coloured, to those that are variegated and non-homogeneous. Different experimental techniques ranging from laboratory, to synchrotron-based experiments have been applied to characterise the samples in order to gain an insight into their chemical and structural properties. This preliminary chapter presents a general introduction to Diamond.

1.2 Diamond History

Carbon in its traditional form has been familiar to Mankind since the discovery of fire, whereas diamond itself has been known as a gemstone for many centuries (*1*). It is difficult to comprehend that behind the glitz and glamour that is associated with diamond that it is just a form of carbon of which the Latin is *carbo,* coal. It is difficult to comprehend that this crystal with its phenomenal 'fire' and brilliance (terms used in the gem trade) which causes it to be a particularly attractive and spectacular gemstone due to its high refractive index of ~2.417, was once inherent deep within the earth's crust with no exposure to light (*2*). It has an energy gap between the valence band and the unoccupied conduction band of ~5.47eV (*3*) which makes diamond a wide-band semiconductor abundant with unique electrical, physical, chemical and mechanical properties (*4*) and a Young's Modulus of 1000GPa (*5*).

Diamonds are mentioned in old Indian manuscripts that date back to around 800 B.C in Golconda, India. They were traditionally gathered from rivers and flats after the erosion of kimberlite pipes and the transportation of the material away from these sources. Up to the 18^{th} century, India was the only significant source of the gemstone up until around 1730 when diamonds were discovered in Brazil, establishing itself as

the world principal supplier until 1866, when diamonds were eventually discovered in South Africa.

Geologists in 1869 discovered that diamonds primarily originate from kimberlite pipes and thus began the production of diamonds at unprecedented rates. In 1888 Cecil Rhodes merged four South African diamond mines into the company that became DeBeers, and came to control almost all of the world's diamond production. Diamonds are these days mined in around 25 countries with the exception of Europe and Antarctica (*6*).

As mentioned earlier, not much research has been carried out on brown diamonds and they were seen as lower quality diamonds. During the great depression of the 1930's the stock of natural diamonds grew. Diamonds were only seen as gem sales of the high quality diamond and therefore the lower quality diamonds were put to one side. As a result stocks grew and it was down to Fergus Rogers who carried out a review into how the lower quality diamonds could be used in industrial applications such as drilling and therefore began the application of diamond into industry, which developed considerably. For further information regarding the Historical developments of Diamond Research in South Africa, a fine summary is presented in the 60th Diamond Conference Proceedings, held at Warwick in 2009 by Rob Caveney (*7*).

1.3 Diamond Structure

Diamond has long been a symbol of wealth and status for thousands of years. It is a mineral composed of Carbon in the form of a crystalline structure with each carbon atom surrounded by four other neighbouring carbon atoms in a tetrahedral arrangement/formation. It was Smithson Tennant in 1796 who discovered that diamond consisted of pure carbon. He observed that it burned to only form carbon dioxide (*8*).

It is this tetrahedral bonding of five carbon atoms that forms an incredibly strong crystal. It is a repeating geometry that creates a highly symmetrical and uniform framework such as shown in figure 1-1 (*6*). It has a crystal structure virtually identical to its common relatives in semiconductor research, silicon and germanium (*3*).

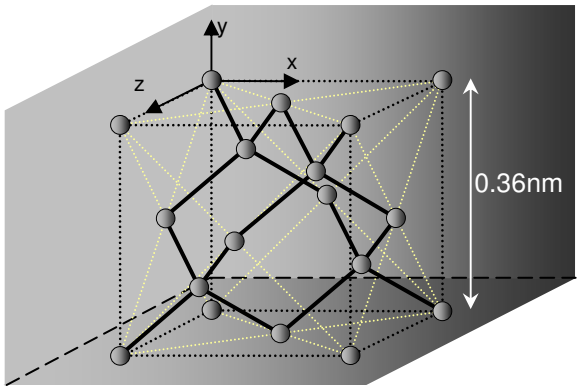

Figure 1-1: Diamond Cubic lattice (FCC). Carbon atoms in tetrahedral formation.

It is a face centred cubic (FCC) Bravais lattice crystalline structure, and can be cut and found with (111), (110) and (100) faces as shown in figures 1-2a, b, c. Diamond forms as two interpenetrating FCC lattices with a lattice constant a=0.36nm (figure 1-1) and a C–C spacing of 1.54Å. With a C–C bond strength of 344 kJ mol^{-1} (*9*) (sp^3 bonded carbon) this structure is responsible for diamond's high melting point and extreme hardness.

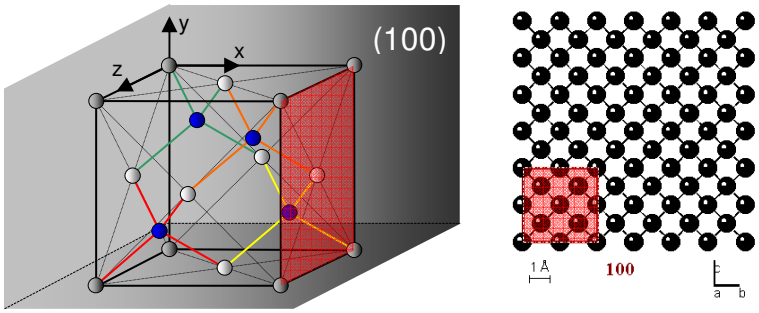

Figure 1-2a: The (100) face. All spheres are Carbon atoms. Dark grey are unit corner carbon atoms, light grey are face centre atoms and the blue atoms are inner unit atoms. ((100) face taken from (10)).

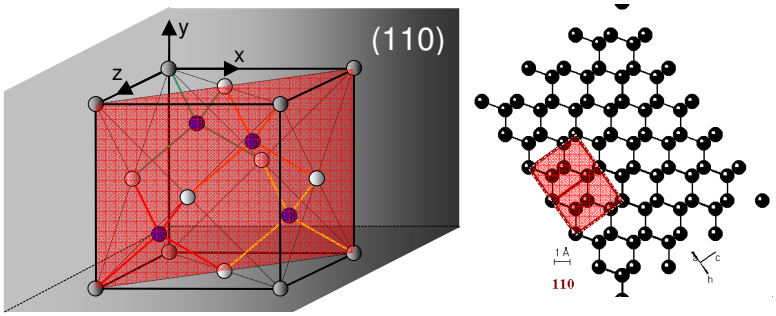

Figure 1-2b: The (110) face. All spheres are Carbon atoms. Dark grey are unit corner carbon atoms, light grey are face centre atoms and the blue atoms are inner unit atoms. ((110 face taken from (10)).

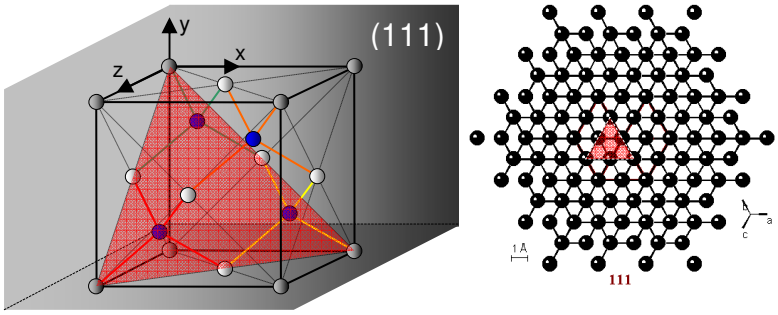

Figure 1-2c: The (111) face. All spheres are Carbon atoms. Dark grey are unit corner carbon atoms, light grey are face centre atoms and the blue atoms are inner unit atoms. ((111) face taken from (10)).

The two important surfaces for diamond are the (100) and (111) surfaces. Reactivity is related to crystal orientation and therefore knowing the exact orientation is a necessary detail in any account of surface reactions on diamond. These can be selectively grown by CVD synthesis by controlling the parameters during the growth process. The surface termination of the dangling bonds on these types of faces create different and useful surface properties each unique for the face orientation. When hydrogen terminated, surface states are removed from the gap and the electron affinity

changes sign and becomes negative. The material as a result becomes prone to transfer doping (*3*). This shall not be delved in further during the course of this thesis. Carbon is a group IV element with an atomic number of 6, it consists of 6 protons and 6 electrons and has the electronic structure, $1s^2 2s^2 2p^2$. Carbon has a valency of four and in the Diamond structure every carbon atom is covalently bonded to four other neighbouring carbon atoms creating a tetrahedral network (red, green orange and yellow – figure 1-2a,b,c). This bonding arrangement is referred to as sp^3 bonding (*4*), typically indicative of diamond and will be referred to often throughout the course of this thesis. In contrast, Graphite has a sp^2 bonded carbon structure.

As an engineering material, Diamond is one of the hardest naturally occurring substances known and has the highest thermal conductivity (room temperature) known of (2×10^3 Wm^{-1} K^{-1}) (*11*). Diamond-studded saws and drills have been used since at least the Napoleonic Wars (*12*). Contention for the hardest material has recently been in the form of, lonsdaleite (hexagonal diamond), wurzite BN and nanodiamonds (*13-16*). Nanocrystalline forms of diamond are known to have scratched diamond (*12*).

Graphite on the other hand (figure 1-3), another allotrope of Carbon, has striking differences to that of Diamond. Graphite is far softer than Diamond (see mohs hardness scale – figure 1-4) and as a result can mark i.e. paper and hence derives its name from the Latin “to write”. Graphite as a result is often used for pencil leads as well as a lubricant due to its relatively greasy texture which is as a result of the weak Van der Waal bonding that exists between the graphitic planes. Graphite was used as a lubricant on USAF aircraft but it was shown to be corrosive to Aluminium when moisture is present and therefore was discontinued (*17*).

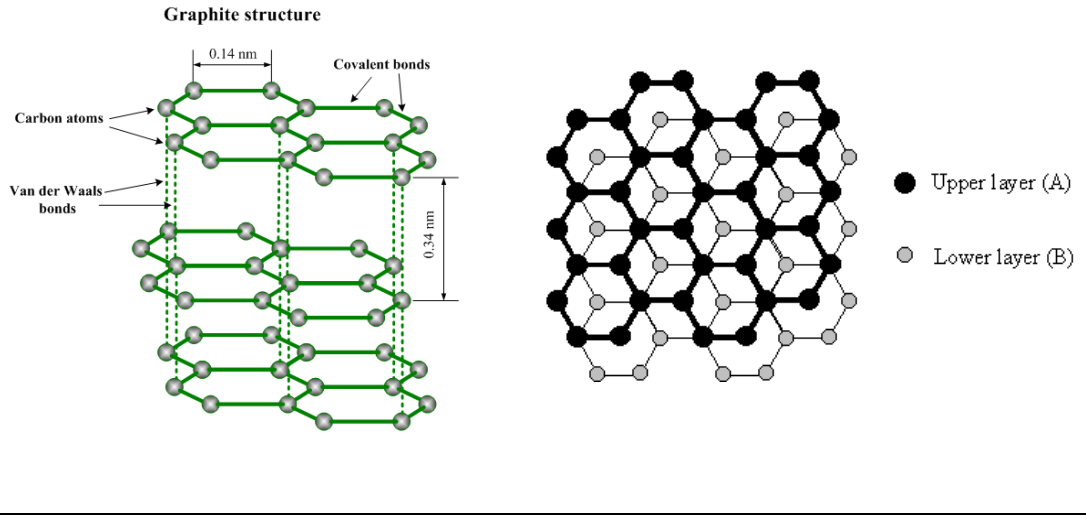

Figure 1-3: The atomic structure of Graphite. Taken from (18) and (19).

Table 1-1 shows the different important discoveries related to carbon over the years. Summarized and adapted from (*8*).

Table 1-1:

Year	Discovery	
1779	Carl Scheele	Demonstrated that graphite burned to form Carbon Dioxide and established that it therefore must be a form of Carbon
1796	Smithson Tennant	Established that diamond was made of pure Carbon and not a compound. Found that it burned to form only Carbon Dioxide
1855	Benjamin Brodie	Laboratory discovery of producing graphite from carbon
1955	Francis Bundy	Demonstrated that Graphite could be transformed into Diamond at high-temperature and high-pressure
1985	Kroto *et al*.	Discovered a new form of Carbon, C_{60}: Buckminsterfullerene (*20*)

As mentioned previously, Graphite is far softer than Diamond and different materials' hardness can be compared using the Mohs scale (figure 1-4).

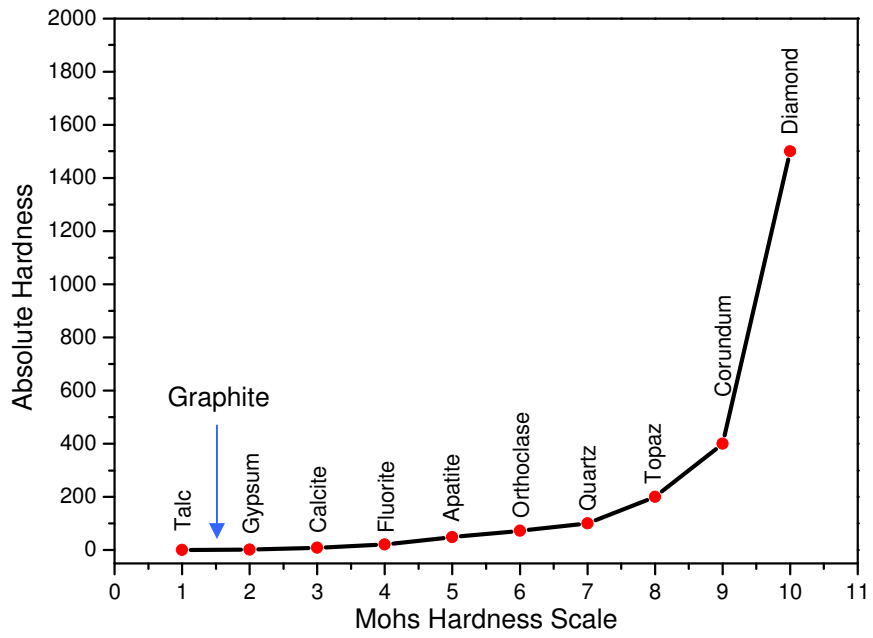

Figure 1-4: Mohs hardness scale – reproduced from (21).

Graphite is extremely soft and has a mohs hardness value of between 1 and 2 (*2*) and for hardness and stiffness it has long been thought that nothing could rival diamond (*12*). Recent work by Roderic Lakes at the University of Wisconsin – Madison and his colleagues have created a material that is nearly ten times stiffer through the embedding of barium titanate in a tin matrix. It gives the material an interesting property of negative stiffness that causes the inclusions to bend in the opposite direction of the applied force. As well as this, at a particular temperature the tendencies cancel each other out and the material scarcely deforms, although it goes on to state that the composite is not particularly hard or strong (*22*). Another material that rivals the hardness of diamond has been revealed in indentation experiments by Pan *et al*. (*16*). Experiments were carried out on wurtzite BN (w-BN) which has a similar bond length to cubic Boron Nitride (c-BN). c-BN is known to be second to diamond as a hard material and the results carried out by Pan *et al*. revealed surprising results when w-BN's hardness rivalled that of diamond from experiments.

Recent work has been undertaken on the melting of Diamond. It was long thought to be impossible to melt diamond at high temperatures – that it transforms to Graphite

rather than melting. A group in New Mexico have heated diamond at high pressure to more than 2000°C inside a microscopic hollow shell of carbon within which they observed the diamond soften. It is apparent that the diamond does not particularly melt, but in-fact fluctuates between crystal forms by continually melting and refreezing, a process called quasi-melting. The graphite-like carbon enclosing the diamond is estimated to produce a pressure of around 400,000 atmospheres and a temperature of 2000°C by contracting when electron beams are incident and as they shrink, the carbon at the centre is transformed from graphite to diamond (*23*).

Polycrystalline diamonds are tougher than single crystal diamonds and are therefore useful for cutting and polishing other hard materials (*24*). Fullerenes, (short for Buckminsterfullerene) a football shaped molecule arrangement, consisting of 60 carbon atoms discovered in 1985, is also an allotrope of carbon along with diamond and graphite (*20*). Each allotrope has different properties, all down to the arrangement of the carbon atoms within their lattices. Carbon is a versatile element which provides an array of crystallographic forms ranging from the three-dimensional Diamond and Graphite, one-dimensional carbon nanotubes and the zero-dimensional fullerenes. A two-dimensional form of carbon also exists and is more often referred to as Graphene – a planar, hexagonal single layer of graphite. In 2004 a simple but effective approach led to a revolution in the field whereby a single sheet of graphene was obtained from a graphite sample through micromechanical cleavage (*25*) (*26, 27*).

The electronic properties of Graphene and Diamond are very different. Diamond is a good insulator with a large energy gap in the electronic spectrum while graphene is a zero-overlap semi-metal. The reason for the differences lies in the fact that both have different electronic states of carbon which form both materials. Carbon has four electrons in its outer shell and in diamond all are involved in strong σ-bonds resulting in a large gap in the electronic band structure. For Graphene and Graphite only three electrons form σ-bonds, the fourth creates a π-bond and is in communal use thus resulting in Graphene and Graphite being good conductors. An essential part of developing wide band-gap materials for optoelectronic devices is to have a good understanding of the local structure, chemistry and optical properties of the material under study.

1.4 Diamond Formation

Natural diamond is typically formed deep underground, at depths of around 200km in the upper portions of the mantle. The mantle temperature and pressure conditions are around 1,000°C and 50 kilo-bars (*6*). The phase diagram in figure 1-5 provides an indication of the pressures and temperatures involved for the different processes (*28*).

1.4.1 Carbon Phases

Figure 1-5 shows the different carbon phases for the formation of diamond and graphite. The relationship between both allotropes is of the thermodynamic and kinetic form as is clearly visible in the phase diagram. A large activation barrier for conversion between graphite and diamond exists between the two allotropes, this is why diamond can exist at all, as the pressures and temperatures are so close between the two different formations of carbon atoms. No simple mechanism exists for the conversion of diamond into graphite or vice versa. The amount of energy required is nearly as much as it would be to completely destroy the lattice and performing a complete rebuild (*29*). Recent work by Evans *et al*. studied the conversion of diamond into graphite with Al as a catalyst (*30*). Once diamond is formed, it cannot convert back to graphite because the barrier is too high. Diamond is therefore said to be metastable, since it is kinetically stable, not thermodynamically stable.

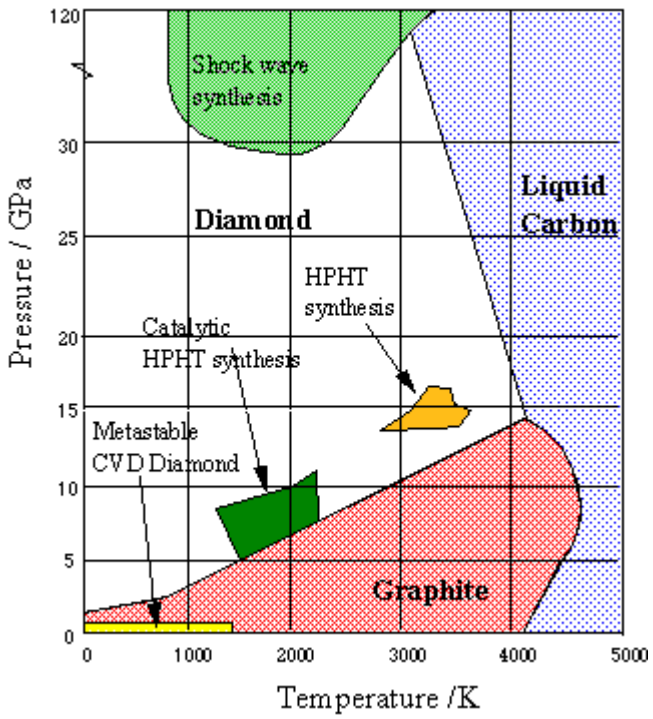

Figure 1-5: The Carbon Phase diagram for Diamond and Graphite taken from (28).

1.5 Diamond Classification

It was Robertson, Fox and Martin in 1934 that revealed that there were significant differences between optical and photoconductivity properties of different diamonds (*31*) and as a result fashioned the diamond classification system. It was later in 1953 that Custers came across p-type conductivity in diamond and further subdivided the type II group (*32*). Today, four groups exist, all with differences that affect their physical, electrical and optical properties.

The diamond type classification system is widely used in diamond research, providing a convenient way of categorising diamond based on their chemical and physical properties. The classification of a sample under study is important to consider when characterising samples in relation to their luminescence properties. The Near-Edge X-ray Absorption Fine Spectroscopy (NEXAFS) and Optically-Detected X-ray Absorption Spectroscopy (OD-XAS) techniques probe the chemical and physical properties of these materials and provide further invaluable information for sample characterisation as will be explained later in this thesis.

Diamonds can be divided into two main types, type I and type II. The division is based on the presence or absence of nitrogen impurities. The type I and II groups are further subdivided to create subgroups according to the arrangement of the nitrogen atoms incorporated in the lattice (isolated or aggregated), as well as the occurrence of boron impurities in some instances.

A pure diamond consists only of carbon atoms. No other elements are present and the atoms are arranged in a regular repeating pattern as previously mentioned. However, in some instances carbon atoms can be replaced by atoms of elements such as nitrogen (one of the most common impurities in diamond) and boron. The way these two impurities are arranged in the diamond lattice governs the type classifications (*33*).

Diamonds can be characterised into four different types as follows:

Type Ia, Ib, IIa and IIb each have specific properties that are different to each other (*1, 6, 31, 34, 35*):

- **Type I** – contain Nitrogen and roughly 98% of the world's diamonds are of this nature.

    - **Type Ia** – this type contains atoms of nitrogen (makes up of up to 0.3% of the diamond) which are clustered together within the carbon lattice. These diamonds absorb blue light and due to this they have a pale yellow or brown colour. 98% of diamonds are of this type.

    - **Type Ib** – are very rare in nature and almost all samples are synthetic. Within these types of diamond the nitrogen atoms are not clustered – they are far more evenly spread out within the carbon lattice and are referred to as isolated nitrogen atoms. These types – as well as type Ia – absorb blue light, but they also absorb green light – thus have a darker colour than type Ia. They appear in colour as orange, brown or green. Less than 0.1% of the world's diamonds are classed as type Ib. Their nitrogen content can be up to 500ppm.

- **Type II** – Diamonds that contain very few or no Nitrogen atoms.

    - **Type IIa** – these are the purest forms of diamond possible. They contain no impurities whatsoever – although if they do – it is minimal and miniscule amounts which are colourless. If the carbon lattice has been deformed and bent out of shape as the diamond rose to the surface of the earth, it may then give it a yellow, brown, pink or red colouration. 1-2% of the world's diamonds are Type IIa.

    - **Type IIb** – these are boron doped diamonds and absorb red, orange and yellow light and due to this appear to be blue. The crystal can be considered a p-type semiconductor due to the boron dopants (*34*). All natural blue diamonds belong to this type IIb – consisting of 0.1% of the world's diamonds.

Figure 1-6 provides a visual aid into the understanding of the type classification as well as a visual summary of the arrangement of the nitrogen and boron atoms in the specific types. Note also that the type Ia subgroup can be further subdivided into type IaA and IaB, which consist of pairs of nitrogen atoms and four nitrogen atoms around a vacancy respectively. Table 1-2 also provides a summary of the types of diamond and the typical colours found.

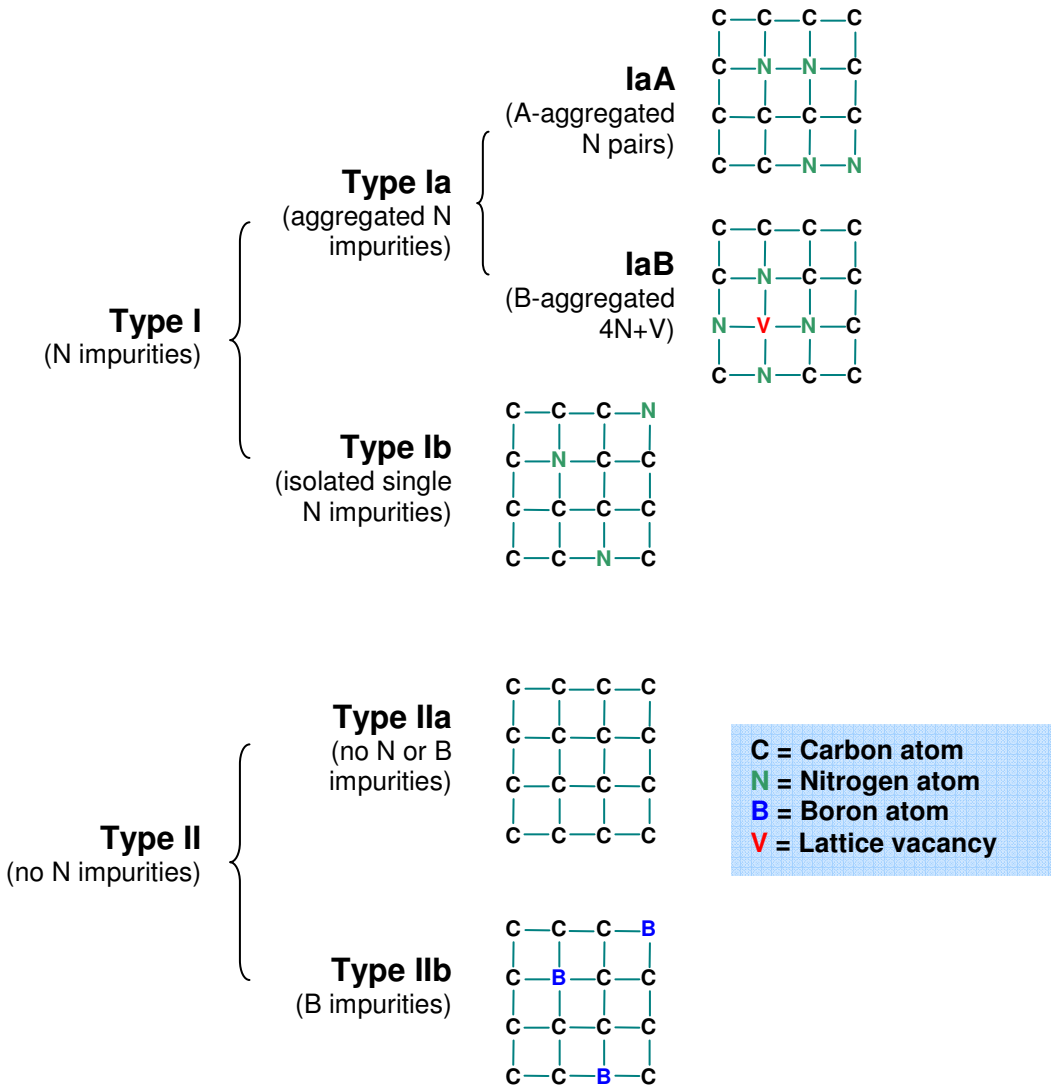

Figure 1-6: Reproduced from (33). Classification of diamond types.

Table 1-2: Type Classification and Colour reproduced from (6)

Type		Natural Abundance	Nitrogen content (ppm)	Colour	Cause	Centre/ Defect/ Inclusion
Type I	Ia	~98%	~10-3000	Colourless	Unknown inclusions	-
				Brown	Unknown centre related to deformation	-
				Pink	Unknown centre related to deformation	-
				Yellow	Aggregates of 3 Nitrogen atoms	N3
	Ib	~0.1%	~25-50	Yellow	Isolated Nitrogen	N
				Brown	Unknown centre related to deformation	-
Type II	IIa	~2%	<10	Colourless	Unknown inclusions	-
				Pink	Vacancy trapped adjacent to isolated Nitrogen	N-V
				Red	Unknown centre related to deformation	-
				Brown	Unknown centre related to deformation	-
	IIb	Rare	None (<0.1)	Blue	Boron	B
				Gray	Boron	B

1.6 Defects in Diamond

The understanding of defects in diamond is of the utmost importance, especially when applying diamonds into optical or electronic applications. The optical and electric properties of the material need to be understood in an effort to control them.

Natural diamond is rarely found without impurities incorporated into its morphology. Up to 44 elements have been identified as impurities in natural diamond (*1*). The most significant of these is Nitrogen (up to 0.3%). The properties of the diamond crystal are significantly governed and affected by these impurities. For example, the presence of substitutional boron (up to 0.25ppm) is sufficient to transform the usually insulating crystal into a p-type semiconductor (*36*).

A perfect diamond is colourless (*37*). It contains no impurities and is very rarely found in nature. The clarity and colour of diamond establish its value as a gemstone and are due to the defects and impurities within its lattice structure. Gem-quality diamonds are typically graded and evaluated in terms of the 'four Cs', carat weight, colour, clarity and cut (*6*).

- Carat weight – this is a measure of the diamond's weight whereby 1 carat = 0.2g.

- Colour – A colour grade table exists ranging from colourless, near colourless, faint yellow, very light yellow and light yellow. Within these groups are subgroups and are shown in table 1-3. Further information on colour in diamond is presented later in this chapter.

Colour Grade	D E F	G H I J	K L M	N O P Q R	S T U V W X Y Z
Colour	Colourless	Near Colourless	Faint Yellow	Very Light Yellow	Light Yellow

Table 1-3: Colour Grade table, reproduced from (6).

- Clarity – Almost all natural diamonds contain flaws and imperfections and clarity is a means of describing these deficiencies. Clarity grades are also available, expressed in the form of a table, but are not presented in this thesis.

- Cut – the cut is the shape of the diamond that brings out light at its most brilliant. It consists of flat polished surfaces and can be of a variety of different shapes ranging from the standard round brilliant, pear-shaped, to heart shaped, but again will not be mentioned further during the course of this thesis.

For more information on the 'four Cs' refer to (*6*).

There are two types of defects typically found in Diamond. Point defects and extended defects. Point defects are typically of the order of 1nm in size and are often no larger than a few atoms or vacancies in size. Extended defects are substantially larger and may well be hundreds of nanometres in size.

1.6.1 Point Defects in diamond

Point defects in diamond can be intrinsic or extrinsic. The misalignment of the diamond structure that have created vacancies or interstitials with no alien elements are classed as intrinsic. Point defects can also be extrinsic whereby foreign elements such as nitrogen have been introduced or are situated within the lattice. Figure 1-7 shows the various point defects that can exist in a crystal.

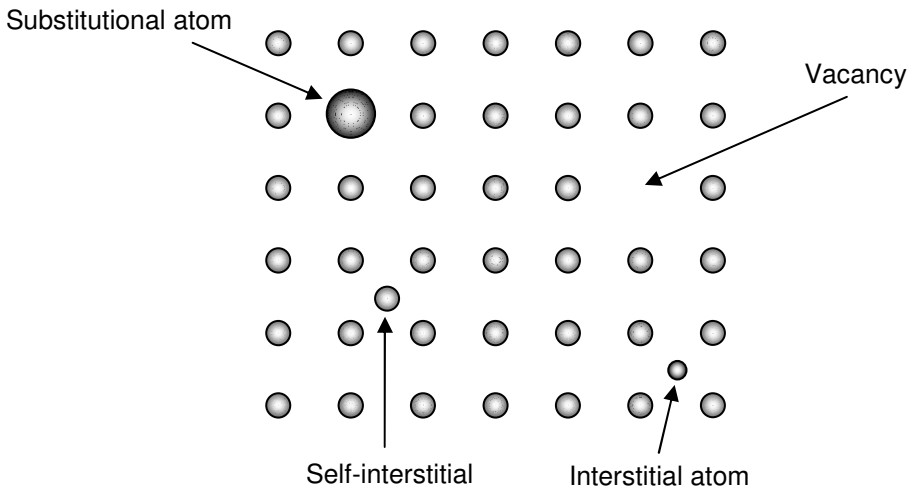

Figure 1-7: An illustration of the various point defects that are typically found in a crystal lattice. Reproduced from (38).

Point defects in diamond have been studied for decades and it has been known for many a year that diamonds can be separated into two groups as mentioned earlier (*31, 39*). The ability to control or regulate the defects or impurities is essential for the production of synthetic diamonds as will be explained in the next section. Point defects can be identified in diamond by Raman spectroscopy (*40*) and in luminescence studies such as Photoluminescence (PL) (*41*).

Some of the main defects and their known properties are listed in table 1-4.

Table 1-4: A summary of a few of the defect centres typically found in Diamond, partly reproduced and adapted from (*41*).

Centre	Structure	ZPL (eV)	Position
A centre	$[N\text{-}N]^0$	3.758, 3.902, 3.928	E_c – 4eV
B centre	$[4N\text{-}V]^0$	-	-
C centre	N sub	-	E_c – 1.8eV
Boron	B sub	-	E_v + 0.38eV
H3 centre	$[2N\text{-}V]^0$	2.463	
H2 centre	$[2N\text{-}V]^-$	1.257	E_c – 2eV
N3 centre	$[3N\text{-}V]^0$	3.0	-
2.156eV	$[N\text{-}V]^0$	2.156	-
W15	$[N\text{-}V]^-$	1.945	-
GR1	V^0	1.673	~E_c – 3.2
ND1	V^-	3.150	~E_c – 3.2
Divacancy (TH5)	$[V\text{-}V]^0$	2.543	-

1.6.1.1 Nitrogen in Diamond

As mentioned earlier nitrogen is one of the most abundant impurity elements found in diamond. It is found in many structural forms. The most significant ones are the single substitutional nitrogen atoms (C-centres), pairs of nearest-neighbouring substitutional nitrogen atoms (A-centres) and complexes of four substitutional nitrogen atoms surrounding a lattice vacancy (B-centres) as shown in table 1-4. Annealing diamond at HPHT conditions has been shown to convert C-centres to A-centres and then from A-centres to B-centres (*42*). Due to the broad vibronic emission bands (as will be shown later in the thesis) of centres such as H3 and N-V, they have been considered for future applications as solid state tuneable femtosecond lasers as a replacement for the current dye lasers that exhibit lower photo and less thermal stability (*43*).

1.6.1.2 Boron in Diamond

Boron is an important impurity in diamond. It results in the diamond being classed as a type IIb diamond (*36*). It forms an acceptor state in the diamond lattice situated at 0.37eV above the valence band (*42*). The doping of boron causes the diamond to become a p-type semiconductor and therefore ideal for uses in electronic applications. The HPHT treatment of a type IIb synthetic diamond has no effect on the single substitutional boron (*42*).

1.6.2 Extended Defects in Diamond

Extended defects in crystals can, like point defects, either be intrinsic or extrinsic. In diamond crystals they are typically in the form of intrinsic defects such as dislocations and stacking faults.

Dislocations are very common in natural and CVD-grown diamond and densities as high as 10^7 cm^{-2} have been observed in type IIa diamonds (*44*). They are reported to lie at or near grain boundaries as well as some that propagate through the thin film from their beginning at the substrate. There has been an advance in the growth of high-quality CVD diamonds whereby the defect density is of the order of 10^4 cm^{-2}. They are typically found as edge dislocations and screw dislocations.

Dislocations can be observed in cathodoluminescence (CL) topographs and photoluminescence (PL) images of diamond. They seem to have a quenching effect on the impurity related luminescence (*45*).

1.7 Synthetic Diamond

1.7.1 High-pressure, high-temperature (HPHT) synthesis

Natural diamonds are very much unique. No other diamond is alike and naturally the impurities or impurity concentration vary from one sample to the next. This is one of the many reasons why they are much more expensive than synthetic diamonds as well as being a valid reason not to include them in electronic applications and other applications such as in dosimetry whereby the synthetic types are more preferred (*46, 47*). Natural samples are too expensive and their purity is also an issue. The production of the first synthetic diamond in 1955 by Bundy *et al.* at the General Electric factory in the United States paved the way for the synthetic diamond synthesis that we know of today. The High-Pressure, High-Temperature (HPHT) technique used consisted of the compression of graphite using a metal catalyst at temperatures exceeding 2000K (*48*).

HPHT synthetic diamond is used predominantly in industrial applications due to its super hard properties. Issues remain on the quality, grain size and production of this type of diamond and there is no clarity on their growth mechanism as of yet as explained by Yang *et al*. (*49*). Their research paper discusses the way in which surface energy influences the growth of diamond since the growth mechanism is still an issue that is not fully understood in the HPHT synthetic process. They go on to explain the formation of natural diamond in terms of HPHT thermodynamic theory. They state that it is important to pay more attention to the influence of hydrogen on surface energy and that hydrogen may be a "bridge" for explaining the formation of HPHT synthetic and natural diamond. The difference in the formation of natural diamond and HPHT synthetic diamond makes it difficult to compare with the growth mechanism of the HPHT diamond due to both types being formed in different ways (*49*).

The ingredients for the production of industrial HPHT synthetic diamond from an inorganic system consists generally of metal and metal alloys being used as solvent-catalysts with graphite as the predominant carbon source, along with pyrophyllite as a pressure-transfer medium. In nature, the production of natural diamonds results from organic and inorganic material.

1.7.1.1 Large Diamond Grown at High Pressure Conditions

The HPHT technique has improved dramatically since the announcement of the first diamond synthesis in 1955. Synthetic diamond is predominantly produced for commercial use in three forms, Single Crystal, Powder and Polycrystalline compact. Single crystals can be grown by a technique developed by the General Electric Research group called the temperature-gradient method whereby a Carbon source, a seed crystal, and a growth media consisting of a metal solvent-catalyst is essential. The Kanda *et al*. group (*50*) has a cell assembly as shown in figure 1-8. All essential ingredients are placed inside a cylindrical graphitic heater with the carbon source sitting at a higher temperature than the crystal seed. The temperature is at its highest at the centre of the cylindrical heater as electrical current passes the heater. NaCl is added to the heater surrounding the seed crystal, the catalyst, the carbon source and the cell are compressed up to a pressure of ~5GPa in a high pressure vessel and heated to 1500°C.

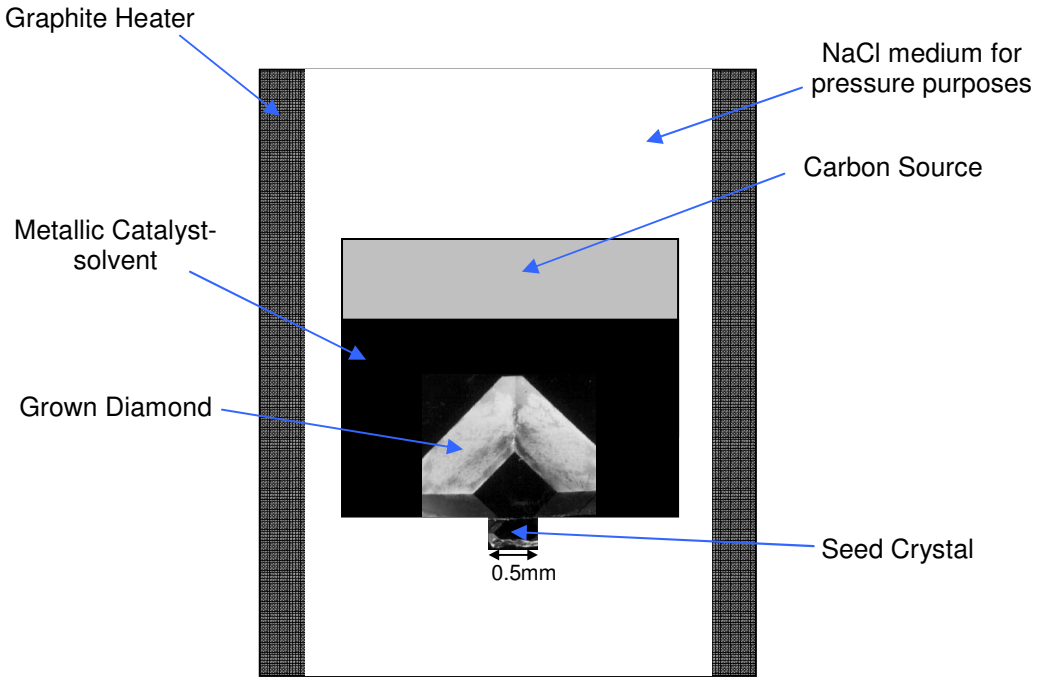

Figure 1-8: Temperature gradient method diamond growth (Kanda group) schematic, seed crystal is 0.5mm is diameter and the grown diamond has grown on top – scanning electron micrograph image taken and incorporated into schematic. Note – cell is not to scale. Diagram reproduced and modified from (50).

1.7.2 Chemical Vapour Deposition (CVD) Synthesis

Another synthetic technique used in the production of diamond is the CVD method. As the name suggests single-crystal and polycrystalline films can be synthesised from the deposition of carbon from hydrocarbon gases onto a variety of substrates (*1*). A pressure of between 1 – 200 Torr is required for the synthesis of CVD diamond as well as hydrogen and a hydrocarbon source such as methane. This is the source of carbon from which the diamond is formed. Hydrogen is crucially important in the CVD synthesis process due to forming a 'hydrogen radical'. Typically under the growth conditions it is graphite that is thermodynamically favoured – this is where the hydrogen radical aids the diamond process by etching away the graphite formed. Hydrogen coverage stabilizes the sp^3 bonding of the carbon atoms and prevents the formation of the graphitic phase (*36*) (*11*). The graphite is removed 10 to 100 times quicker than it would to etch away diamond. The hydrogen radicals are formed by hot filaments, microwaves and even blowtorches, this is a high energy consuming process and thus expensive (*51*).

For the production of single crystal CVD diamond the initial substrate has to be diamond. The conditions for diamond growth are already met and the diamond during this process is grown in layers (*51*).

CVD can also be applied to graphite (*52*). Laser-Assisted Chemical Vapour Deposition (LCVD) of graphite by Tyndall *et al*. succeeded in growing a carbon film on a silicon substrate. The analysis of the film by Auger electron spectroscopy and Raman spectroscopy confirmed its graphitic nature. Further work on this type of synthesis could be utilized in producing a single monolayer of graphite on a silicon substrate as a means of growing graphene for electronic purposes due to its excellent electronic properties (*26, 27*).

As mentioned above Raman spectroscopy is often used for the characterization of CVD films and a good means of the analysis of their quality as well as being a non-destructive technique. It is used as a diagnostic tool for the evaluation of the phase purity and perfection of CVD diamond films (*53, 54*).

1.8 Diamond Applications

The exceptional hardness, strength, chemical and thermal stability as well as radiation hardness and optical transmission, to name but a few of diamond's properties make it an invaluable material for application in electronic and wear resistant coatings (*55*).

The volume synthesis of diamond through the CVD technique has led to a substantial reduction in the cost of production of the material and thus to the utilization of the product for optical, thermal, electrochemical, chemical and electronic applications. CVD diamond are these days used in tweeters for the high frequency part of loudspeakers, and radiation detectors (*5*). The material offers tremendous potential for a wide range of applications and is reflected in BAE Systems (British Aerospace) attaining a 50% stake in 'Diamond Detectors Ltd' in 2008 (*5*).

Diamond has recently been applied to electrochemistry and biotechnology as a substrate for biosensors or DNA chips due to its excellent blend of electrical, optical chemical, thermal and biotechnical properties (*56*).

1.8.1 Diamond in Medicine

Diamond is often used in medicine for the purpose of radiation detection. Its advantages for such uses are that it is a biocompatible material with the ability to be sterilised as well as being non-toxic (*57*). The key specifications that make it such an ideal material in instances such as this is its high radiation resistance, high-temperature operation, fast time response and its atomic number (carbon Z = 6) equivalent to that of human tissue and water-effective atomic number of Z_{eff} = 7.4 (*41, 42*). Another valuable characteristic of the use of diamond in clinical dosimetry is the fact that small detectors can be developed of relatively small sizes such as 1-2 mm^3 as well as being chemically inert (*47*). The performance of a CVD diamond for applications such as dosimetry depends significantly on the quality of the material (*47*). High quality CVD diamonds are most often used as diamond dosimeters compared to HPHT synthesised diamonds. Studies by Marczewska *et al.* show that HPHT synthesised diamonds demonstrated characteristics approaching that of commercial natural diamond dosimeters and CVD detector grade dosimeters but work

is still required to understand fully the relation to the electronic structure of the material due to the defect and impurity content (*47*). These types of properties were revealed by high-quality natural diamond as it is very difficult to obtain such energy spectrometer grade detectors from natural diamond. Natural diamonds are expensive and rare as well as the fact that natural diamonds would cause difficulty in obtaining a wide range of natural diamond dosimeter devices, providing the same reproducible results (*57, 58*). All natural diamonds are different. The application of natural diamond dosimeters is severely fraught with the requirement of testing many natural stones before a suitable dosimetry detector can be found to be capable of producing correct and consistent results (*47*).

The recent progress and emergence in the synthesis of high quality diamond crystals from HPHT and CVD methods have provided higher quality diamond for radiation dosimetry spectroscopy with the significance of providing more accurate results and therefore offer more possibilities in this field (*47, 58*). Disadvantages lie with small crystal polycrystalline diamond due to charge loss at grain boundaries, although recently, larger polycrystalline diamonds are now available.

1.8.2 Other uses of Diamond in Medicine

Diamond is used in cutting implements and due to being hydrophobic has a very low friction against living tissue. The image in figure 1-9 below shows a significant difference in the edges of a steel scalpel and a diamond scalpel.

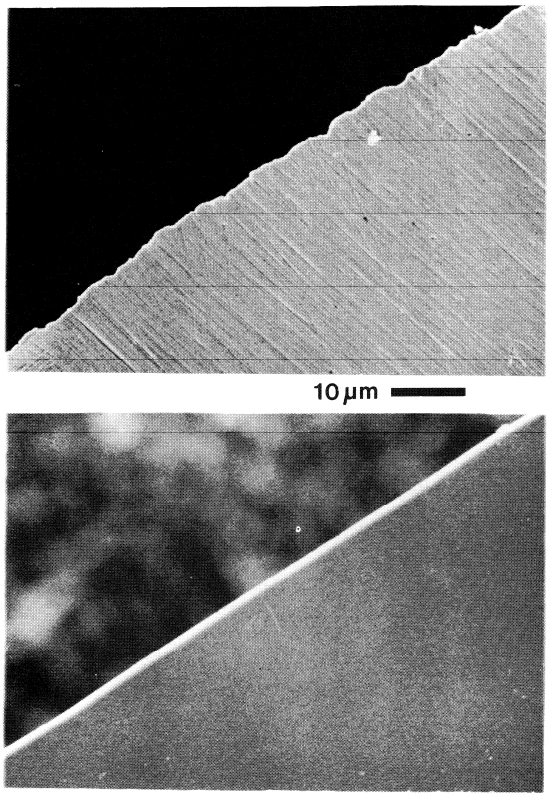

Figure 1-9: Image taken from (1) showing two scalpel edges, the top image is that of a steel scalpel and the bottom is that of a diamond scalpel.

Studies reveal that a diamond blade causes less stress on the tissue with less cells being damaged while an incision is being made. This results in a more rapid healing process and as a result reduced scarring. They are also implemented in the removal of cataract whereby the use of a diamond blade provides the surgeon with greater control of incisions with less stress being applied to the cornea (*1*). Synthetic diamond are being considered for use in the treatment of eye cancer sufferers in the instrument's optics to deliver a more precise way of proton therapy due to the target location being so small. The current challenges are to deliver the therapy precisely and uniformly without damage to the health tissue in the surrounding vicinity (*59*).

Smith *et al*. have researched into the preservation of DNA samples through the utilization of diamond as a substrate to preserve and anchor the DNA for i.e. forensic storage. Successful preliminary work (2007) has been made on the anchoring of single stranded DNA to diamond (*60*). As well as DNA anchoring purposes recent work by Stacey *et al*. (2010) have applied diamond in biological sensing that could one day be incorporated in the eye to assist the blind.

1.9 Future Diamond applications

Recent work carried out by Stoneham has touched upon whether a *"Room-Temperature, solid-state quantum computer"* is possible (*61*). The use of diamond as a *quantum* computer has been explored due to the markets' constant demand for faster, smaller and more power efficient computers. Some work demonstrating the critical steps has been done as far back as the late 80s at room temperatures, using the nitrogen-vacancy $[N\text{-}V]^-$ centres in diamond for the transfer of quantum information (*61-63*).

1.10 Colour in Diamonds

The hype and interest towards coloured diamonds can be said to have been accelerated in October 1987 when a 0.95-carat red diamond was auctioned for nearly $1million (U.S) in new york (*6*).

1.10.1 Coloured Material

As stated earlier, the main purpose of this thesis over the past four years has been to identify and find the cause of the brown colouration within brown diamonds. It is therefore important to understand how any material appears to be coloured.

White Light consists of all colours – it is the additive suppression of all the colours as one. i.e.

Red + Orange + Yellow + Green + Blue + Indigo + Violet = White

The electromagnetic spectrum is shown in figure 1-10.

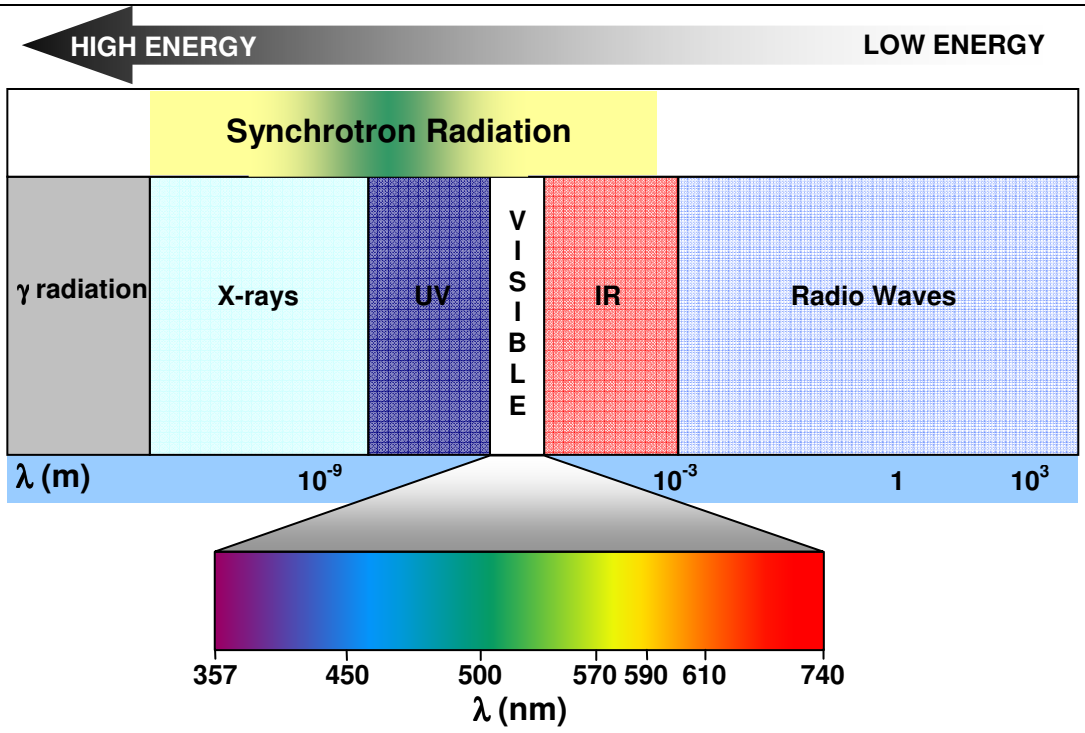

Figure 1-10: The Electromagnetic spectrum (not to scale). Green region is the energy region available at the MPW6.1 (40-450eV) beamline at the SRS, Daresbury predominantly used for the investigations in this thesis.

When a material appears to be a certain colour, we can gather that the light emitted by the object has been modified. Certain colours present within the white light incident upon the material are absorbed by the material. The apparent colour of the material has not been absorbed and therefore is of that particular colour.

An example is a red material. The red material absorbs mostly Green light and thus appears red to our eyes. It is the same in the case of coloured diamonds.

1.10.2 Colouration in Diamond

A "yellow" diamond basically consists of a combination of green, yellow, orange and red. The rest of the colours have been absorbed by the diamond. *Coloured* diamonds absorb a part of the visible spectrum, whereas *colourless* diamonds do not absorb at all.

Diamond is an exception to other gems whereby their colour is due to metal impurities located within the lattice. The colouration often found in diamond is typically due to nitrogen doping, an element rarely found in other types of gems. Defects within a diamond's structure can also have a colouring effect.

Colour is due to the absorption of a particular wavelength (energy). In some instances the incident light is absorbed and can excite electrons from the valence band up into a particular energy level. A perfect diamond is colourless with no defects or impurities. It contains no defect states within its band gap and therefore when light of a particular wavelength (energy) is incident on the sample, the light energy is not sufficient to excite electrons from the valence band into the higher level, in this instance for a colourless diamond, the conduction band. As a result no visible light/energy is absorbed due to its high band-gap (valence band to conduction band energy spacing) of ~5.5eV. For coloured samples, states exist within this band-gap and therefore light of lower energy can excite electrons into that particular level. Absorption occurs as a result and produces colour.

The inclusion of nitrogen incorporated into a diamond's structure provides a defect level within the band gap. The different forms of these are listed in table 1-4. The N3 centre which consists of a vacancy surrounded by three nitrogen atoms, is a colour centre and the A aggregate and B aggregate do not absorb light individually but can become part of more complex colour centres. H3 and H4 centres are also found in nitrogen containing diamonds and are related to heat-treatment, formed when a vacancy becomes trapped at an A or B aggregate respectively. An N-V centre can be formed when a vacancy captures an isolated N atom (*6*). Missing atoms can also have an effect on the diamond's colour, the simplest form is that of the carbon vacancy (table 1-4), the GR1 centre, whereby a carbon atom is missing from the lattice.

1.10.3 Brown Diamond and HPHT treatment

The origin of colour in brown diamonds has attracted much attention in recent years, and resulted in many attempts to characterise the responsible defect, whether it related to a doping of some sort, or a particular defect. Many samples contain stark brown colouration and others a lighter shade. As well as this, samples exist that contain stark brown and colourless bands, known as banded diamonds, sometimes referred to as 'zebra diamonds'.

Brown diamonds are the most commonly mined diamonds in the world. They have been found set in Roman rings, dating as far back as between the first and third centuries C.E. Brown diamonds are found as natural and synthetic forms, grown from techniques such as chemically vapour deposited (CVD) diamond and also exist in both type I and II which makes it difficult to exactly determine the source of the colour. The fact that type I and type II diamonds can be found with brown colouration could suggest that nitrogen is therefore not the responsible defect although as mentioned in the diamond classification section, it is possible that natural type II diamonds can contain very few nitrogen atoms.

The cause of brown colouration is still not fully understood may be due to the significantly less research that has been implemented on these types of diamonds. Diamond studies have always been particularly inclined towards high purity, high quality materials whereby brown diamonds have been disregarded, perhaps for their low commercial value especially when it comes to the gem trade. Brown diamonds have always been difficult to sell in the gem trade and efforts have been made to make diamond more appealing to potential customers by advertising them as 'champagne diamonds' (*6*) and so forth. The recent discovery that the High-Pressure, High-Temperature (HPHT) treatment of brown diamonds eliminates the brown colouration and makes them virtually colourless, has brought upon renewed interest in brown diamond.

The implication of the change in colour is that the brown diamonds once deemed unattractive in appearance within the gem trade have had their appearance significantly enhanced and thus as a result, increased their commercial value. It is

therefore crucial to understand the nature and source of the brown colouration and the nature in which the treatment has affected the colour. It is highly important to be able to identify treated diamonds, due to the potential false advertising of previously brown diamond as colourless, specifically for the protection of the consumer (*64*). The probing of the diamonds' structure by a variety of techniques could be one way of identifying whether a diamond is treated or not due to the HPHT process resulting in i.e. band elimination. The microscopic mechanisms involved in the removal of the brown colour remain unclear.

Colour in diamond is typically associated with some impurity content but the origin of colouration in brown diamond (type IIa for example) is not a result of impurity. They can be as pure as a colourless type IIa specimen (*65*). Recent studies suggest that the colouration is related to vacancies or vacancy clusters (*65*) as a trend has been observed with the depth of colour and the size of the vacancy clusters. Positron annihilation studies have revealed that the size of the cluster decreases with decreasing brown colouration (*66*). Positron annihilation is an efficient technique for studying crystallographic defects that have an open volume. The vacancy in fact cannot be detected after HPHT treatment. Studies have revealed that dislocations alone can account for the strength of the observed absorption in brown diamond (*67, 68*).

Whilst the nature of brown colour in natural diamond is relatively well understood to be largely due to N and vacancy defects, the origin of the brown colour in synthetic diamonds is still under discussion (*65, 69-72*). For example, it appears that extended vacancy defects may play a role and it has been shown theoretically that such defects would lead to significant discolouration (*70*). Further observations in support of the removal of brown colour when a brown natural diamond sample is subjected to high-pressure and high-temperature (HPHT) treatment resulting in near-colourless stones have been made by Collins *et al.* and Van Royen *et al.* (*37, 73*).

Positron annihilation studies have revealed a reduction in extended vacancies with increasing temperature and pressure and high resolution transmission microscopy has shown that vacancy clusters are more common in darker synthetic diamonds (*66, 74*). There is some indication from Raman spectroscopy that brown diamonds exhibit a

greater concentration of sp^2 diamond. Up to now the clearest indication of non-diamond carbon in brown diamonds has been TEM measurements using local electron absorption at the C K-edge (*69*). However, such measurements involve severe sample processing and high energy density electron beams and there is a need to confirm these measurements using less destructive methods.

A recent review by Fisher (*64*) has suggested a strong case for the cause of brown colouration to be associated with vacancy clusters as has also been suggested by Maki *et al*. (*74*) and Bangert *et al*. (*75*). Maki *et al*. found that natural brown diamond (type IIa) contained active vacancy clusters of the order of around 40-60 missing atoms. They noted that the clusters gradually disappeared with HPHT treatment and that the samples treated up to a temperature of 2500°C resembled colourless samples optically with similar positron lifetimes and as a result concluded that the brown colour originates from the vacancy clusters and that their removal by HPHT treatment causes the loss in colouration (*74, 76*). An interesting statement is that the removal of brown colouration from CVD diamond by thermal treatments can occur at lower temperatures of ~1600°C, but no correlation is observed with the observation of vacancy clusters (*76*).

As well as the synthesis of diamonds from HPHT growth, it has been noted that the HPHT treatment of coloured diamond such as brown diamonds cause them to become colourless due to the treatment. One of these types, a natural type IIa sample has been studied for the purpose of this thesis which will be mentioned further in detail later in the thesis.

The HPHT treatment annealing effects on CVD diamond have also been studied in the literature (*77*). Ueda *et al*. observed a decrease in the band-A emission of their samples which is related to crystal defects within the diamond. Their conclusion was that the HPHT treatment decreased the crystalline defects and improved the optical and electronic properties. The main reason for the HPHT treatment of the CVD diamond in this case was to try and improve the CVD crystal quality. It has been observed that the H3 centre increases in intensity in CVD diamond after HPHT treatment (*77*), an interesting observation and comparison with some of the results obtained for the purpose of this research are to be found later in the thesis. As well as

this the HPHT process is also known to convert C-centres to A-centres followed by A-centres to B-centres (*42*).

The HPHT process is well documented and known to eliminate the brown colouration from brown diamond. Kupriyanov *et al*. have also studied the effects of HPHT treatment on the spectroscopic features of type IIb (boron doped) synthetic diamonds (*42*). They found that single substitutional boron was not affected by the treatment and agrees with work carried out by Goss and Briddon (*78*) that a high activation energy is required for the migration of substitutional boron atoms within the diamond lattice (*42*).

HPHT treatment has an effect on nitrogen incorporated in the diamond lattice. It is responsible for many optical systems that are incorporated into the lattice as individual atoms (C-centres) during HPHT growth of synthetic diamond. The annealing of diamond at temperatures exceeding 1500°C stimulates nitrogen migration in the diamond lattice creating aggregation pairs (A-centres) or complicated complexes containing up to 4 nitrogen atoms (B-centres) (*79*).

CVD brown diamonds are different to naturally brown diamonds when HPHT treated. The brown colouration disappears at lower temperatures in CVD compared to natural diamond suggesting a less stable defect. As well as this, positron annihilation experiments have found different lifetimes than those found in natural diamonds (*70*). Jones *et al.* also mention that the brown centres in natural diamonds are multivacancy clusters of globular nature in agreement with TEM studies (*70, 80*).

1.11 Summary

This initial chapter has introduced diamond as a material that has a variety of properties for different applications. Further information on diamond could be presented here due to it being a well researched material that has been studied for many years. The next chapter introduces Synchrotron facilities, an invaluable source of experimental apparatus without which, most of this thesis' data could not have been acquired.

1.12 References

1. J. E. Field, *The Properties of Natural and Synthetic Diamond*. (Elsevier Academic Press, 1992).
2. http://www.enmu.edu/services/museums/miles-mineral/diamond.shtml. (2010).
3. J. Ristein, *Applied Physics a-Materials Science & Processing* **82**, 377 (2006).
4. R. Kalish, *Journal of Physics D-Applied Physics* **40**, 6467 (2007).
5. D. J. Twitchen, paper presented at the The 60th Diamond Conference, Warwick, 2009.
6. G. E. Harlow, *The Nature of Diamonds*. (Cambridge University Press, 1998).
7. R. Caveney, paper presented at the The 60th Diamond Conference, Warwick, 2009.
8. http://www.chemicool.com/elements/carbon.html. (2010).
9. W. J. Huisman *et al.*, *Surface Science* **387**, 342 (1997).
10. http://www.chm.bris.ac.uk/pt/diamond/dstruc.htm. (2010).
11. P. W. May, *Philosophical Transactions of the Royal Society of London Series a-Mathematical Physical and Engineering Sciences* **358**, 473 (2000).
12. P. Ball, in *New Scientist*. (2009).
13. F. P. Bundy, J. S. Kasper, *Journal of Chemical Physics* **46**, 3437 (1967).
14. N. Dubrovinskaia *et al.*, *Applied Physics Letters* **90**, (2007).
15. M. R. Salehpour, S. Satpathy, *Physical Review B* **41**, 3048 (1990).
16. Z. C. Pan, H. Sun, Y. Zhang, C. F. Chen, *Physical Review Letters* **102**, 055503 (2009).
17. http://graflex.org/speed-graphic/lubricants.html. (2010).
18. http://www.substech.com/dokuwiki/doku.php?id=graphite_as_solid_lubricant. (2010).
19. http://www.spmtips.com/hopg. (2010).
20. H. W. Kroto, J. R. Heath, S. C. Obrien, R. F. Curl, R. E. Smalley, *Nature* **318**, 162 (1985).
21. http://www.allaboutgemstones.com/mohs_hardness_scale.html, (2010).
22. T. Jaglinski, D. Kochmann, D. Stone, R. S. Lakes, *Science* **315**, 620 (2007).
23. P. Ball, in *Nature*. (Nature Publishing Group, Nature News, 2007), vol. 448, pp. 396-397.

24. S. Fukura, T. Nakagawa, H. Kagi, *Diamond and Related Materials* **14**, 1950 (2005).
25. K. S. Novoselov *et al.*, *Science* **306**, 666 (2004).
26. K. S. Novoselov, in *The KIAS Newsletter 2009*. (Korea Institute for Advanced Study, 2009), pp. 20-25.
27. A. C. Ferrari *et al.*, *Physical Review Letters* **97**, (2006).
28. F. P. Bundy, *Journal of Geophysical Research* **85**, 6930 (1980).
29. http://www.ch.ic.ac.uk/rzepa/mim/century/html/diamond_text.htm, (2010).
30. Owain Rhys Roberts, The University of Wales, Aberystwyth (2009).
31. R. Robertson, J. J. Fox, *Philosophical Transactions of the Royal Society of London Series a, Containing Papers of a Mathematical or Physical Character* **232**, 463 (1934).
32. J. F. H. Custers, *Physica* **18**, 489 (1952).
33. C. M. Breeding, J. E. Shigley, *Gems & Gemology* **45**, 96 (2009).
34. http://www.bris.ac.uk/Depts/Chemistry/MOTM/diamond/diamond.htm. (2010).
35. http://www.24carat.co.uk/diamondtypes1a1b2a2bframe.html. (2010).
36. C. Goeden, G. Dollinger, *Applied Physics Letters* **81**, 5027 (2002).
37. J. Van Royen, Y. N. Pal'yanov, *Journal of Physics-Condensed Matter* **14**, 10953 (2002).
38. J. C. Anderson, K. D. Leaver, P. Leevers, R. D. Rawlings, *Materials Science for Engineers*. (Nelson Thornes Ltd, ed. 5, 2003).
39. W. Kaiser, W. L. Bond, *Physical Review* **115**, 857 (1959).
40. S. Prawer, I. Rosenblum, J. O. Orwa, J. Adler, *Chemical Physics Letters* **390**, 458 (2004).
41. K. Iakoubovskii, A. Stesmans, *Journal of Physics-Condensed Matter* **14**, R467 (2002).
42. I. N. Kupriyanov *et al.*, *Diamond and Related Materials* **17**, 1203 (2008).
43. V. G. Vins, E. V. Pestryakov, *Diamond and Related Materials* **15**, 569 (2006).
44. N. Fujita, R. Jones, S. Oberg, P. R. Briddon, *Diamond and Related Materials* **17**, 123 (2008).
45. M. P. Gaukroger *et al.*, *Diamond and Related Materials* **17**, 262 (2008).
46. M. Benabdesselam *et al.*, *Radiation Protection Dosimetry* **120**, 87 (2006).
47. B. Marczewska *et al.*, *Diamond and Related Materials* **16**, 191 (2007).

48. F. P. Bundy, H. T. Hall, H. M. Strong, R. H. Wentorf, *Nature* **176**, 51 (1955).
49. Z. J. Yang *et al.*, *Chinese Science Bulletin* **53**, 137 (2008).
50. H. Kanda, *Brazilian Journal of Physics* **30**, 482 (2000).
51. "Synthesis of Diamond Using Chemical Vapur Deposition" (Element Six).
52. G. W. Tyndall, N. P. Hacker, *Chemistry of Materials* **6**, 1982 (1994).
53. C. D. O. Pickard, T. J. Davis, W. N. Wang, J. W. Steeds, *Diamond and Related Materials* **7**, 238 (1998).
54. S. Prawer, K. W. Nugent, P. S. Weiser, *Applied Physics Letters* **65**, 2248 (1994).
55. B. E. Williams, J. T. Glass, *Journal of Materials Research* **4**, 373 (1989).
56. H. Kozak *et al.*, *Diamond and Related Materials* **18**, 722 (2009).
57. C. Descamps *et al.*, *Diamond and Related Materials* **15**, 833 (2006).
58. J. H. Kaneko *et al.*, *Diamond and Related Materials* **14**, 2027 (2005).
59. "Hope for more precise Proton Therapy for Eye Cancer sufferers" (Element Six).
60. C. I. Smith, M. C. Cuquerella, D. S. Martin, P. Weightman, J. E. Butler, paper presented at the The 58th Diamond Conference, Warwick, 2007.
61. S. Stoneham, *Physics* **2**, 34 (2009).
62. P. Kok, W. Lovett, in *Nature*. (Nature Publishing Group, Nature News, 2006), vol. 444, pp. 49.
63. S. T. Nakagawa *et al.*, *Nuclear Instruments & Methods in Physics B* **267**, 1226 (2009).
64. D. Fisher, *Lithos* **112**, 619 (2009).
65. R. Barnes, U. Bangert, P. Martineau, *Physica Status Solidi a-Applications and Materials Science* **203**, 3081 (2006).
66. V. Avalos, S. Dannefaer, *Physica B-Condensed Matter* **340**, 76 (2003).
67. B. Willems, P. M. Martineau, D. Fisher, J. Van Royen, G. Van Tendeloo, *Physica Status Solidi a-Applications and Materials Science* **203**, 3076 (2006).
68. D. Howell *et al.*, paper presented at the The 60th Diamond Conference, Warwick, 2009.
69. R. Barnes, U. Bangert, A. Scott, *Physica Status Solidi a-Applications and Materials Science* **204**, 3065 (2007).
70. R. Jones, *Diamond and Related Materials* **18**, 820 (2009).
71. L. S. Hounsome *et al.*, *Physical Review B* **73**, (2006).

72. N. Fujita, R. Jones, S. Oberg, P. R. Briddon, *Diamond and Related Materials* **18**, 843 (2009).
73. A. T. Collins, H. Kanda, H. Kitawaki, *Diamond and Related Materials* **9**, 113 (2000).
74. J. M. Maki, F. Tuomisto, C. J. Kelly, D. Fisher, P. M. Martineau, *Journal of Physics-Condensed Matter* **21**, 364216 (2009).
75. U. Bangert, R. Barnes, M. H. Gass, A. L. Bleloch, I. S. Godfrey, *Journal of Physics-Condensed Matter* **21**, 364208 (2009).
76. F. Tuomisto, J. M. Maki, paper presented at the The 60th Diamond Conference, Warwick, 2009.
77. K. Ueda, M. Kasu, A. Tallaire, T. Makimoto, *Diamond and Related Materials* **15**, 1789 (2006).
78. J. P. Goss, P. R. Briddon, *Physical Review B* **73**, (2006).
79. A. P. Yelisseyev, J. W. Steeds, Y. V. Babich, B. N. Feigelson, *Diamond and Related Materials* **15**, 1886 (2006).
80. U. Bangert *et al.*, *Philosophical Magazine* **86**, 4757 (2006).

Chapter

2

2.0 Synchrotron Radiation Facilities

2.1 Introduction

Presented in this chapter is an explanation and description of a typical Synchrotron Radiation Source facility. A brief overview of what it entails, its concepts and components are discussed, as well as the key features that make it a powerful probing tool for the analysis of materials. Its high penetrating depth for uses in applied experimental techniques for the provision of obtaining profiles, analysis of local chemical bonding and the physical structural nature in materials of interest, is also considered.

2.2 What is a Synchrotron?

Over the years the synchrotron has become a significant and powerful research tool for a wide range of applications. It is used as a structural probe by a myriad of scientific researchers such as, physicists, chemists, biologists and geologists, as well as engineers. The synchrotron it is seen by all as an invaluable research asset for the provision of informative studies on surfaces, bulk materials, crystals and viruses as well as for the spectroscopic analysis of solids, liquids and gases (*1*).

A desirable feature that makes synchrotron radiation so attractive for different types of experimental applications is that synchrotrons provide a wide range of photon

energies which are continuous from the infra red (IR) region up to high energy x-rays with the addition of being many orders-of-magnitude more intense than conventional light sources as well as the provision of many wavelengths not available from other sources (*2, 3*). A precise time structure – relative to the radiofrequency of the accelerator system (more details on this later in this chapter) is also a key factor and characteristic of an individual synchrotron source (*3*). Synchrotrons also provide a tightly collimated and narrow beam of high intensity even after monochromatization along with a divergence that is smaller than some laser sources – this is of the utmost importance for experiments that require high resolution (*2*). Another desirable feature is its high degree of polarization although this significant property was not utilized in the gathering of data for the purpose of this thesis and research. It is an excellent means of identifying molecular orientations of molecules bound to surfaces in samples such as the angular dependence of the Nitrogen K-edge NEXAFS for SnPc on S:GaAs for example (*4*).

Generally, important properties relative to Synchrotron radiation are, high intensity, broad spectral range, high polarization, pulsed time structure and natural collimation. In addition, synchrotron radiation produced by storage rings offer, high-vacuum environment, small source spot size as well as stability (*5*). Any one of these properties would make synchrotron radiation an important experimental tool, but the combination of all of them makes it a unique and completely extraordinary source.

2.3 History

The development of the Synchrotron was seen as a landmark step in the structural study of materials. Results of old experimental techniques could now be re-visited due to the provision of much better signals and higher incident intensities produced by synchrotron radiation. These techniques as a result have become more powerful, and in turn, phenomena once considered to be quite peculiar have now become routine techniques (*6*).

Synchrotrons have evolved from the first circular electron storage rings called cyclotrons built by Ernest Orlando in 1932 (*1*). A conscious disregard for Health and Safety during research on radiation was one of the key factors in the birth of

Synchrotron radiation (*7*). A 70MeV synchrotron was built at the General Electric Laboratories by Herbert Pollock *et al*. which had a 29.2cm equilibrium orbit radius (*8*). A "very quick glimpse" by Floyd Haber (Pollock's assistant at the General Electric Research Laboratory) with the aid of a mirror around the corner of the radiation shield on the 24th of April 1947, was noted historically as the first visual observation of man-made synchrotron radiation (*7, 9*).

2.3.1 Daresbury Laboratories

In 1964 the Daresbury Laboratory was created to house NINA (figure 2-1), a 6 GeV synchrotron accelerator built for the study of particle physics. Synchrotron radiation is emitted as a result of high energy electrons being accelerated as they travel through a magnetic field. A substantial amount of energy was lost as the bending magnets deflected the beams of charged particles in synchrotron accelerators and, initially, synchrotron radiation was seen as a nuisance to the high energy accelerator designers. When NINA closed in 1977, plans had already been set to build a Synchrotron Radiation Source (SRS) as a result of experiments carried out on NINA prior to 1977 (*3, 6*). The Second generation light sources were developed in the 60s and 70s with electron rings specifically designed for the emission of synchrotron radiation. Experiments began at the SRS facility in 1981 (*10*).

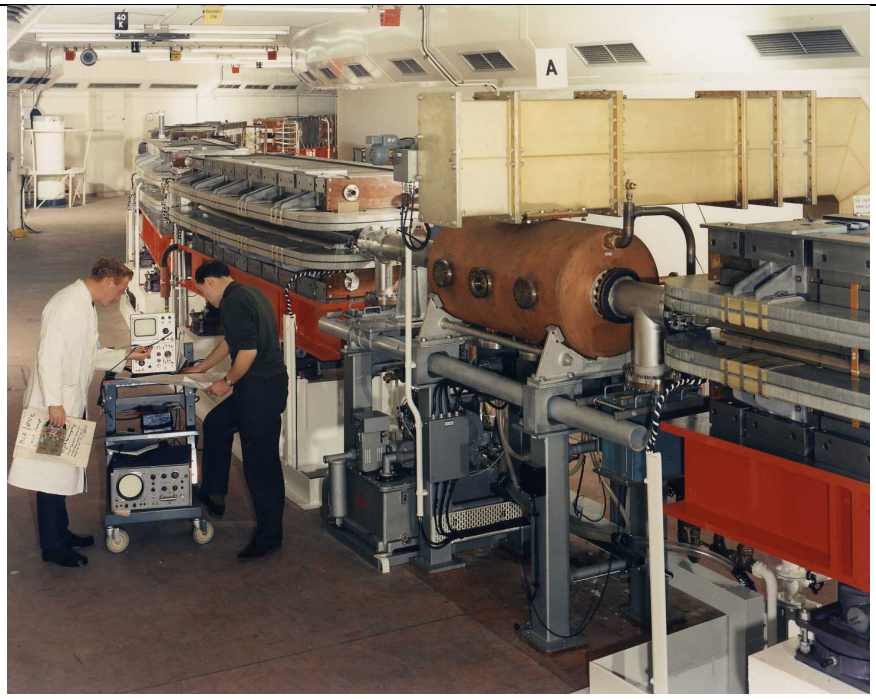

Figure 2-1: Photograph of NINA, the 6GeV synchrotron accelerator. Reproduced from (11)

After a contribution of 2 million hours of science over a 28 year period the SRS (figure 2-2) was decommissioned in August '08. It was the World's first centre dedicated to the production of synchrotron radiation in the X-ray region (*1*). The SRS at Daresbury was the first second-generation light source to produce x-rays, with its operation solely for the provision of synchrotron radiation for multiple simultaneous user experiments. The Daresbury Synchrotron since the first publications in 1981 (*12, 13*) has provided many advances in technology and has influenced world leading research such as the large magnetic memory used in ipods (*14*).

The SRS has six insertion devices (of which will be introduced later) comprising of, two X-ray (high field superconducting) wigglers (5T and 6T wiggler magnets with characteristic wavelengths of 0.093nm and 0.078nm respectively), the maximum power output from these magnets is 170 and 200mW/(mA mrad) respectively (*1*). It also has a VUV-SXR 0.33T planar undulator magnet and three multipole wigglers (two 2.0T and one 2.4T multipole wiggler magnets). The storage ring serves experimental stations which are situated tangentially to the main storage ring. In 1991 there were 28 experimental stations each with their own optical system for beam focus and characteristic energy (*3, 15*).

Figure 2-2: Photograph of the SRS prior to it's build showing the locations of the Booster Ring and the Main Storage Ring, photograph taken from (11).

2.4 How do Synchrotrons work?

Electrons are firstly created by a hot filament and as a result photons are created from these electrons travelling around within a storage ring which, as they change direction, experience acceleration. The electrons pass through a linear accelerator (linac) and experience high energy radio waves that create a pulsed electron beam. For example, at the SRS at Daresbury the electrons are ejected from the linear accelerator (linac) with an energy of 12MeV. In the linac they experience an acceleration that accelerates them close to the speed of light '*c*' when exiting the linac and on to the Booster Ring which increases their energy to around 600MeV. The electrons are then fed in 'pulses' into the main storage ring of which has a 96m circumference and is under high vacuum, typically ~10^{-11} Torr.

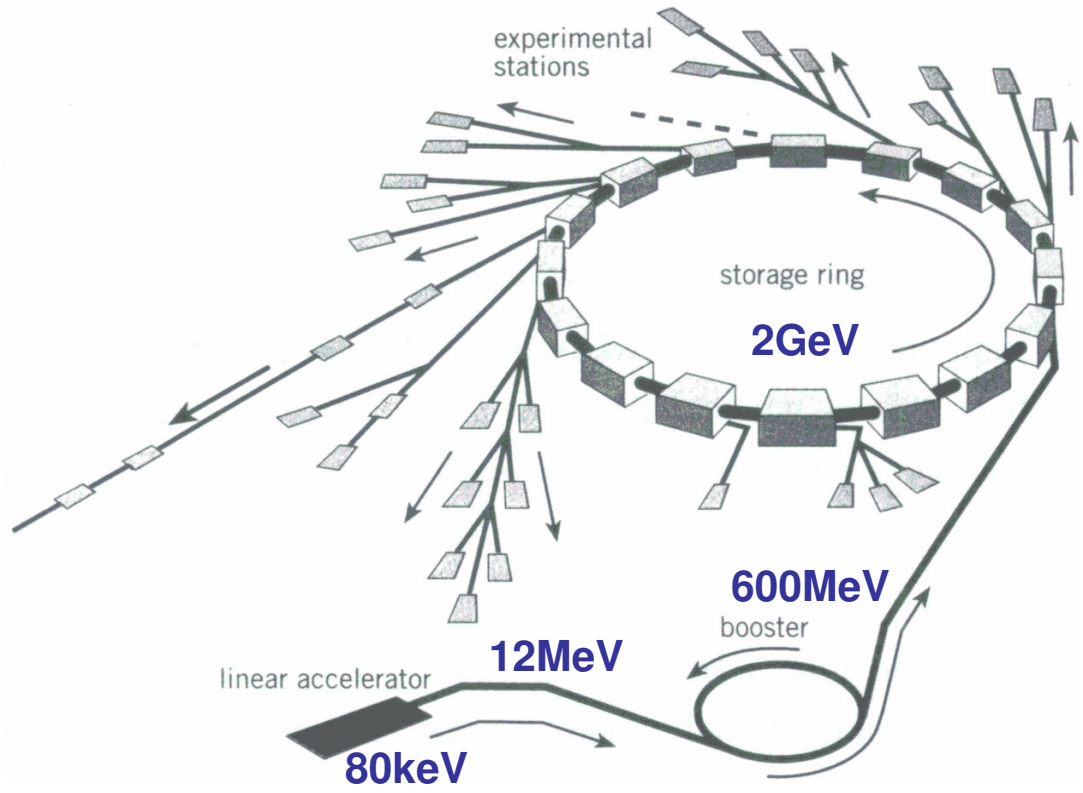

Figure 2-3: Schematic diagram of Daresbury Synchrotron taken from (16) showing the main sections of the synchrotron facility.

The storage ring generally consists of a tube under high vacuum where electrons are free to circulate around. The ring itself is not in fact perfectly circular. It is more of a polygon shape with straight linear sections followed by a corner and then another straight linear section and so forth. At these corners bending magnets are present which provide a magnetic turning field that bend the synchrotron beam and turn it towards the next straight section, therefore forcing it to keep on going around the ring without colliding into the sides. They experience acceleration as they change direction and therefore radiate each time they come to a bend (figure 2-4).

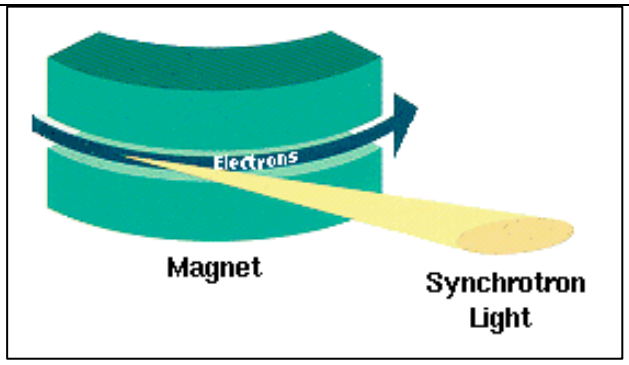

Figure 2-4: Electrons radiate as they come to a bend. Taken from (17)

At the straight sections there are periodic magnetic structures called undulators or wigglers (depending how strong the field is – see section on Insertion Devices 2.5) to keep the electrons on track through the straight sections.

Whenever a charged particle is accelerated, Electromagnetic Radiation is produced and the deflection of a beam is a form of acceleration. Due to the fact that the beam is made to circulate a ring through the guidance of bending magnets, the beam experiences energy losses and slows down. As the high energy particles hit the curved parts of the storage ring, a proportion of their energy is lost as synchrotron radiation, which is as a result emitted tangentially to the curved sections as mentioned earlier. As a means of overcoming the energy loss that occur at these bends, a radio frequency (RF) cavity is present on the main ring which supplies an occasional "kick" to the particles, therefore increasing their Kinetic Energy to around 2GeV (see figure 2-3 for a schematic of the energies at the relative sections of the SRS). The RF cavities are not operational when high energy electrons pass through, but are active when less energetic electrons (due to radiative emission) enter the cavity. This as a result causes the electrons to travel around the storage ring in bunches and therefore all remain high in energy. The storage ring current is in the 150mA to 300mA range and the maximum number of electron bunches are 160 with an electron bunch width (FWHM) of 180ps. Figure 2-5 show a typical SRS beam profile taken in the summer of 2008 during a particular beamtime. The electron bunches can clearly be seen.

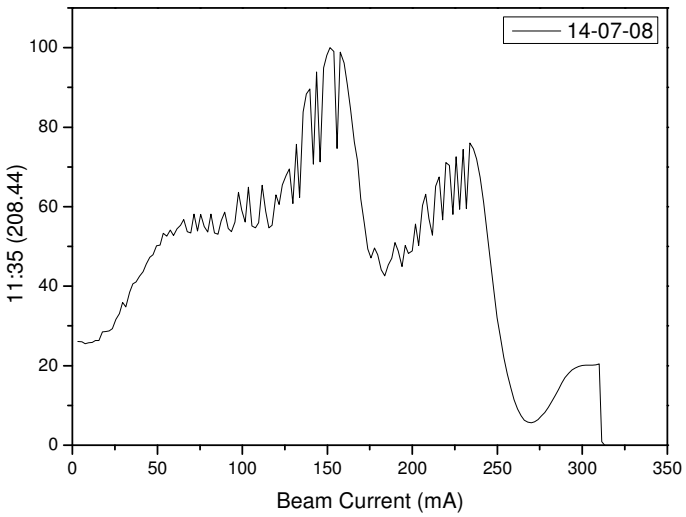

Figure 2-5: A typical Synchrotron beam profile taken on the 14/07/08 clearly showing the electron multi bunches.

The electrons circulate the main ring (figure 2-7) with a circulating frequency of 500MHz. At low energies the electron beam travels in the shape of a toroid and as the particles approach the speed of light the process becomes relativistic and the radiation is emitted in a forward direction such as a Car headlight (*6*) (figure 2-6).

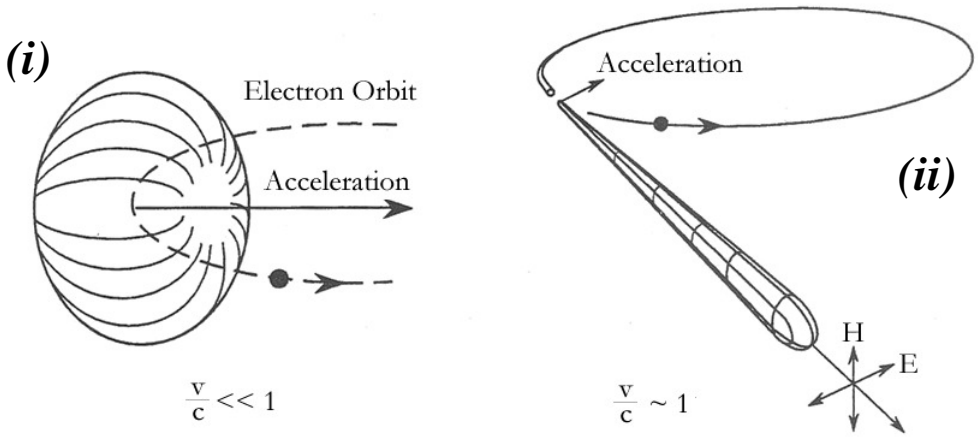

Figure 2-6: Above is a schematic of the Electron orbit at two significant cases. In (i) the electron travels at a velocity 'v' where 'c' is the speed of light. This is the non-relativistic case, whereby the electrons radiate in a dipole pattern. In case (ii) 'v' is very close to the speed of light as shown by the equation. At relativistic energies such as these the pattern becomes sharply peaked in the direction of motion. H and E are the magnetic and electric component vectors of the electromagnetic radiation (reproduced from (18)).

The electrons have a current decay lifetime when stored in the main ring of around 20-30 hours before the addition of electrons is required. Usually the SRS would be used on a daily basis, 24 hours a day and 7 days a week which consisted of one re-fill every 24 hours. For re-fill, dumping of the beam is required and subsequently refilling occurs which takes around 1 to 2 hours. Significant shielding is present that allows users in the experimental areas to work without the necessity to wear dosimeter badges (*15*). The requirement of re-filling has been overcome by 3rd generation synchrotrons such as the Diamond Light Source in Oxford, UK. A top-up system is in operation whereby electrons are continually injected into the storage ring for a continuous beam and therefore uninterrupted experiments.

Figure 2-7: Photograph taken at Daresbury Laboratories, Warrington. Direction of beam is shown (yellow arrow) relative to the storage ring (Main ring circumference, 96m).

2.5 Insertion Devices

Insertion devices are magnetic devices that are in place usually on the main storage ring. In some instances bending magnets have been replaced by two devices to be used as an alternative. These are undulators and wigglers. They deflect the beam in one direction and then the other and are designed to produce synchrotron radiation of specific characteristics and control the electron beam path within the synchrotron.

2.5.1 Undulators

Undulators are an insertion device typically used on synchrotron beamlines for the provision of changing the electrons' path. This is done due to the arrangement of a closely packed array of vertical magnets of alternating polarity and as a result causes the electrons to oscillate as they travel through. The angle of each bend in each pole is of the order of mc^2/E so that the small angular divergence due to the emission pattern of synchrotron radiation is not significantly increased, as a result the brightness of the synchrotron radiation is conserved in the horizontal and vertical planes (*19*). Due to the path changing induced by these types of insertion devices synchrotron radiation is as a result emitted. The electrons emit cones of radiation at each bend along their path which overlap to create a highly collimated beam of radiation.

2.5.2 Wigglers

Wigglers are also a fundamental part of a synchrotron. They are similar to undulators but with the exception that they have a higher magnetic flux and produce a continuous radiation spectrum of higher flux. It also consists of a succession of alternating polarity magnets which bends the electron beam. The magnet is designed so that the deflections to the beam cancel out and as a result no net bending is produced. The radiation's flux and brightness is enhanced by a factor roughly equal to the amount of poles. A more detailed explanation and further information on insertion devices can be found in (*1*) and (*19*). A schematic of an undulator and wiggler radiation envelope can be seen in figure 2-8.

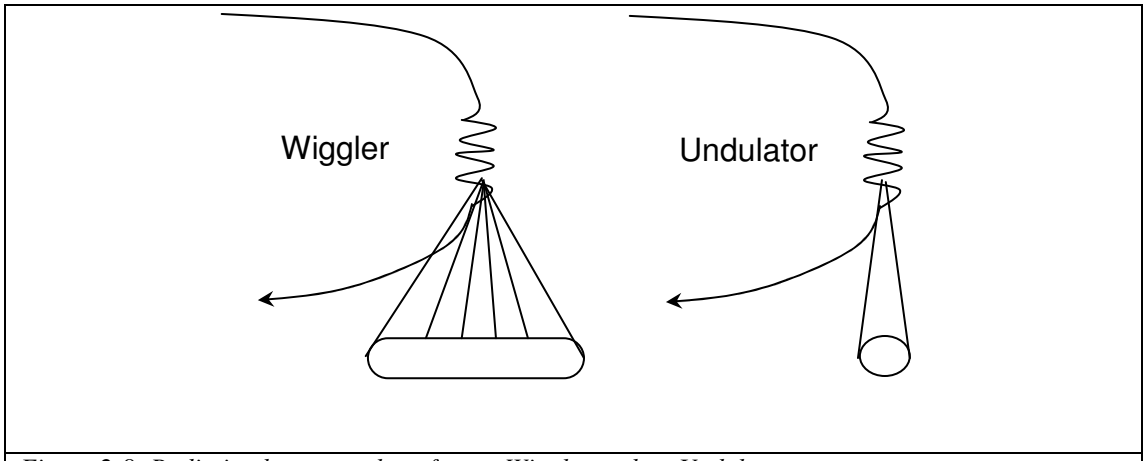

Figure 2-8: Radiation beam envelope from a Wiggler and an Undulator.

2.6 Beamlines

Beamlines are essentially tangential to the main synchrotron ring and transport synchrotron radiation into end stations whereby the synchrotron light can be used for experiments.

2.6.1 Beamline 3.1 at the SRS, Daresbury

Beamline 3.1 with the provision of an energy range of 4-31eV (*20*) was used for the band-gap measurements taken for the type Ia diamond (results shown in chapter 7). It consisted of a vacuum 1m Wadsworth monochromator and the wavelength range of 30nm to 300nm was provided by two interchangeable diffraction gratings (*21*).

2.6.2 MPW6.1 Beamline at the SRS, Daresbury

The tangentially emitted radiation is carried down a beamline into experimental stations such as with the MPW6.1 beamline (figure 2-9) which was predominantly used for all the synchrotron data presented in this thesis. It consisted of a multipole wiggler that allowed 10 times the amount of normal beam flux with revolving powers of up to 4000 over the energy range of 40-450eV (*22*). This beamline was ideal for the probing of the sp^2 and sp^3 bonded-carbon region as well as the Carbon K-edge that all lie within the 280-320eV region.

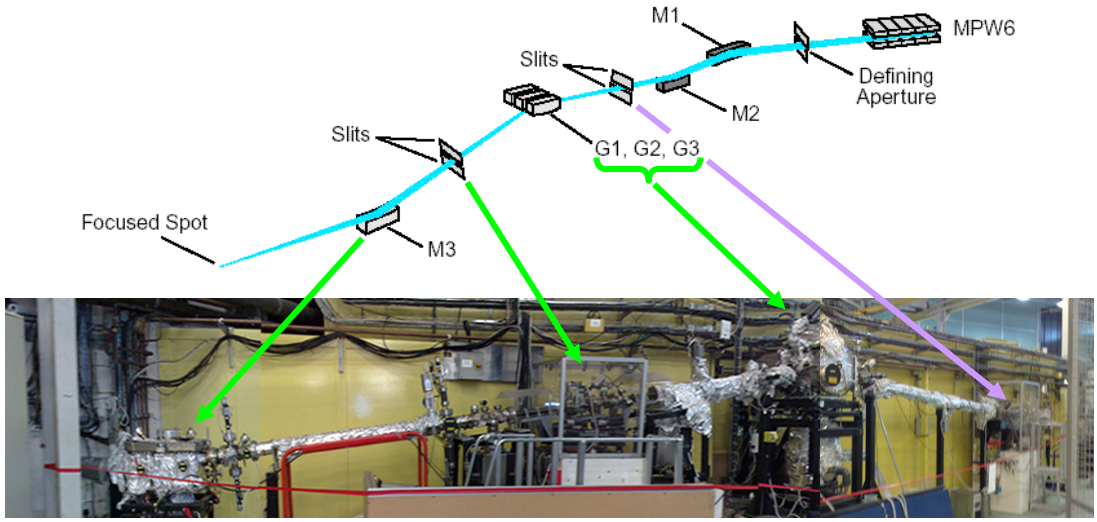

Figure 2-9: A schematic (taken from (23)) of the MPW6.1 beamline at the SRS along with a photograph of most of the schematic components. The end-station itself is to the left with the synchrotron main storage ring to the right.

All of the XEOL, OD-XAS spectra and images have been gathered using the CLASSIX instrumentation system on beamline MPW6.1 at the SRS Daresbury Laboratories. The focussed spot shown in the schematic in figure 2-9 is located within the experimental chamber of CLASSIX on the sample itself. The need for a synchrotron source was crucial for these types of experiments due to their powerful intense radiation that is easily tuneable to the required energies.

The MPW6.1 beamline optical components consists of three mirrors, a spherical grating Monochromator inclusive of three interchangeable gratings (table 2-1) (*24*) and two slits – entrance and exit.

Table 2-1 (reproduced from (*24*)):

Gratings	Energy range (nominal)	Surface Coating	Substrate Material
Grating 1 (G1) (LEG)	40-80eV	Gold (30nm)	Fused Silica
Grating 2 (G2) (MEG)	80-160eV	Gold (30nm)	Fused Silica
Grating 3 (G3) (HEG)	160-340eV	Nickel (30nm)	Fused Silica

Low Energy Grating (LEG), Medium Energy Grating (MEG), High Energy Grating (HEG)

Mirrors	Material	Coating	Profile
Mirror 1 (M1)	Silicon, Water Cooled	Gold (30nm)	Spherical (radius, 120m)
Mirror 2 (M2)	Silicon, Water Cooled	Gold (30nm)	Spherical (radius, 160m)
Mirror 3 (M3)	Fused Silica	Gold (30nm)	Toroidal (tan. Rad. 51m)

The purpose of the mirrors are to focus the beam spot. Mirror 1 (M1) is a horizontal deflecting and focus mirror which removes half the radiation fan for use on the beamline and the other half for beamline 6.2. The Mirror 2 (M2) function is similar but it vertically deflects and focuses the beam onto the entrance slits of the monochromator, whilst Mirror 3 (M3) both focuses vertically and horizontally along with vertical deflection and focussing monochromatic light on the sample position (*24*).

2.7 Monochromators

Monochromators are typically found on a synchrotron beamline along with curved mirrors which are often used to focus the synchrotron light into a focussed beam. The monochromator is used to select the photon energy required for experimentation. It is essentially a diffraction grating and for its use with x-rays it is designed for the purpose of reflecting the incident radiation from its surface. Any incident waves that are in phase will interfere constructively and any out of phase will interfere destructively. A slit is present after the reflection which blocks all unwanted photon energies. For further detailed information on monochromators, refer to (*19, 25*).

2.8 Summary

A brief description of how Synchrotron Sources operate has been introduced and forms a foundation to the rest of the thesis whereby the use of Synchrotron Source has been vital for the acquirement of data. This chapter leads directly to the next, whereby the Instrumentation Systems used at both Synchrotron and Laboratory are introduced.

2.9 References

1. P. J. Duke, *Synchrotron Radiation Production and Properties*. (Oxford University Press, 2000).
2. M. L. Perlman, E. M. Rowe, R. E. Watson, *Physics Today* **27**, 30 (1974).
3. W. Gelletly, *Measurement Science & Technology* **3**, 239 (1992).
4. Alex Raymond Vearey-Roberts, The University of Wales, Aberystwyth (2004).
5. H. Winick, S. Doniach, *Synchrotron Radiation Research*. (Plenum Press, 1980).
6. S.S. Augustithis, *Synchrotron Radiation Applications in Mineralogy and Petrology*. (Theophrastus Publications, 1988).
7. G. C. Baldwin, *Physics Today* **29**, 9 (1975).
8. H. C. Pollock, R. V. Langmuir, F. R. Elder, J. P. Blewett, A. M. Gurewitsch, *Physical Review* **70**, 798 (1946).
9. J. P. Blewett, *Journal of Synchrotron Radiation* **5**, 135 (1998).
10. Arthur L. Robinson. (http://xdb.lbl.gov/Section2?Sec_2-2.html).
11. M. W. Poole, *75 years of Accelerator Innovation in the UK (a personal viewpoint of highlights) presentation*. (2007).
12. G. N. Greaves, P. J. Durham, G. Diakun, P. Quinn, *Nature* **294**, 139 (1981).
13. G. N. Greaves, A. Fontaine, P. Lagarde, D. Raoux, S. J. Gurman, *Nature* **293**, 611 (1981).
14. http://www.srs.ac.uk/srs/. (2010).
15. Daresbury SRS user guide & Information. (http://www.srs.dl.ac.uk/ulo/User_Guide/the_srs.htm, 2006).
16. A. R. Vearey-Roberts, Prifysgol Aberystwyth University (2004).
17. M. W. Poole, *75 Years of Accelerator Innovation in the UK*, (Presentation 2007).
18. Owain Rhys Roberts, The University of Wales, Aberystwyth (2009).
19. *Synchrotron Radiation Sources*. H. Winick, Ed., (World Scientific, 1994).
20. C. R. Howle, S. Ali, R. P. Tuckett, D. A. Shaw, J. B. West, *Nuclear Instruments and Methods in Physics Research Section B: Beam Interactions with Materials and Atoms* **237**, 656 (2005).
21. SRS Daresbury. (http://www.srs.ac.uk/srs/stations/station3.1.htm, 2003).

22. M. Bowler *et al.*, *Surface Review and Letters* **9**, 577 (2002).
23. The Extreme Ultra-Violet Spectroscopy Group. (http://srs.dl.ac.uk/XUV-VUV/science/mpw6.1/layout.html, 2002).
24. The Extreme Ultra-Violet Spectroscopy Group. (http://srs.dl.ac.uk/XUV-VUV/science/mpw6.1/details.html, 2002).
25. H. Winick, S. Doniach, *Synchrotron Radiation Research*. (Plenum Press, New York, 1980).

Chapter

3

3.0 Instrumentation

3.1 Introduction

Presented here is a detailed overview of the End Station apparatus and equipment that have been used at the SRS end station on (predominantly for the purpose of this thesis) beamline MPW6.1.

Laboratory based techniques used in the characterization of the diamond samples are also introduced towards the end of this chapter.

3.2 Mobile Luminescence End-Station (MoLES)

The **Mo**bile **L**uminescence **E**nd-**S**tation (MoLES) (*1*) was developed for use on multiple beamlines at the SRS, Daresbury. It is a dedicated instrumentation system, built in 2003 for the sole provision of volume integrated luminescence studies. It has been extensively utilized for many experimental applications such as monitoring corrosion layers on copper, Band-gap measurements on Boron Nitride (BN), luminescence efficiencies of wide band-gap materials and probing electron transfer processes on YPO4:Ce, Sm, as well as Diamond studies (*2-8*).

The MoLES spectrometer provides the user with the detection of luminescence light from solid-state samples in the 190 – ~1000nm emission range (1.2–6.5eV) (930nm

GaAs photocathode tube for detection over extended photon ranges or a 860nm bialkali tube (Electron Tubes, 9111WB) used for high-sensitivity broad-band luminescence detection (*1*)). A self-contained system such as MoLES consists of a compact ultra-high vacuum chamber with an internal diameter of 13cm coupled to a closed-cycle cryogenic refrigeration unit (Gifford McMahon with a cooling power of 0.4W at 8K and 2.5W at 20K) for the purpose of sample cooling at temperatures in the ~8K – 300K range.

Techniques such as X-ray Excited Optical Luminescence (XEOL), Photoluminescence (PL), Thermoluminescence (TL) and Optically Detected X-ray Absorption Spectroscopy (OD-XAS) can be utilised with this flexible system (*6*), as was indeed done for the provision of data for the purpose of this thesis.

Eight ports are available for optical access and the schematic diagram in figure 3-1 shows a typical set-up for the experiments carried out and will be mentioned in more detail later in the thesis. Coupled to the chamber is a dedicated turbo pumping system for the provision of pressures of typically 10^{-8} torr at room temperature and $<10^{-10}$ torr at 10K. The Ultra high vacuum (UHV) (MoLES) chamber can be directly mounted onto a soft x-ray synchrotron beamline. Higher (harder) x-ray energies requires an Aluminised Mylar window to be mounted, so that the MoLES chamber can be under UHV but without the necessity of the hard x-rays due to being able to travel through air.

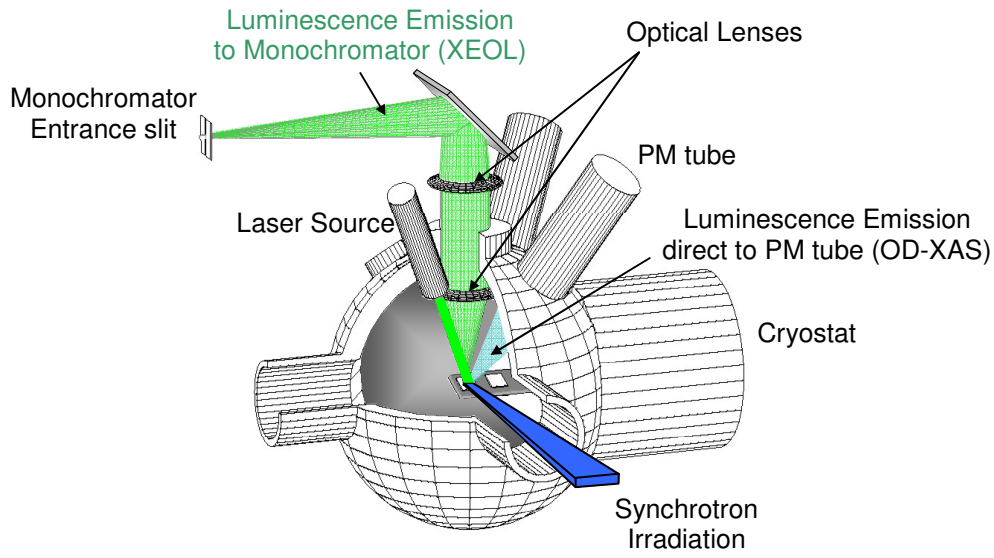

Figure 3-1: Schematic of MoLES End Chamber reproduced and adapted from (1).

MoLES consists of two photomultiplier detectors (Hamamatsu) (figure 3-2) that offer optical detection in the 190nm – 1000nm range with a maximum resolution of 0.01nm and a minimum resolution of 6nm with 2mm slits. The detectors are mounted externally, the first mounted directly on an aperture window and therefore collects all of the luminescence emission (TLY) for the purpose of measurements such as Optically-Detected X-ray Absorption Spectroscopy (OD-XAS). The second is fitted to a monochromator (Triax Jobin-Yvon) exit aperture whereby the luminescence light generated by incident x-rays from a synchrotron or x-ray source is measured through the monochromator and gathered at the second PMT, this type of measurement is X-ray Excited Optical Luminescence (XEOL) or if a laser source is used instead of a synchrotron or x-ray source then Photoluminescence (PL) can be measured.

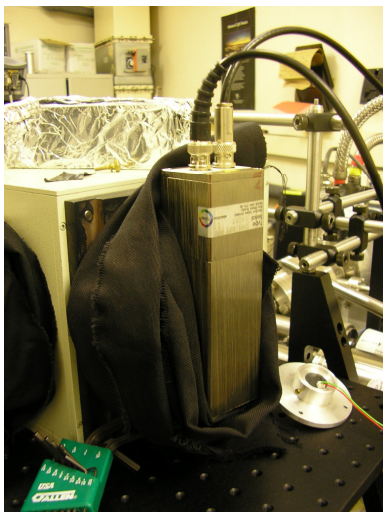

Figure 3-2: PMT mounted to the monochromator exit aperture for XEOL/PL measurements.

3.2.1 Low Temperature Measurements

The sample cooling involves a water cooled liquid helium cryostat that connects to a copper cold finger where the samples are mounted to a sample holder for the provision of sample cooling down to ~10K (figure 3-3). A heater is also attached for the purpose of temperature ramping (i.e. 10 – 300K with a ramp rate of 10K/min) or temperature control i.e. continuously maintained at 150K where the temperature regulator switches on the heater as and when is it needed (figure 3-4). The sample cold finger can be moved in and out of the beam for sample selection and therefore analysis, and around 3-4 samples can be mounted on the sample holder at any one time (dependent on sample size). Low temperature measurements are essential for luminescence studies due to the non-radiative emission being directly dependent on temperature (figure 3-5).

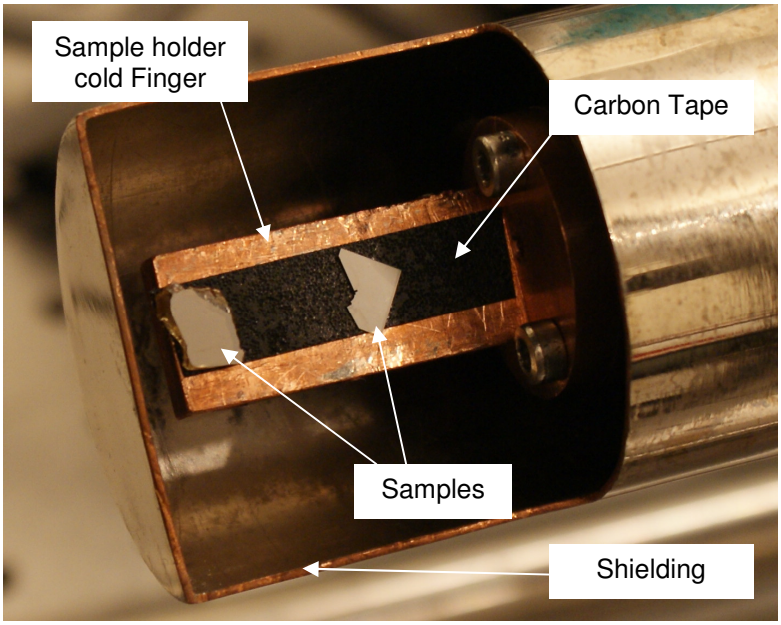

Figure 3-3: Two diamond samples mounted on the copper cold finger (MoLES spectrometer) with carbon tape.

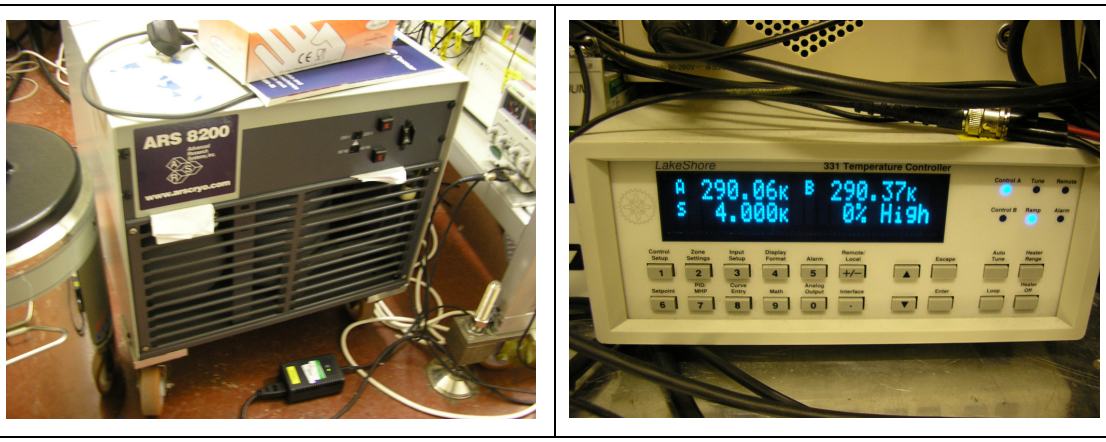

Figure 3-4: Closed Cycle Liquid Helium Cryostat (left) and temperature regulator/controller (right).

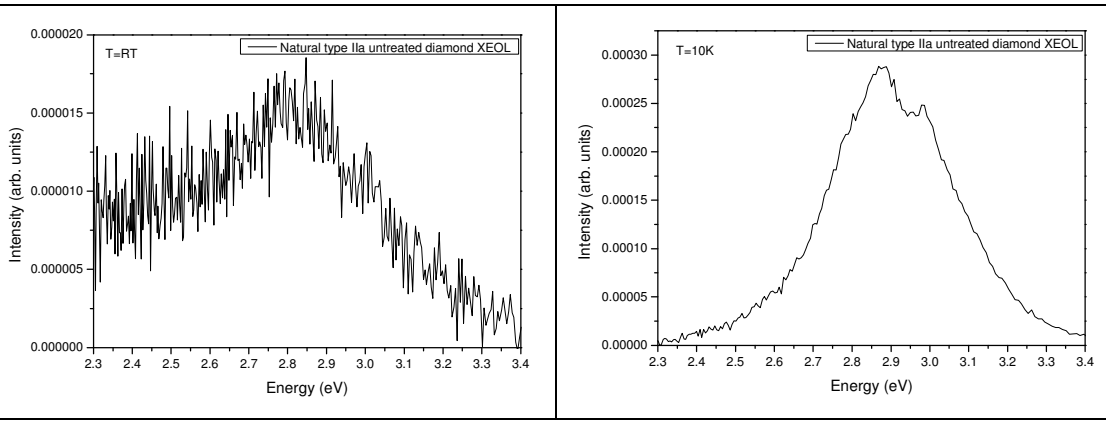

Figure 3-5: XEOL spectra for the untreated type IIa natural sample at room temperature (RT) (left) and at 10K (right) showing the significant difference in the quality of the luminescence spectra at different temperatures.

3.2.2 Monochromator

MoLES consists of a 190 Triax Jobin-Yvon (figure 3-6) with a spectral range of 200-1000nm in which it gathers the luminescence emission emitted from luminescent samples when irradiated through its entrance aperture and collected by the PM tube mounted to the exit aperture. There are three Bragg type diffraction gratings within the monochromator, each with its own optimum response for the particular wavelength range selected by the user. The resolution of the monochromator is dependent on its entrance slit width, giving 3nm resolution per 1mm slit width. These slit widths can be adjusted for the optimum luminescence signal and resolution as shown in figure 3-7.

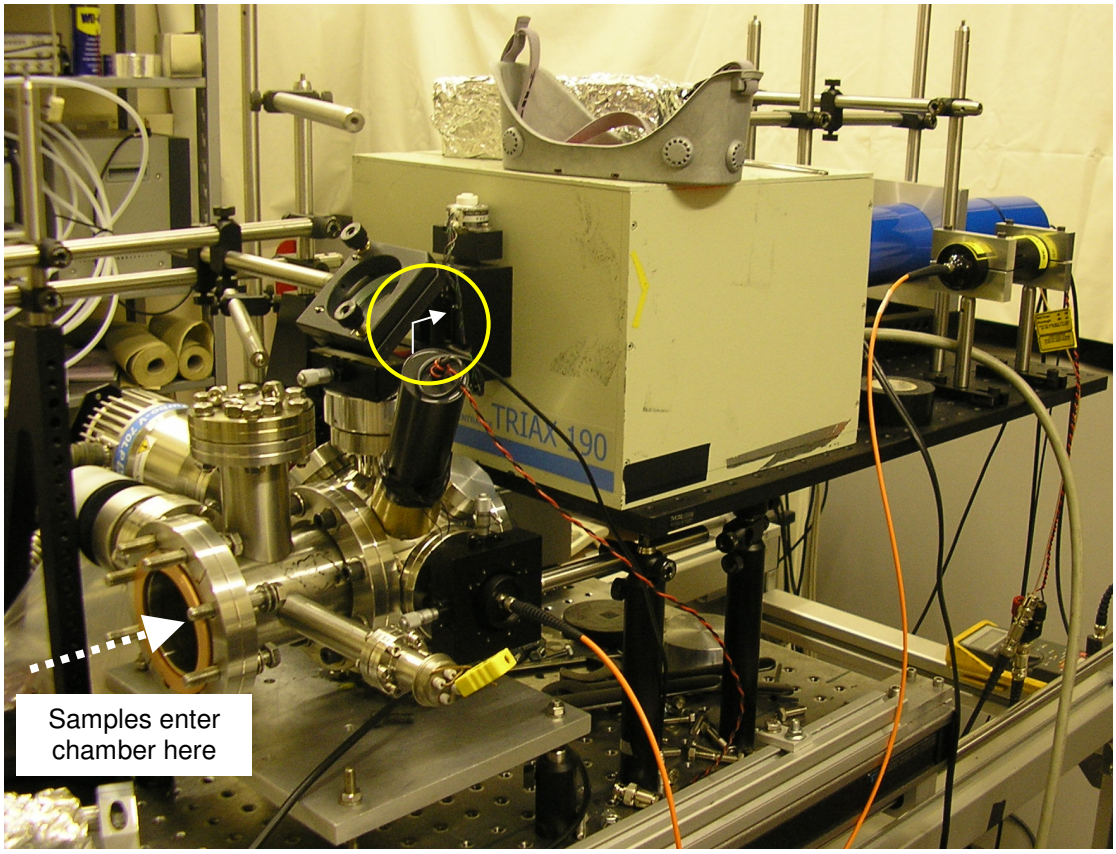

Figure 3-6: The monochromator on the MoLES spectrometer. White arrow within yellow circle indicates luminescence emission light coming from sample within the chamber and being reflected by the mirror into the monochromator for XEOL/PL measurements. Dashed white arrow indicates where the cryostat arm along with samples enters chamber. NOTE: MoLES spectrometer has casing as a surround to minimize background light – casing has been removed for image purposes.

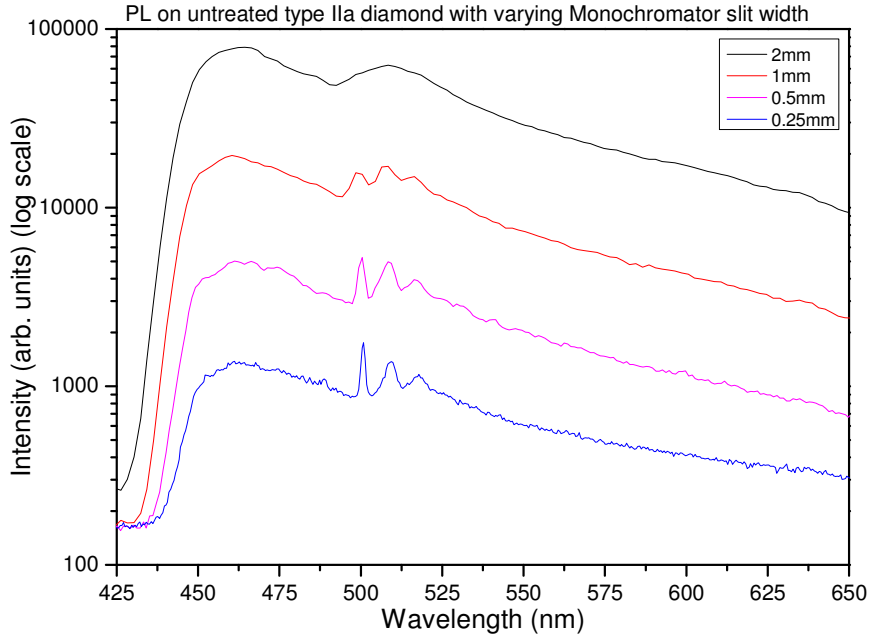

Figure 3-7: Spectra showing how the resolution improves with the narrowing of the slit width, although the intensity decreases. Graph displayed in logarithmic form for clarity.

Figure 3-7 shows how the decrease in slit-width at the monochromator entrance and exit slits enhances the finer structures. Zero Phonon Lines (ZPL) are much more visible and more pronounced, with finer detail being able to be resolved, although with the added detail, a decrease in intensity occurs as a result. Less light enters the monochromator due to decreasing slit-width.

3.2.3 Computer Interface

The MoLES spectrometer can be completely controlled via a computer that can also incorporate the beamline computer in "slave mode" for the incident synchrotron energy control for measurements such as OD-XAS where the incident energy is ramped in certain allocated energy steps designated by the user from i.e. in this study of diamond, 280eV to 320eV at 0.2eV steps. The entrance and exit slit-widths, grating selection, scan parameters and data storage/gathering is also controlled by the computer via the LabVIEW programming interface as shown in figure 3-8.

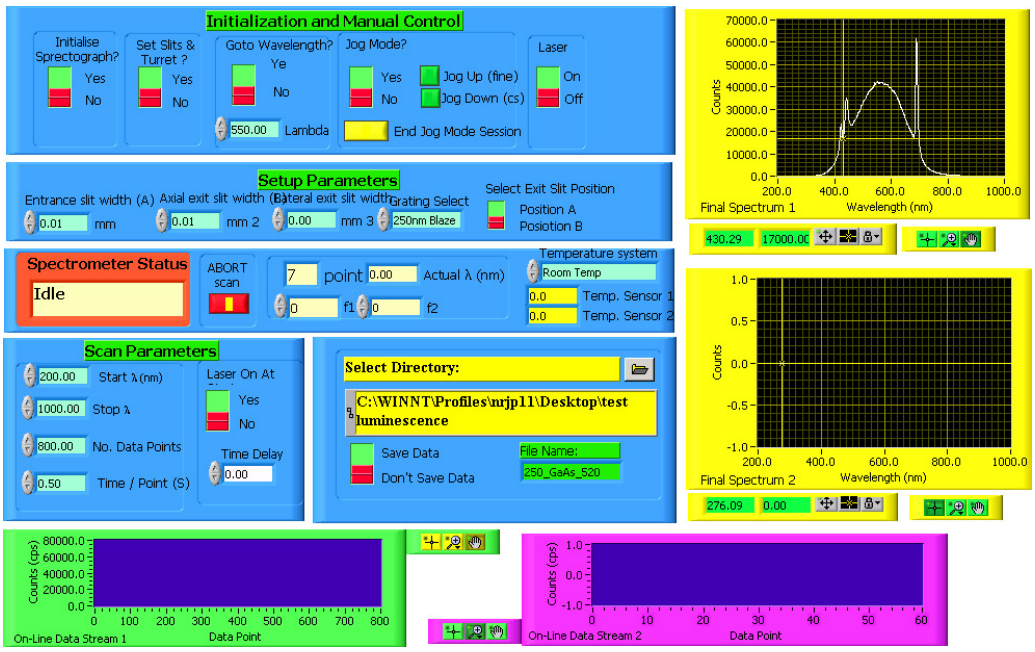

Figure 3-8: MoLES spectrometer computer control LabVIEW interface.

3.2.4 Optical Filters/Lenses

Optical filters are often used to block a certain signal from reaching the PMT. They can be mounted prior to the PMT entrance, i.e. a neutral density filter – if the signal is too strong (therefore saturating the PMT), or prior to the monochromator – to stop any laser light coming through and/or 2nd order laser light.

MoLES is an extremely efficient and powerful instrument for the analysis of uniform and homogeneous samples where the region of analysis upon the sample is not particularly significant. Due to the uniformity of the sample, the signal would be expected to be invariable all over the sample.

For non-homogeneous samples such as banded diamonds the region of analysis is much more significant with regards to the location of the probing, i.e. on a brown band or not. Due to the alternating bands and regions on variegated samples containing different information with regards to the chemical and structural bonding of the sample under study, the CLASSIX spectrometer is therefore crucial in implementing the analysis for these types of samples and is introduced in the next section.

3.3 Chemistry, Luminescence and Structure of Surfaces by micro-imaging X-ray Absorption (CLASSIX)

3.3.1 Introduction

The name CLASSIX is an acronym for **C**hemistry, **L**uminescence **A**nd **S**tructure of **S**urfaces by micro-**I**maging **X**-ray absorption (*9*). It is a mobile spectrometer system specially designed to fit onto a Synchrotron end-station for the purpose of micro-imaging x-ray absorption features of solids through their Luminescence emission. It was developed by Dr Nigel Poolton *et al.* (*9*) at the SRS at Daresbury and is now based at Aberystwyth with the capabilities of taking it to synchrotrons across the world for studies due to its ease of mobility. It has been used previously as a tool to study nanoscience, the optical band-gap of cubic and hexagonal boron nitride (BN), micro-imaging of synchrotron-laser interactions in wide band-gap luminescent materials, as well as other materials including this study of diamond (*3, 5, 10-14*).

The optical detection of the x-ray absorption is gathered by a CCD. A micro-image is therefore obtained and a direct link between x-ray features and the luminescence characteristics of a sample is possible. Due to the pixelated formation of the image (512 x 512 pixels) (see figure 3-9) information is present relative to the luminescence spectra, therefore it is possible to correlate between spectra and the sample probing location i.e. a luminescence spectra is obtained for the very region that is probed – a powerful technique especially for variegated luminescent samples.

From solids' luminescence emission the micro-imaging of their X-ray absorption features is possible with the instrumentation system. Excitation energies in the range of UV to hard X-rays, 4eV to 7keV are useable. Measurements in imaging mode are rapidly developing into a major area of interest coupled with the fact that third generation light sources provide a combination of high flux and small beam sizes.

The CLASSIX spectrometer (*9*) is extremely similar to MoLES, it consists of a cold finger where samples are mounted for the purpose of cooling to temperatures of ~8 – 10K. The cold finger is situated within a UHV-compatible bespoke chamber.

Magnified imaging optics are also present on a computer controlled turn-table for magnification selection by the user. Spectral dispersion elements for the purpose of the luminescence emission analysis are also available as well as a 2-D detector array. The CCD used is an Andor Technology iXon DV887 512 x 512 pixel back-illuminated system with enhanced UV capability. It has the provision of high-sensitivity capable of single photon detection capability when thermoelectrically cooled to 200K in the 200-1000nm spectral range. A computer controls the functioning of the CLASSIX system as well as the beamline energy selection for XAS scanning. The CLASSIX instrumentation system can be directly coupled to synchrotron beamlines for VUV/soft X-ray applications or fitted with aluminised Mylar X-ray windows for deployment on hard X-ray stations or X-ray gun sources, such as the ones that will be introduces in the next part of this chapter that also have been/can be used on the MoLES spectrometer as mentioned previously.

As a means of showing the capabilities of the CLASSIX spectrometer, figure 3-9 provides a typical CCD gathered image on a cubic Boron Nitride (c-BN) sample consisting of 100μm c-BN crystals (*15*).

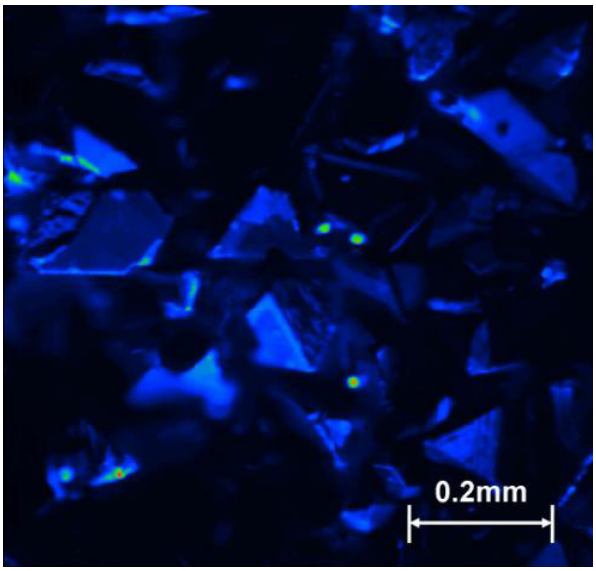

Figure 3-9: Luminescence image taken with the CLASSIX spectrometer at 185eV of 100μm c-BN crystals in total luminescence yield (TLY) (15). A XEOL or OD-XAS spectrum can be obtained anywhere on the CCD pixel image, in either Single, 3x3, 5x5, 7x7, 9x9, 11x11 or 15x15 pixel array.

Figure 3-10 shows a schematic representation of the hardware involved within the CLASSIX spectrometer. Synchrotron light irradiates the sample mounted on the sample holder which is cooled by the cryostat (liquid He) cold finger. The luminescent light that occurs as a result of the irradiation is measured through an objective selected by the user at the beginning of the experiment. CLASSIX has a x2, x10, x50 visible transmitting lenses and a x20 and x80 UV transmitting lenses. The light once passed through the objective goes through a particular filter, again selected by the user for partial luminescence yield (PLY) or through no filter, for total luminescence yield (TLY) measurements. The resultant light is then gathered in the CCD and an image (relative to intensity) (512 x 512 pixel) is generated. Each pixel contains an OD-XAS spectra relative to the sample itself. Table 3-1 provides a summary of the objectives' magnification pixel dimensions used for this research.

Table 3-1:

Magnification Objective	**Pixel Dimension**
x2	8 x 8μm
x10	1.6 x 1.6μm
x20	0.8 x 0.8μm

XEOL measurements can also be made by irradiating with a fixed energy (i.e. ~280eV for diamond). The MoLES spectrometer scans through with the monochromator and XEOL measurements are taken with the PMT. CLASSIX rotates the filter wheel through all filters in the 200 - ~1000nm range (figures 3-13 – 3-16), the CCD gathers the light, thus generating an image along with a XEOL spectrum at each pixel.

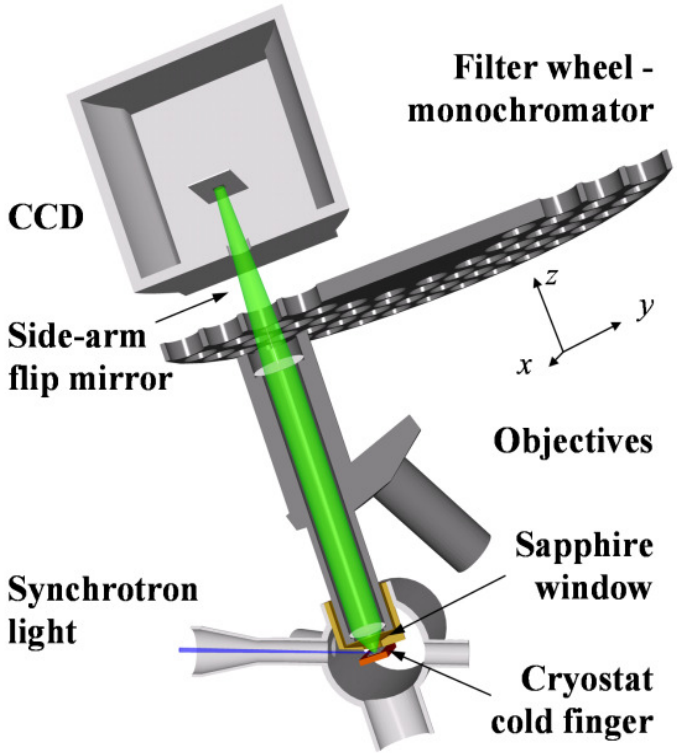

Figure 3-10: Schematic Diagram of the CLASSIX instrumentation system showing the main components. Schematic taken directly from (9).

For XEOL measurements a specific energy is selected that lies below that of the absorption edge of the sample in question. In diamond's case it is around 284.8eV – as previously mentioned, the Carbon K-edge. An energy of 280eV was selected as the intensity is at its highest just before the edge, thus resulting in a high intensity signal – a high luminescence yield. The filter wheel is then rotated, with each filter comprising of a section that lies within the 200-1000nm range. An image is gathered at each filter and therefore obtaining a XEOL image spectra. It is virtually the same as for the MoLES setup – but for MoLES the CCD and filter wheel are not present and a PMT and Monochromator are used instead, therefore limiting to homogeneous samples as previously mentioned.

In OD-XAS measurements, the energy is scanned from (for diamond) in steps of 0.2eV in the 280-320eV range, to cover the absorption edge, π and σ resonance regions, which have been of particular interested during the course of this research.

The CLASSIX spectrometer takes an image at each energy step. Figures 3-11 and 3-12 show the apparatus at the MPW6.1 beamline at the Daresbury Laboratories.

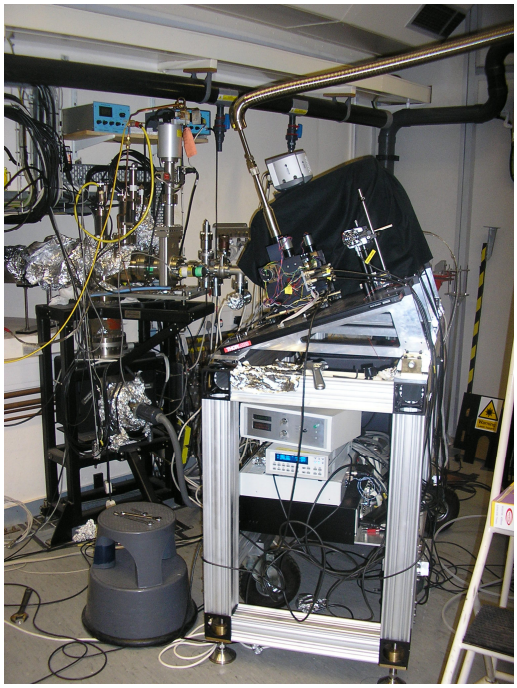

Figure 3-11: CLASSIX spectrometer mounted to synchrotron beamline.

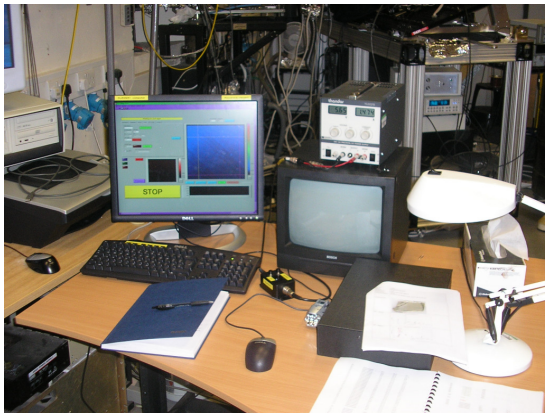

Figure 3-12: Control Computer on synchrotron beamline.

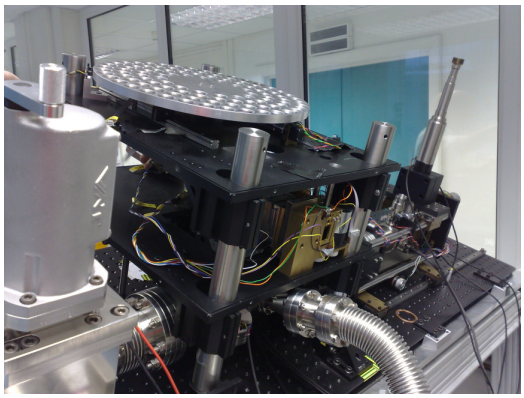

Figure 3-13: CLASSIX spectrometer with casing removed, filter wheel is visible and CCD removed.

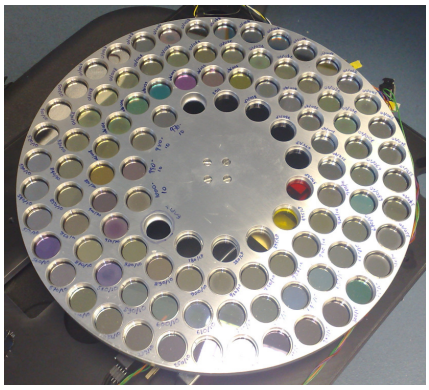

Figure 3-14: Filter wheel with all filters in place.

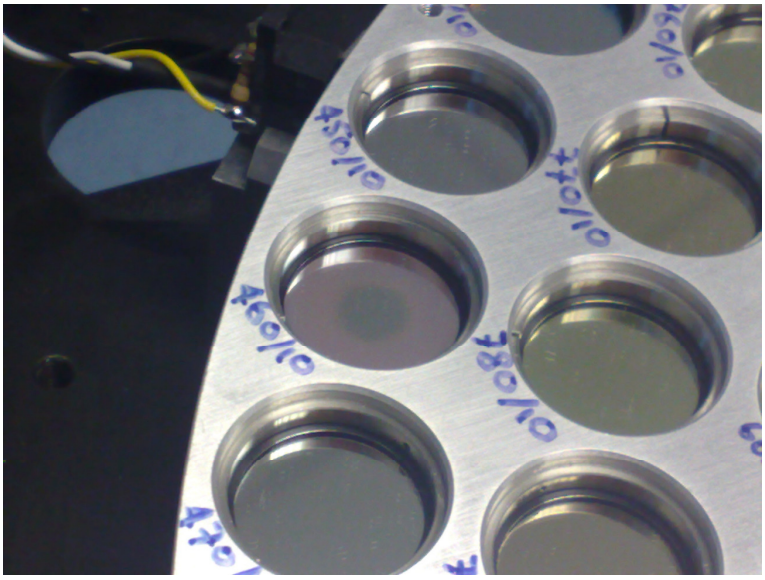

Figure 3-15: Close-up of filters

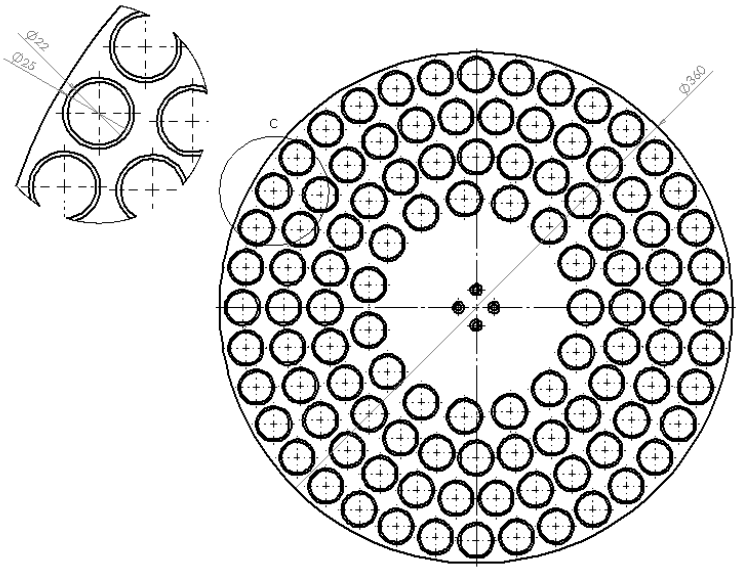

Figure 3-16: Filter Wheel dimensions

The system consists of a similar type of cryogenically cooled cold finger to MoLES, but unlike MoLES where the system used a closed cycle liquid helium cryostat, CLASSIX has to use a Liquid He Dewer due to possibilities of vibrational interference affecting the CCD gathered image. Vibrational influences have no effect on the MoLES spectrometer due to no CCD being used.

Figure 3-17: CLASSIX sample holder for diamond samples.

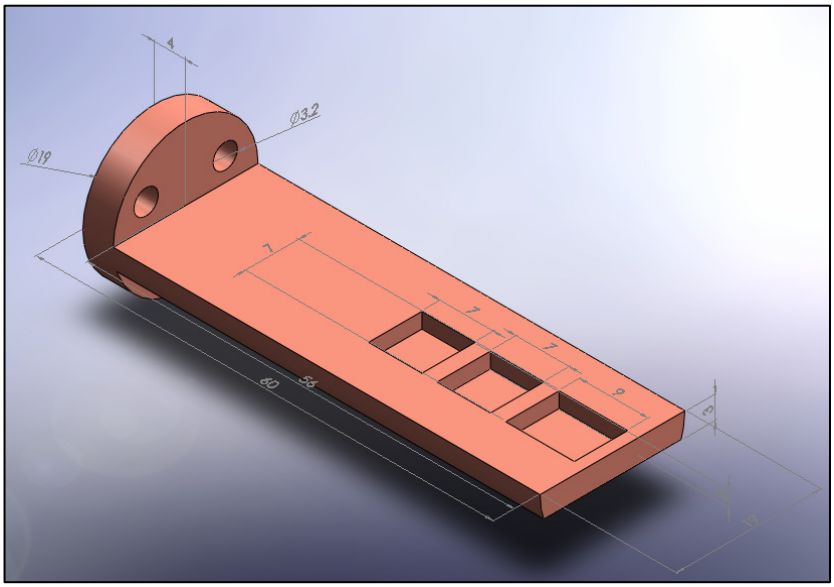

Figure 3-18: CLASSIX sample holder dimensions.

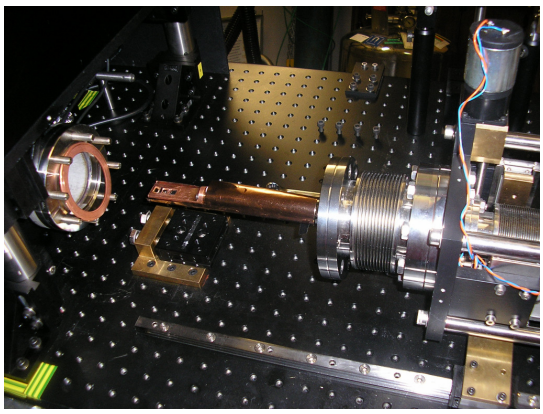

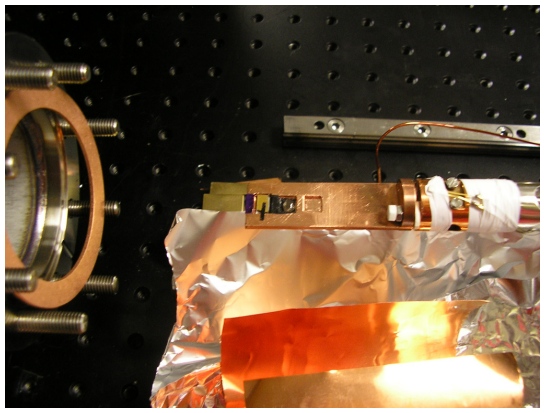

Figure 3-19: CLASSIX cryostat arm and cold finger near chamber opening with samples mounted.

Note how the CLASSIX sample holder (figure 3-17) differs to that of the MoLES sample holder (figure 3-3). This is due to the fact that focussing is important for the imaging in CLASSIX – the tops of the samples therefore have to be flush (or as close to being flush as possible) with the CLASSIX sample holder surface.

The build of CLASSIX 2 is currently underway. It consists of a new build with significant differences to CLASSIX 1. The filter wheel is replaced in favour of a liquid crystal unit. This will significantly improve the spectrometer resolution due to this being a significant limitation of CLASSIX 1. The incorporation of Raman measurements will also be possible as well as a closed cycle cryostat unit similar to that of MoLES but with significantly less vibration and interference connected to a cryostat arm that will be mounted vertically due to the operation of the cryostat.

3.3.2 Data Correction – Reference sample

Due to the fact that diamond consists of carbon atoms and that there is carbon present on the beamline in the focussing mirrors, gratings etc. it is important to have a reference sample that does not contain carbon for correction. A quartz high purity (resonator grade) (SiO_2) sample was used for this purpose as shown in the luminescence gathered image, figure 3-20 on the CLASSIX spectrometer. A reference sample was measured at each interval between moving from one sample to another – so that any change in the synchrotron beam (that occurs as the day goes on prior to the next re-fill) is also accounted for in the correction reference sample. Correction is also to be made for the PMT response and relative to the grating selected on the Monochromator on the MoLES spectrometer as well as for the carbon present on the beamline with quartz.

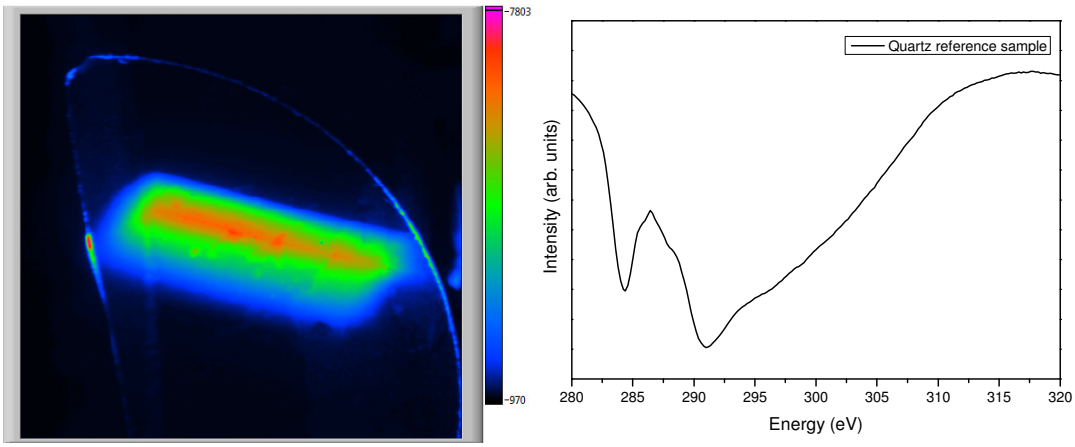

Figure 3-20: High purity (resonator grade) Quartz reference sample. Synchrotron beam (~3x1mm spot) is clearly seen in the centre for the purpose of obtaining a reference scan. This was taken on the CLASSIX spectrometer, the image above is the luminescence intensity (red is high intensity) taken by the CCD. On the right a Volume Integrated plot is shown of the Quartz sample used as a reference sample for correction due to carbon being present on the beamline.

3.4 Offline Measurements at Aberystwyth

The MoLES and CLASSIX spectrometers can also be used offline at Aberystwyth for the purpose of performing further in-house measurements without the need for a synchrotron source. Evidently OD-XAS measurements cannot be undertaken due to the requirement of a variable tuneable excitation source in the range of 280-320eV (for Diamond).

XEOL measurements can be undertaken with the aid of an X-ray source (as mentioned previously in the MoLES section) to provide the fixed incidence excitation energy required for the MoLES and CLASSIX spectrometers to be utilized in XEOL mode and measuring the luminescence light emission through a monochromator (MoLES) or through the filter wheel (CLASSIX). The excitation source is not as intense and has the provision of a sizeable beam-spot, compared to the SRS which has high-flux and small beam sizes, but can still provide the necessary irradiation for measurements such as XEOL and TL. Beam-size can be varied by the addition of different collimator hole dimensions (diameters, 1mm/2mm/3mm) to the x-ray shutter unit (section 3.4.1).

Photoluminescence (PL) and low-temperature Thermoluminescence (TL) measurements have also been undertaken on the diamond samples using the MoLES spectrometer, just a few of the range of experimental features and techniques the spectrometer has to offer. The experimental techniques will be explained further in the next chapter.

3.4.1 X-ray Unit

The images on the next few pages show the development of the window aperture for attachment to an x-ray source unit with a coupled shutter system, designed and developed by myself with the aid in construction of the Aberystwyth University Physics Workshop (figures 3-21 – 3-25).

A stainless steel casing was developed to enclose the x-ray source's opening that required the provision of a collimator prior to the shutter system. Due to the x-ray source providing hard x-rays that can travel through air, the whole shutter system was not required to be under UHV, although UHV was required for the MoLES chamber for the provision of sample cooling. An Aluminised mylar Window was coupled to a modified flange and placed over the usual synchrotron/source chamber entrance along with the x-ray source coupled to the shutter assembly.

Figure 3-21: A modified chamber aperture blank flange with recessed rubber 'o-ring'.

Figure 3-22: Aluminised Mylar 'window' cut and ready to be mounted. Note – Al coating on the outside for earthing purposes.

Figure 3-23: Mounted Aluminised Mylar window, ready for attaching to synchrotron entrance on spectrometer MoLES or CLASSIX.

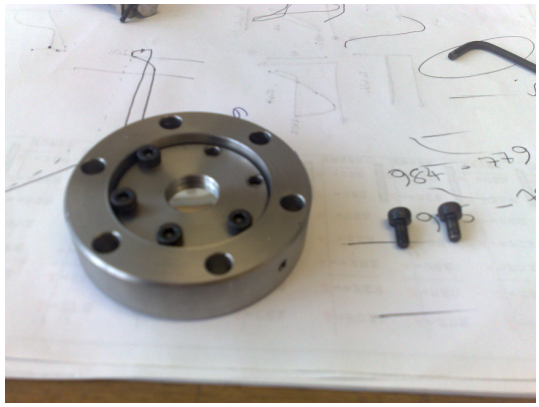

Figure 3-24: Aperture had to be modified slightly – comparing pic (left and right) it can be seen that the mylar window fitting is recessed into the flange.

The testing of the window was carried out on an 'Edwards' vacuum chamber and the initial vacuum obtained went down to ~4x10^{-7} mbar (figure 3-25).

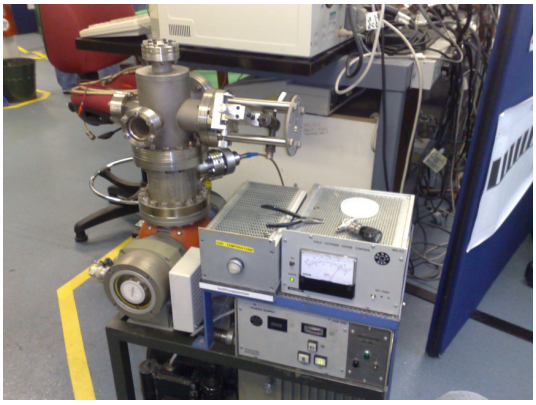

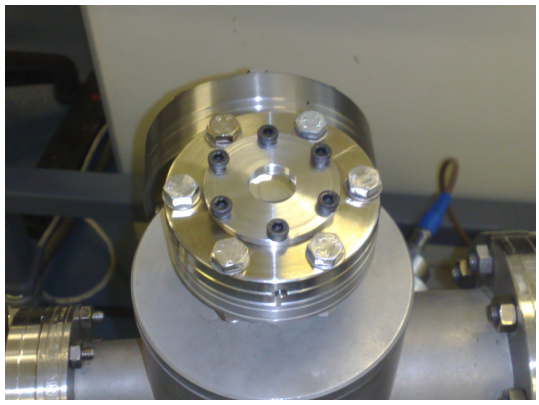

Figure 3-25: Initial testing of Al Mylar on 'Edwards' vacuum chamber. Initial vacuum went down to ~4x10^{-7} mbar.

The XEOL measurements were undertaken in-house at the recently built Luminescence Lab at Aberystwyth with an Oxford Instruments 50kV, 1mA Cu K_α x-ray source. The X-ray source has been coupled to a shutter system for the purpose of controlling exact irradiation times. The x-ray source was limited to provide a 30kV output, due to the shutter blade blocking limitation being of this value. This provided an instantaneous "switch off" system for irradiation. The x-ray source was ramped up (voltage) for use and ramped down to switch off. The unit also allowed PP

measurements to be carried out – an instantaneous x-ray "switch off" is essential for these types of experiments (figures 3-26 – 3-33).

3.4.1.1 Development of the shutter unit

Figure 3-26: The Uniblitz shutter. Capable of blocking x-ray energy up to 30keV

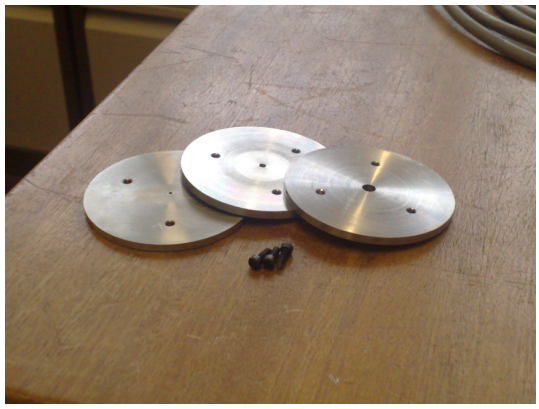

Figure 3-27: Collimators ranging from 1, 2 and 3mm diameter size.

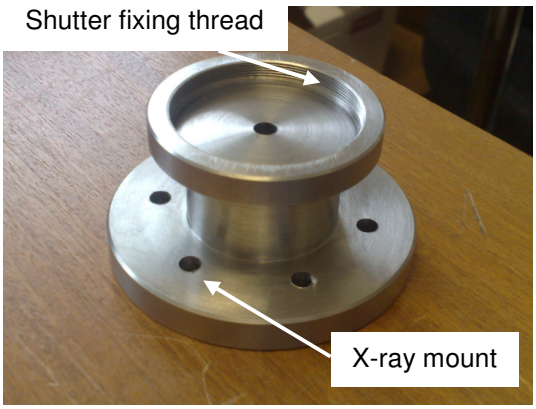

Figure 3-28: The pre-shutter section with collimator and attachment to the x-ray source.

Figure 3-29: The Uniblitz shutter complete with collimators and x-ray source cable connection.

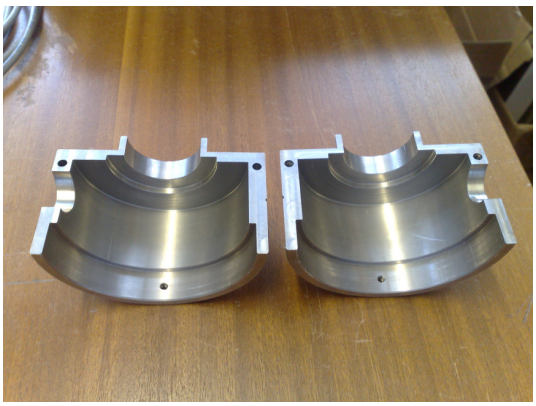

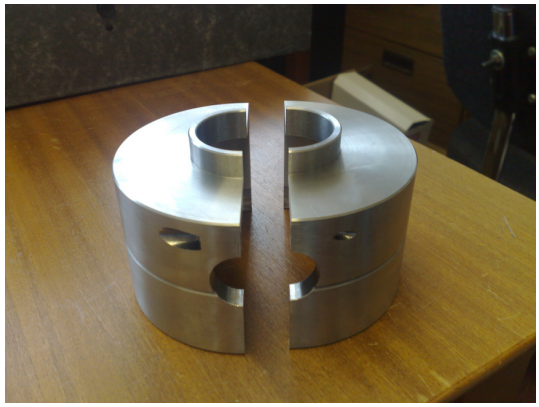

Figure 3-30: Stainless steel casing for the shutter unit.

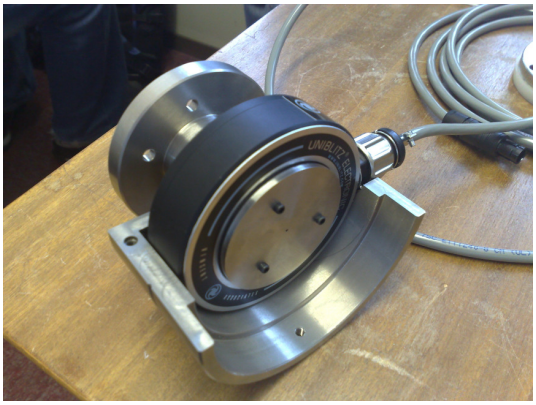

Figure 3-31: Shutter mounted in stainless steel casing.

Figure 3-32: Mounting ring connection between mylar window aperture and shutter casing.

Figure 3-33: X-ray source control box.

The final product is shown in figure 3-34 (with half of casing missing for image purposes). The schematic for the whole set-up is shown in figure 3-35.

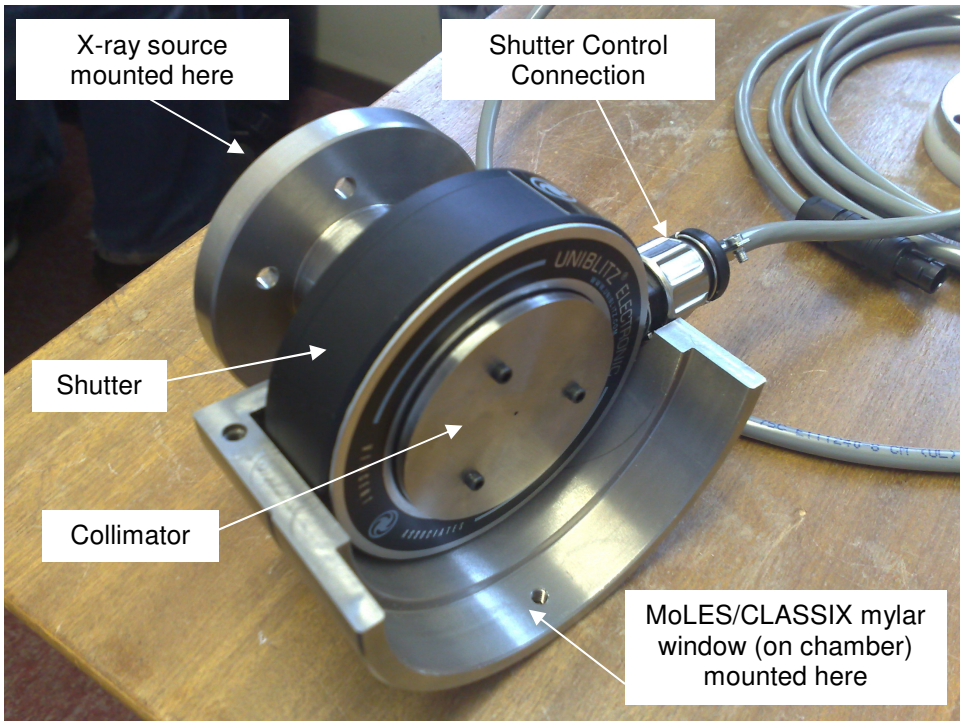

Figure 3-34: Image showing where the X-ray source and Mylar chamber window are mounted.

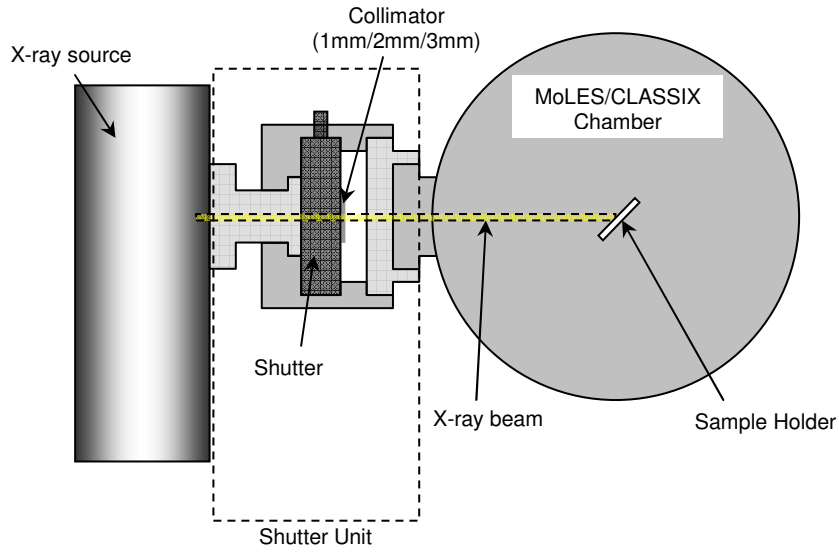

Figure 3-35: Schematic of the x-ray source and shutter unit developed at Aberystwyth mounted to either the MoLES or CLASSIX spectrometer.

3.4.1.2 Safety Considerations

Safety is vitally important when using radiation sources and steps are required to be implemented in reducing the possibility of accidents and incidents.

3.4.1.2.1 Interlock

All safety issues are required to be considered and addressed, including introducing an interlock system if the x-ray unit was removed whilst still switched on to shut the power supply to the source itself (figure 3-36).

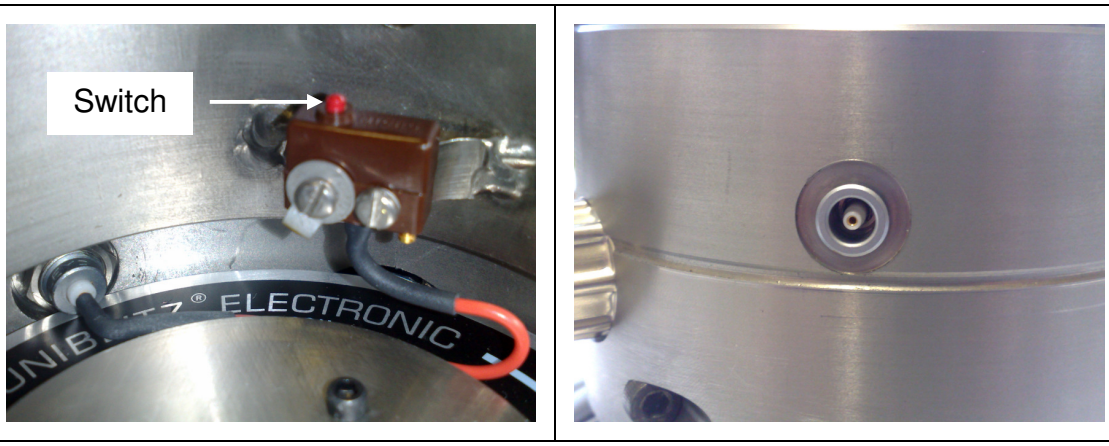

Figure 3-36: Interlock system – shuts down power to x-ray source if shutter casing/unit is removed from spectrometer/mylar window aperture.

3.4.1.2.2 Pressure and Temperature trip-switches

Consideration to safety aspects was also in place for the chamber pressure – if not low enough then the chamber could be open, thus exposing the user to scattered x-rays. A relay system was available on the pressure gauge and coupled to the X-ray control unit. A temperature switch (set to 50°C) was also mounted on the surface of the x-ray source along with a cooling fan. The temperature switch if triggered would trip the power supply to the x-ray source via the x-ray control box, thus limiting its usage when overheating occurs. This aids in maintaining the life-time of the source as well as safety considerations including fire.

3.4.1.2.3 X-ray source alignment

For the purpose of alignment of the x-ray source collimated beam-spot a fluorescent sticker was adapted and mounted on the sample holder. The MoLES chamber was closed and the conditions met for the x-ray source to be activated. The x-ray spot could be viewed through a lead-glass window mounted to the MoLES chamber and therefore the rough height of the location of the spot could be foreseen for the purpose of mounting the samples at the correct height (see figure 3-37 and 3-38). The lateral movement of finding the x-ray spot can be done by using the PMT and moving the cryostat arm further in/out of the chamber and optimizing the PMT counts (figure 3-38).

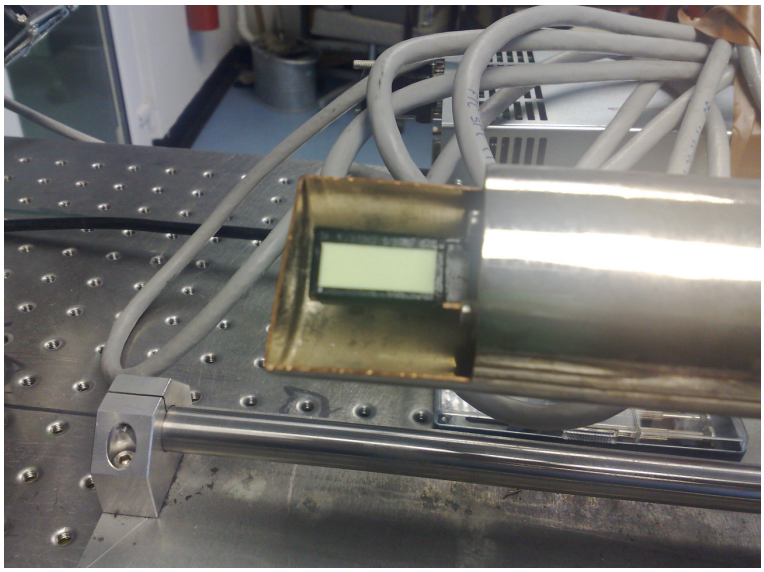

Figure 3-37: Yellow rectangle mounted on the sample holder cold finger is a fluorescent sticker. This was to align the collimated x-ray beam aiding in directly irradiating the samples.

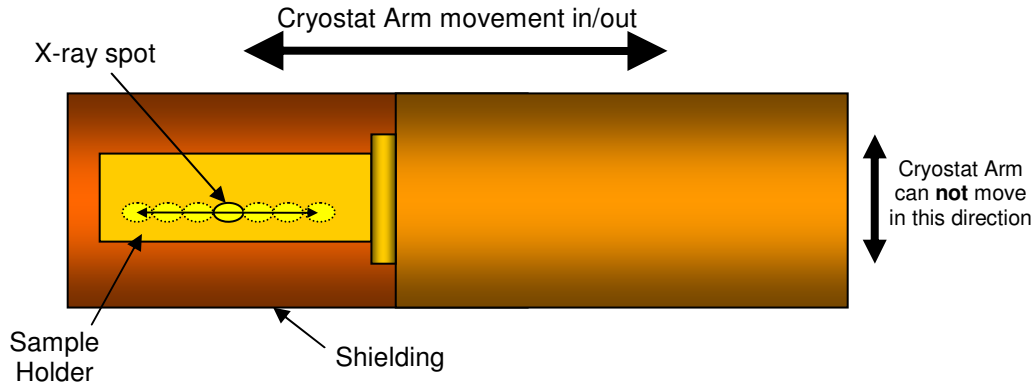

Figure 3-38: Schematic of the type of situation regarding the x-ray spot location – i.e. lower than the centre of the sample holder. Samples would therefore be required to be mounted on carbon tape so as to be directly irradiated by x-ray source. This is important due to the cryostat arm (sample holder) not being able to move laterally – only in or out as depicted in the schematic diagram.

Figure 3-39 shows the complete and fully functioning x-ray unit mounted to the MoLES spectrometer along with the control boxes in the luminescence lab at Aberystwyth University.

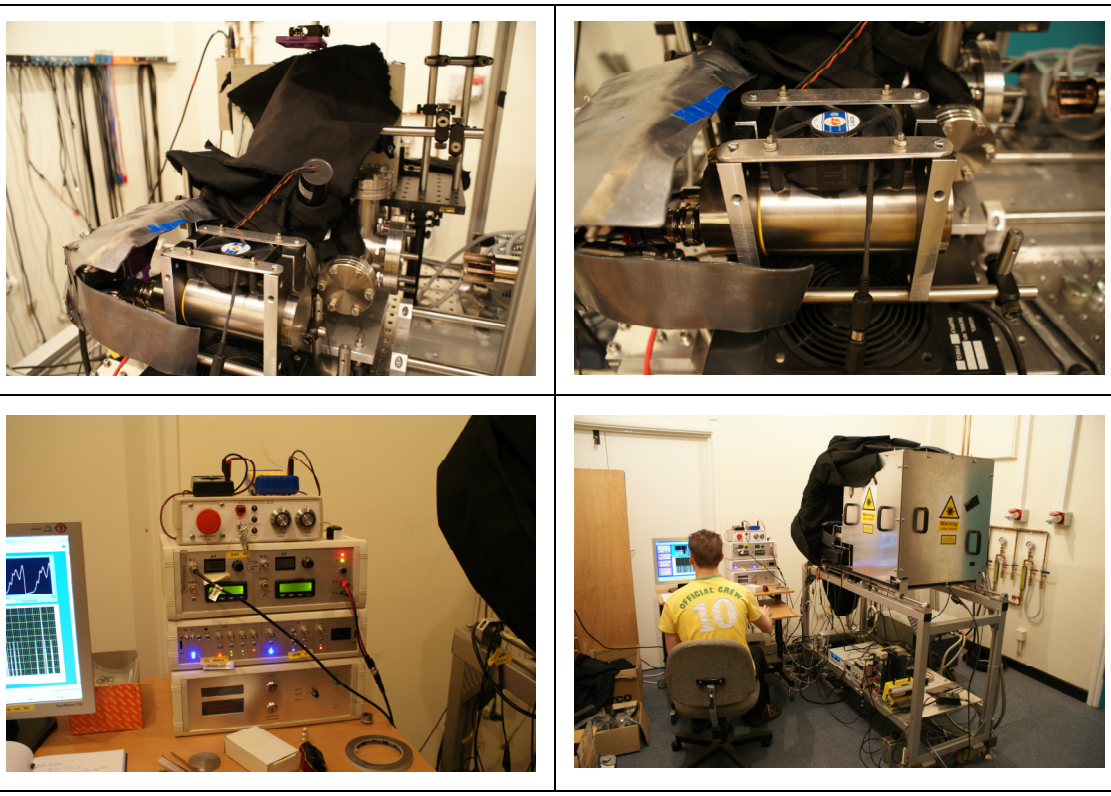

Figure 3-39: (Top left clockwise) The mounted x-ray source on MoLES complete with shutter casing, fan cooling, and lead protection. MoLES working offline at the laboratory in Aberystwyth – note that casing is now present surrounding the spectrometer to minimize background measurements. X-ray, laser and PMT control boxes.

3.5 Raman Instrument System

Raman measurements in standard mode and in imaging mode were carried out on a Horiba Jobin Yvon LabRam HP Raman Spectrometer with a Class 3B HeNe laser (632.8nm) at the Materials Laboratory at Aberystwyth University (figure 3-40). The homogeneous samples were measured using the standard Raman system and the non-homogeneous, variegated diamonds in Raman mapping mode (see chapter 6 for the Raman results).

Figure 3-40: The Horiba Jobin Yvon LabRam HP Raman Spectrometer at the Materials Laboratory at Aberystwyth University.

3.6 Atomic Force Microscopy (AFM)

Initial AFM measurements were carried out on a few samples at Aberystwyth University (figure 3-41) to clarify whether it was possible to pick up the brown banding in some samples using an AFM in contact mode. It was confirmed that the brown bands could not be observed through the AFM technique. Some AFM images are shown in the Results section of this thesis, clearly showing banding in the images, but banding that crosses the actual brown bands and very much variable in direction over the whole sample – identified as polishing lines.

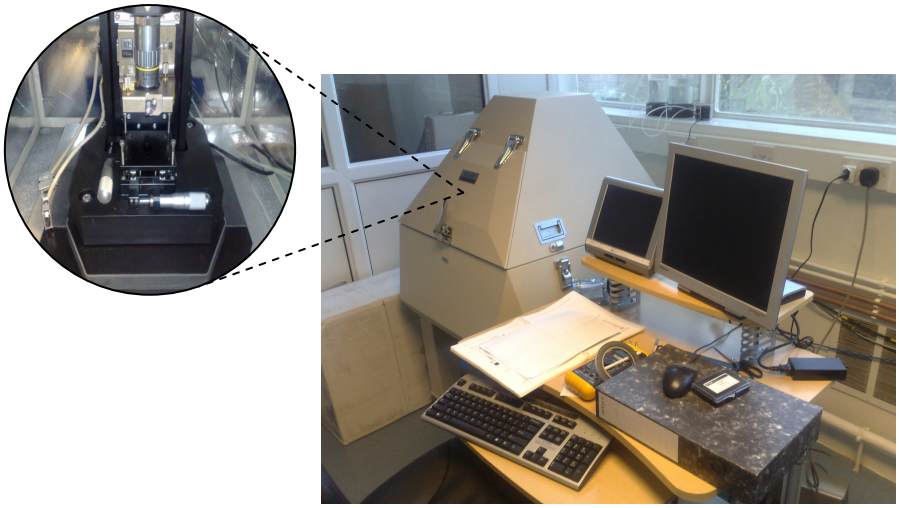

Figure 3-41: AFM kit at the Laboratory in Aberystwyth. Detail shows the internal parts of the AFM system complete with magnification, x-y table and laser.

A commercial XE-100 AFM from PSIA Corporation was used for the purpose of gathering the AFM images at room temperature and ex-situ. The first Non-Contact mode AFM (NC-AFM) was developed by Martin *et al.* in 1987 (*16, 17*). A typical AFM consists of a tip attached to a cantilever. As the sample is moved relative to the tip, the bending or deflecting of the cantilever occurs as a result of the tip interaction with the sample. A laser is shone on the rear of the cantilever which is coated with metal. The reflection that occurs as a result of this laser beam is measured by a position sensitive photo detector (PSPD) (see schematic in figure 3-42).

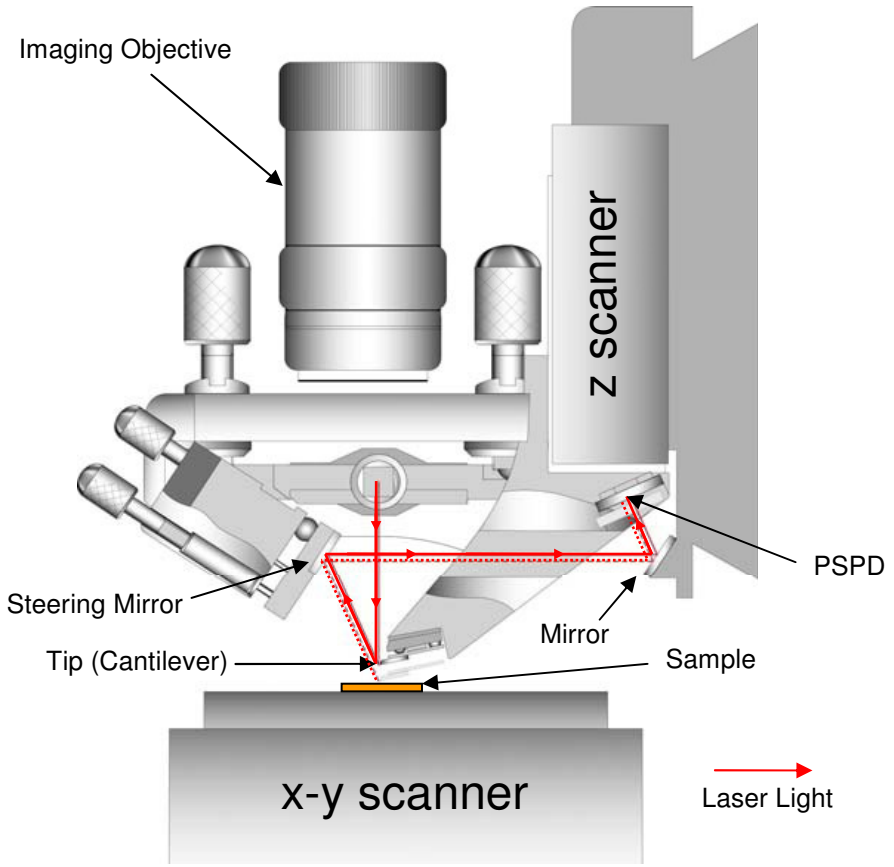

Figure 3-42: Schematic of the XE-100 AFM. Taken and adapted from (16)

As the AFM tip approaches the surface of the sample the atoms of both the tip and surface begin to interact with each other. The van der Waals attractive force between the tip and the surface affect the cantilever and as a result affect the cantilever vibration and it is these changes that are monitored to control the tip distance. Figure 3-43 shows the tip-sample interaction.

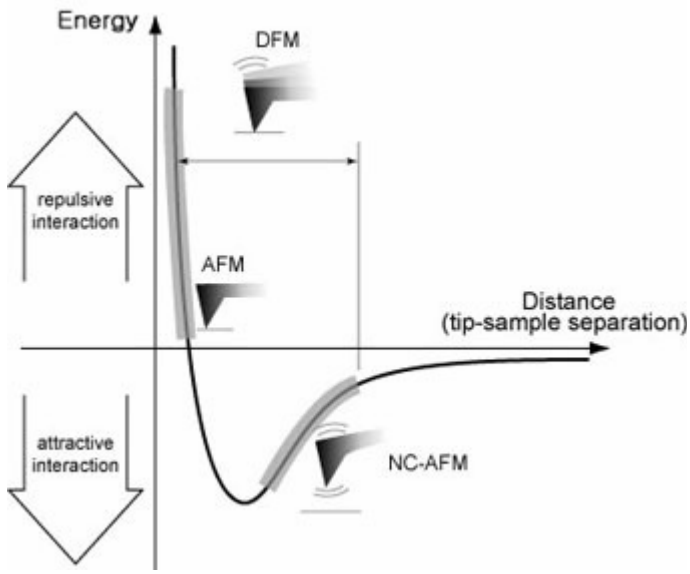

Figure 3-43: Tip interaction reproduced from (18).

As shown in figure 3-43 the AFM can be utilized in three different modes, contact mode (C-AFM), non-contact mode (NC-AFM) and Dynamic Force Microscopy (DFM).

3.7.1 C-AFM

The tip is very close to the sample surface and measurements are taken by measuring the repulsive forces between the tip and the sample. The interatomic repulsive forces are around 1~10nN and can be measured due to the spring constant of the cantilever being very small (< 1N/m) – the cantilever is sensitive to the smallest of forces (figure 3-43 and 3-44).

3.7.2 NC-AFM

In NC-AFM the tip is much further away from the sample surface as depicted in figure 3-43. As a result of this the forces upon the cantilever are small and of attractive interaction. The small forces are not sufficient so as to cause the bending of the cantilever and thus the surface topology of the sample in question is measured via the cantilever being piezo-mechanically vibrated. Changes in both amplitude and the phase of the cantilever vibration is monitored.

3.7.3 DFM

The Dynamic Force Microscopy method is similar to the NC-AFM method. The tip is allowed to gently come into contact with the surface of the sample in each oscillation period. As the tip approaches the surface ready for contact, the repulsive forces softly bounce the tip away from the surface and as a result increase the effective spring constant thus causing the amplitude to decrease. As with the NC-AFM technique the AFM corrects the cantilever position until the attractive forces (van der Waals) govern once again.

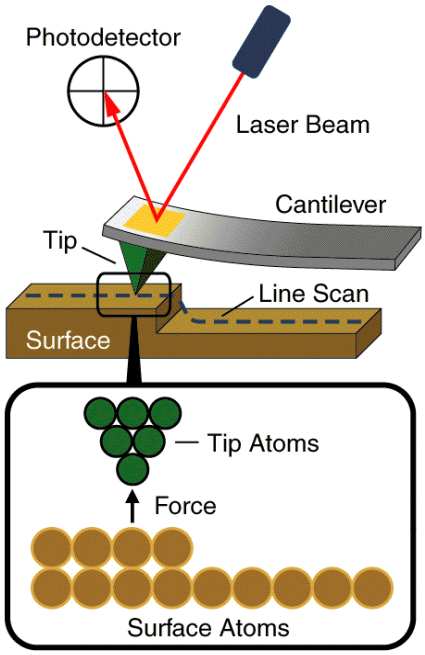

Figure 3-44: Image taken from (19) showing how the beam is deflected as the cantilever moves over the surface of the sample.

Measurements on some of the diamond samples for the purpose of the thesis were utilized in contact mode (C-AFM) only.

3.8 Summary

The invaluable instrumentation systems have been introduced in this chapter for the purpose of relating the data obtained to the techniques used. The instruments vary from bespoke purpose built luminescence analysis apparatus such as MoLES and CLASSIX to commercially available spectrometers such as the Raman instrument. In their own right, MoLES and CLASSIX are powerful stand-alone versatile instruments to acquire XEOL, OD-XAS, PL, and PP measurements. Along with other techniques such as Raman Scattering, the characterization of diamond samples can be achieved and studied. The next chapter goes on to discuss the science and theoretical aspects involved with the experimental equipment.

3.9 References

1. F. Quinn *et al.*, *Journal of Synchrotron Radiation* **10**, 461 (2003).
2. M. G. Dowsett *et al.*, *Analytical Chemistry* **80**, 8717 (2008).
3. D. A. Evans *et al.*, *Journal of Physics-Condensed Matter* **20**, (2008).
4. G. O. Jones *et al.*, *In Press*, (2010).
5. D. A. Evans *et al.*, paper presented at the Hasselt Diamond Conference, 2009.
6. N. R. J. Poolton, B. Hamilton, D. A. Evans, *Journal of Physics D-Applied Physics* **38**, 1478 (2005).
7. N. R. J. Poolton, A. J. J. Bos, G. O. Jones, P. Dorenbos, *Journal of Physics-Condensed Matter* **22**, 185403 (2010).
8. N. R. J. Poolton *et al.*, *Journal of Luminescence* **130**, 1404.
9. N. R. J. Poolton, B. M. Towlson, B. Hamilton, D. A. Evans, *Nuclear Instruments & Methods in Physics Research Section B-Beam Interactions with Materials and Atoms* **246**, 445 (2006).
10. S. Larcheri *et al.*, *Review of Scientific Instruments* **79**, (Jan, 2008).
11. N. R. J. Poolton, B. M. Towlson, B. Hamilton, J. Wallinga, A. Lang, *Journal of Physics D-Applied Physics* **40**, 3557 (Jun, 2007).
12. D. A. Evans *et al.*, paper presented at the DeBeers Diamond Conference, 2008.
13. G. O. Jones *et al.*, paper presented at the DeBeers Diamond Conference, 2009.
14. G. O. Jones *et al.*, paper presented at the DeBeers Diamond Conference, 2010.
15. A. G. McGlynn, Aberystwyth University (2010).
16. PSIA, *PSIA XE-100 Product Datasheet*. (http://210.34.15.15/PSIAINC/psiainc/DSR-XE100-R1.pdf).
17. Y. Martin, C. C. Williams, H. K. Wickramasinghe, *Journal of Applied Physics* **61**, 4723 (1987).
18. PSIA, *XE-100 High Accuracy Small Sample SPM Version 1.0*. (http://research.fit.edu/nhc/documents/XE100UserManual.pdf, 2002).
19. A. V. Clemente, K. Gloystein, *Principles of Atomic rinciples Force Microscopy*. (http://www.mansic.eu/documents/PAM1/Frangis.pdf, 2008).

Chapter

4

4.0 Experimental Techniques

4.1 Introduction

In this chapter the theoretical aspects of each experimental technique used during the course of this research is considered. It is a continuation from the previous chapter whereby the Instrumentation Systems used were introduced and discussed.

The first part of this chapter presents X-ray Absorption Spectroscopy (XAS). It will predominantly be concentrated on Near-Edge X-ray Absorption Fine Structure (NEXAFS) and Optically-Detected XAS (OD-XAS). These are the most significant techniques used for the study of Diamond during the course of this research. Luminescence induced by laser (Photoluminescence (PL)), X-rays (X-ray Excited Optical Luminescence (XEOL)) and Electron beams (Cathodoluminescence (CL)) will follow and tie in with the XAS section due to being of similar nature. The theoretical aspects of Raman spectroscopy will then be introduced – another powerful characterisation technique used during the course of this research.

4.2 X-ray Absorption Spectroscopy (XAS)

4.2.1 Introduction

The discovery of X-rays by Wilhelm Roentgen in 1895 (*1*) paved the way to x-ray experimental use as we know of today on the interaction of x-rays with materials. Not only did he discover x-rays, he also studied these new rays' properties and laid the foundations for significant x-ray detection techniques such as fluorescence of a phosphor, photographic plate darkening and the ionization of a gas. He also brought about radiography but more relevant to this thesis, he applied x-ray absorption to analytical chemistry.

The development of synchrotron sources (chapter 2) allowed access to higher coherent sources of light that ranged from the far infra-red region of the electromagnetic spectrum (see chapter 1) to high energy x-rays. Photons (light quanta) are a useful tool with which to study matter through a myriad of techniques. Photons of different wavelengths are suited to probing different samples. For example IR radiation is of a similar energy to atomic and molecular vibrations, while hard x-rays are of the required wavelength for probing the crystal structure of materials.

The well established X-ray Absorption Spectroscopy (XAS) technique was first used in the 1920s for structural investigations of matter (*2*) and has accelerated the research into the local chemical, electronic and structural properties of materials providing an insight into the chemistry and structure of materials of interest. Before exploring the main principals, theoretical and instrumental details of XAS itself, it is worthwhile to note that the interaction of light with matter is the main concept with regards to these experimental techniques.

In 1887, Hertz was the first to observe electrons being emitted from a material when irradiated with ionizing radiation and called it the photoelectric effect. Therefore, as well as the interaction of light with matter, it is vital to introduce x-ray absorption and the x-ray absorption cross-section, which describes the interaction of light with electrons in solids.

4.2.1.1 X-ray Absorption

The absorption of x-rays is a fundamental part in the understanding of how x-rays interact with matter. If we consider x-rays of intensity I_1 travelling into a sample of thickness 'Δx' some of the initial x-rays are absorbed (Figure 4-1). The physical process which x-ray absorption relates to, can be governed by Beer's Law.

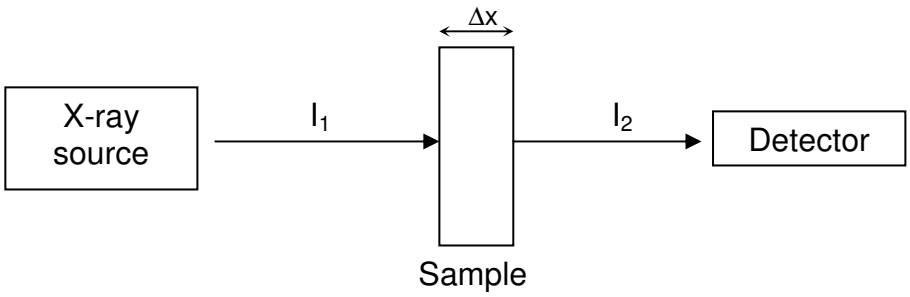

Figure 4-1: Schematic showing x-rays incident of initial intensity I_1 on a sample of thickness' Δx' and with a resultant intensity I_2 due to sample absorption.

For the schematic in figure 4-1 Beer's Law may be written in the form,

$$\log\left[\frac{I_1}{I_2}\right] = k\,\Delta m = k_d\,\Delta x$$

Whereby, *'m'* is the mass, 'Δx' is the sample thickness and the values of the proportionality constants *'k'* and *'k_d'* depend on the wavelength and elements within the sample. For a sample of unit area, *'k_d'* is *'k'* times the density (*1*). *'I'* is the intensity.

For fully absorbing samples such as Diamond, similar information can be gathered from photoelectron emission secondary relaxation events and fluorescence emission.

4.2.1.2 The X-ray Absorption Cross-section

At the atomic level in an atom or molecule the X-ray absorption Cross Section (σ_x) is defined as the number of electrons excited per unit time divided by the number of

incident photons per unit time per unit area and is usually measured in cm^2 or barn ($1cm^2 = 10^{24}$ barn) (*2*) (Equation 4-1).

$$\sigma_x = \frac{P_{if}}{F_{ph}} \qquad \textit{Equation 4-1}$$

Where F_{ph} is the photon flux – the number of photons per unit time per unit area. The exciting of an electron from an initial state *'i'* to a final state *'f'* has a transition probability P_{if}, and can be calculated from Fermi's "Golden Rule" (*2*) of a 1st order driven harmonic time-dependent perturbation probability

$$P_{if} = \frac{2\pi}{\hbar} \left|\langle f \left|\Delta\right| i \rangle\right|^2 \rho_f(E) \qquad \textit{Equation 4-2}$$

Whereby $\left|\langle f \left|\Delta\right| i \rangle\right|$ is the matrix element $\left|M_{fi}\right|$ and ρ_f (E) is the energy density of final states, Δ is the perturbation.

The matrix element can be derived from the Hamiltonian and expressed in terms of the incident photon vector field (**A**) and the electron momentum operator (**p**)

$$H = V(r) + \Delta \qquad \textit{Equation 4-3}$$

$$H = V(r) + \frac{e}{2mc}(\mathbf{A}\cdot\mathbf{p} + \mathbf{p}\cdot\mathbf{A}) - e\phi(r,t) + \frac{e^2}{2mc^2}\left|\mathbf{A}\right|^2 \qquad \textit{Equation 4-4}$$

Whereby, $\left|\mathbf{A}\right|$ and $\phi(r,t)$ are the vector and scalar potentials respectively. **p** is the momentum operator and *V(r)* is the Hamiltonian.

The $\left|\mathbf{A}\right|^2$ term in the above equation (equation 4-4) which refers to the photon-photon interaction. It is small for the experimental investigations carried out during the course of this research and can be considered insignificant.

The application of the Coulomb gauge, the scalar potential $\phi(r,t)$ is a constant with time and can be incorporated within the time independent term *V(r)*. As well as this, by considering the momentum vector $\mathbf{p} = i\hbar\nabla$ the following commutation can be applied,

$$\mathbf{A}\cdot\mathbf{p} + \mathbf{p}\cdot\mathbf{A} = 2\mathbf{A}\cdot\mathbf{p} + i\hbar(\nabla\cdot\mathbf{A}) \qquad \textit{Equation 4-5}$$

and substituting into equation 4-4 along with the final term that reduces to zero, the perturbation Hamiltonian can be simplified to,

$$\Delta = \frac{e}{mc}(\mathbf{A}\cdot\mathbf{p}) \qquad \textit{Equation 4-6}$$

Substituting equation 4-6 into equation 4-2 gives the transition probability as,

$$P_{if} = \frac{2e^2\pi}{\hbar m^2 c^2}\left|\left\langle f\left|\mathbf{A}\cdot\mathbf{p}\right|i\right\rangle\right|^2 \rho_f(E) \qquad \textit{Equation 4-7}$$

The vector potential can be written in the form of a plane electromagnetic wave of wave vector $\boldsymbol{k}$, frequency ω, and unit vector $\boldsymbol{e}$.

$$\mathbf{A} = \boldsymbol{e}\,A_0\cos(\boldsymbol{k}\cdot\mathbf{x} - \omega t) = \boldsymbol{e}\frac{A_0}{2}(e^{i(\boldsymbol{k}\cdot\boldsymbol{x}-\omega t)} + e^{-i(\boldsymbol{k}\cdot\boldsymbol{x}-\omega t)}) \qquad \textit{Equation 4-8}$$

The $e^{-i(\boldsymbol{k}\cdot\boldsymbol{x}-\omega t)}$ term can be discarded due to describing the emission of a photon if an atom had an inner shell hole. The vector can be further simplified due to the fact that the electron energies for this research are below 1keV and therefore it can be approximated that **A** is a constant due to the atomic separation being significantly larger than the photon wavelength. It is therefore only the first term that is required and we can approximate that $e^{i(\boldsymbol{k}\cdot\boldsymbol{x})} \approx 1$. The transition probability can therefore be expressed as,

$$P_{if} = \frac{e^2\pi}{2\hbar m^2 c^2}A_0{}^2\left|\left\langle f\left|\boldsymbol{e}\cdot\mathbf{p}\right|i\right\rangle\right|^2 \rho_f(E) \qquad \textit{Equation 4-9}$$

The photon flux (F_{ph}) can be obtained by dividing the energy flux of the electromagnetic field by the photon energy,

$$F_{ph} = \frac{{A_0}^2 \omega}{8\hbar\pi c} \qquad \textit{Equation 4-10}$$

Diamond has a low absorption cross-section for X-rays and a review can be found in (*3*). Through combining equation 4-9 with equation 4-10 we can obtain,

$$\sigma_x = \frac{4e^2\pi^2}{m^2 c\ \omega}\left|\langle f|\boldsymbol{e}\cdot\mathbf{p}|i\rangle\right|^2 \rho_f(E) \qquad \textit{Equation 4-11}$$

4.3 X-ray Absorption Spectroscopy (XAS) Theory

Research into the chemical and structural properties of materials has been accelerated and aided with the development of X-ray Absorption Spectroscopy (XAS) techniques over the past few years. Synchrotron based techniques such as those mentioned in chapter 2 have been key to the understanding of materials at the atomic level. The main principles of X-ray Absorption Fine Structure (XAFS) for example, (more information later in this chapter) have been known since the 1930s due to Kronig's explanation of the oscillatory fine structure in an x-ray absorption spectrum. The 1970s provided synchrotron radiation and provided an ideal source for x-ray absorption experiments and it became apparent that XAFS was potentially a powerful tool in providing information on the local structure in the local surroundings of atoms.

The XAS technique essentially consists of x-rays being absorbed by matter and promoting an electron situated within the absorbing atom's core shell into a higher unoccupied state or the continuum (the photoelectric effect). It can obtain structural information in the immediate surroundings of the absorbing atom. The x-ray absorption increases rapidly when the x-ray energy is sufficient to reach the binding energy of a particular electron in a particular shell, when this occurs it is called the absorption edge. They are different for each particular element due to different nuclear charges and the different orbitals involved (*4*).

XAS involves the study of the x-ray absorption as a function of the irradiating incident excitation energy as shown in figure 4-2 whereby photons get absorbed by an electron in a core level which as a result is then excited into an unoccupied state above the Fermi Level.

The reason for the sudden rise in the absorption that goes against the trend of the gradual decrease in absorption as the excitation energy is increased is due to the fact that the energy has reached an ionization threshold of a core electron shell as is illustrated in figures 4-2 and 4-3. The schematic diagram depicts the origins of the K (highest energy – nearer to the nucleus) and L edges. The three absorption edges that are observed here relate to the 2s orbital at the higher energy and the 2p orbital which splits into two features, the $2p_{1/2}$ (L_2 edge) and the $2p_{3/2}$ (L_3 edge – at the lowest energy) (see figure 4-2).

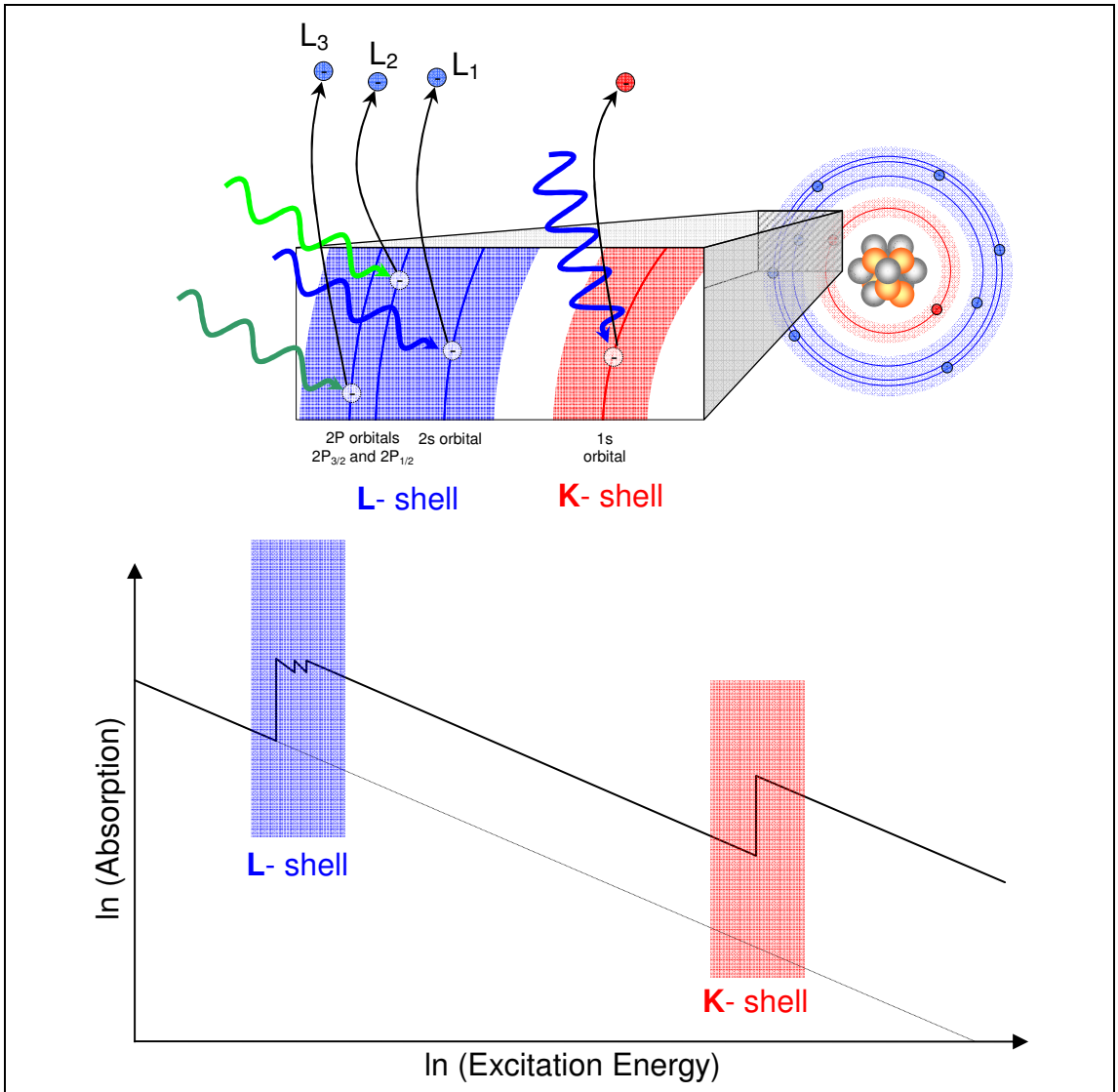

Figure 4-2: Schematic of the absorption edges in terms of absorption vs energy (log scale). The inset shows a schematic representation of a typical atom along with the Protons and Neutrons at the Nucleus and the corresponding excitations relative to the K and L edges. Note the shorter wavelength of the incident wave in exciting an electron from the K-shell, core level (1s) indicative of the requirement of higher energy. Red electrons correspond to K-sell electrons and blue electrons correspond to L shell electrons.

The inset in figure 4-2 shows a schematic representation of a typical atom along with the Protons and Neutrons at the Nucleus and the corresponding excitations relative to the K and L edges. Higher energy is required to excite a K-shell electron out of the 1s core level, due to being closer to the nucleus and therefore strongly bound.

Figure 4-3 below shows a schematic representation of the excitations involved in figure 4-2.

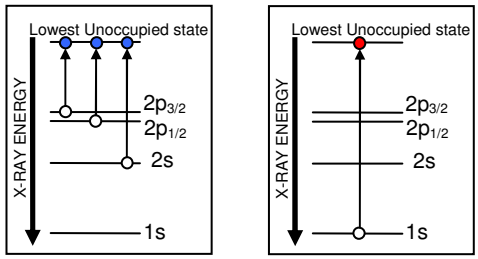

Figure 4-3: Schematic of excitation relative to the absorption edges similar to as depicted in figure 4-3.

The graph below shows how the K-edge binding energies vary for the first 9 elements (figure 4-4).

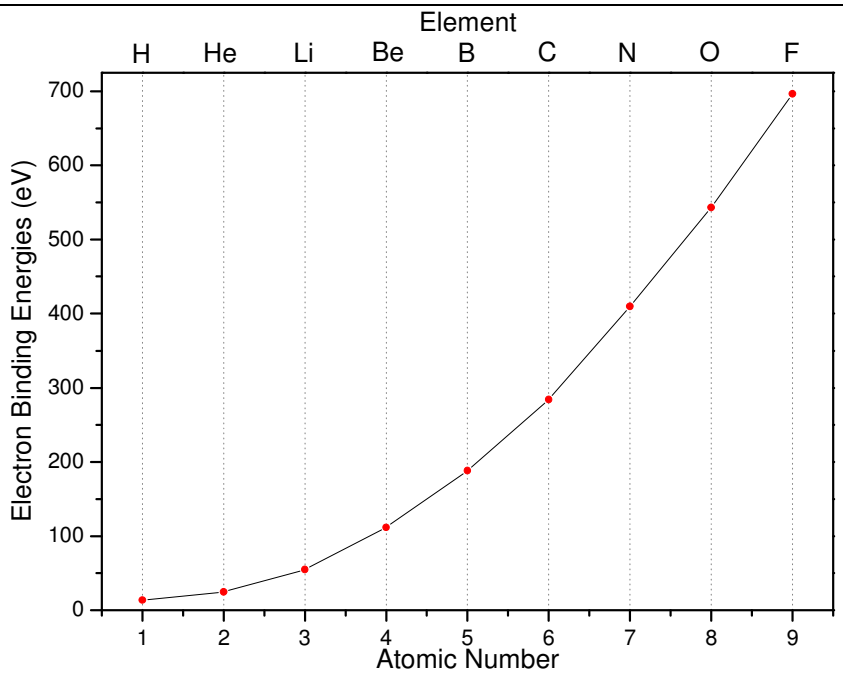

Figure 4-4: Electron Binding energies of the first 9 Elements (5).

During the course of this research, studies have concentrated around the K-edge of Carbon which has an electronic structure, $1s^2\ 2s^2\ 2p^2$. Figure 4-5 shows the finer detail situated around the K-edge of carbon when studying Diamond. The red spectrum is a typical Diamond NEXAFS spectrum and will be further explained in the next section.

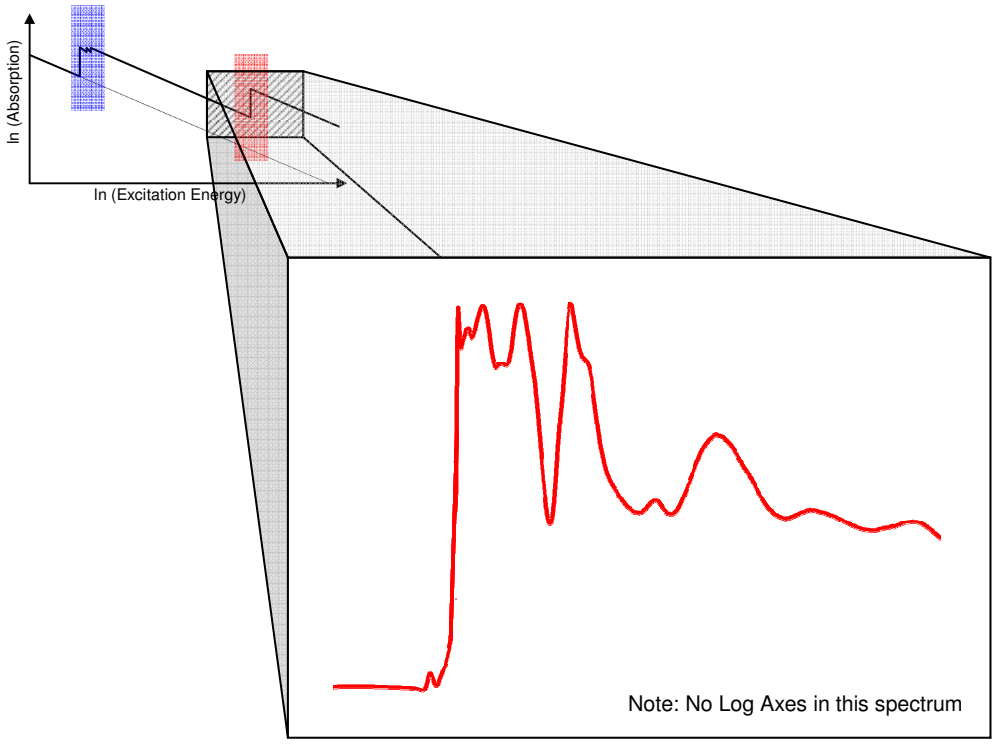

Figure 4-5: Schematic of the K-edge region showing more detail. It is these regions that are studied for the purpose of this thesis. Features are indicative of features specific to different materials. In this instance the red NEXAFS spectrum shown is for the Diamond Carbon K-edge (spectrum has been taken from excitation energy of ~280eV to ~320eV).

The XAS spectrum can be divided into the relevant regions as depicted in figure 4-6 below. There is no apparent division for the regions and it is often found that the XANES and NEXAFS regions are often modelled together (*4*).

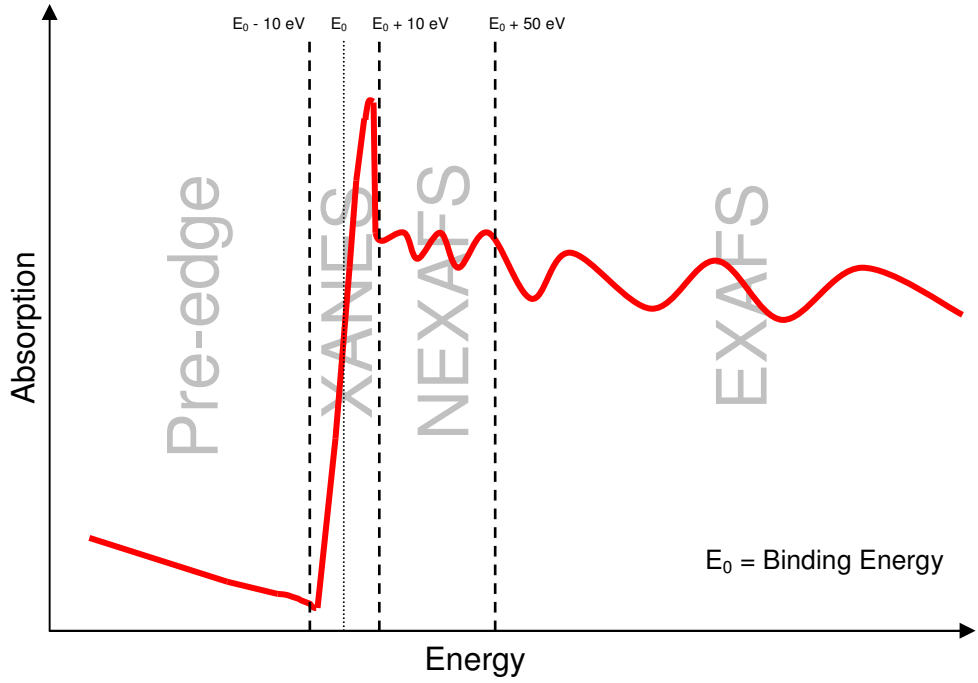

Figure 4-6: Reproduced and adapted from (6) showing the different regions of XAS analysis.

For the purpose of this research we predominantly studied the Pre-edge and NEXAFS (inclusive of XANES) regions of the spectrum as well as the OD-XAS technique that will be introduced later in this section.

The EXAFS region is predominantly observed as ripples once the absorption edge has been reached. These ripples depict the constructive and destructive interference that occurs as a result of an out-going wave and a back-scattered wave from neighbouring atoms affecting the absorption of a particular energy as shown in figure 4-7. The enhancement (constrictive) or reduction (destructive) of the absorption at a particular energy is what is observed in the EXAFS region.

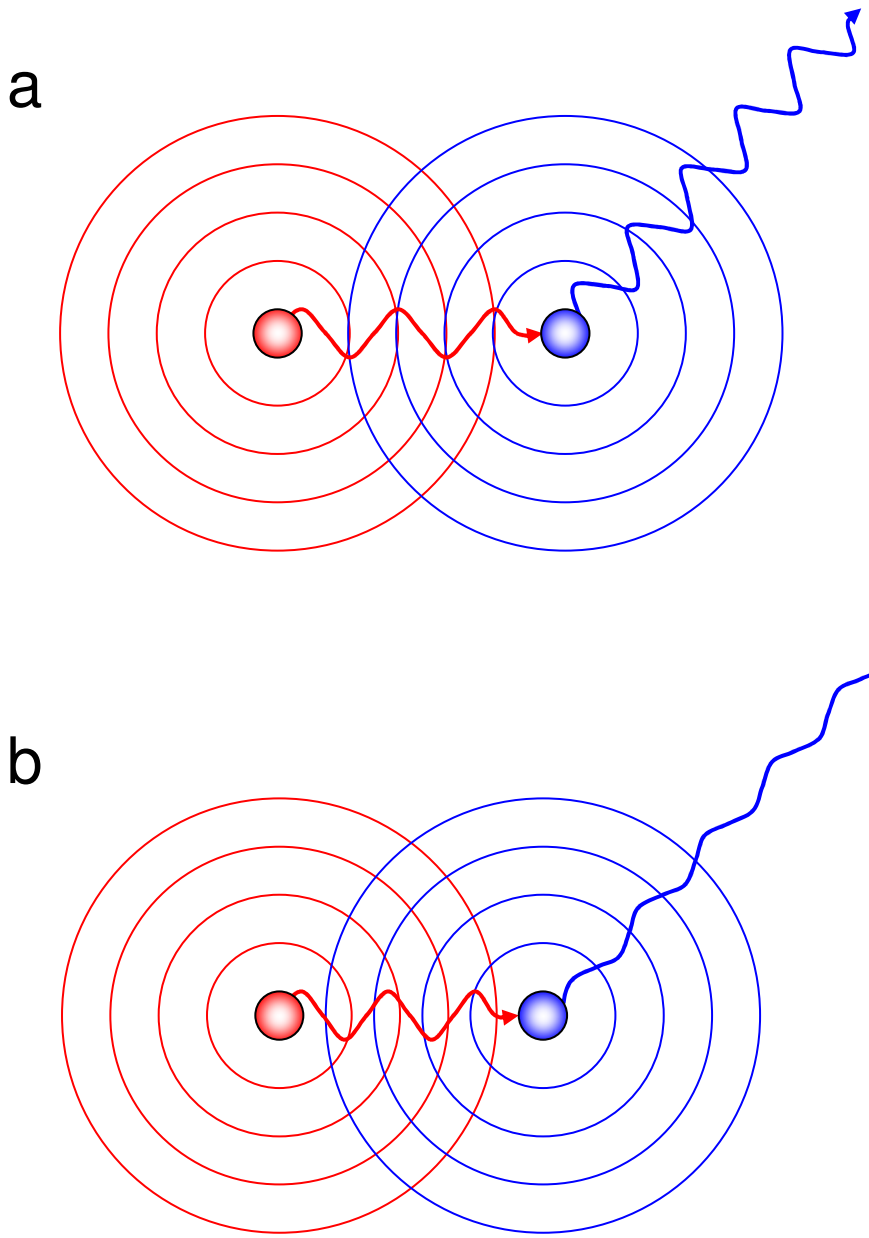

Figure 4-7: Schematic showing the constructive (a) and destructive (b) interference that occurs between the outgoing electron wave and the back scattered wave due to neighbouring atoms that give rise to EXAFS oscillations.

The EXAFS region of the spectrum was not studied during the course of this research and shall not be explored further in this thesis.

4.4 Near-Edge X-ray Absorption Fine Spectroscopy (NEXAFS)

4.4.1 Introduction

The Near-Edge X-ray Absorption Fine Spectroscopy (NEXAFS) technique is a significant XAS technique for the study of molecules bonded to surfaces as well as to probe the chemical, structural properties and geometric structure of materials. It was developed in the 1980s and is a synchrotron based technique with the aim of probing the structure of molecules that were bonded to surfaces. Low Z molecules were then and still are now, significantly of special interest in surface science and consist of organic molecules containing important building blocks such as hydrogen, nitrogen, oxygen, fluorine and predominantly the significant element predominantly studied during the course of this research, carbon (*2*). One of NEXAFS' strengths is the ability of identifying particular molecular bonding such as C – C, C = C, C ≡ C and C – H bonds in hydrocarbons (*2*) as well as the ability of determining the orientation of surface molecules through angular resolved NEXAFS – a technique that was not implemented during the course of this research. NEXAFS can detect in the molecules the presence of specific bonds and determine their lengths and orientation. It is an important study in the understanding of how molecules bond to surfaces and to the understanding of how oxygen bonds to the heme group in myoglobin and haemoglobin (*2*), a fundamental concept in the study of oxygen transport in blood through the body.

The NEXAFS technique is a well established synchrotron based technique involving the collection of induced photo-electrons due to the incident synchrotron radiation. It involves the interaction of light with matter and can give rise to information on the electronic and geometric structure of a material. The synchrotron source predominantly used for the gathering of the experimental data was at the MPW6.1 end-station at the Daresbury Laboratories, Warrington (see chapter 2).

As already mentioned in the Introduction (chapter 1) the NEXAFS of graphite and diamond have key indicative features as are shown in figure 4-8.

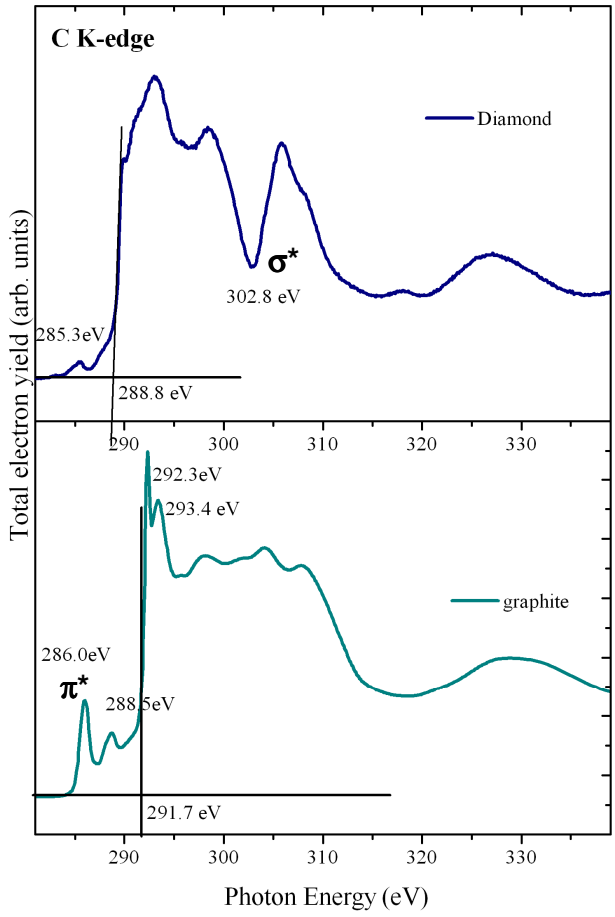

Figure 4-8: Typical NEXAFS spectrum for Diamond and Graphite showing the π (sp^2 carbon-bonding) and σ* (sp^3 carbon-bonding) indicative features in graphite and diamond respectively.*

In NEXAFS studies, the incident energy from a tuneable source such as a synchrotron is scanned from an energy value below the absorption edge of the material, through the absorption edge. For NEXAFS measurements on graphite and diamond for example, a typical NEXAFS scan would consist of ramping the synchrotron energy from ~280-320eV over the significant features i.e. the π* (indicative of sp^2-bonded carbon in graphite) and the σ* resonance (indicative of sp^3-bonded carbon in diamond). The position of the σ-resonance was realized as a sensitive measure of the intramolecular bond length in 1983 through the study of CO, formic acid (HCOOH) and methanol (CH_3OH) on Cu(100) (*2*).

Identifying the specific bonding involved was the main objective of the experiments carried out in this research on brown diamond via the NEXAFS and OD-XAS techniques. The NEXAFS technique has been applied to the study of single crystal

CVD diamonds of uniform colouration for the purpose of providing information relative to the chemical bonding of the CVD diamond in obtaining an explanation for the brown colour which has long been a topic of interest to scientists and geologists. It has been applied in parallel with the OD-XAS technique (introduced later in this chapter) to prove that both techniques provide the same information regarding the local chemical structure of the sample under study, but from different origins, electrons in NEXAFS study and luminescent light for OD-XAS.

4.4.2 X-ray Photoemission Spectroscopy (XPS)

The X-ray photoemission spectroscopy (XPS) technique or more accurately photo-emission spectroscopy (PES) can be utilized for the provision of mapping out the density of occupied states (DOS) in the valence band (VB). High ionizing energy x-rays are used to remove electrons from bound states out of the sample entirely creating core holes. Studying diamond for example at Aberystwyth University Materials Laboratory using a 1257eV Mg K-α x-ray source produces elastically scattered electrons from the top layers of the diamond sample (~5nm). It is vital that the samples used for this technique are clean. Information on the C 1s is thus gathered whereby electrons are measured with a Kinetic Energy (K.E.) of,

$$E_{KIN} = h\nu - E_B - \Phi \qquad \textit{Equation 4-11}$$

E_{KIN} is the Kinetic Energy, $h\nu$ is the excitation source energy (eV), E_B is the Binding Energy (i.e. ~284eV for the C 1s) and Φ is the Work Function. This technique was not utilized during this research and therefore shall not be further explored in this thesis.

Figure 4-9 shows two instances during the NEXAFS experiment. The left panel shows the information obtained via NEXAFS when the incident energy is below that of the K-edge energy. The right hand panel depict the NEXAFS spectrum obtained when the energy is scanned above the K-edge energy, mapping out the density of unoccupied states in the conduction band. The XPS technique spectrum is also shown as it maps out the density of occupied states within the valence band for theoretical and image consistency and completion.

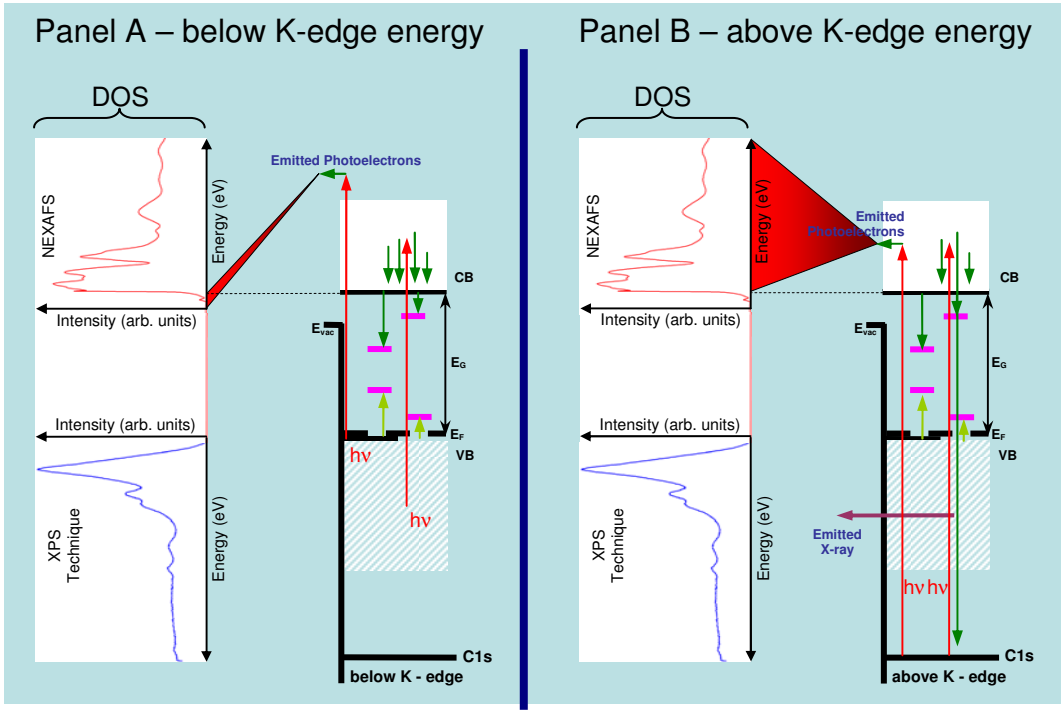

Figure 4-9: Schematic diagram of the processes involved. Panel A shows the transitions that occur when energy below that of the K-edge is incident upon the sample. The XPS technique can be used to map out the density of occupied states (DOS) in the VB. Optical luminescence occurs as the electrons recombine back down from the CB into the VB. Panel B shows the transitions that occur when higher energy is incident on the sample (above K-edge energy).

Further information on the specific regions of the NEXAFS spectrum can be found on the following pages.

4.4.3 Pre-edge region

X-rays of energy below the K-edge energy but above the ionization energy (the energy required to remove an electron from a neutral atom) of a material under study excite electrons from the valence band (VB) across the band gap (E_g) into the conduction band (CB).

In the pre-edge region, the energy is not sufficient to excite electrons from the K shell. Electrons situated in the high DOS of the valence band are excited up into the high DOS of the conduction band (the continuum), there is no reference level to excite from – excitation occurs everywhere and is referred to as non-resonant excitation. There is no reference point for excitation as depicted in figure 4-10.

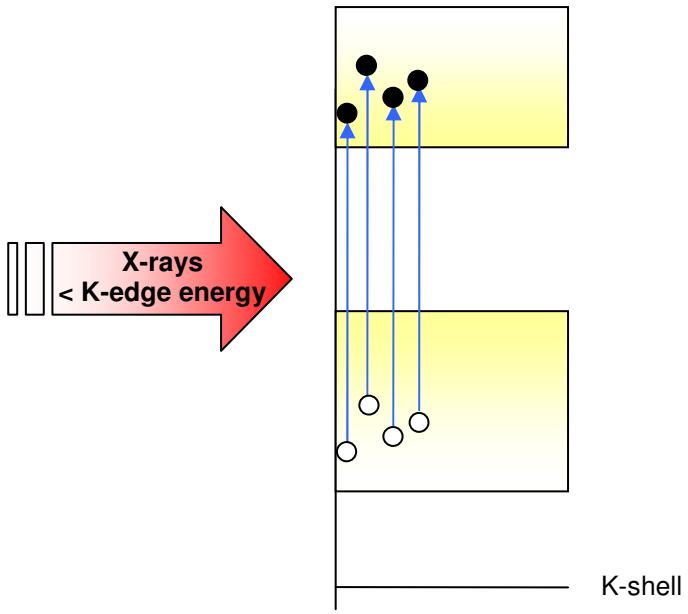

Figure 4-10: Pre edge case, energy below the K-edge excited electrons from a high density of states in the VB into a high density of states in the CB, there is no reference level – i.e. it is a non-resonant case where excitation occurs everywhere (region 'a' in figure 4-11).

The pre-edge spectrum as shown highlighted in figure 4-11 is obtained.

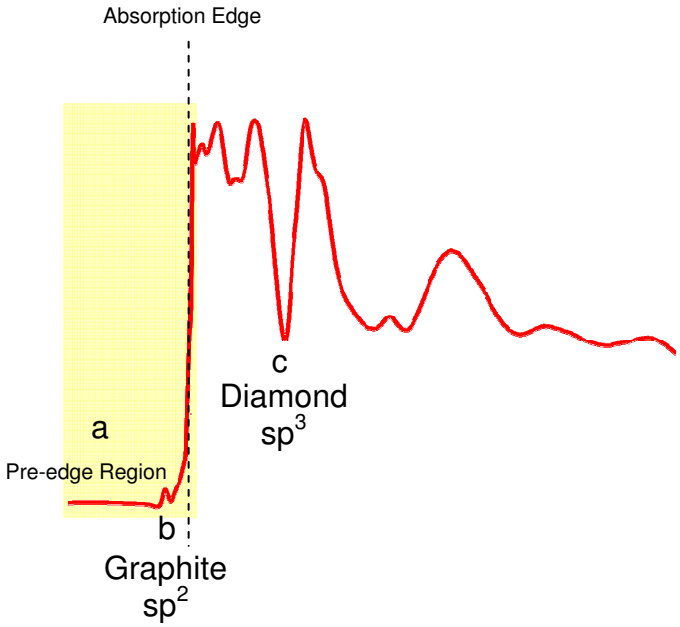

Figure 4-11: Schematic depicting the pre-edge region (highlighted) in the NEXAFS spectrum.

For instances whereby features are seen in the NEXAFS spectrum pre-edge, as is the case for graphite (see figure 4-8) it can be gathered that features exist within the band-gap as shown in the schematic in figure 4-12.

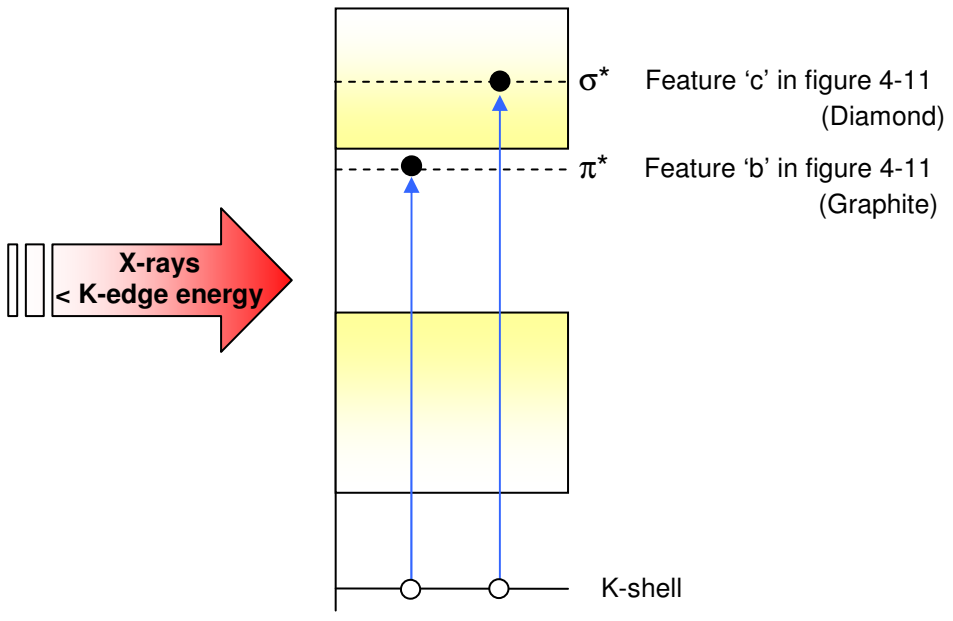

Figure 4-12: Pre-edge case, but with a π state and a σ* situated within the band-gap. Features can be observed in the pre-edge spectrum (figure 4-11) in some instances i.e. Graphite.*

4.4.4 Absorption Edge

The X-ray Absorption Near Edge Structure (XANES) region is concentrated at the onset of the edge and is the energy at which the transition of an electron from the core level to the lowest unoccupied state occurs (figure 4-13).

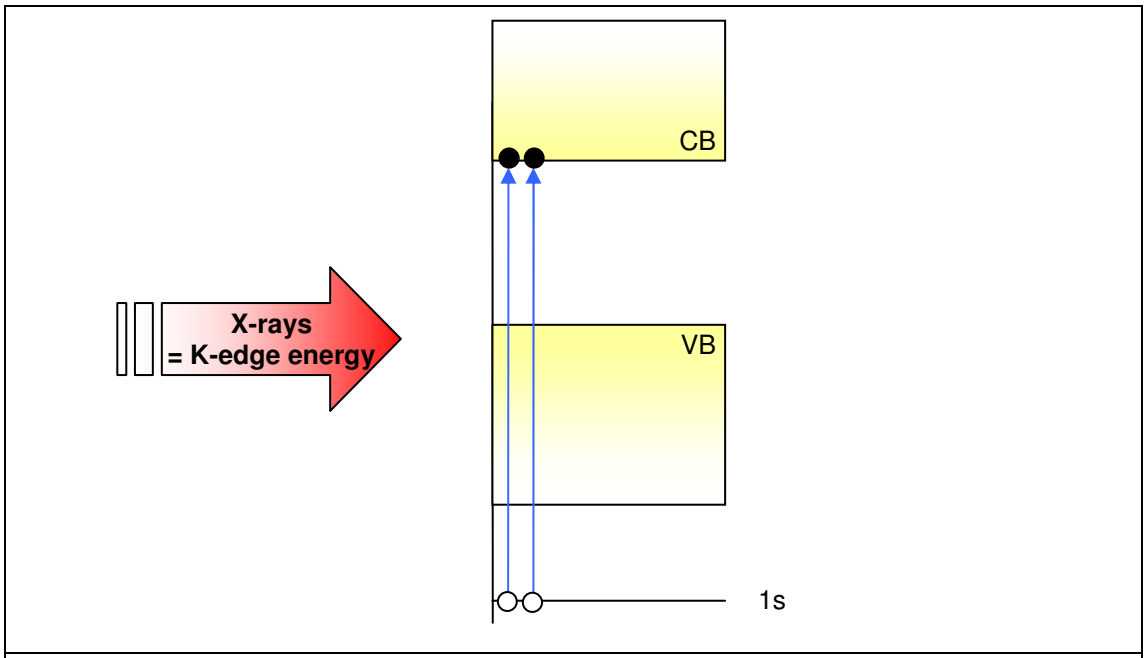

Figure 4-13: Schematic of X-ray absorption at the K-edge

The spectral region is highlighted in the figure below (figure 4-14).

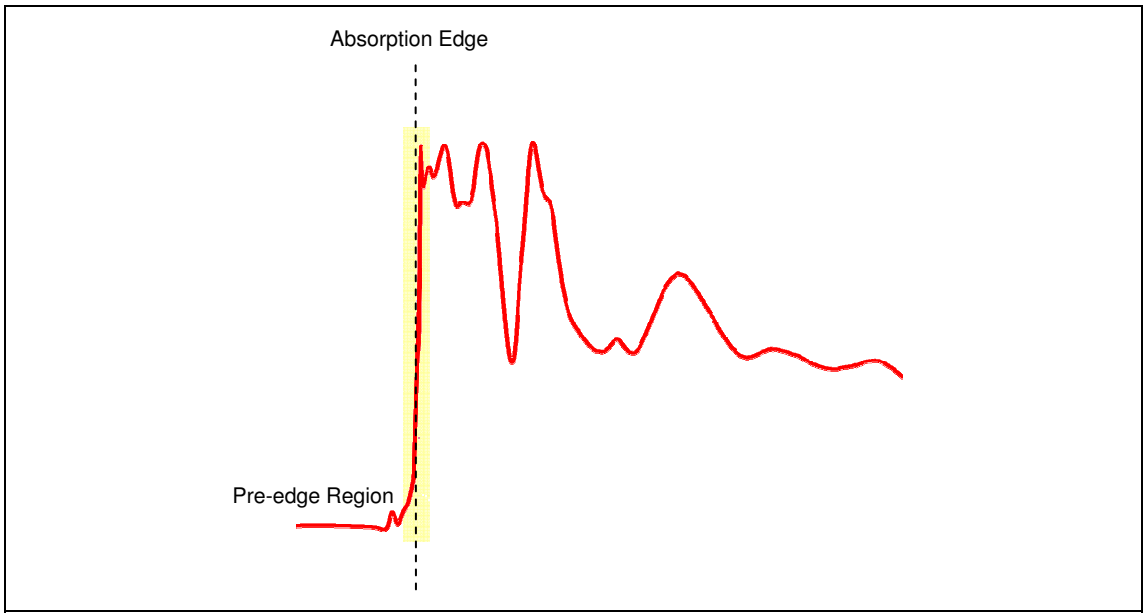

Figure 4-14: Absorption edge region on NEXAFS spectrum.

At the absorption edge, an increase in the signal occurs due to the increase in the absorption compared to the pre-edge level. A resonance level has been met. An excitation from the core level (K-shell) to the lower unoccupied state occurs as depicted in figure 4-13.

4.4.5 Above-edge

As the incident energy is further increased up to the binding energy of the 1s shell (284.25eV in carbon) and beyond, the excited electrons originate from the 1s core level and are excited up into the VB, this higher excitation energy has opened up a new channel for x-ray absorption and results in more electrons being excited into the CB – the number depends on the density of states in the CB and again a collection of these electrons gives a NEXAFS spectrum. Absorption has increased due to the fact that more electrons are present. This occurs due to the fact that as the energy reaches the binding energy of the 1s (core level) it excites an electron up into the CB. The core hole (now present) is highly energetic and causes an electron in the VB to drop down to fill the hole in the K shell. In order to do this that electron must lose energy to get there and it does this by transferring its energy to another electron and as a result "kicks" this (ionizes) into the CB as shown in figure 4-15 (red arrow indicates transfer of energy). This is known as an Auger electron emission.

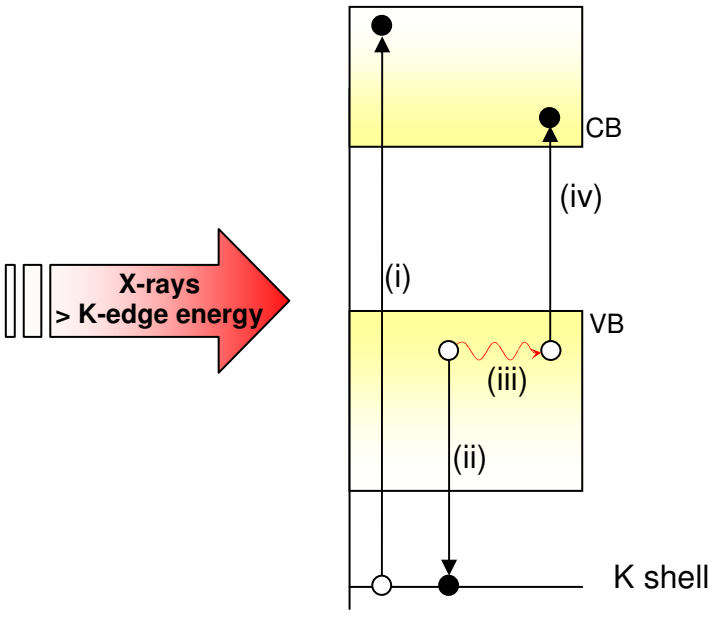

Figure 4-15: The Auger emission process. Excitation of an electron from the 1s shell to the CB (i). Electron re-combines (ii), and in order to do so, must loose energy. This loss of energy is transferred to another electron (iii), which results in that electron being ionized into the CB (iv).

Figure 4-16 shows the highlighted region of the NEXAFS spectrum at energies above that of the K-edge.

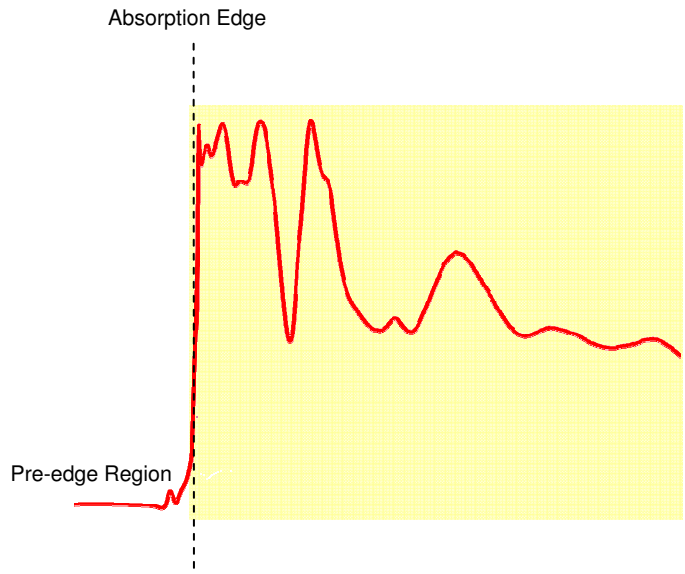

Figure 4-16: NEXAFS spectrum showing the higher energy (above K-edge binding energy) region.

4.4.6 Secondary Relaxation Events

As electrons are excited into the CB, holes are created as a result in the valence and core states. A relaxation event is when a system that has been irradiated and therefore has excited electrons into the CB, leaving highly energetic holes in the VB. These holes are filled via recombination processes resulting in a stable system. Three relaxation patterns exist for the recombination processes that occur, Fluorescence X-ray emission, the Auger process (already introduced) of which is more likely for low Z elements than x-ray decay, charge transfer and luminescent emission.

4.4.7 Fluorescence X-ray emission

The simplest recombination relaxation event results in a fluorescent x-ray emission whereby an electron recombines down into a core hole (situated in the 1s shell) as shown in figure 4-17 from a higher energy state. For the electron to recombine down to the core hole it must loose energy (the energy keeping it in the VB). As the electron recombines down into the 1s core state level the energy is lost and emitted as x-ray emission.

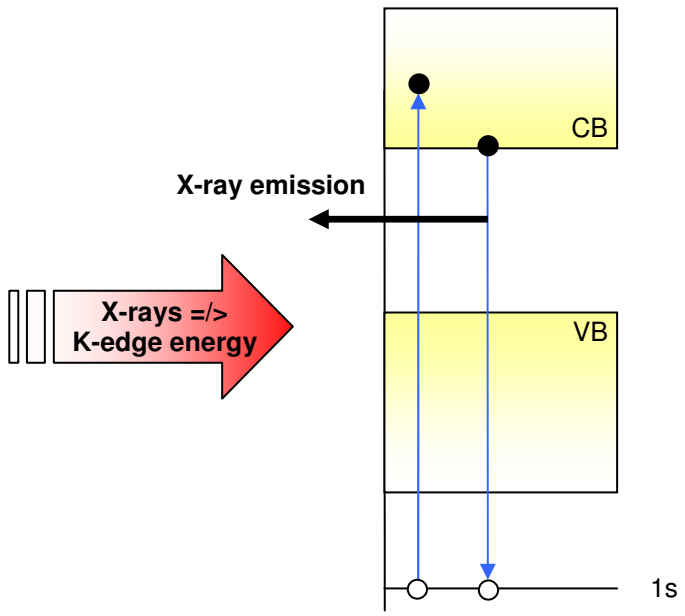

Figure 4-17: Schematic diagram of the fluorescence recombination process.

In 1985-1986 an important development occurred whereby the first demonstration of fluorescence was detected, it was firstly observed at the sulphur K-edge (2470eV) and then at the carbon K-edge (284.2eV) (*2*).

4.4.8 Charge Transfer and Surface Sensitive Luminescent Emission

The sampling depth and surface sensitivity is dependant upon the scattering of electrons within the sample. An electron's mobility within the material is governed by the inelastic mean free path which relates to the distance an electron can travel before being inelastically scattered, figure 4-18. Electrons that have been excited with an incident radiation such as x-rays move within the continuum with the kinetic energy that they have absorbed from the incident radiation and it is the mean free path that governs this mobility.

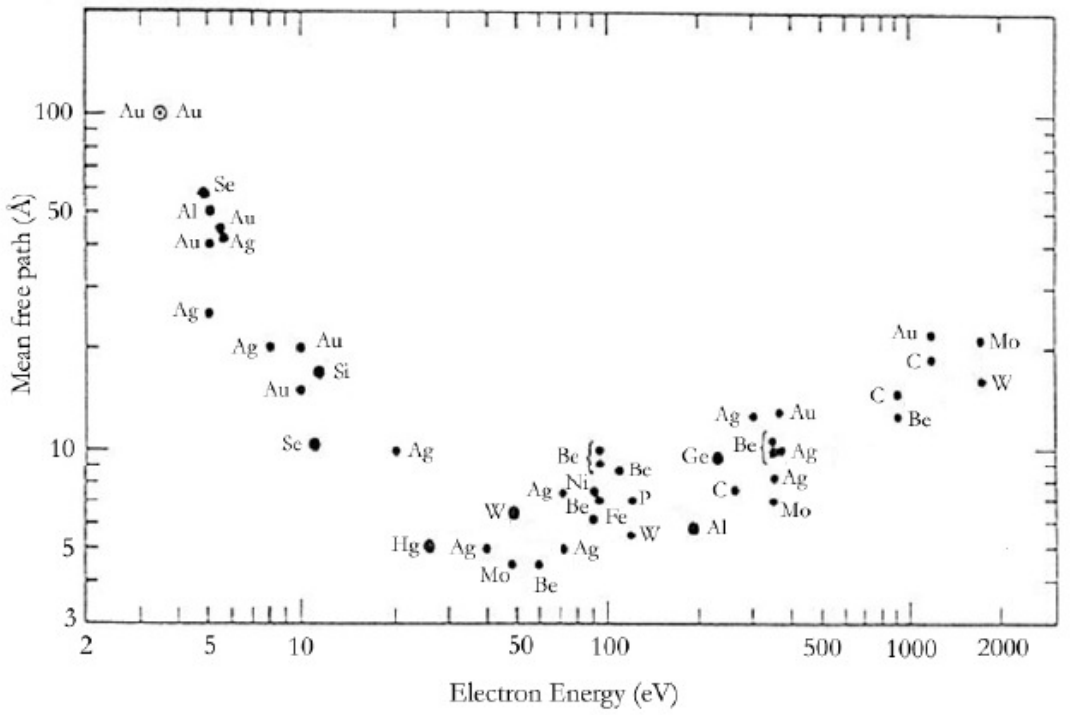

Figure 4-18: Inelastic mean free path of electrons experimentally measured in angstroms (7).

As the electron loses its energy it results in electrons populating the lowest conduction band states and holes populating the highest valence band states. The electrons recombine across the band-gap with the holes and emit energy. Optical Luminescence can occur when defect states are present within the band-gap and the electrons recombine back down via these defect states. This is the process that is involved during X-ray Excited Optical Luminescence (XEOL) whereby the X-ray source at a fixed incident energy is used as the excitation energy, to excite electrons up into the conduction band, the recombination results in the emission of light which can be measured using a monochromator and a PMT that give rise to information relative to the defects within that particular material. Further information on XEOL is provided later in this chapter as well as Photoluminescence (PL) – a similar process.

4.5 Optically Detected X-ray Absorption Spectroscopy (OD-XAS)

4.5.1 Introduction

NEXAFS has been introduced as a powerful research tool for the provision of information on the chemical structure and properties of materials utilized with the MoLES spectrometer mounted to a synchrotron beamline. The technique is well suited for samples that are uniform in nature and those that do not contain any features that may affect the chemical and optical properties of the sample, such as some of the single crystal samples used in this research.

For non-homogeneous samples such as the variegated samples used in this research the NEXAFS technique does not provide the spatial resolution or the accuracy of probing the chemical structure of individual bands or features commonly seen on non-uniform diamond samples. OD-XAS can provide this spatial resolution as will be explained here.

4.5.2 OD-XAS Theory

The Optically Detected X-ray Absorption Spectroscopy (OD-XAS) is a similar technique to NEXAFS. It works in a similar manner by the synchrotron generated excitation of electrons, from the VB into the conduction band by ramping incident x-rays in increments set by the user at energies ranging from below the absorption edge to above. A typical scan when studying i.e. Carbon would be from 280-320eV in order to scan over any possible pre-edge resonances (π^*, sp^2 bonded-carbon species) and resonances at higher energies (σ^*, sp^3 bonded-carbon species). The excited electrons now situated in the CB cascade/filter back down into the VB via defect states situated within the band-gap and as a result the recombination process produces luminescent light emission – it is this that is measured experimentally. The luminescent light provides the *same* information as the NEXAFS (electrons) signal but through a different source – light emission.

X-rays penetrate around 200nm into the diamond – fluorescent x-rays and optical photons originate within this region and hence the technique probes the bulk material

giving rise to an OD-XAS signal containing information that originates from deep within the bulk. Photoelectrons (measured in the NEXAFS technique) originate from within the topmost 1-10nm and hence probe the surface region. NEXAFS is therefore very sensitive to surface contaminants, i.e. sp^2 bonded carbon on the surface of the sample would be picked up in the spectrum quite significantly.

In conclusion, NEXAFS spectroscopy is much more sensitive to surface anomalies and fails in providing information on samples of which our interest lies in the bulk. It is also limited in the provision of localised information from inhomogeneous samples of which the spatial variation and visible differences are of particular interest – the actual probing regions of the sample cannot be identified.

Samples have been specially selected for the purpose of this thesis to provide the spatial variation required to provide a direct comparison of specific regions locally on the same sample.

The sample preparation for the purpose of these investigations consisted primarily of polishing not only to provide a flat surface for uniformity and limited light scattering but also for the provision that the brown coloured regions are situated as close to the surface as possible (see figure 4-19).

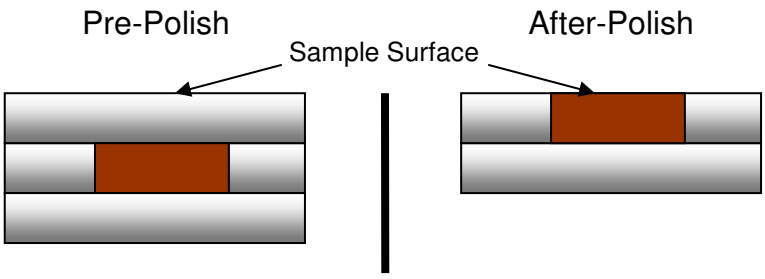

Figure 4-19: Schematic showing pre-polish and after-polish instances. The brown feature/colour that is of particular interest has been brought closer to the surface. Note – schematics ***not*** *to scale.*

The main emphasis of the experiment was to observe if any correlation exists between the sample colour and its local chemical structure.

NEXAFS spectroscopy's main limitation is that it fails in providing the lateral analysis of inhomogeneous samples and as a result for the purpose of identifying and gathering information on the local chemical structure of the variegated samples in this thesis, the OD-XAS technique was adopted coupled to the MoLES spectrometer (*8*) for homogeneous uniformly coloured samples and to the CLASSIX spectrometer (*9*) for the variegated samples for imaging purposes.

Figure 4-20 below shows a similar schematic to that in figure 4-9 for the NEXAFS technique. The schematic illustrates how the same information regarding the density of unoccupied states in the conduction band, can be gathered via the luminescence light that occurs as the electrons recombine back down to the valence band via defect states. The gathered light measured by a PMT (MoLES) or a CCD (CLASSIX) provides the OD-XAS spectrum which is very similar to that of the NEXAFS spectrum. The main differences are that the NEXAFS technique only probes around 1-10nm into the sample, therefore only providing information on the very surface of the sample in question. The OD-XAS technique probes much further into the sample, ~200nm, therefore providing information that originates from deeper within the bulk of the sample, limiting any surface anomalies. The OD-XAS technique is thus a bulk technique and is therefore much more apt for the analysis of the diamond structure particularly when analysing variegated diamond.

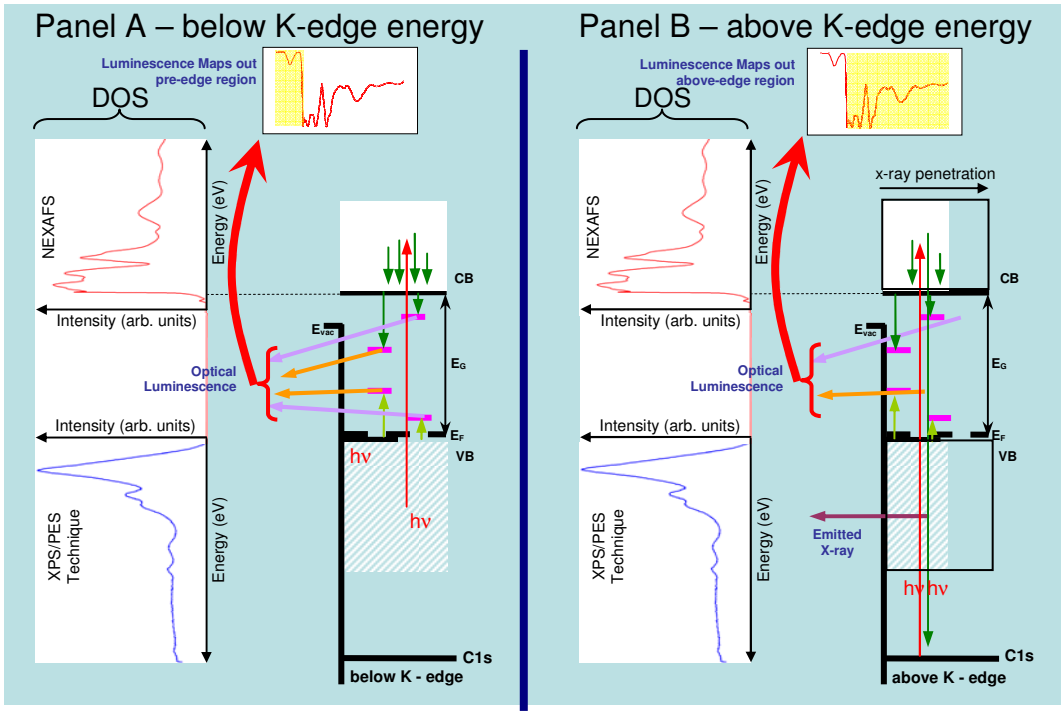

Figure 4-20: Schematic diagram of the processes involved. Panel A shows the transitions that occur when energy below that of the K-edge is incident upon the sample. The XPS technique can be used to map out the density of occupied states (DOS) in the VB. Optical luminescence occurs as the electrons recombine back down from the CB into the VB. Panel B shows the transitions that occur when higher energy is incident on the sample (above K-edge energy). Note how the x-ray penetration depth has changed at energies above the K-edge.

In the pre-edge situation, electrons are being excited from the valence band up into the conduction band throughout the X-ray sampling depth. Luminescence emission occurs as a result of the electrons recombining back down via the defect states situated within the band-gap and as for the NEXAFS case provides a non-resonant background level. At the absorption edge – a resonant excitation occurs as an electron from the core 1s level is excited up to the lowest conduction band site.

A typical NEXAFS spectrum taken in total electron yield (TEY) at room temperature (RT) and an OD-XAS spectrum taken in total luminescence yield (TLY) at low temperature (LT) for a diamond sample with graphitic features is shown in figure 4-21. This is similar to the types of spectrums that have been obtained during the course of this thesis.

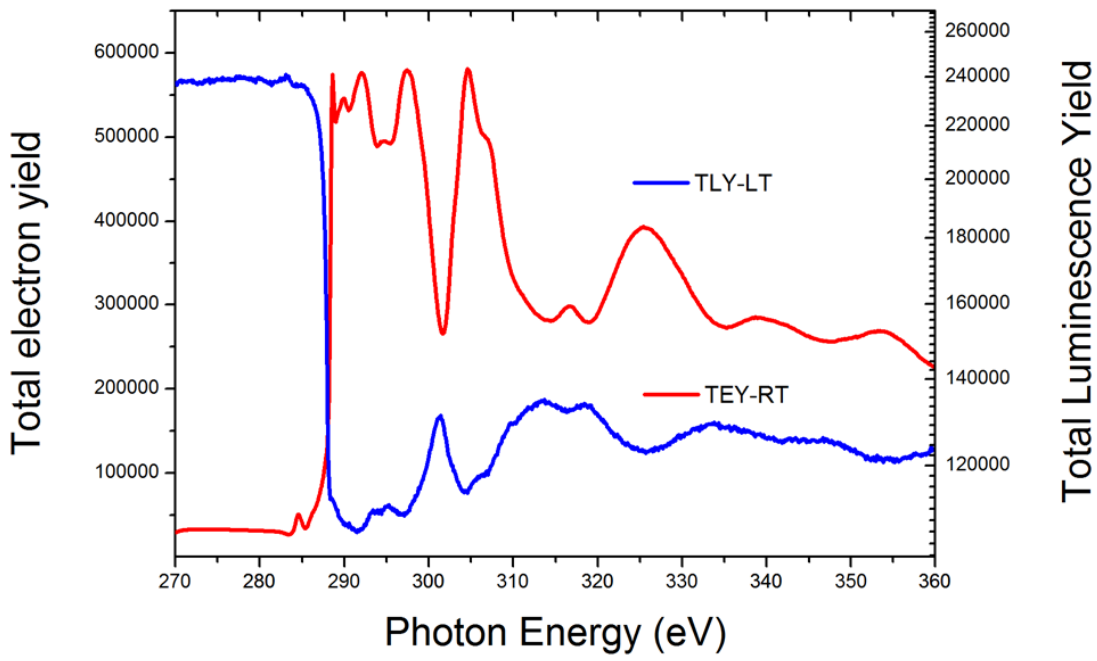

Figure 4-21: Schematic representation of the processes involved during XAS, along with the transitions involved relative to the spectrum obtained.

The OD-XAS technique is one of the few methods possible of directly relating the luminescence properties of solids to their structure and physical chemistry. Some examples of where it has been implemented are for the monitoring of corrosion on copper (*10*), porous silicon (*11, 12*), CaF_2 (*13*), aluminosilicates (*14*), organic light emitting materials (*15*) as well as rare-earth defects (*16, 17*).

4.5.3 Sample Thickness Studies

There are relative differences in the OD-XAS spectrum for a thin sample and a thick sample. The pre-edge region of the OD-XAS spectrum is typically the background non-resonant signal, and that at this instance the entire sample is being irradiated. This non-resonant background signal is therefore proportional to the amount of material being irradiated. In a thick sample this signal is large, and much larger than that for a sample of thickness that is less than the x-ray penetration depth.

In a thin sample, of which the thickness of the sample is less than that of the penetration depth, the x-ray penetration depth remains constant for this sample. The pre-edge level of the OD-XAS spectrum is again the background non-resonant level and in this instance is significantly less that that of a thicker sample. As the irradiation energy reaches the K-edge an increase in the luminescence yield is observed in the spectrum (figure 4-22a).

In a thick sample, as the energy is ramped up to the K-edge the signal decreases significantly due to the effective penetration depth reducing and therefore has an effect on the total volume of sample that's being irradiated with x-rays being absorbed, this is depicted by the decrease in the luminescence intensity of the signal (figure 4-22b).

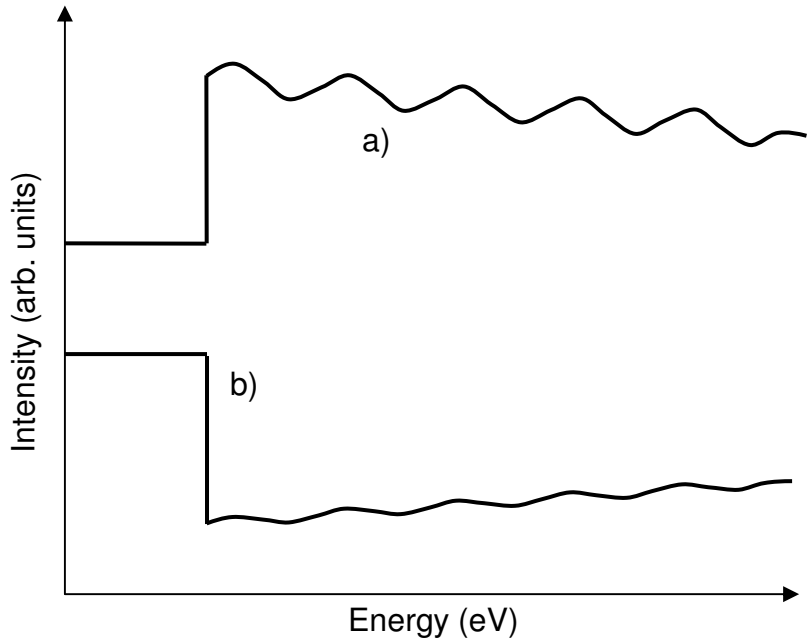

Figure 4-22: OD-XAS spectrum for a thin sample (a) and a thick sample (b) reproduced and adapted from (18).

4.5.4 Temperature effects on Luminescence

Temperature has a stark effect on luminescence in crystalline materials. There are two relaxation processes involved in luminescence. One is a radiative relaxation and the other is a non-radiative relaxation process.

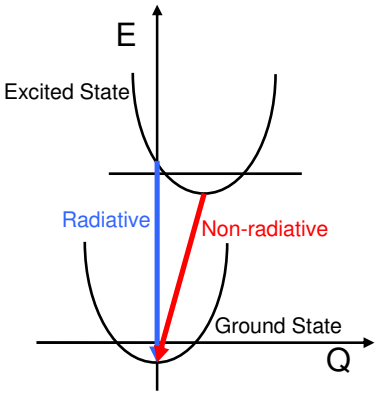

Figure 4-23: Luminescence recombination processes in a crystalline material.

A radiative emission is a process in which light is emitted and therefore can be measured by a PMT. A non-radiative emission dispels its energy thermally and can not be measured directly by a PMT for example. Temperature has a significant effect upon this component. The most significant effects can be observed at low temperatures whereby the luminescence signal is far stronger and more pronounced with more features present. At higher temperatures or whereby the temperature is increased, a quenching effect occurs. This is due to the increased probability of the decay/recombination of an excited electron being predominantly a non-radiative process. The rate of change in the population of the excited state can be described by,

$$\frac{dN_2}{dt} = G - \frac{N_2}{\tau_{radiative}} - \frac{N_2}{\tau_{non-radiative}} \qquad \textit{Equation 4-12}$$

N_2 is the population of the upper state (assumed to be proportional to the emission intensity I), G is the excitation rate and $\tau_{radiative}$ and $\tau_{non\text{-}radiative}$ are the radiative and non-radiative relaxation times.

Intensity remains constant when $\frac{dN_2}{dt} = 0$, a steady state. If G and $\tau_{radiative}$ are independent of temperature they can be assumed to remain constant, but $\tau_{non\text{-}radiative}$ has an activated temperature dependence given by,

$$\frac{1}{\tau_{non-radiative}} = Ae^{-\frac{E_A}{k_B T}} \qquad \textit{Equation 4-13}$$

E_A is the thermal activation energy of a non-radiative luminescent centre and A is the non-radiative recombination rate. By substituting into the previous equation and solving (for $\frac{dN_2}{dt} = 0$) the thermal quenching relationship can be obtained,

$$Intensity = \frac{I_0}{1 + B\,e^{-\frac{E_A}{k_B T}}} \qquad \textit{Equation 4-14}$$

($I_0 = G \times \tau_{radiative}$ and B is the ratio of $\tau_{radiative}$ to $\tau_{non\text{-}radiative}$).

The above equation is the standard equation used to describe thermal quenching of luminescence in a solid.

4.5.5 Temperature Effects on Electron Yield

Significant differences can be observed in the NEXAFS spectrum for the same sample when measured at low temperatures and room temperatures as shown in figure 4-24. At low temperatures and UHV conditions the sample effectively attracts impurities from its surroundings and causes them to settle on the surface. This yields a significant increase in the pre-edge features as is shown in the NEXAFS spectrum at low temperature (LT) (figure 4-24). It can be gathered that for experiments and investigations into the cause of the brown colour in diamond, room temperature (RT) measurements are more accurate at depicting the NEXAFS spectrum than at LT.

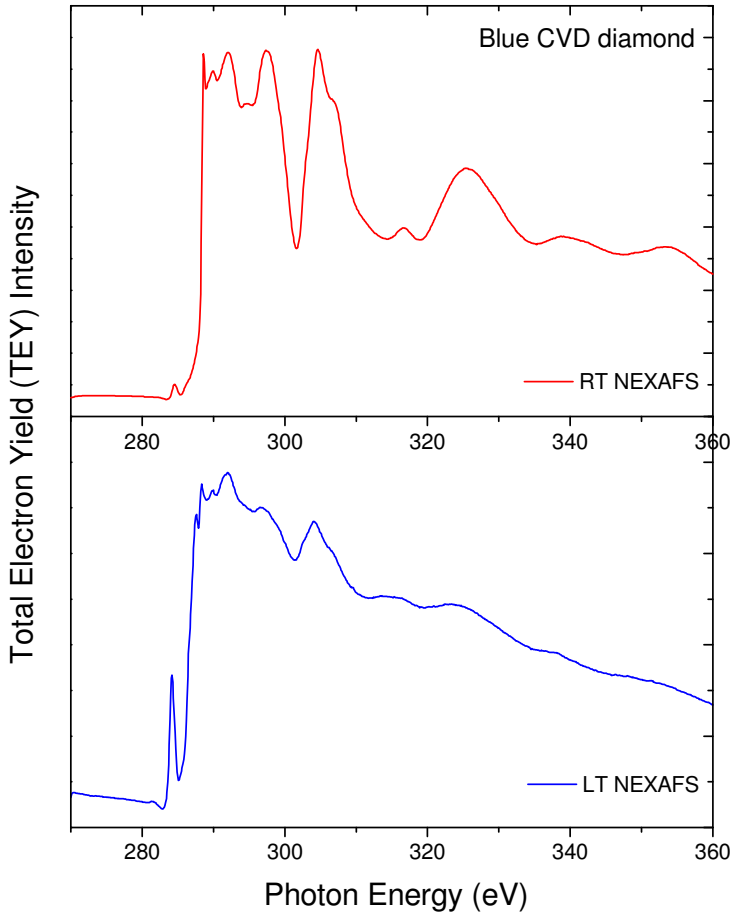

Figure 4-24: NEXAFS spectrum taken for the Blue CVD diamond at room temperature (RT) and low temperature (LT) showing a significant difference especially pre-edge, due to impurities on the surface of the sample being more prominent and of a higher amount.

4.5.6 Partial Luminescence Yield OD-XAS measurements

OD-XAS measurements are initially measured in total luminescence yield (TLY) typically to observe the whole OD-XAS spectrum and to see whether any features are observed in the spectrum. If particular features are observed then a PLY measurement can be obtained relative to the XEOL spectrum gathered for the sample in question.

If a particular band exists at i.e. 500nm in the XEOL spectrum for a sample under study, a PLY OD-XAS measurement can be taken through a filter that lies around the 500nm region. Results are then obtained to see whether the features observed in TLY are present in the PLY, and potentially can be attributed to a particular band in the XEOL and in turn identify the defect responsible. This correlation of the XEOL

emission to the PLY OD-XAS measurement can potentially directly link luminescence emission to its chemical origin. Measurements such as these have been carried out during the course of this research as well as for mixed phase samples (*19, 20*).

A summary of the Synchrotron Stimulated Luminescence techniques and their features used during the course of this research on diamond is presented in table 4-1.

Table 4-1: A summary of Synchrotron Stimulated Luminescence techniques.

Technique	**Energy (eV)**	**Energy Step (eV)**	**Detection**	
NEXAFS	280-320	0.2	Fixed: TEY (not via monochromator) PEY (particular monochromator wavelength)	MoLES (PMT)
XEOL	Fixed Energy: 280	---	Ramp Through: MoLES (monochromator) CLASSIX (Filter Wheel)	MoLES (PMT) CLASSIX (CCD)
OD-XAS	280-320	0.2	Fixed: TLY (No Filter) PLY (Particular Filter)	CLASSIX (CCD)

4.6 Luminescence Studies

4.6.1 Introduction

The study of the interaction of electromagnetic radiation with matter is referred to as spectroscopy and the measurement of luminescent centres, Luminescence Spectroscopy (*21*). Luminescence emission occurs as a result of an electron progressing from a higher energy state to a lower energy state whereby the difference in energy has to be lost and as a result is released as a photon. It is these photons that are studied during the course of luminescence spectroscopy experiments. The electron initially must be excited to a higher energy state for it to recombine and release a photon. This can be achieved by some form of irradiation such as UV or visible light (Photoluminescence (PL)), a beam of energetic electrons (Cathodoluminescence (CL)) or by x-rays (X-ray excited luminescence (XEL)). Another case is Thermoluminescence (TL) whereby the sample is stimulated by heating after initially being irradiated for the excitation of electrons in a different way, i.e. Beta Radiation or X-rays.

Key to the characterization of luminescent materials is its quantum yield. This is the ratio of the number of photons emitted by the sample relative to the number initially absorbed. Luminescence spectroscopy is a study of this quantum yield and lifetime.

A large quantum yield results in high luminescence intensity and the lifetime of the sample is related to the average time the electron spends in the excited state before recombining back down to the ground state.

The general equation of the electronic transition between two energy levels E_1 and E_2 (E_2>E_1) is,

$$\frac{hc}{\lambda_0} = E_2 - E_1 \qquad \textit{Equation 4-15}$$

'λ_0' is the radiation emission wavelength. '*c*' is the speed of light (2.997 x 10^8 ms^{-1}) and *h* is Planck's constant (6.626 x 10^{-34} J s).

4.6.2 Photoluminescence (PL)

Photoluminescence (PL) is the spontaneous emission of light from a material when excited by an optical source such as a laser. The material's band-gap and defect states can be investigated and is a non-contact and non-destructive technique. Excitation arises therefore from the absorption of photons.

4.6.2.1 Photoluminescence Concepts

The population of states occurs as the incident light is absorbed by the material. The radiative transitions of the electrons back to the electronic and associated vibronic levels of the ground state result in a narrow line-structure which composes of a sharp zero-phonon line (ZPL) and vibronic side-band. All defects have their own spectral shape and are unique for each optical centre. This allows for the identification of defects and in turn the characterisation and knowledge of the material for its implementation in a particular concept (*22*).

4.6.3 X-ray excited optical luminescence (XEOL)

XEOL measurements provide the user with detailed emission spectrum that can then be fitted with Gaussian fits that indicate the relative trapping parameters that give rise to the emission spectrum obtained. These can be attributed to defect states within the sample under study as well as the nature and identification of the doping involved.

XEOL measurements are comparable with PL studies, but have the added advantage over PL of providing a higher excitation energy resulting in a complete excitation of the sample under question i.e. for Diamond – band gap of ~5.5eV – by using a 404nm laser source it can only probe 3.07eV "into" the band-gap. Thus any deeper traps cannot be probed or even identified as being present with PL. XEOL provides

complete coverage of the 5.5eV band-gap thus gathering all of the relative information on the luminescence properties and trapping parameters.

XEOL studies have previously been applied in the study of Boron Nitride (BN) samples of different chemical structure or polytypes, mainly hexagonal (h-BN) and cubic (c-BN) (*23*). Differences were found in the emission spectrum for both samples in the 2 – 5eV energy range which consisted of a number of broad overlapping emission bands (*23*).

The mechanical properties of BN and C are very similar. The h-BN and c-BN are similar to the carbon equivalents of graphite and diamond respectively but when it comes to their electronic properties they are significantly different. In this study, diamonds of different types have been investigated using different luminescent excitation sources such as, Synchrotron Radiation at the Daresbury Laboratories in Warrington, 404nm Laser Excitation (for PL) and a hard X-ray Cu K_α source (for XEOL) both of which are situated in house at Aberystwyth University. The X-ray Excited Optical Luminescence (XEOL) measurements are obtained via the recently purchased Cu-K_α X-ray source. The incorporation of this source including an enclosed shutter system has been fitted to the mobile end station, MoLES (*8*) (see chapter 3, section 3.4.1) for offline XEOL investigations.

4.6.3.1 XEOL measurements for samples

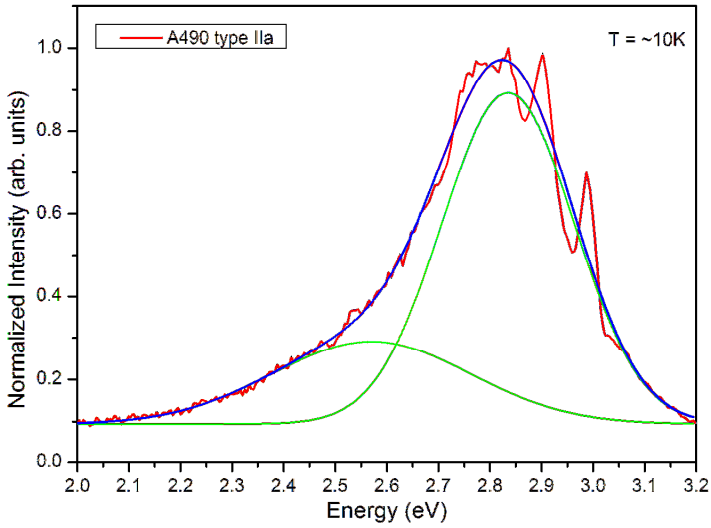

Figure 4-25: XEOL spectrum taken at ~10K of a type IIa naturally brown diamond sample showing two components relative to the emission spectrum with peaks situated at 2.57eV and 2.84eV excitation energies.

Figure 4-25 shows a typical XEOL spectrum that has been gathered using the MoLES end station spectrometer for a type IIa naturally banded diamond. This brown banded sample's (see photograph in Results foreword) XEOL spectrum was gathered over the whole area of the sample. MoLES doesn't provide the spatial resolution required to exactly identify a signal that comes from a brown banded region. Further analysis and comments on the XEOL spectrum can be found in chapter 5.

4.6.4 Cathodoluminescence (CL)

Cathodoluminescence is also a technique whereby the luminescence spectrum of a particular luminescent sample can be obtained.

Instead of excitation by a laser or x-rays as in Photoluminescence and XEOL respectively, CL provides excitation by the bombardment of a beam of electrons.

In contrast to photoluminescence (PL), cathodoluminescence (CL) will lead to all of the possible radiative channels in the sample. However, negatively charged defects will not be excited.

CL was not a technique used during the course of this research and shall not be delved into further, although results and features appear in CL as well as in PL and therefore some CL papers have been referred to during analysis of the data obtained.

4.6 Raman Spectroscopy

4.6.1 Introduction

Raman spectroscopy was firstly theoretically predicted by A. Smekal in 1923 (*24*) and then in 1928 C. V. Raman studied the scattering of light by a dense medium (*25*). The effect was later named after him (*26*).

Raman has become a widely used method of analysing semiconductor layers, and the quality of CVD diamonds (*27-31*). It provides the required sensitivity to monolayer thickness as well as being a non-destructive technique. The evolution of equipment has led to the Raman technique being implemented in imaging mode with lateral probing of, for example, variegated samples as in this research. It can also be utilized to probe variable depths.

Raman spectroscopic analysis provides information in identifying materials and compounds. It can also provide information on the layer orientation, stress and crystalline perfection, as well as a sample's electronic properties. In this section the basic principals of Raman scattering are introduced and discussed. It is very sensitive to the molecular bonding and structure of a sample lattice under study. A distinct spectral pattern can be obtained for an individual sample, characteristic of features that are incorporated within.

4.6.2 Theory

The Raman process can be described as follows, when a sample is irradiated with monochromatic radiation such as a 632.8nm HeNe laser, it can induce an electronic transition if energetic enough. If not, then this incident photon can be weakly scattered predominantly by the sample lattice or generally in one of three different ways. One of which is Rayleigh scattering, caused by the polarizability of the sample whereby there is no energy loss and provides no information in Raman spectroscopy – it is a weak scattering process. Secondly, Tyndall Scattering consists of the incident light being scattered from dust particles or impurities within the sample.

The third form of scattering also occurs at different frequencies to that of the source. This is the frequency shift as will be explained further in the next section.

4.6.3 Principles of Raman Spectroscopy

Inelastic light processes are studied in Raman spectroscopy. It is the scattering processes that occur as energy is transferred from an incident photon of energy $\hbar\omega_I$ and the sample under study. As a result a scattered photon of different energy $\hbar\omega_S$ is generated. The transferred energy corresponds to the eigenenergy $\hbar\Omega_j$ of an elementary excitation labelled *'j'* in the sample such as a phonon, a polariton, a Plasmon, a coupled plasmon-phonon mode or a single electron or hole excitation (*32*).

The equation for the processes involved is shown below,

$$\hbar\omega_S = \hbar\omega_I \pm \hbar\Omega_j \qquad \textit{Equation 4-16}$$

The ± symbol refers to the Raman processes of Stokes ('–') and anti-Stokes ('+') as is illustrated in figure 4-26.

The source usually used consists of a monochromatic light source such as a visible, near infrared or near ultraviolet laser. In this instance a Horiba Jobin Yvon LabRam HP Raman Spectrometer coupled to a Class 3B HeNe laser (632.8nm) has been used. As laser light interacts with phonons or other excitations in the system, the energy of the laser photons are either shifted up or down. The shift in energy gives information relative to the phonon modes within the system.

The sample is irradiated with the HeNe laser and the light from the illuminated region of the sample is collected through a lens and passed through a monochromator. Filtering occurs, whereby the wavelengths close to that of the laser line, due to Rayleigh scattering are filtered out and the rest of the gathered light is directed onto a CCD detector.

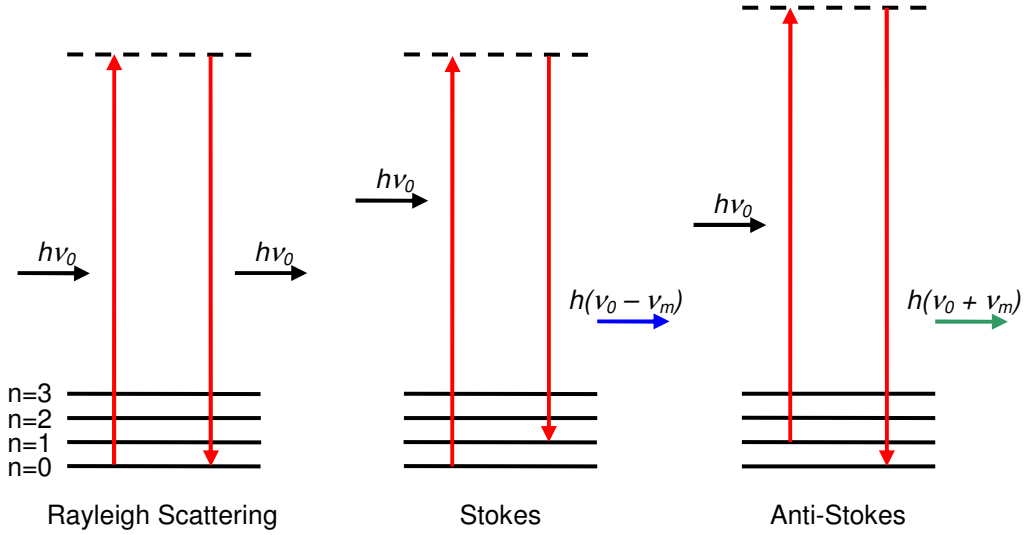

Figure 4-26: Raman processes. (Vibrational energy transitions) with an incident photon of energy $h\nu_0$.

As depicted in figure 4-26, the vibrational frequency ν_m is measured as a frequency shift from the incident beam ν_0. The energy shift of the scattered light can be described as,

$$E = h\nu_m = hc\tilde{\nu} \qquad \textit{Equation 4-17}$$

where *'h'* is the Plank constant, *'c'* is the speed of light and '$\tilde{\nu}$' is proportional to the scattered light's energy loss or gain in units of reciprocal centimetre.

$$[\tilde{\nu}] = \left[\frac{\nu_m}{c}\right] = cm^{-1} \text{ with } 1cm^{-1} \cong 1.24\times10^{-4}\ eV \qquad \textit{Equation 4-18}$$

Raman spectroscopy can be performed at various excitation energies; however, sample fluorescence is reduced by using near-infrared excitation. Fluorescence is undesirable as it can obscure the Raman signal. Red wavelength excitation is also less likely to cause photo-decomposition or thermal damage due to absorption. Work has been carried out on the study of diamond with different excitation sources of different wavelength (*33*).

4.6.3.1 Diamond and Graphite Raman Signatures

Raman spectrums provide the user with a wide range of structural and phase information regarding the sample under study and has the added advantage of being a non-destructive tool with the capabilities of surface region analysis within a few nm below the surface as well as deeper regions up to the μm range (*32*). The samples can be characteristically analysed to provide information relating to the physical properties such as shown in figure 4-27 for diamond and graphite.

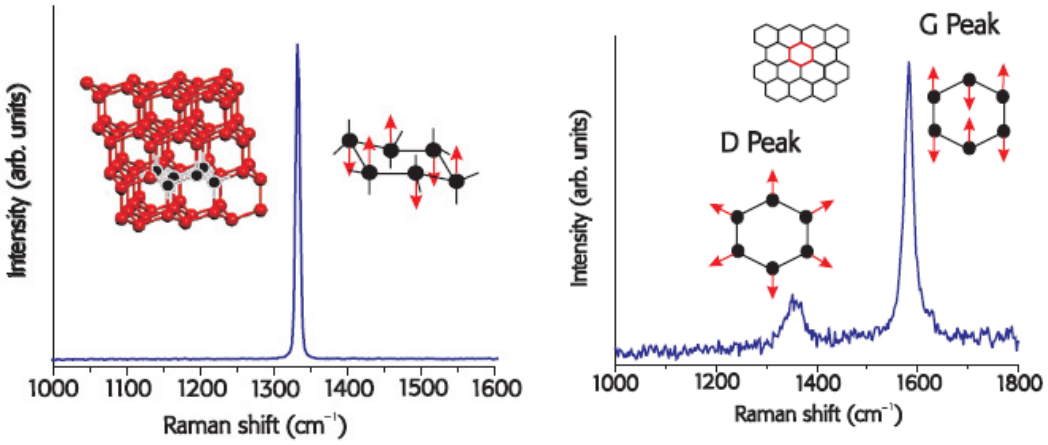

Figure 4-27: Typical Raman spectrum for diamond (left) and graphite (right), taken from (28).

Diamond signatures relating to its Raman spectrum consists of a single sharp peak at 1332cm^{-1}. This is indicative of a high quality crystalline diamond (*34, 35*). This peak relates to the sp^3-bonded carbon present within the diamond crystal.

Signatures typically indicative of Graphite or sp^2-bonded carbon species are found around the 1500-1600cm^{-1} region (*36*) further information on these types of features is presented later in the thesis.

The Raman technique is a well established and widely used experimental tool for the analysis of semiconductor layers, heterostructures and interfaces. Among the main reasons for its wide-spread application is its sensitivity for thin films down to monolayer (ML) thickness, combined with its variable information depth. The Horiba Jobin Yvon LabRam HP Raman Spectrometer at the materials laboratory in Aberystwyth has these Raman mapping capabilities and has been used for the purpose

of characterizing the brown colouration and brown banding within the diamond samples for the purpose of this thesis primarily utilized in imaging mode for Raman mapping measurements.

4.7 Summary

This chapter has introduced the main concepts in relation to XAS techniques. An understanding of the theory is vital for the correct determinations and analysis of the results (see chapter 8). The luminescence principles have also been introduced as well as the Raman technique, all of which have been applied in the study of brown and brown banded diamonds during the course of this research. The following section provides a foreword introducing the samples studied along with the experiments that have been performed during the course of this research.

4.8 References

1. H.A. Liebhafsky, H.G. Pfeiffer, E.H. Winslow, P. D. Zemany, *X-ray Absorption and Emission in Analytical Chemistry*. (Wiley, 1960).
2. J. Stohr, *NEXAFS Spectroscopy*. (Springer, 1996).
3. A. L. Ruoff, *Acc. Chem. Res.* **21**, 223 (1988).
4. www.chemphys.lu.se/research/techniques/xrayxas. (2010).
5. A. C. Thompson, D. Vaughan, *X-ray Data Booklet*. (Lawrence Berkley National Laboratory, 2001).
6. http://www.chemphys.lu.se/research/techniques/xrayxas/.
7. A. Zangwill, *Physics at Surfaces*. (Cambridge University Press, 1988).
8. F. Quinn *et al.*, *Journal of Synchrotron Radiation* **10**, 461 (2003).
9. N. R. J. Poolton, B. M. Towlson, B. Hamilton, D. A. Evans, *Nuclear Instruments & Methods in Physics Research Section B-Beam Interactions with Materials and Atoms* **246**, 445 (2006).
10. M. G. Dowsett *et al.*, *Analytical Chemistry* **80**, 8717 (2008).
11. D. A. Hill *et al.*, *J. Phys IV France* **7**, 553 (1997).
12. G. Dalba *et al.*, *Physical Review B* **62**, 9911 (2000).
13. A. Bianconi, D. Jackson, K. Monahan, *Physical Review B* **17**, 2021 (1978).
14. N. Poolton *et al.*, *Journal of Physics D-Applied Physics* **36**, 1107 (2003).
15. Y. F. Hu *et al.*, *Review of Scientific Instruments* **73**, 1379 (2002).
16. L. Soderholm, G. K. Liu, M. R. Antonio, F. W. Lytle, *Journal of Chemical Physics* **109**, 6745 (1998).
17. M. Ishii *et al.*, *Applied Physics Letters* **78**, 183 (2001).
18. S. Emura *et al.*, *Physical Review B* **47**, 6918 (1993).
19. D. A. Evans, A. R. Vearey-Roberts, N. R. J. Poolton, *Applied Physics Letters* **89**, (2006).
20. N. R. J. Poolton, E. Pantos, B. Hamilton, P. M. Denby, O. Johnsen, *Physica Status Solidi B-Basic Research* **241**, 3656 (2004).
21. M. Gaft, R. Reisfeld, G. Panczer, *Luminescence Spectroscopy of Minerals and Materials*. (Springer, 2005).
22. K. Iakoubovskii, G. J. Adriaenssens, *Physical Review B* **61**, 10174 (2000).
23. D. A. Evans *et al.*, *Journal of Physics-Condensed Matter* **20**, (2008).
24. A. Smekal, *Naturwiss* **11**, 873 (1923).

25. C. V. Raman, K. S. Krishnan, *Nature* **121**, 501 (1928).
26. T. R. Gilson, P. J. Hendra, *Laser Raman Spectroscopy*. (Wiley-Interscience, 1970).
27. P. K. Bachmann *et al.*, *Diamond and Related Materials* **3**, 1308 (1994).
28. J. Filik., *Spectroscopy Europe* **17**, 10 (2005).
29. D. S. Knight, W. B. White, *Journal of Materials Research* **4**, 385 (1989).
30. C. D. O. Pickard, T. J. Davis, W. N. Wang, J. W. Steeds, *Diamond and Related Materials* **7**, 238 (1998).
31. P. Ascarelli, E. Cappelli, G. Mattei, F. Pinzari, S. Martelli, *Diamond and Related Materials* **4**, 464 (1995).
32. Günther Bauer, Wolfgang Richter, *Optical Characterization of Epitaxial Semiconductor Layers*. (Springer, 1996).
33. G. Niaura, R. Ragauskas, A. Dikcius, B. Sebeka, Z. Kuodis, *Chemija* **20**, 78 (2009).
34. A. C. Ferrari, J. Robertson, *Physical Review B* **63**, (2001).
35. S. Prawer, R. J. Nemanich, *Philosophical Transactions of the Royal Society of London Series a-Mathematical Physical and Engineering Sciences* **362**, 2537 (2004).
36. J. E. Field, *The Properties of Natural and Synthetic Diamond*. (Elsevier Academic Press, 1992).

Part II

Results - Foreword

Introduction

This second part of the thesis dedicates itself to the results obtained through the various techniques that have been applied to the study of brown and brown banded diamond. This foreword is a short introduction to the samples studied and a summary of all the experiments undertaken on the diamond samples

Samples studied, an introduction

Diamond samples were supplied with much gratitude form the Diamond Trading Company (DTC) and Element Six Ltd. All samples have been carefully selected to provide the depth of colour and colour variation required for the purpose of this research.

The Mix-phased materials such as the natural and synthetic banded diamonds have been carefully selected and purposely grown to provide the non-homogeneity required for the purpose of identifying the brown regions present in the samples as well as to identify the chemical and physical structure that is responsible for the variety in colour that is found within a sample.

The extended bands, highlighted in these samples by polishing perpendicular to their direction are the focus of this study.

A summary of all the samples studied for the purpose of this research are presented on the following pages.

Natural Diamonds

Uniformly Coloured samples

Sample Name	**A455-13-04**	**A455-13-02b**
Photograph		
Type	IIa	IIa
Orientation	-	-
Dimensions	3.85 x 3.71 x 1.38mm	1.94 x 3.36 x 1.76mm
Colour	Uniform Brown	Brown prior to HPHT treatment, Colourless
Carat	0.34 ¢	0.14 ¢
Treatment	NONE	HPHT (~10GPa, 2550°C for 1hr)

Sample Name	**A330-20**	**typeIIa_1**
Photograph	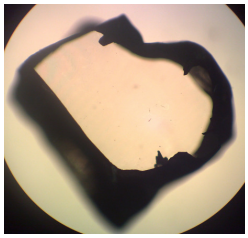	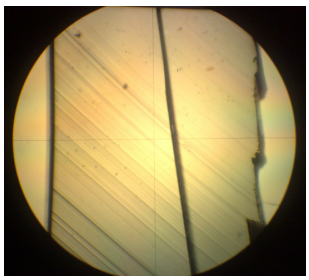
Type	IIa	IIa
Orientation	-	{100}
Dimensions	4.06 x 3.34 x 1.77mm	3.92 x 6.92 x 1.35mm
Colour	Naturally Colourless	Naturally Colourless
Carat	0.24 ¢	-
Treatment	NONE	NONE: note – polishing lines are visible in image above.

Banded Diamond samples

Sample Name	**A465-40-03**	**A465-40-04**	**A490-159**
Photograph			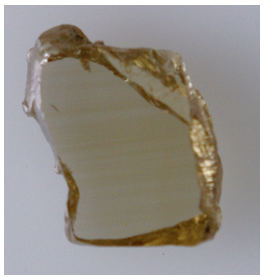
Type	Ia	Ia	IIa
Orientation	{110}	{110}	{110}
Dimensions	5.48 x 5.40 x 1.28mm	4.48 x 5.47 x 1.07mm	6.43 x 7.92 x 2.54mm
Colour	Diagonal Brown Bands	Diagonal Brown Bands	Horizontal Brown Bands
Carat	0.26 ¢	0.37 ¢	1.50 ¢
Treatment	NONE	NONE	NONE

Synthetic Diamonds

Uniformly Coloured

Sample Name	**Blue CVD**	**0473906**	**0473904**
*Photograph**	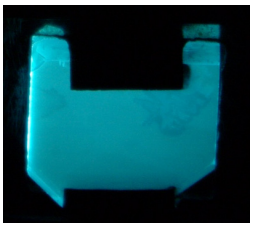	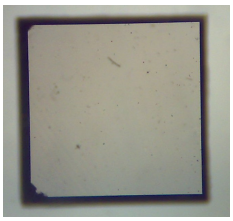	
Type	Single Crystal CVD	Single Crystal CVD (small)	Single Crystal CVD (large)??
Orientation	{100}	{100}	{100}
Dimensions	7.5 x 7.5 x 1.5mm	3.82 x 3.98 x 2.61mm	7.78 x 8.43 x 2.71mm
Colour	Blue	Brown	Brown
Carat	-	0.70 ¢	1.90 ¢
Treatment	NONE	NONE	NONE

*Photograph for the Blue Single Crystal CVD was taken when irradiated with X-rays.

Diamonds Inclusive of Brown Features

Sample Name	**0673803****	**0542715*****
Photograph	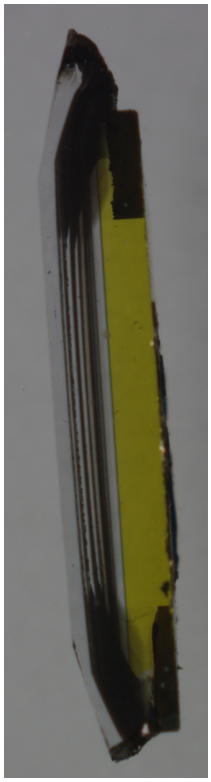	 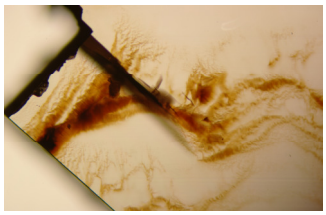
Type	CVD	CVD
Orientation	{100}	{100}
Dimensions	0.80 x 5.36 x 0.85mm	5.67 x 6.10 x 0.36mm
Colour	Layered Brown	Brown Features
Carat	0.06 ¢	0.15 ¢
Treatment	Features grown by varying gases/temperatures	Features grown by varying gases/temperatures

** CVD sample has been grown on a HPHT substrate shown on the right part of the sample from above photograph. Grown from right-to-left.

*** CVD sample has been grown perpendicularly ‘out of the paper’.

Birefringence

Small differences in crystal orientation at different parts of a diamond which may have solidified under unsatisfactory conditions would result in enormous stresses and strains being present during the crystal growth. These stresses can be revealed when the sample is placed between two polarisers with light shining through. Diamonds with internal flaws or inclusions therefore unsurprisingly exhibit birefringence, the absence of birefringence is a good test of crystal perfection (*1*). In Raman's paper in 1944, he states that cleavage plates once with birefringence observed within could be freed from stresses when they break off. This could be due to the stresses upon them originating directly from faults or irregularities elsewhere in the crystal.

The birefringence patterns of the samples studied during the course of this study are briefly touched upon in this thesis with significant differences apparent between natural and synthetic diamonds. As well as this, differences are observed when two type IIa diamonds of the same origin i.e. cut from the same original stone and with one HPHT treated are compared.

Previous studies such as those by Raman (*1*) show that a relationship exists between the direction of the brown bands and the birefringence pattern in the samples studied. The birefringence images were gathered by using two Polaroid filters at 90° to each other and putting the sample for study in between the polarisers as shown in the schematic in figures (i) and (ii).

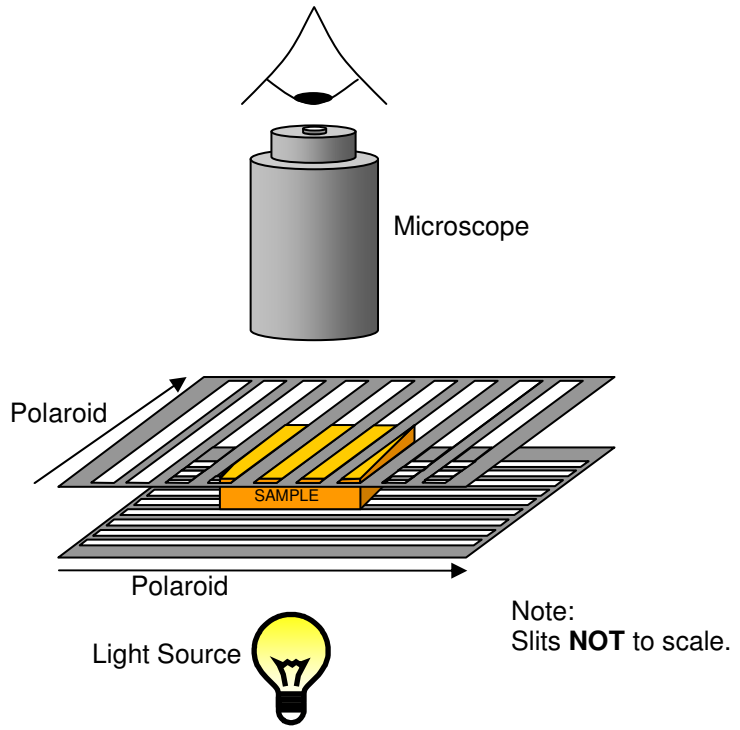

Figure (i): Schematic setup of the birefringence measurements taken for the diamond samples.

Applying the above setup (figure (i)) with a diamond sample sandwiched between two polarisers and at 90° to each other provides the image shown in figure (ii). A completely dark image is expected when no sample is present, with no light transmitted at all. An image is obtained when a diamond sample is present. Through this setup a birefringence image was obtained showing the stress lines within the diamond sample created as the diamond was formed deep in the earth's crust from temperature and pressure changes. In order to view this type of image it is clear from the schematic diagrams above that the diamond sample has in some way twisted the polarised light.

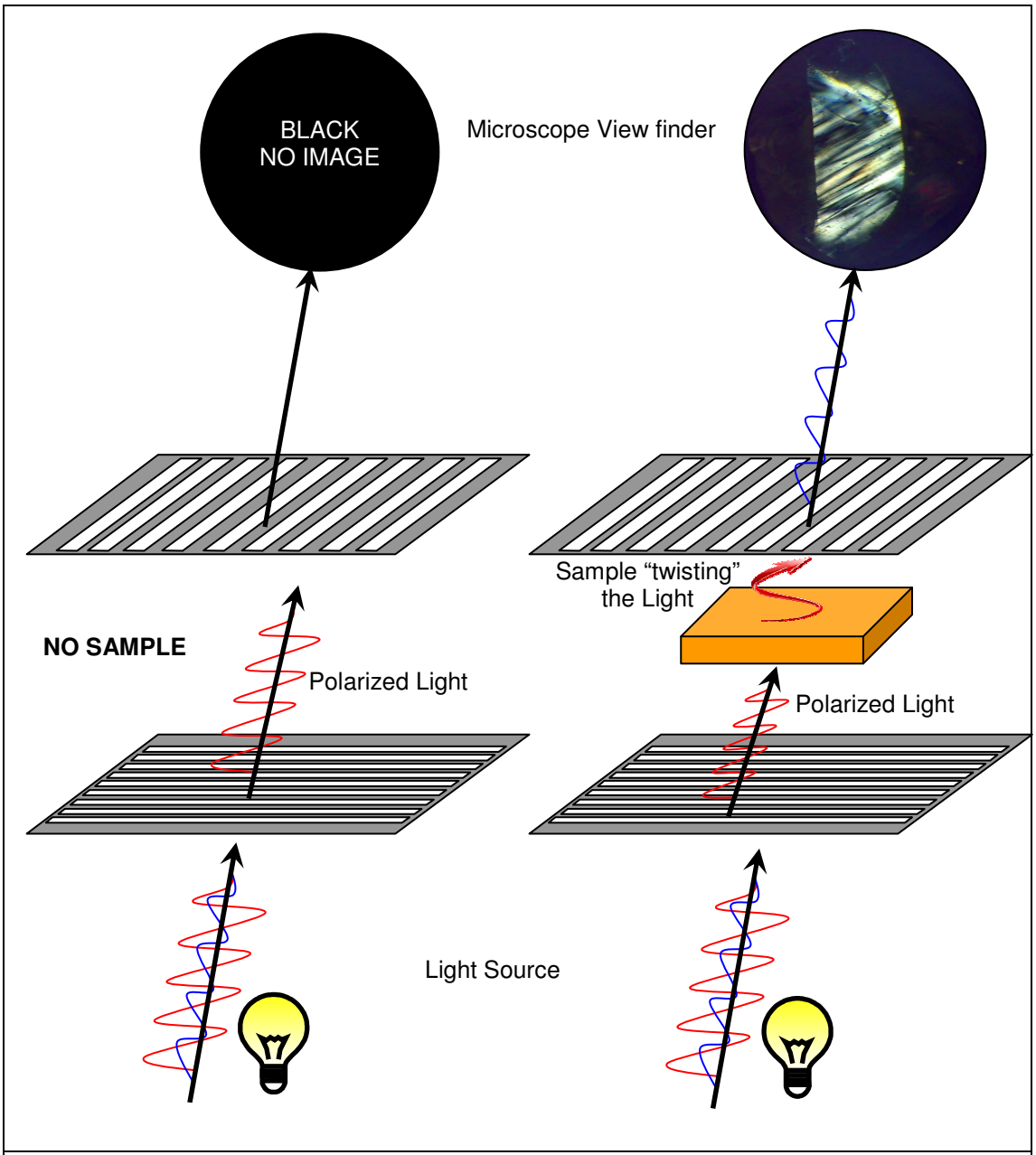

Figure (ii): Schematic of Birefringence observations with no sample present on the left therefore producing a dark observation and a type Ia naturally banded sample (for example purposes) on the right. Clearly shown here is the diamond "twisting" the light.

The birefringence images for the diamond samples are often provided with the diamond photograph in the results section of this thesis for the reader's interest as the banding correlates with the direction of the birefringence pattern in most cases.

AFM measurements

Initial measurements on the brown banding were required to be made via AFM. This was to clarify that the brown bands present in some of the diamond samples were not due to polishing effects or surface effects.

Figure (iii) provides an AFM image gathered for the A490 type IIa naturally banded diamond.

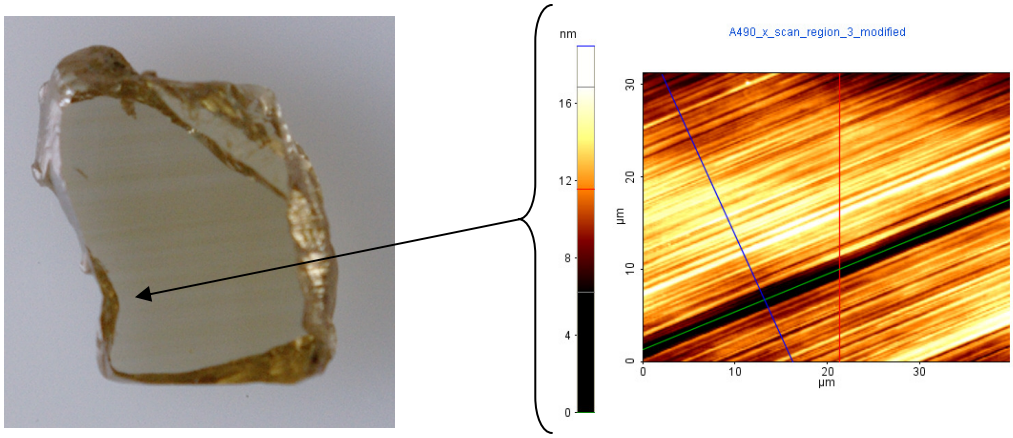

Figure (iii): AFM image taken from indicated region for the naturally banded type IIa diamond sample.

Images such as the one presented in figure (iii) were obtained for all samples and due to the banding observed in the AFM image not correlating with the brown banding direction, it therefore confirmed that the brown banding could not be measured with the AFM. The banding observed in figure (iii) are the polishing lines with an average mean roughness of ~4nm.

References

1. C. V. Raman, G. R. Rendall, *Proc. Indian. Acad. Sci* **A19**, 265 (1944).

Experiment Summary – Characterisation Techniques

Location	**Aberystwyth University Materials Laboratory**					**TU Delft/Aberystwyth**		**Synchrotron Based**								
	PL	**Raman**	**Raman Mapping**	**PP**†	**XEOL (Aber)**	**TL**†		**XEOL**	**NEXAFS**	**OD-XAS**	**OD-XAS**					
Instrument/ Spectrometer	MoLES	Horiba Jobin Yvon	Horiba Jobin Yvon	MoLES	MoLES	MoLES		MoLES/ CLASS	MoLES	MoLES	CLASSIX					
											PLY			TLY		
Temperatures	Low Temp	Room Temp	Room Temp	Low Temp	Low Temp	Low Temp**	High Temp**	Low Temp	Low Temp	Low Temp	Low Temp					
											Objectives					
											x2	x10	x20*	x2	x10	x20*
Samples																
A455-13-04 (untreated)	√	√		√	√	√	√	√			√	√	√	√	√	√
A455-13-02b (HPHT treated)	√	√		√	√	√	√	√			√	√	√	√	√	√
A330-20 (nat. colourless – type IIa)	√	√			√	√	√									
0673803 (CVD layered)			√		√			√			√	√	√	√	√	√
A490-159	√		√		√	√		√			√	√	√	√	√	√

0542715 (CVD plan)	√		√		√			√			√	√	√	√	√	√
naturally colourless type IIa								√						√		√
A465-40-03	√				√			√			√	√	√	√	√	√
A465-40-04	√		√		√			√			√	√	√	√	√	√
Blue Single Crystal CVD		√						√	√	√						
0473906 (small brown single crystal CVD)		√			√	√		√	√	√	√	√	√	√	√	√
0473904 (large brown CVD)		√			√	√		√	√	√						

* x20 objective is a UV lens.
** Low temperature TL measurements were undertaken from 10K-300K and High Temperature from 300K-723K.
† Results not presented in this thesis

Diamond Colour Key:

Uniform Brown | Banded Brown | Brown Features | Blue | Colourless

Chapter

5

5.0 XEOL and PL investigations on natural and synthetic diamond

5.1 Introduction

The chapter has been set out into two parts. The first part will present the results obtained for the uniformly coloured samples, synthetic diamonds followed by the naturally uniform samples. The second part will consist of the variegated, non-homogeneous samples comprising firstly of the synthetic CVD samples and lastly the naturally banded samples. The XEOL and PL techniques have been used in conjunction in this chapter to characterise the different samples utilizing either, the SRS at Daresbury, the in-house X-ray source at Aberystwyth or a Laser source. The source used and the spectrometers utilized will be stated at each individual sample section. Calibration was made using a HeNe (632.8nm) laser.

5.2 Uniformly Coloured Diamond

The data for these types of samples has predominantly been obtained using the MoLES spectrometer (*1*) due to the uniformity of the samples in question and therefore the use of a CCD on the CLASSIX spectrometer (*2*) for imaging purposes was not required.

5.2.1 Synthetic Diamond

5.2.1.1 Blue and Brown Single Crystal CVD diamond

Optically Detected X-ray Absorption Spectroscopy (OD-XAS) and X-ray Excited Optical Luminescence (XEOL) have been applied in parallel to characterise the chemical structure of two single crystal CVD diamonds. One CVD sample is a Blue, highly Boron doped diamond (~10^{16} atoms per cm^3) of which its depth of colour is a good indication to the degree of doping involved and the other is a brown CVD sample. Both samples have been carefully selected to provide the significant difference in colouration required for the purpose of probing correlations between colour, luminescence and their local chemical structure – the main purpose of this investigation.

Soft x-ray studies were carried out at the Synchrotron Radiation Source (SRS). XEOL and OD-XAS measurements were undertaken using the mobile spectrometer, MoLES (*1*) at temperatures of ~10K and sample cooling was achieved using a liquid He closed-cycle cryostat. XEOL measurements were taken using a fixed excitation energy of ~280eV and the emitted light analysed at wavelengths of ~200-1000nm using a monochromator coupled to a PMT (for specification see chapter 3 – Instrumentation).

The OD-XAS measurements which will be discussed further in chapter 8, were recorded for both samples in total electron yield (TEY), total luminescence yield (TLY) and partial luminescence yield (PLY). The excitation energy was scanned from ~280-320eV to cover the Carbon K-edge binding energy (284.2eV) and the π^*

(indicative of graphite, sp^2-bonded carbon) and σ^* (indicative of diamond, sp^3-bonded carbon) regions.

Nitrogen and hydrogen are the main impurities typically found in CVD diamonds. Techniques such as Photoluminescence (PL), Cathodoluminescence (CL) and X-ray Excited Optical Luminescence (XEOL), are sensitive, non-destructive tools in identifying low concentration defects and impurities in wide-band semiconductor samples such as diamond (E_g = ~5.5eV) and boron nitride (BN) (*3*). Measurements such as PL are often limited to lower optical energies due to the sub-band-gap energy of the excitation source e.g. 404nm, 3.07eV laser. The XEOL technique consists of an x-ray source that provides a higher penetration depth compared to PL and can therefore cover the complete energy region of a sample such as diamond, giving rise to a complete luminescence spectrum, thus providing information relating to the doping (identity) or impurity content of the sample under study.

Figure 5-1 is a plot of the XEOL spectrum intensity (in arbitrary units) versus the Energy (eV) of the luminescent light (emission) generated by the sample under study when excited by a SRS beam fixed at 280eV (below the main C absorption edge). Noticeable differences are apparent between both samples. The spectrum obtained are typical of a highly doped boron (blue CVD diamond) and nitrogen containing samples (brown CVD diamond).

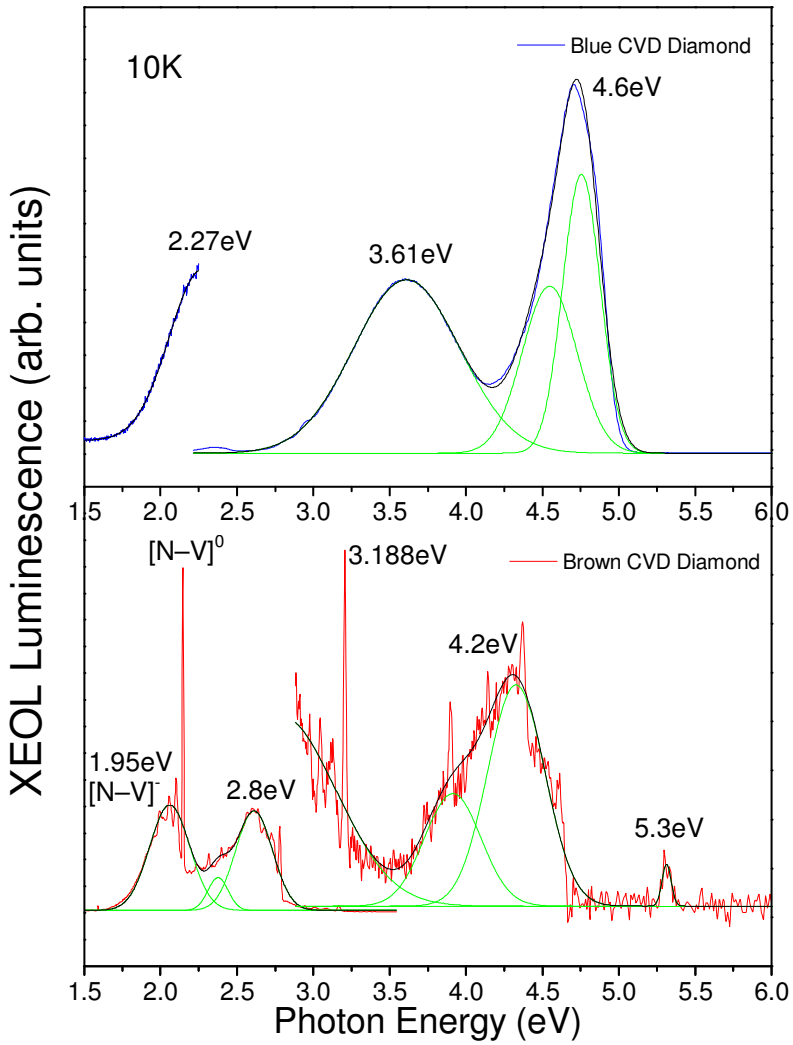

Figure 5-1: XEOL spectrum for the Blue and Brown CVD single crystal diamond samples, taken at 280eV at the SRS (measurements taken at a temperature of 10K).

5.2.1.1.1 Brown CVD Diamond

Investigations into the luminescence of natural nitrogen-containing diamonds have long been an area of interest for several years. The CL and PL of CVD diamond films prepared by various deposition techniques have been investigated (*4-6*). The XEOL spectrum obtained for the brown CVD sample (red curve) is a typical XEOL spectrum measured from a single crystal CVD diamond containing nitrogen atoms and is similar to a PL spectrum that has previously been reported for brown diamond (*7*).

A strong line known as a Zero Phonon Line (ZPL) dominates the spectrum at 2.15eV and from this sharp line to ~1.97eV, three other weak, broader lines are observed on a reddish luminescence band. These weaker lines are associated phonon replicas of the 2.15eV ZPL and are situated at 2.102, 2.055 and 1.992eV. The 2.15eV ZPL is attributed to a nitrogen vacancy complex and is a clear indication that nitrogen is incorporated in the brown CVD single crystal sample. It is attributed to $[N\text{-}V]^0$ centres and there is mention in the literature (*4*) that a link exists between the intensity of the 2.156eV ZPL and the depth of brown colouration i.e. the more intense the ZPL, the browner the film sample. Our brown CVD diamond is very much a dark brown and the intensity of the 2.156eV obtained in the XEOL spectrum confirms this, the colouration and intensity of the 2.156eV ZPL was used as an indication of the Nitrogen doping in this instance. Substitutional nitrogen provides a yellow colouration to a diamond and blue colour is obtained by boron doping.

At ~1.95eV a ZPL is present with a significantly weaker intensity to that of the $[N\text{-}V]^0$ centres (2.15eV). The 1.95eV ZPL is a well known optical band that has been reported previously by Rzepka *et al.* (*7*) and is attributed to $[N\text{-}V]^-$ centres that occur at a centre with trigonal symmetry at which an electronic transition from a ground state to an excited state occurs (*8*). The low intensity of this ZPL may be due to the fact that all of the nitrogen vacancy centres may well have been put into the neutral charge state $[N\text{-}V]^0$, thus accounting for such a high ZPL signal at 2.15eV.

Extending from 2.1 to 2.8eV a blue/green emission is observed in the XEOL spectrum, inclusive of many intense, sharp bands peaking at 2.778, 2.724, 2.679, 2.638, 2.598, 2.565, 2.445, 2.397, 2.316, 2.282, 2.237 and 2.18 eV with an average

separation of ~59meV. Some of these lines have been previously reported by Rzepka *et al.* using near UV-laser excitation and at lower intensities in CL studies (*7*).

A peak is present at ~2.316eV. It has previously been reported (*9, 10*) and is observed in CVD diamond and is often found to be one of the dominating features along with the 2.156eV centre in CVD diamond films (*9*).

A clear optical signature relating to N is the emergence of narrow-line point defect spectrum such as the 2.156 and 3.188eV peaks. These are due to the complexing of N with vacancies or self interstitial C atoms (*11*). A good indication of significant N in CVD-diamond films is when these lines are strong. Peaks present at ~2.78eV and 3.18eV are produced by electron irradiation and are known to become stronger after annealing at 600°C (*8*). The 3.188eV peak is readily formed through N^+ ion implantation in CVD-diamond films and is a common feature (*9*). It is thought to be a defect interstitial-related feature, possibly a nitrogen interstitial. Previous studies have also observed similar localized vibrational modes and it has been shown that these centres involve a single nitrogen atom associated with a radiation damage product (*12, 13*). We can thus gather that the 1.95eV and 2.156eV centres are associated with vacancies and that the 2.807eV and 3.188eV centres are associated with interstitial atoms (*8, 9*).

A complex band has been observed in our XEOL spectrum located at 4.2eV as well as in other reports with the band previously deconvoluted into main contributions at 4.06eV and satellite peaks at 4.08, 4.28 and 4.49eV (*7*).

The ~5.3eV band observed in our XEOL spectrum has also been previously reported at ~5.2218eV and is speculated to be possibly related to near-band-gap edge emission due to impurity bounded excitons (*7*). Studies on polycrystalline films and CVD samples show that the single crystal CVD samples exhibit strong, intrinsic 'edge-emission' at around 5.3eV due to the recombination of the free exciton (*14*).

5.2.1.1.2 Blue CVD Diamond

The XEOL spectrum obtained for the Blue single crystal CVD sample consists of mainly three bands in the 1.5eV to 5eV range. Peaks are situated at around, 2.27eV, 3.61eV and 4.6eV and can been attributed to features that are typically associated with boron-doped diamond (*15, 16*). The 2.27eV peak (540nm) is referred to in the literature as the Green Band and is commonly seen in CVD and HPHT synthetic diamonds. It has been attributed to donor-acceptor pair recombination (*9, 15*). It is likely that boron acts as the acceptor and probably nitrogen as the donor (*15*). However, the band is clearly Boron related (*17*).

The ~4.6eV peak with a FWHM of 0.4eV has been observed in the XEOL spectrum for the Blue single crystal CVD sample and has been reported in previous PL studies of boron doped diamond samples with the addition that the band is only found in boron-doped diamond and is more commonly found in CVD samples than those produced by HPHT methods (*15*). The 4.6eV band only appears in samples that contain immeasurably low concentrations of atomically dispersed nitrogen and the band intensity appears to increase with increases in the boron doping. Studies by Lawson *et al.* have revealed that the 4.6eV band is temperature dependant (*15*). A comparison of the ~3.5eV band in the XEOL spectrum that was taken at ~10K with work undertaken by Lawson *et al.* at 113K, could also suggest that the 3.5eV band is also temperature dependent.

5.2.2 Natural Diamond

Natural diamond are also found to be uniform in colour. XEOL studies have been undertaken, again using the MoLES spectrometer (*1*).

5.2.2.1 Untreated and HPHT treated type IIa diamond

X-ray Excited Optical Luminescence (XEOL) measurements have been undertaken on two sister type IIa diamond samples cut from the same original stone. Both samples were initially uniformly brown in colouration and one of the two was subjected to high-pressure, high-temperature (HPHT) treatment (~10GPa and a temperature of 2550°C for 1hr) of which the process is known to eliminate the brown colouration (*18*).

The resultant samples for study therefore consist of two uniformly coloured type IIa diamonds, one brown and therefore untreated and the other colourless (HPHT).

Hard x-ray studies were carried out at the Luminescence Laboratory in Aberystwyth using the 50kV Cu K_α x-ray source as previously introduced in chapter 3. The XEOL measurements were undertaken using the mobile spectrometer, MoLES (*1*) at temperatures of ~10K. Sample cooling was achieved using a liquid He closed-cycle cryostat. XEOL measurements were taken using the x-ray source at 30kV and the emitted light analysed at wavelengths of ~200-1000nm using the MoLES monochromator coupled to a PMT.

Figure 5-2 is a plot of the Normalized XEOL spectrum intensity (in arbitrary units) versus the energy (eV) of the luminescent light (emission) generated by the sample under study when excited by a 30kV x-ray source. Both spectrum shapes are very similar and display a broad luminescence band at ~2.9eV – the well known band-A luminescence that is typical of type IIa natural diamond. It is one of the most characteristic features found in diamond and is often observed in natural diamonds, CVD films and HPHT synthetic diamonds (*19*). The A-band is significantly strong in low-nitrogen diamonds and therefore ties well with the samples studied in this case

(type IIa – low nitrogen content – see chapter 1). The dislocation-related A-band can be observed in CL, only in type IIa diamonds of relatively high purity (*19*). Dean in 1965 provided evidence that suggested that the band-A emission situated around ~2.8eV was due to donor-acceptor pairs (*20*). Although Ruan *et al.* in 1992 provided evidence and concluded that the ~2.83eV band was due to dislocations within the diamond (*17*).

The band-A peak usually lies around 2.88eV with a FWHM of 0.22 to 0.45eV (*19*) of which values are comparable with the values obtained for both the untreated type IIa diamond sample and the HPHT treated diamond, 2.90eV (FWHM = 0.32eV) and 2.91eV (FWHM = 0.31eV) respectively.

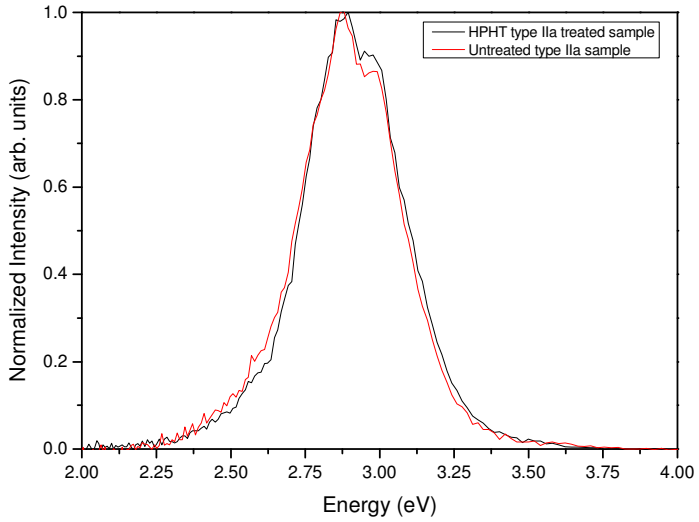

Figure 5-2: XEOL spectrum of both the untreated and HPHT treated type IIa sister diamonds.

At the low energy side of the XEOL spectrum, differences can be clearly observed. A broader feature is present at around the 2.3-2.6eV region. This was observed in all instances, whereby the monochromator slit widths were varied to optimize the resolution.

The PL spectrum obtained in figure 5-3 and 5-4 for this sample further confirms the feature and provides an explanation. The PL measurements were undertaken on MoLES at the Luminescence laboratory in Aberystwyth with a 404nm (3.07eV) laser coupled to the system instead of the x-ray source. Two Schott BG39 filters (see

specifications in Appendix) were mounted prior to the monochromator entrance to block any laser light from coming through and damaging the PMT.

The PL spectrum obtained with variable slit width are shown below in figure 5-3. Differences can clearly be seen between both XEOL and PL techniques.

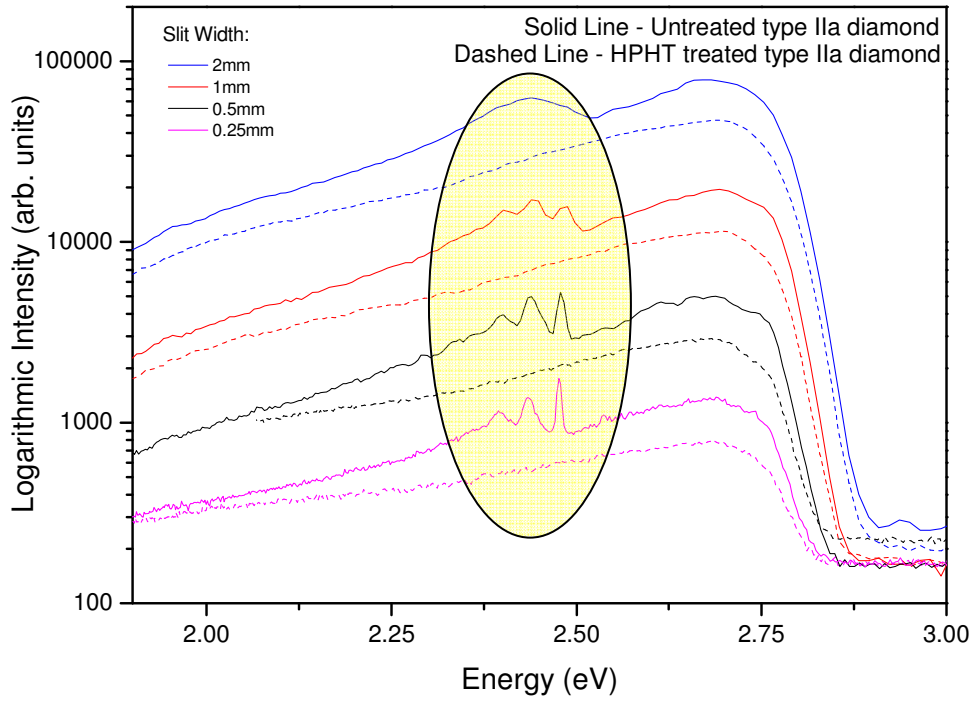

Figure 5-3: PL spectrum for the two sister type IIa samples, one of which has been HPHT treated. The yellow oval highlights the specific region where the differences are observed.

XEOL measurements suggest that there are features present in the untreated that are missing in the HPHT treated sample. Photoluminescence (PL) measurements have confirmed these differences and have revealed a significant feature that is present only in the untreated brown type IIa diamond as shown in figure 5-3. The feature is completely absent in the HPHT treated type IIa diamond.

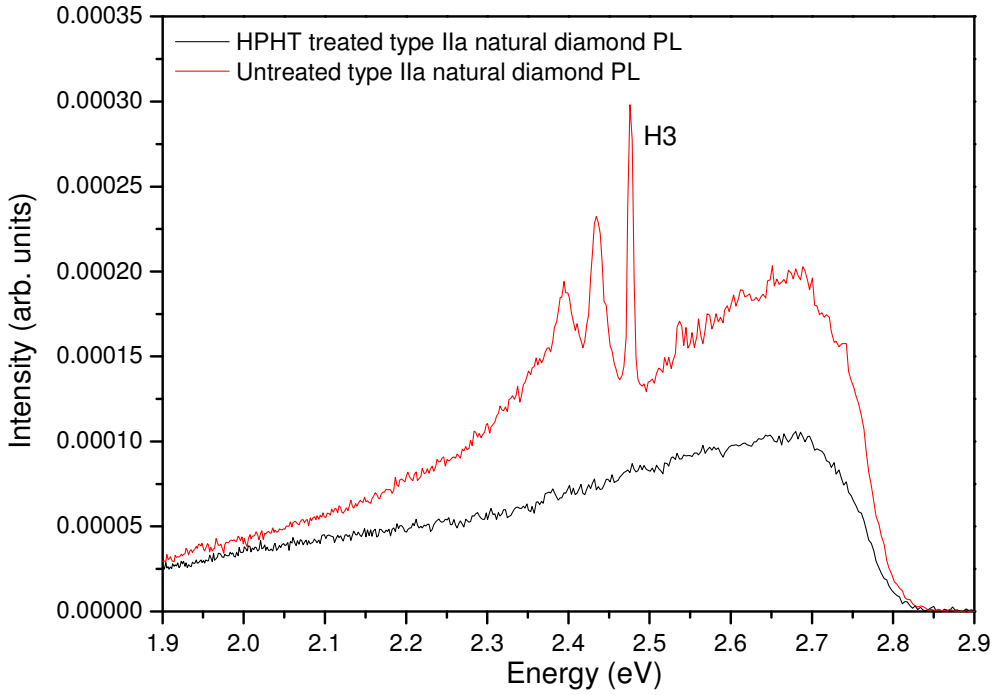

Figure 5-4: The above PL spectrum is for the untreated and the HPHT treated type IIa natural diamonds (monochromator entrance and exit slit width at 0.25mm). It is clearly seem that the features in the 2.3 to 2.6eV region are present in the untreated samples and absent in the HPHT treated sample. This is the H3 centre.

The feature observed in the untreated sample can be attributed to the H3 centre and is typically found around 2.463eV (503nm) (*8*). The spectrum obtained for the untreated sample has a ZPL at 2.476eV with phonon replicas situated at 2.434 and 2.394 with vibration energy of ~41meV comparable with that found in the literature (*19, 21*).

The H3 centre consists of two nitrogen atoms around a vacancy with a neutral charge. It is one of the most common naturally occurring optical features observed in nitrogen-containing diamonds (*19*). It could be surprising to see it in type IIa diamond due to the only statement in Zaitsev stating that it is readily created in type IIa diamond by N+ ion implantation and annealing at temperatures above 800°C.

The H3 centre is responsible for green photoluminescence (*22*) and the luminescence due to the H3 centres vary with the concentration of nitrogen present (*23*).

The PL spectrum clearly confirms that the HPHT treatment has eliminated the H3 centre. Evidence of this is found in the literature (*19, 24, 25*). The well known H3 centre arises as a result of a vacancy being trapped at the A form of Nitrogen, resulting in a N-V-N structure.

The HPHT treated type IIa diamond has experienced ~10GPa (100kBar) of pressure and a temperature of up to 2550°C for ~1 hour. Collins – through private communication – mentions that the HPHT treatment typically enhances the H3 centre up to around 1900°C (*24, 25*). This is also observed during the sintering of diamond powders, the interaction of dislocations introduces vacancies into the diamond and at above 550°C the vacancies are mobile. The vacancies become trapped at higher temperatures at singly substituted nitrogen atoms or A aggregates of nitrogen to form N-V centres (1.945eV) or H3 centres (2.463eV) respectively (*8*). At above 1900°C the H3 centre decreases and by ~2500°C the H3 centre would have been destroyed (*24*). The H3 centre is typically found at dislocation regions (*19*), the HPHT treatment has eliminated this centre – this may account for the higher concentration of sp^2 bonded carbon species that have been observed in the OD-XAS spectrum for this HPHT treated sample – chapter 8. The HPHT treatment may have eliminated the H3 centres and left dangling bonds at these dislocations, therefore contributing to the increase in sp^2 bonded carbon. The HPHT treatment may have also brought small vacancy-clusters closer together to create larger vacancy-clusters and therefore made it far more sensitive to be observed in the Raman measurements as well as OD-XAS investigations (see chapter 6 and 7). This could account for the larger concentration of sp^2-bonded carbon observed in the HPHT treated sample.

Differences between both samples are also observed in the birefringence image and the luminescence image (figure 5-5b and 5-5c). When the samples are placed between two crossed-polarisers, the birefringence image for the untreated image is orderly and in a predominantly uniform direction. When the HPHT treated sample is viewed between two crossed-polarisers, the birefringence image is very much different to the untreated (figure 5-5b). It seems to be much more disordered with no specific direction. The luminescence image also confirms this from the observations carried out when both samples were studied side-by-side on the CLASSIX spectrometer cold-finger with the synchrotron spot overlapping both samples as shown in figure 5-5c.

The luminescence intensity emitted from the untreated sample is significantly greater than that of the HPHT treated sample (Red = high intensity). The light seems to be much more dispersed and disordered with lower intensity see figure 5-5c.

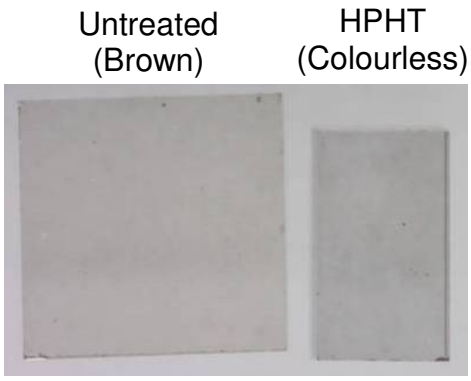

Figure 5-5a: A photograph of the untreated (left) and HPHT treated (right). The untreated sample is brown and the HPHT treated sample is colourless due to the treatment.

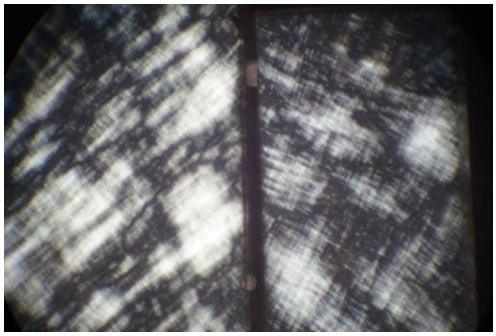

Figure 5-5b: A birefringence image of both samples. The birefringence pattern observed for the untreated sample (left) is much more ordered than the HPHT treated sample (right) which also appears to be much more disperse.

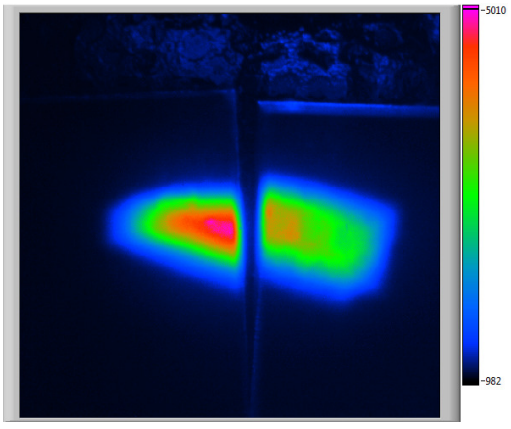

Figure 5-5c: The luminescence image also suggests and confirms what is shown in the birefringence image. The luminescence light intensity is much less and more dispersed in the HPHT treated sample (right) compared to the untreated sample (left). (Red = High Intensity)

The dispersion in the HPHT treated sample could be as a result of the H3 centre being eliminated or perhaps the small vacancy-clusters merging together to form larger ones.

The H3 centre is the most common naturally occurring optical feature found in nitrogen-containing diamond. It is almost always accompanied by the N3 centre (*19*). Zaitsev goes on to state that the HPHT treatment suppresses the H3 centre as has been observed in the PL study on the untreated and HPHT treated diamonds (*8, 19, 24, 25*).

The H3 centres decorate individual dislocations (*19*), such as proposed in the model in figure 5-6. When the sample is HPHT treated for experimental analysis it has been observed that the H3 centres disappears is some way and as a result may leave dangling bonds. These in turn may result in sp^2 vacancy clustering and is supported by the increase in the sp^2-bonded carbon observed in OD-XAS measurements in the HPHT treated sample. The HPHT treatment due to the high temperature may also have caused vacancies to become mobile.

A proposed model for the elimination of the H3 centre in the HPHT treated diamond is shown in figure 5-6 and 5-7.

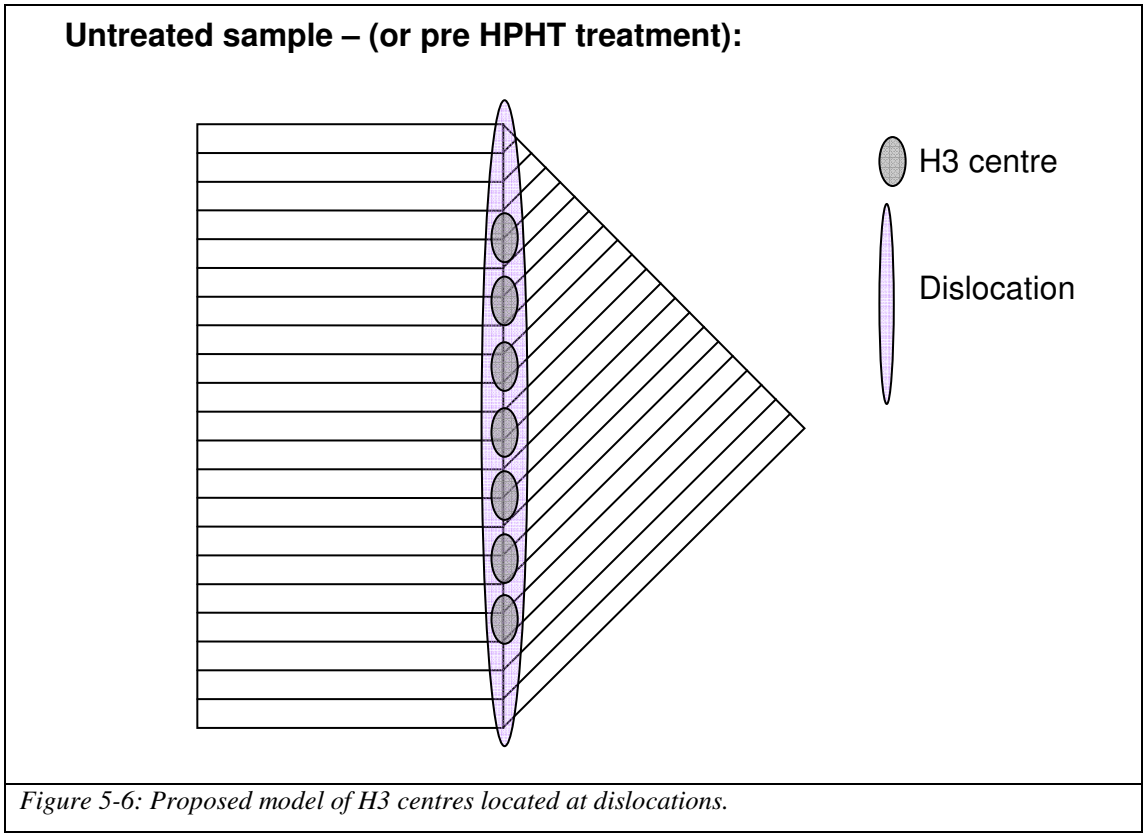

Figure 5-6: Proposed model of H3 centres located at dislocations.

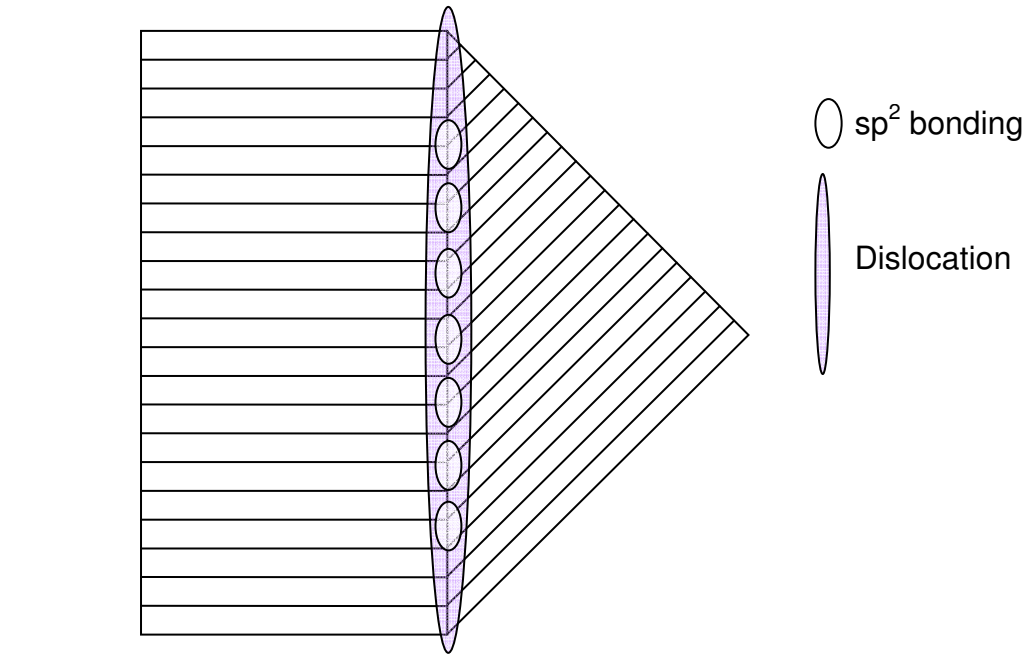

Figure 5-7: Proposed model of H3 centres being eliminated or removed from the dislocation sites and leaving sp^2 dangling bonds.

A higher concentration of sp^2 bonding was observed in the HPHT treated samples compared to the untreated sample when analysed via the OD-XAS technique (chapter 7). Raman measurements carried out on the same two samples also supports this analogy due to a higher concentration of sp^2 bonded carbon species being found in the HPHT treated sample. The proposed model here suggests that these sp^2 bonded species are much more local and thus easier to stimulate using synchrotron excitation – thus resulting in a higher probability of observing the sp^2 (π^*) resonances in OD-XAS measurements (more on this in chapter 7).

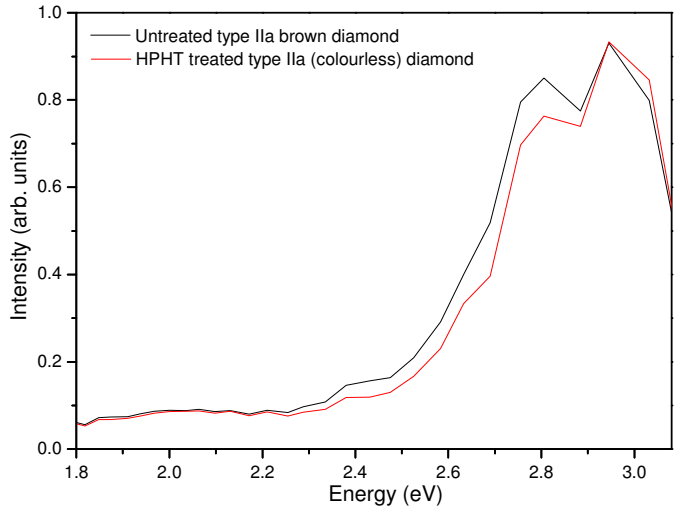

Figure 5-8: Volume Integrate XEOL spectrum taken with CLASSIX at the SRS, Daresbury. The peak around 2.8eV in the HPHT treated type IIa diamond is less intense than the untreated sample.

The XEOL acquired on the CLASSIX spectrometer shown in figure 5-8 also shows a decrease in intensity around the 2.8eV region, this may be due to the decrease/elimination of the H3 centre which may have been contributing to the band-A luminescence itself.

5.2.2.2 Naturally Colourless type IIa diamond

A naturally colourless type IIa diamond (A330-20) has also been studied for comparison with the untreated and HPHT treated diamonds. No XEOL spectrum taken on the MoLES spectrometer exists for XEOL comparison with the other two type IIa samples, but PL measurements were taken for the naturally colourless sample. The measurements were undertaken on the MoLES spectrometer using the same PL setup as before; a 404nm laser with two BG39 filters (see Appendix for specification) prior to the monochromator entrance.

Figure 5-9 shows the acquired PL spectrum for the type IIa naturally colourless sample.

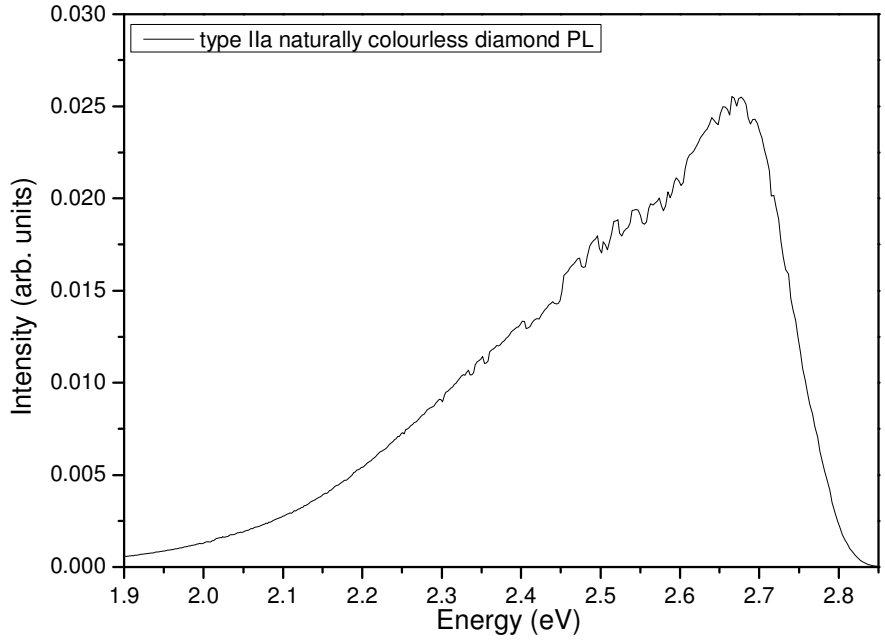

Figure 5-9: PL spectrum for the type IIa naturally colourless sample.

Clearly absent from the PL spectrum in figure 5-9 is the H3 centre. Slight featured remnants may be present around the 2.463eV region, but comparable to the untreated brown type IIa it is virtually absent.

It is worthwhile to note that the band-A luminescence is still present for all three type IIa PL spectrum, but due to the filter cutting the higher energy part of the spectrum to

block out the laser source (3.07eV) it is difficult to tell whether the N3 centre typically found at around 2.985eV could also be present in the PL. The band A luminescence is caused by intrinsic defects within the diamond lattice and has been mentioned in the literature to be related to dislocations (*17, 19*). Lipatov *et al.* suggest that the band A maximum must be localized in energy close to the centre of the diamond band gap at ~455nm (2.73eV) – similar to the values mentioned earlier and in Zaitsev (*19*). Lipatov *et al.* also mention that it is quite likely that the optical centres such as N3, H3, N, and B can be superimposed on band-A and affect the position of the band A maximum. Walker mentions that the band-A luminescence could display some structure due to the superimposed luminescence or absorption of other systems such as the N3 centre (*11*).

Figure 5-10 is the Volume Integrated XEOL spectrum obtained for another type IIa colourless diamond. The x20 (UV) lens was utilized due to being UV compatible thus allowing the XEOL spectrum to range into the UV.

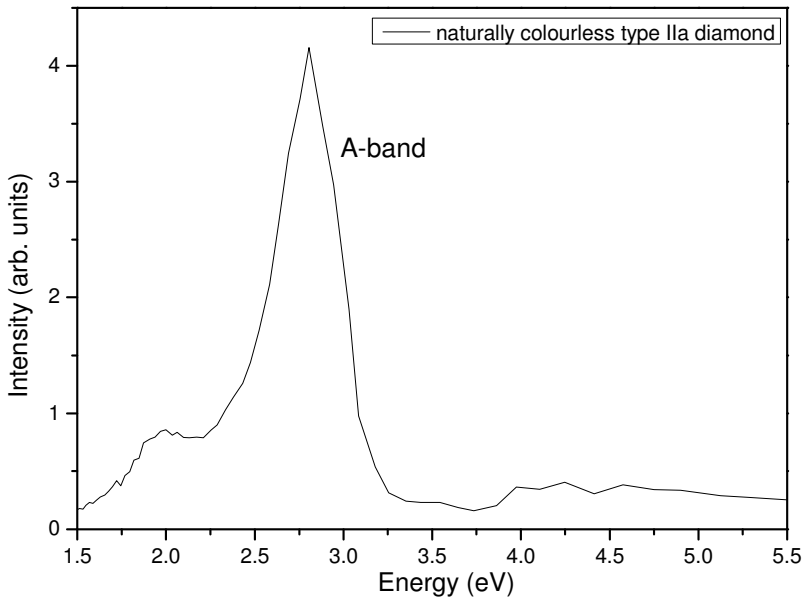

Figure 5-10: Volume Integrated XEOL spectrum for another type IIa colourless sample taken on the CLASSIX spectrometer. The A-band is still the most prominent feature.

A broad band is situated at around 1.8eV which is associated with an artefact – plasma from the Ion-gauge.

5.3 Variegated Diamonds

X-ray Excited Optical Luminescence (XEOL) measurements have also been applied to characterise variegated diamonds of which either contain features which are brown or banded in both synthetic and natural forms.

For the purpose of probing correlations between colour, luminescence and local chemical structure the CLASSIX spectrometer (*2*) utilized on beamline MPW6.1 at the SRS, Daresbury was predominantly used for the provision of data. Samples were cooled to ~10K using a supplied liquid He Dewer. XEOL measurements were taken using a fixed excitation energy of ~280eV and the emitted light analysed through magnification optics and a variety of filters ranging from ~200nm to 1000nm into a CCD (see chapter 3). PL and in-house (at Aberystwyth) XEOL measurements have also been undertaken in order to compare with the Volume Integrated mode on the CLASSIX spectrometer whereby the spectrum obtained in the Volume Integrated mode corresponds to the total luminescence signal from the whole of the sample being measured i.e. not relative to any brown or bright region specifically.

5.3.1 Synthetic Diamond

5.3.1.1 CVD sample (0542715)

The CVD sample (0542715) has been purposely grown by request to include brown regions. Figure 5-11a shows a photograph of the CVD diamond in transmitted light along with a luminescence image of the same sample taken with the CLASSIX spectrometer CCD (figure 5-11b). The brighter colours indicate high intensity and dark colours, low intensity.

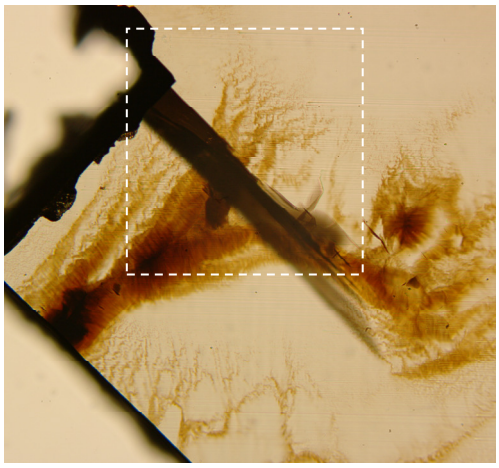

Figure 5-11a: Photograph of the CVD diamond (0542715) sample studied during the course of this research. The white boxed region is the region analysed by the CLASSIX spectrometer.

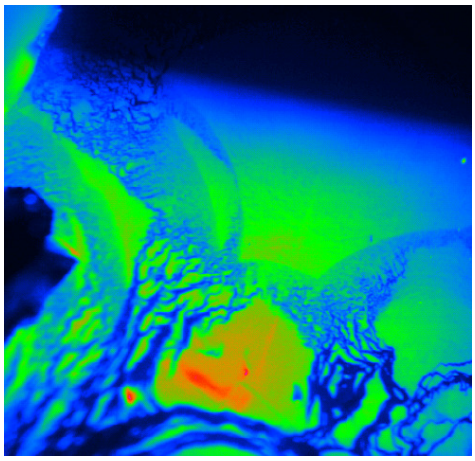

Figure 5-11b: Luminescence image of the CVD sample taken by the CCD on the CLASSIX spectrometer.

Clearly evident in figure 5-12a is the luminescence image acquired for the sample that has been concentrated and focussed on a brown region. The luminescence image correlates exactly with an image taken using transmitted or reflected light (figure 5-11a). The spectrum obtained in figure 5-12b is the Volume Integrated plot over the white rectangle in figure 5-12a. This contains the luminescence from the dark *and* bright regions of the sample.

Figure 5-12c is the same sample but in this instance the XEOL spectrum has been obtained from a bright region on the sample – see cross hatch on figure 5-12c with a 3x3 pixel array spectrum shown in figure 5-12d. This spectrum is quite similar to that

of the Volume Integrated plot. Figure 5-12e has the red cross hatch on a dark region with the corresponding spectrum (3x3 pixel array) in figure 5-12f. The intensity is much lower as expected due to being a dark region and therefore not much light resulting from that part of the sample. The spectrum is also quite different around the 2.5eV region.

Volume Integrated

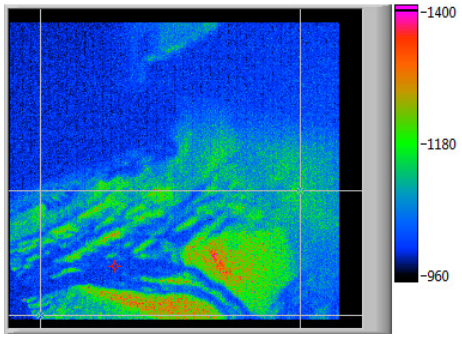

Figure 5-12a: Luminescence image of the CVD (0542715) diamond with a x10 objective. The luminescence image here is taken with incident energy of 280eV, through filter ~480nm with a bandwidth of 8.9nm.

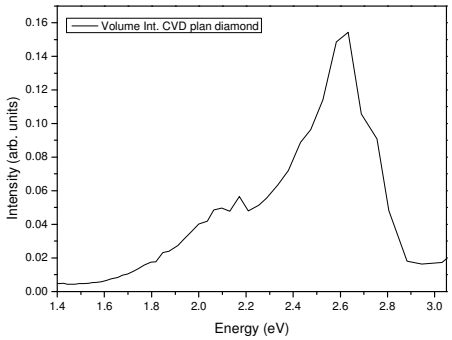

Figure 5-12b: A Volume Integrated XEOL scan of the complete region (white rectangle) in Figure 5-12a.

Bright Region

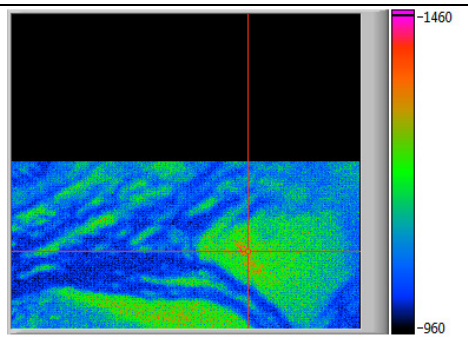

Figure 5-12c: Luminescence image of the CVD (0542715) diamond with a x10 objective. The luminescence image here is taken with incident energy of 280eV, through filter ~480nm with a bandwidth of 8.9nm. The red cross hair is situated at a bright region.

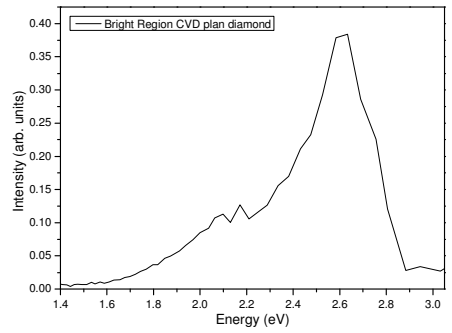

Figure 5-12d: A XEOL scan of the bright region in Figure 5-12c. It is a 3x3 pixel array. Bands are clearly visible in this range.

Dark Region

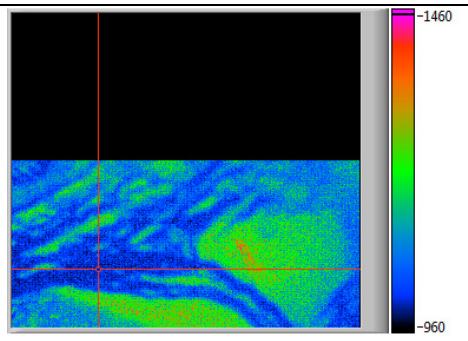

Figure 5-12e: The same as figure 5-12c but looking at a dark region of the CVD sample.

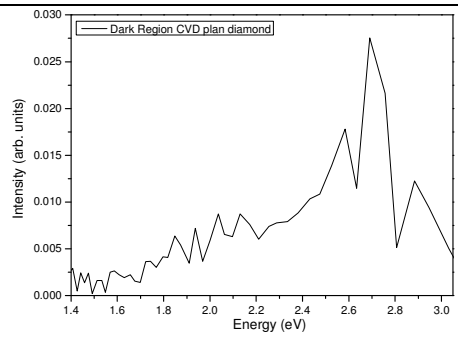

Figure 5-12f: A XEOL scan of the dark region in Figure 5-12e (3x3 pixel array).

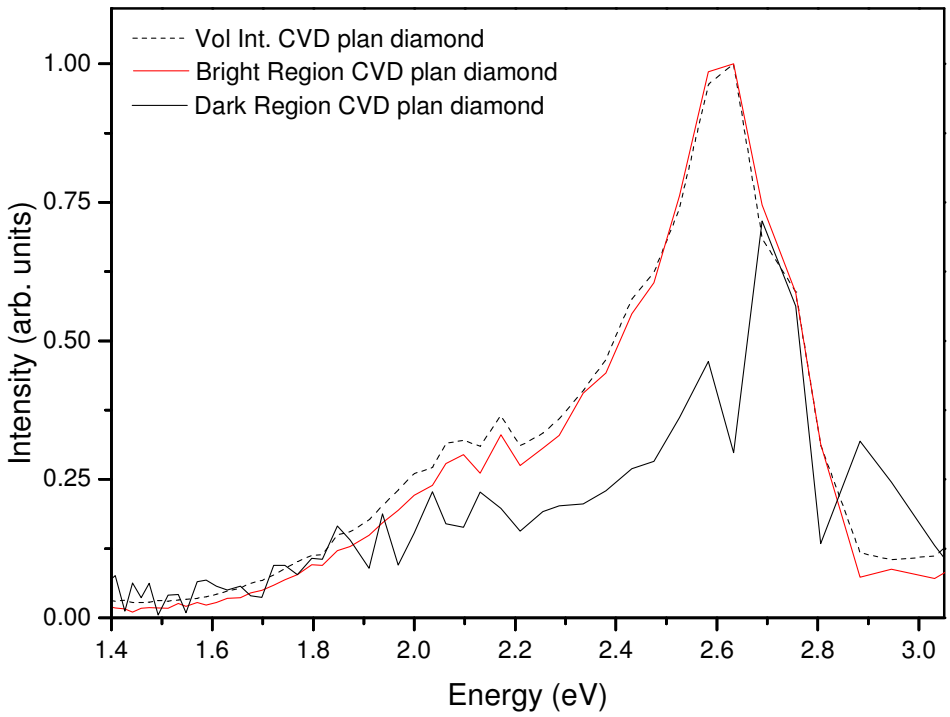

Figure 5-13: All three spectrum normalized for comparison. Differences are clearly visible between the bright and dark region. The ~2.6eV band is much more enhanced in the bright region compared to the dark region where the band's intensity is much less.

Figure 5-13 clearly shows a significant similarity in the Volume Integrated plot with the bright XEOL spectrum. They are virtually identical and this result poses the suggestion that the XEOL spectrum is much more dominant and intense than that originating from the dark region. In figure 5-13 the results have been normalized (Vol Int and Bright XEOL) but the dark XEOL spectrum has been scaled up to try to fit within the band. In doing so it is evident that there is a decrease in a band situated at ~2.5eV but again it is difficult to get any significant information from the measurements.

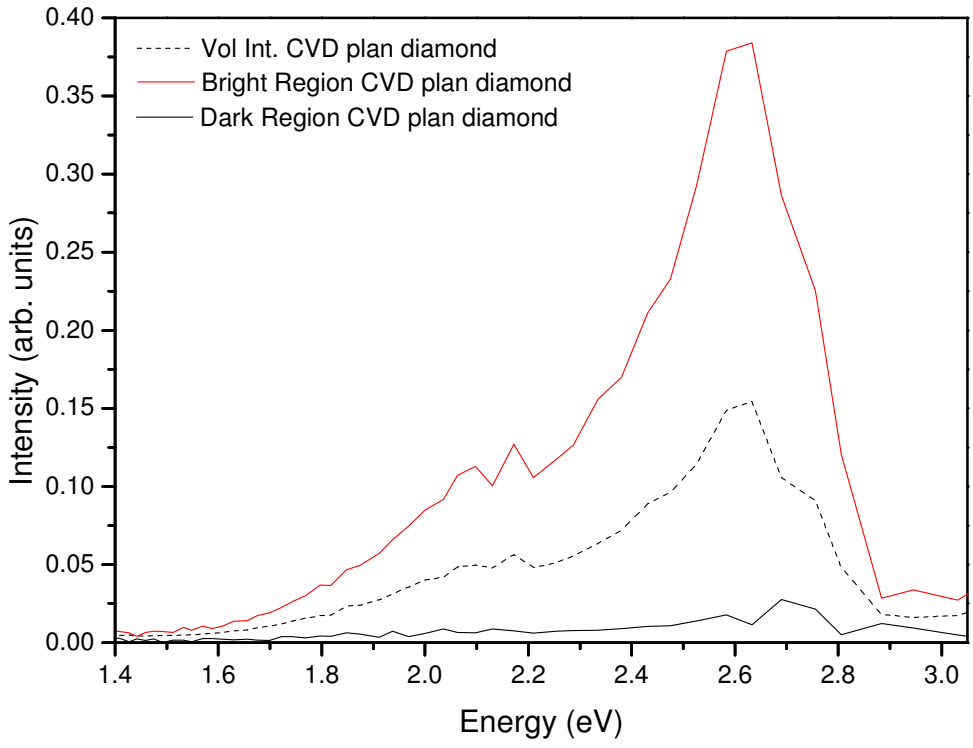

Figure 5-14: Original data (not normalized)

The comparison of the three spectrum reveals a significant feature that is missing in the dark region of the sample. It is difficult to gather any specific detail to the exact origin of the missing band or optical feature such as the H3 centre due to the resolution of the CLASSIX spectrometer. Due to the XEOL being measured through filter (for imaging purposes) there are limitations with regards to the spectral bandwidth of each filter. By scanning from 222nm – 1001nm the bandwidths of the 79 narrowband filters range from 8.0-13nm, whereby the MoLES spectrometer consisted of a monochromator setup with significantly better resolution (as mentioned previously in chapter 3). Any information relative to ZPLs or such features can not therefore be obtained from the CLASSIX spectrometer XEOL spectrum. XEOL measurements were also undertaken with the x20 magnification and provided information from the UV region. No differences were observed at those regions, but did also show the change in intensity of the features shown in figure 5-14.

The PL spectrum for the same CVD plan diamond is shown in figure 5-14. The spectrum was taken with the MoLES spectrometer thus providing much better resolution due to the monochromator but without the lateral sampling region capabilities.

Figure 5-14 provides a fit of the PL for the CVD diamond (0542715).

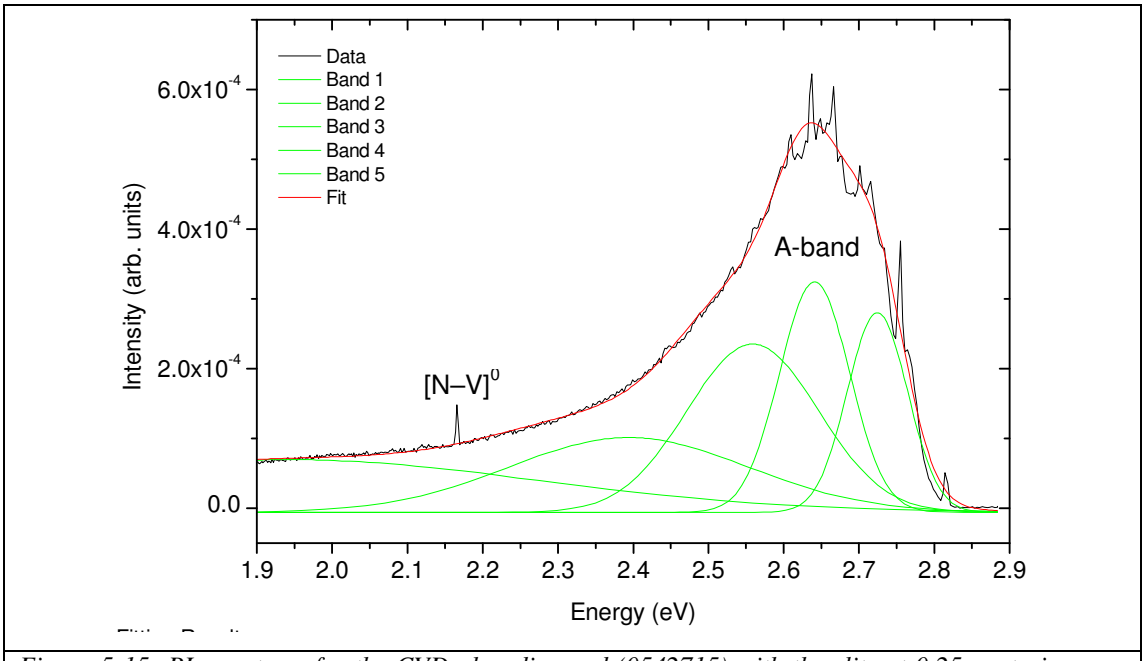

Figure 5-15: PL spectrum for the CVD plan diamond (0542715) with the slits at 0.25mm to improve the resolution.

A good PL spectrum has been obtained for the plan CVD diamond. Although it does not correspond directly to the bright or brown regions relative to the sample it can be compared with the Volume Integrated spectrum obtained with the CLASSIX spectrometer. The 404nm laser was utilized once again to acquire the spectrum at a temperature of ~10K.

This PL spectrum (figure 5-15) is good comparison with the Volume Integrated plot obtained with the CLASSIX spectrometer, it was found with the CLASSIX spectrometer that the Volume Integrated plot and the Bright region XEOL were very similar – but specific features such as ZPLs could not be identified. The PL may aid in identifying the location of the missing/significantly less intense peak that was observed in the dark region XEOL spectrum.

The feature observed in the PL (figure 5-15) at around 2.16eV is the $[N\text{-}V]^0$ centre previously mentioned in chapter 1 and at the beginning of this chapter. The band peaking at around 2.6-2.7eV is the band-A luminescence also mentioned previously but found at a lower energy, which could be due to the quality of the sample (*26*).

The features observed relating to the shape of the PL spectrums obtained for the different samples with regards to some features that are narrow and other broad can be explained by the amount of distortion the defect is submitted to when exciting an electron. Sharp features are typically observed when there is little, or no distortion between the ground and excited electronic levels, resulting in good overlap between the vibrational levels. The broader features observed are due to an increase in distortion resulting in a decrease in the overlap of the lowest vibrational levels. The recombination is as a result down to a set of vibrational states in the ground state resulting in a broader emission spectrum. For diamond, some of the broad bands that have been observed by other research groups are still under discussion as to what is directly responsible for the particular band or feature.

5.3.1.2 CVD layered sample (0673803)

The CVD layered sample (0673803) was also studied using the CLASSIX spectrometer and the results obtained are shown in figures 5-16a-f.

Volume Integrated Region:

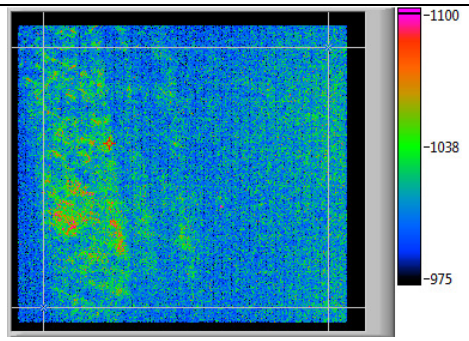

Figure 5-16a: Luminescence image of the CVD diamond (0673803) taken with the x20 (UV) objective.

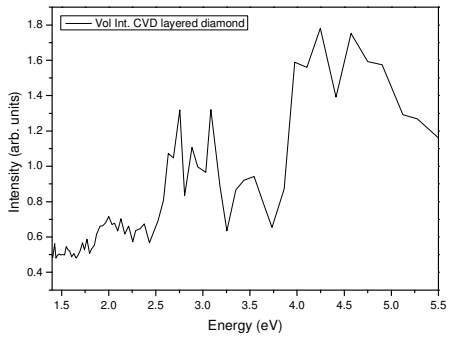

Figure 5-16b: The Volume Integrated XEOL scan ranging from ~1.5ev to 5.5eV for the white rectangular section in figure 5-16a.

Bright Region:

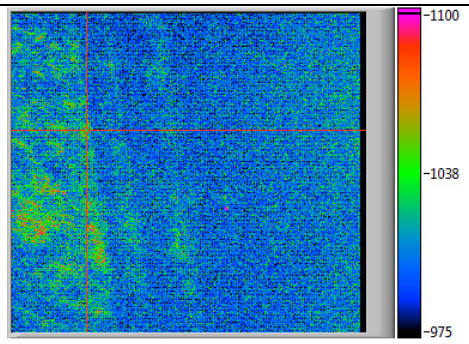

Figure 5-16c: Luminescence image of the CVD diamond (0673803) taken with the x20 (UV) objective with the red cross hair on a bright region.

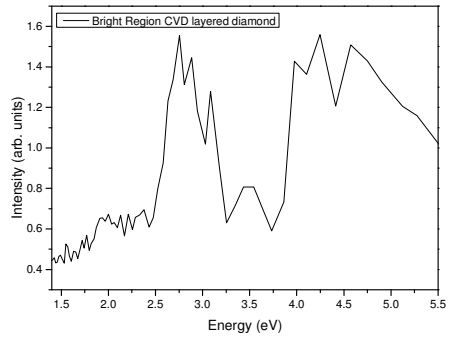

Figure 5-16d: The (15x15 pixel array) XEOL scan ranging from ~1.5ev to 5.5eV for the bright region in figure 5-16c.

Dark Region:

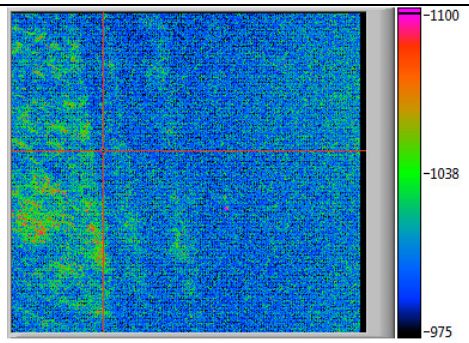

Figure 5-16e: Luminescence image of the CVD diamond (0673803) taken with the x20 (UV) objective with the red cross hair on a dark region.

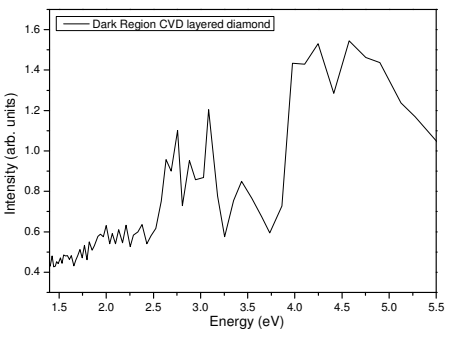

Figure 5-16f: The (15x15 pixel array) XEOL scan ranging from ~1.5ev to 5.5eV for the dark region in figure 5-16e.

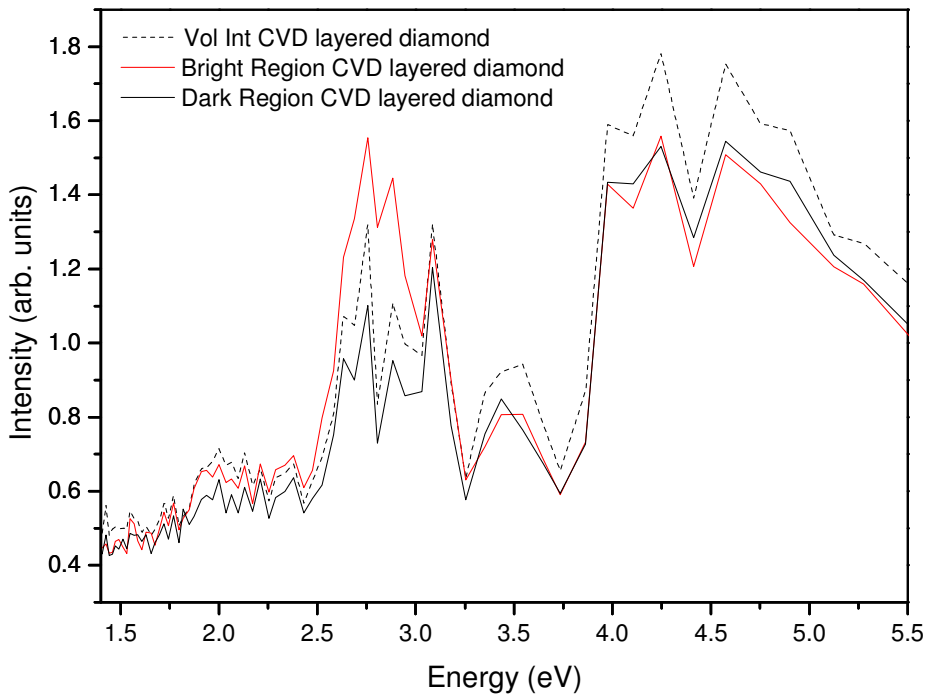

Figure 5-17: The XEOL spectrum (CVD-0673803) obtained with the CLASSIX spectrometer for all three spectrum. No apparent differences are observed in the UV region of the spectrum but there are differences in the 2.5 to 3.25eV range.

The x20 objective was used for the acquirement of the XEOL data for the layered CVD sample (0673803) shown in figure 5-17. The x20 sample is a UV lens that allows XEOL measurements to be undertaken into the UV on the CLASSIX spectrometer. As seen in the 3.75-5.5eV region no significant changes are observed between a dark region and a bright region.

PL for the CVD layered diamond:

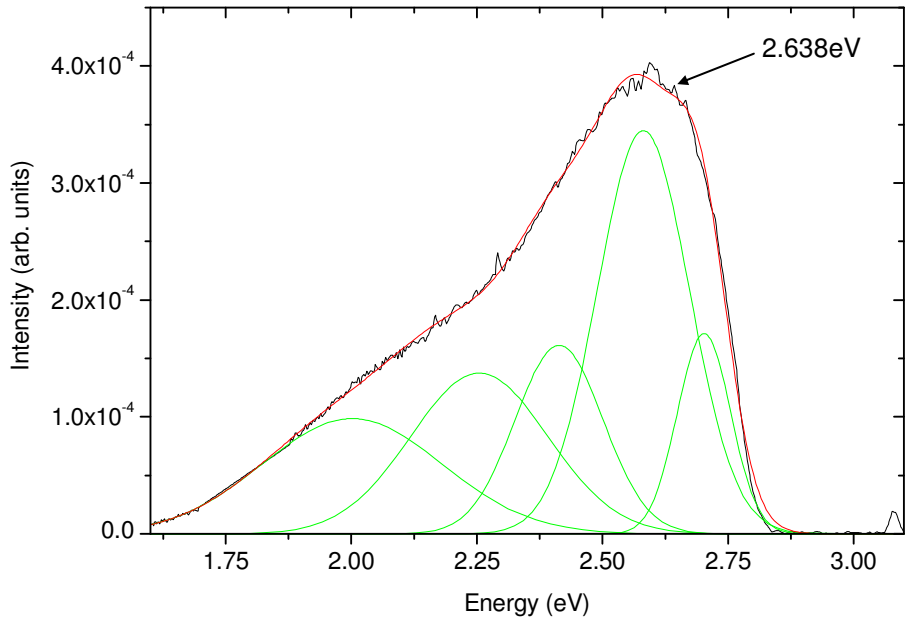

Figure 5-18: PL spectrum for the CVD layered sample. The peak situated at around 3.07eV is the (404nm) laser break through.

The PL shown in figure 5-18 is for the CVD layered sample (0673803). It is similar to the CVD (0542715) sample but there is a slight broadening present around 2.0eV which could be attributed to the $[N\text{-}V]^0$ sideband. A feature is present at around 2.638eV and could be attributed to the TR12 centre which is a typical radiation centre found in diamond (*19*). The feature of narrow lines that are observed at ~2.67 accompanied by other narrow lines at 2.64, 2.55, 2.49, 2.46, 2.41, 2.29 and 2.16eV are observed. These lines are attributed to donor-acceptor recombination that occurs possibly between nitrogen and boron (*19*).

5.3.2 Natural Diamond

5.3.2.1 Type Ia naturally banded diamond (A465-40-04)

The A465-40-04 and the A465-40-03 samples are from the same original sample. The results for A465-40-04 are presented here.

Volume Integrated:

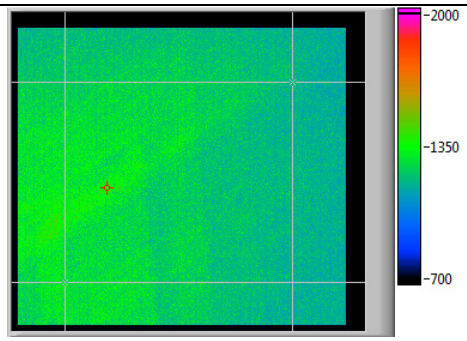

Figure 5-19a: Luminescence image taken at 280eV with a X20 (UV) objective. Bands are clearly visible that correlate with the brown banding in the sample.

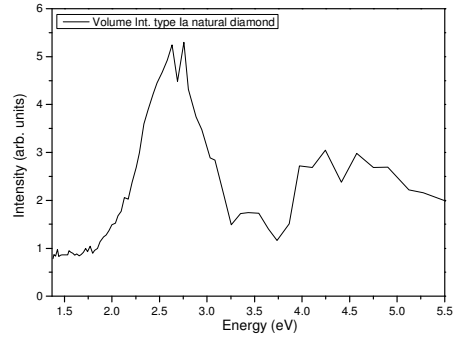

Figure 5-19b: Volume Integrated XEOL spectrum for the white rectangle in figure 5-19a. This XEOL spectrum contains both XEOL emission from the bright and dark bands of the diamond.

Bright Region:

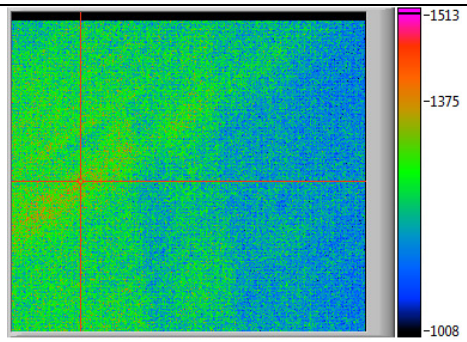

Figure 5-19c: Luminescence image as above (white rectangle) with red cross hair on a bright band.

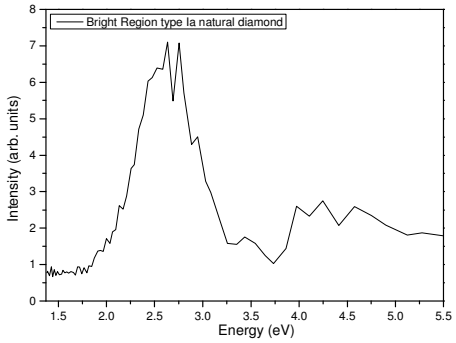

Figure 5-19d: XEOL spectrum for the bright band in figure 5-19c (7x7 pixel array).

Dark Region:

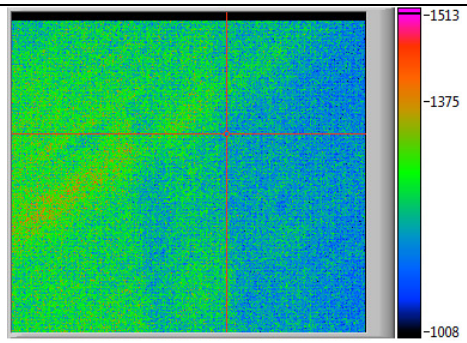

Figure 5-19e: Red cross hair at a dark band.

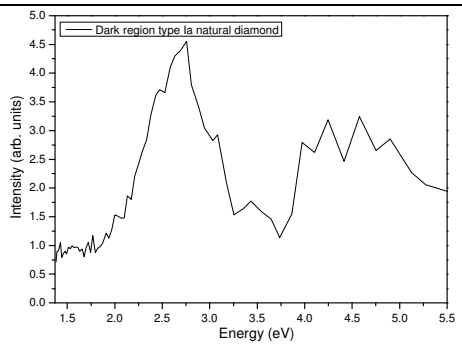

Figure 5-19f: XEOL spectrum for the dark band in figure 5-19e (7x7 pixel array)

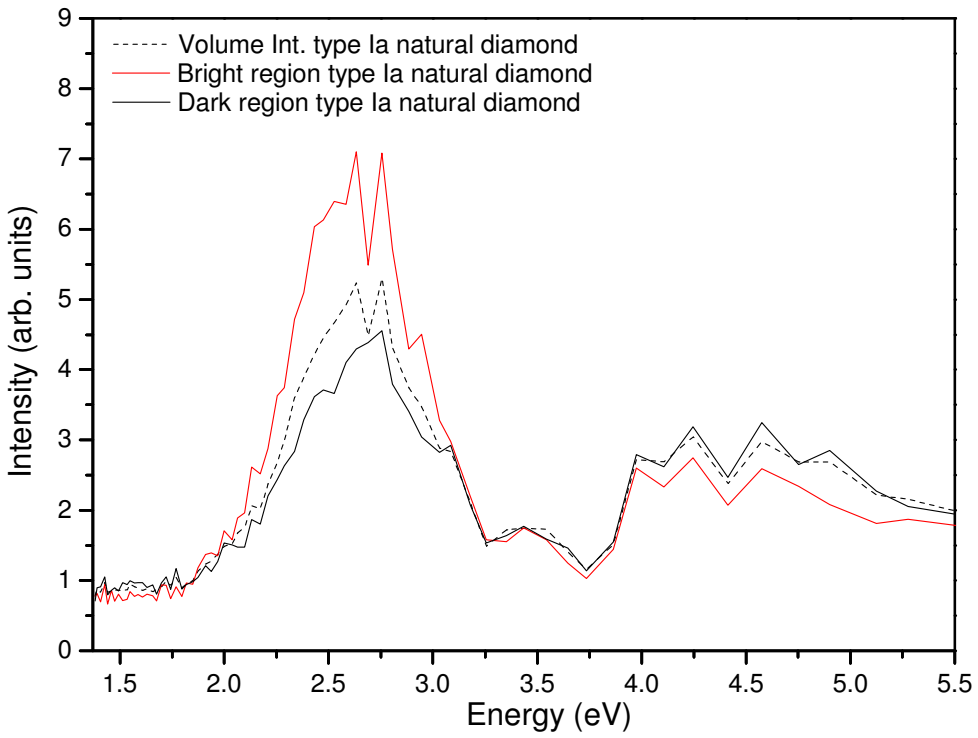

Figure 5-20: The above spectrum is the XEOL spectrum gathered using the CLASSIX spectrometer at beamline MPW6.1 at the SRS, Daresbury. Variations are seen between the different sampling regions in the 2.0-3.0eV range.

The fact that the low energy feature in the 2.0-3.25eV range has significantly reduced may indicate that that band is not as prominent at the darker regions of the sample in question. Further measurements on the same sample (next pages) show that the H3 centre is present in this sample and its location is typically found around 2.463eV. This feature could be decreasing in intensity at these browner regions but it is difficult to quantify due to the poor resolution of the CLASSIX spectrometer. No differences are apparent in the 4-5.5eV region.

In-house XEOL at Aberystwyth (visible region XEOL):

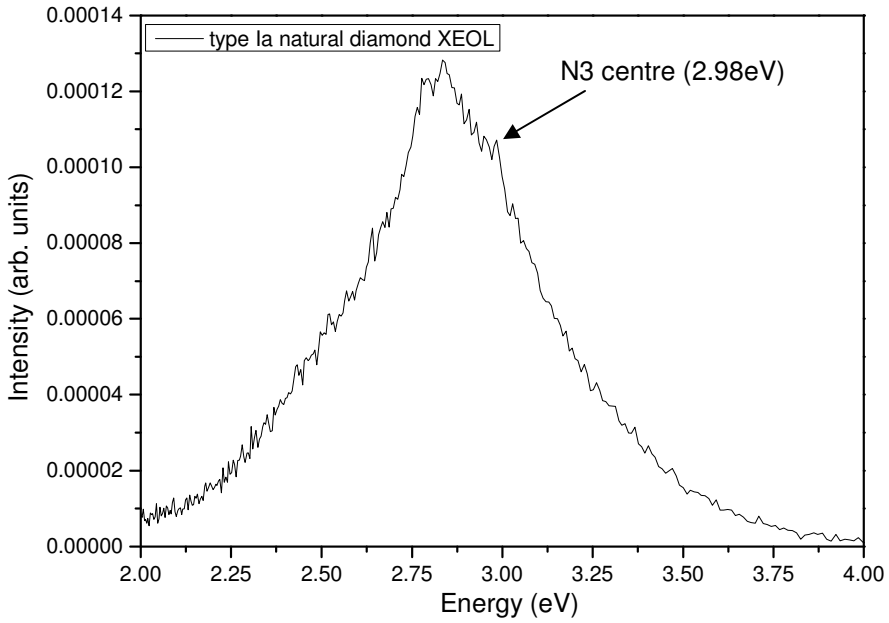

Figure 5-21: An in-house XEOL measurement taken with MoLES using the x-ray source clearly shows the N3 centre ZPL at around 2.98eV.

The in-house XEOL measurement (figure 5-21) clearly shows a slight feature before 3eV at around 2.98eV. This is the N3 centre. The measurement supports what is observed in the PL spectrum obtained for this sample in figure 5-22.

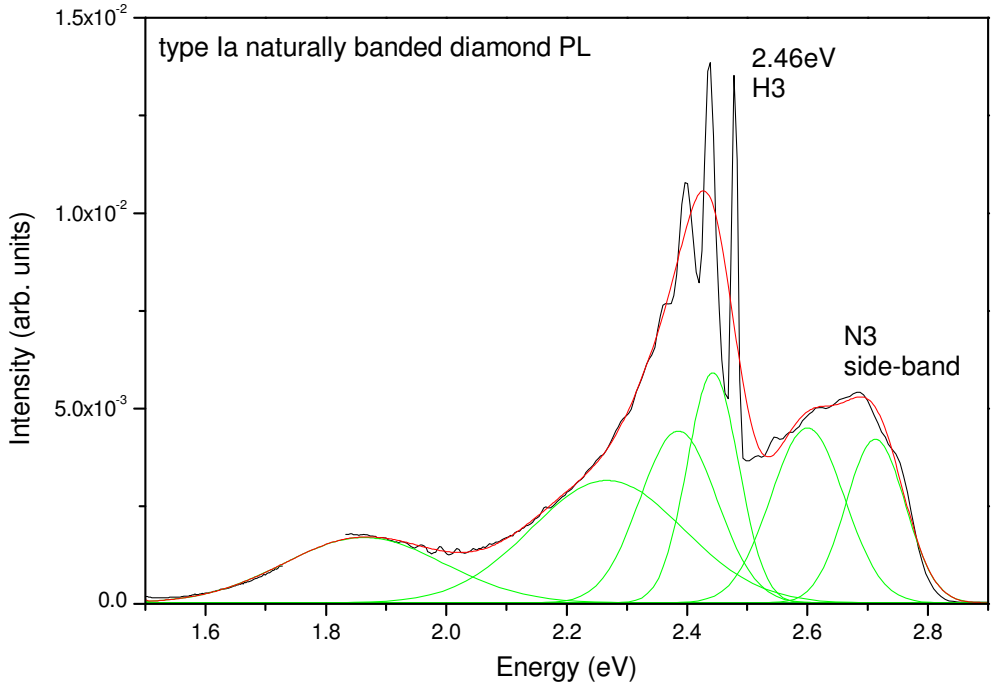

Figure 5-22: PL spectrum for the type Ia banded diamond obtained using a 404nm laser on MoLES.

The PL spectrum obtained for the type Ia banded diamond is typical of a brown type Ia nitrogen containing diamond when excited by a 404nm laser with the sample cooled to a temperature of ~10K. Two BG39 filters (see Appendix for specifications) are mounted prior to the monochromator entrance which results in the cut off above 2.8eV in order to block out the laser from damaging the PMT.

A broad band feature is situated at ~1.875eV with a FWHM of ~0.266eV. This broad band luminescence has previously been observed by De Weerdt *et al*. (*27*) and has been found to be present in natural brown type Ia diamond which show evidence of plastic deformation of which can be observed when the sample is placed between two crossed polarisers – the strain produced by the plastic deformation is clearly visible (Results foreword – prior to chapter 5).

De Weerdt *et al*. observe a maximum at ~1.75eV and state that the precise location of the maximum is sample dependent which bodes well with the maximum location in the XEOL in this investigation which is centred at ~1.875eV. The H3 centre is clearly visible in the acquired spectrum for the type Ia diamond (A465-40-04) at ~2.46eV as well as the N3 side band whereby the N3 ZPL is typically found at ~2.985eV. The N3 ZPL is missing due to the use of a 404nm (3.07eV) laser with two BG39 filters which block out from ~2.8eV and higher. The N3 centre can be observed in the XEOL in figure 5-21.

As mentioned previously the H3 centre is ascribed to a N-V-N arrangement (*19, 27-29*) and it is created when a nearest neighbour nitrogen pair (A-aggregate) capture a vacancy (*29*). The N3 centre consists of three Nitrogen atoms surrounding a vacancy (*28*). It is a very common optical feature in most type Ia natural diamonds containing B-aggregates of nitrogen (*19*).

5.3.2.2 Type IIa natural banded diamond (A490-159).

XEOL studies have also been carried out on a natural type IIa diamond at the MPW6.1 beamline at the SRS, Daresbury using the CLASSIX imaging spectrometer. The CLASSIX setup for XEOL mode for the analysis of Diamond consists of fixing the incident energy at around 280eV (pre C K-edge) and scanning the luminescence light emission through the filters on the filter fly wheel, obtaining an image at each filter using the CCD (see Chapter 3 and 4 for schematic of CLASSIX setup and further details on the XEOL technique respectively).

Volume Integrated

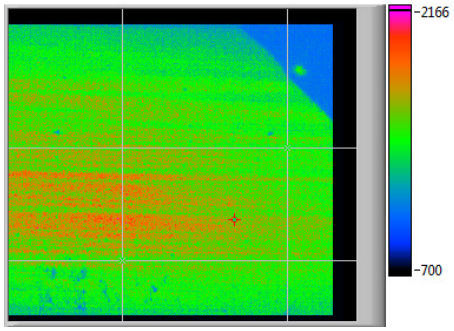

Figure 5-23a: Luminescence image of the type IIa natural diamond (x10 objective). Incident energy ~280eV. The luminescence image here is taken with incident energy of 280eV, through filter ~430nm with a bandwidth of 9.2nm.

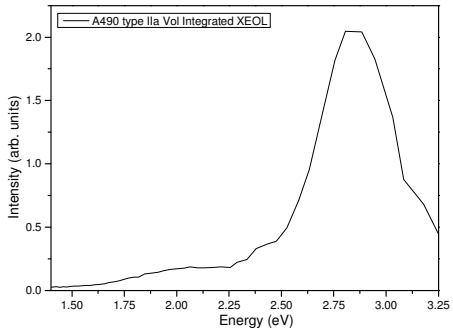

Figure 5-23b: A Volume Integrated XEOL scan of the complete region in Figure 5-23a.

Bright Region

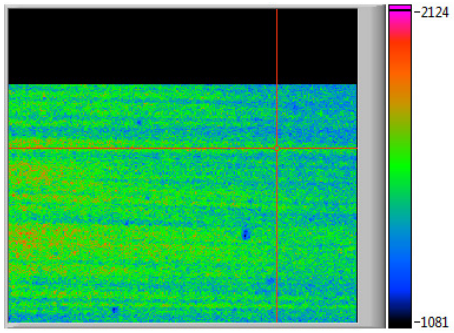

Figure 5-23c: Luminescence image of the type IIa natural diamond (x10 objective) again. Red cross hair is situated on a bright band.

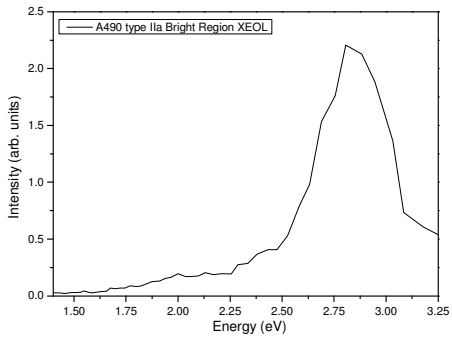

Figure 5-23d: A XEOL scan of the bright region in figure 5-23c. (3x3 pixel array)

Dark Region

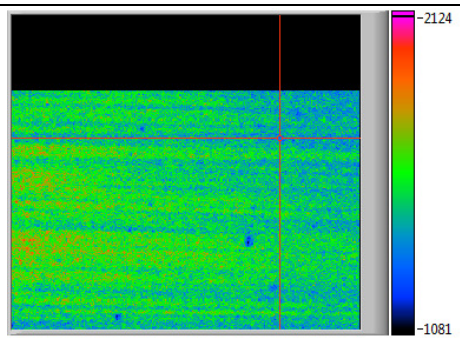

Figure 5-23e: Luminescence image of the type IIa natural diamond (x10 objective) again. Red cross hair is situated on a dark band.

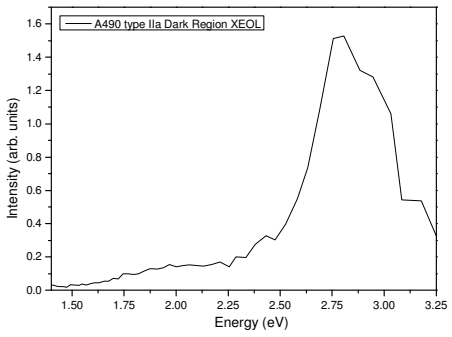

Figure 5-23f: A XEOL scan of the dark region in Figure 5-23e. A significant difference is also present between the bright and dark regions.

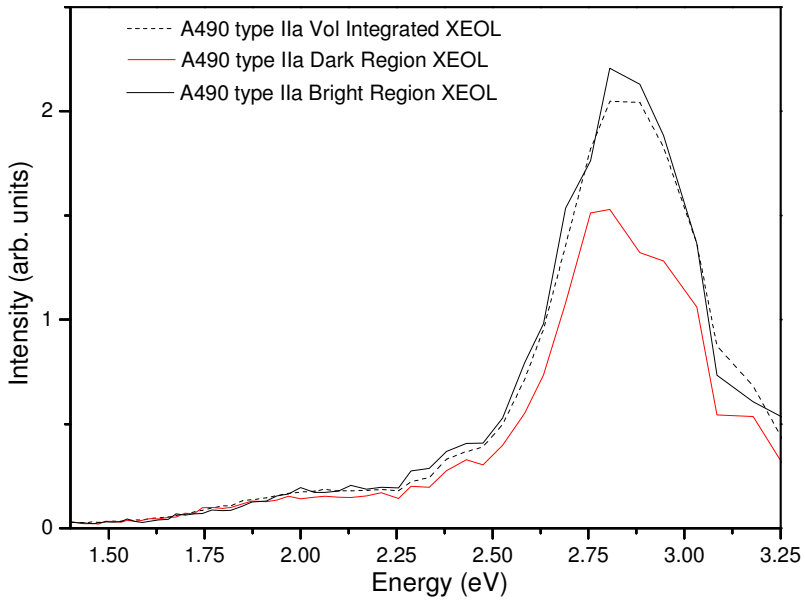

Figure 5-24: All three XEOL spectrums for comparison. Differences are clearly visible between the bright and dark region. The ~2.8eV band is much more enhanced in the bright region compared to the dark region where the band's intensity is much less.

XEOL in house at Aberystwyth using the MoLES spectrometer:

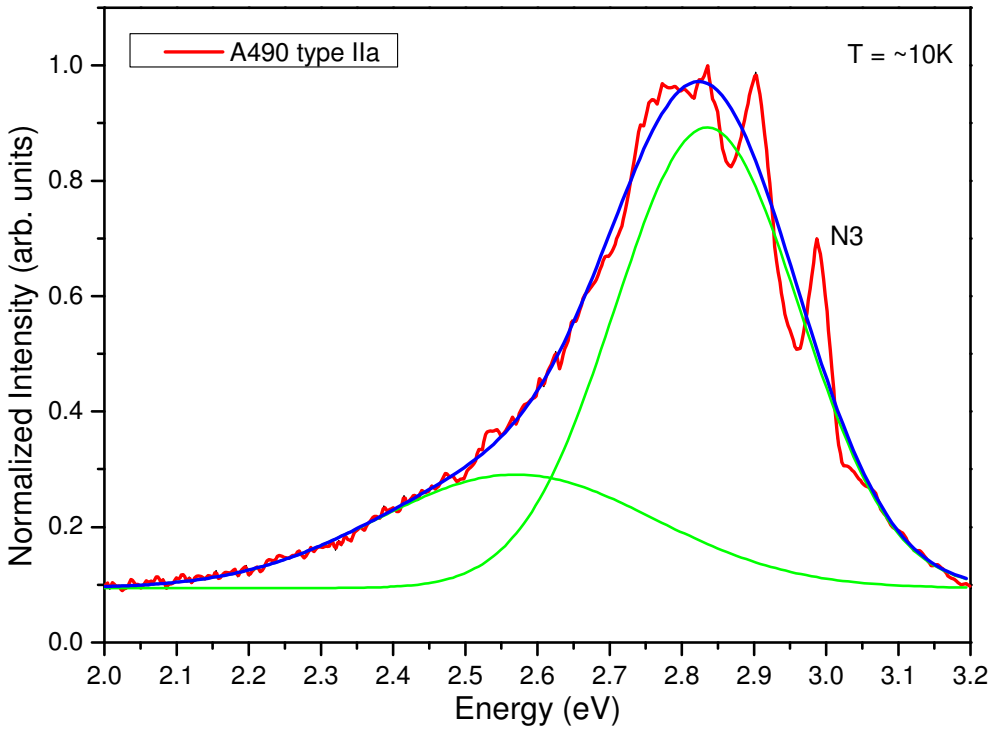

Figure 5-25: Fittings for the type IIa A490 diamond XEOL spectrum.

The XEOL spectrum acquired at Aberystwyth using the Cu K_α x-ray source (figure 5-25) clearly shows the N3 centre located at 2.985 along with the phonon replica lines at lower energies with vibrational energies of 93meV (*19*). There could also be a weak feature of the H3 centre present at around 2.463eV.

The PL spectrum for the A490 type IIa natural diamond in figure 5-26 reveals a small peak located at ~2.156eV which can be attributed to $[N\text{-}V]^0$ and features indicative of the H3 centre at ~2.463eV, as has been previously mentioned in this chapter.

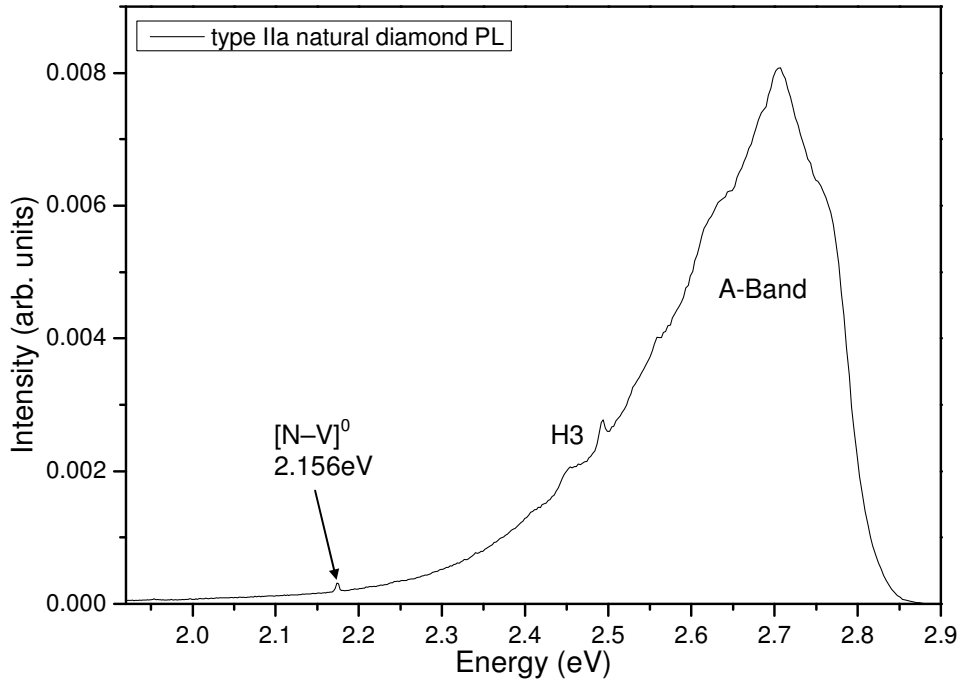

Figure 5-26: PL spectrum for the A490 type IIa natural diamond.(404nm laser).

The well known band-A luminescence band is observed in the XEOL spectrum for this type IIa sample as well as the N3 centre. Which consists of three Nitrogen atoms surrounding a vacancy (figure 5-27). There is mention in the literature that the band-A luminescence changes in intensity with temperature (*8*).

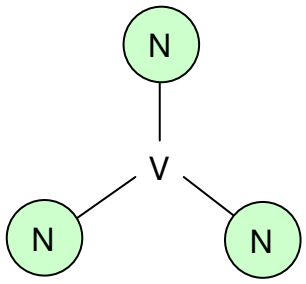

Figure 5-27: The N3 centre, consisting of three nitrogen atoms surrounding a vacancy when looking in the 111 direction.

5.4 Summary

The XEOL and PL spectrum for all samples have been acquired and some have been presented here in this chapter. A summary of the features observed can be found in table 5-1.

Table 5-1:

Sample	Type	Features Observed
Brown CVD Diamond	CVD	1.95eV $[N–V]^-$ 2.156eV $[N–V]^0$ Bands + Features 2.1-2.8eV ~2.316eV – dominating feature in CVD diamond 3.188eV – defect interstitial related feature ~4.2eV – Complex Band ~5.2218eV – possibly near-band gap edge emission
Blue CVD Diamond	CVD	2.27eV – The Green Band commonly seen in CVD + HPHT synthetic diamonds. ~3.61eV – feature typically associated with boron doped diamond. ~4.6eV – appears in samples that have immeasurably low concentrations of atomically dispersed nitrogen (temperature dependent band).
Untreated natural	type IIa	~2.9eV – Band-A luminescence – dislocation related. ~2.463eV – H3 centre
HPHT treated (natural)	type IIa	~2.9eV – Band-A – dislocation related.
Natural colourless	type IIa	~2.9eV – Band-A – dislocation related.
CVD (0542715)	CVD	~2.156eV $[N–V]^0$ Band-A luminescence – dislocation related.
CVD layered (0673803)	CVD	Possible $[N–V]^0$ side-band. Possible TR12 centre (~2.638eV)
Type Ia banded (A465-40-04)	type Ia (natural)	~1.875eV. ~2.46eV H3 centre. ~2.985eV N3 centre (side-band).
Type IIa banded (A490)	type IIa (natural)	~2.156eV $[N–V]^0$ ~2.465eV H3 centre. ~2.7eV Band-A luminescence. ~2.985eV N3 centre.

Features that are typical of the different types have been identified and observed. The different techniques coupled with the different instruments introduced in chapter 3 show how powerful the techniques are in identifying different impurities and species within a particular sample. It is unfortunate that the CLASSIX spectrometer does not provide the resolution that is desperately required in the XEOL spectrum to make analytical statements on the XEOL spectrum originating from a dark and bright region specifically.

The upgrade for CLASSIX due for completion in the near future consists of the filter wheel being replaced by a liquid crystal filter unit. This will undoubtedly significantly improve the resolution of the system, as well as still providing the lateral resolution required for the analysis of variegated samples. The possibilities of identifying the specific defects are extremely likely and may result in many questions being answered as well as posing new ones. The next chapter discusses the Raman results that have been obtained for the diamond samples under study.

5.5 References

1. F. Quinn *et al.*, *Journal of Synchrotron Radiation* **10**, 461 (2003).
2. N. R. J. Poolton, B. M. Towlson, B. Hamilton, D. A. Evans, *Nuclear Instruments & Methods in Physics Research Section B-Beam Interactions with Materials and Atoms* **246**, 445 (2006).
3. D. A. Evans *et al.*, *Journal of Physics-Condensed Matter* **20**, (2008).
4. P. Kania, P. Oelhafen, *Diamond and Related Materials* **4**, 425 (1995).
5. R. J. Graham, T. D. Moustakas, M. M. Disko, *Journal of Applied Physics* **69**, 3212 (1991).
6. H. Sternschulte, J. Horseling, T. Albrecht, K. Thonke, *Diamond and Related Materials* **5**, 585 (1996).
7. E. Rzepka, F. Silva, A. Lusson, A. Riviere, A. Gicquel, *Diamond and Related Materials* **10**, 542 (2001).
8. J. E. Field, *The Properties of Natural and Synthetic Diamond*. (Elsevier Academic Press, 1992).
9. A. M. Zaitsev, *Optical Properties of Diamond*. (Springer, 2001).
10. P. M. Martineau *et al.*, *Gems & Gemology* **40**, 2 (2004).
11. J. Walker, *Reports on Progress in Physics* **42**, 1605 (1979).
12. A. T. Collins, G. S. Woods, *Journal of Physics C-Solid State Physics* **20**, L797 (1987).
13. A. T. Collins, S. C. Lawson, *Journal of Physics-Condensed Matter* **1**, 6929 (1989).
14. A. T. Collins, M. Kamo, Y. Sato, *Journal of Physics D-Applied Physics* **22**, 1402 (1989).
15. S. C. Lawson, H. Kanda, H. Kiyota, T. Tsutsumi, H. Kawarada, *Journal of Applied Physics* **77**, 1729 (1995).
16. H. Kawarada, Y. Yokota, Y. Mori, K. Nishimura, A. Hiraki, *Journal of Applied Physics* **67**, 983 (1990).
17. J. Ruan, K. Kobashi, W. J. Choyke, *Applied Physics Letters* **60**, 3138 (1992).
18. A. T. Collins, H. Kanda, H. Kitawaki, *Diamond and Related Materials* **9**, 113 (2000).
19. A. Zaitsev, *Optical Properties of Diamond A Data Handbook*. (Springer, 2001).

20. P. J. Dean, *Physical Review* **139**, A588 (1965).
21. G. Davies. (Personal Communication, 2010).
22. V. G. Vins *et al.*, *Diamond and Related Materials* **19**, 829 (2010).
23. E. J. Brookes, J. D. Comins, R. D. Daniel, R. M. Erasmus, *Diamond and Related Materials* **9**, 1115 (2000).
24. A. T. Collins. (Personal Communication, 2010).
25. A. T. Collins, A. Connor, C. H. Ly, A. Shareef, P. M. Spear, *Journal of Applied Physics* **97**, (2005).
26. N. Fujimori, Y. Nishibayashi, *Diamond and Related Materials* **2**, 762 (1993).
27. F. De Weerdt, A. T. Collins, *Diamond and Related Materials* **16**, 512 (2007).
28. K. Iakoubovskii, A. Stesmans, *Journal of Physics-Condensed Matter* **14**, R467 (2002).
29. K. Iakoubovskii, G. J. Adriaenssens, N. N. Dogadkin, A. A. Shiryaev, *Diamond and Related Materials* **10**, 18 (2001).

Chapter

6

6.0 Raman Measurements on Natural and Synthetic Diamond

6.1 Introduction

Raman spectroscopy is a technique that can be applied to solids, liquids and gas samples and consists of the detection of inelastically scattered light from an irradiated sample. Molecular vibrations within the sample provide shifts in wavelength that are characteristic of different samples and that can be used to analyze the interaction between different chemical bonds that are present within (see chapter 4).

Laser Raman spectroscopy is widely used as a diagnostic tool due to its sensitivity to different carbon microstructures. It makes it one of the best at identifying the physical properties and characterising carbon based materials such as diamond and chemical vapour deposited (CVD) diamond films. It is an invaluable non-destructive technique, requiring very little or no sample preparation whatsoever and is popular in Material research due to each carbon allotrope providing a clearly identifiable Raman signature.

Presented in this chapter are the Raman results obtained for the uniformly coloured and variegated diamond samples that have been carried out on a Horiba Jobin Yvon LabRam HP Raman Spectrometer coupled to a Class 3B HeNe laser (632.8nm). Ex-

situ, Room Temperature measurements were undertaken at the Materials Laboratory in Aberystwyth. Studies have revealed correlations with brown regions and allotropes of carbon of specific wavenumbers (cm^{-1}). The x10 objective was used for data acquisition and characterisation of these diamonds.

6.2 Raman spectroscopy of Diamond

Within two years of the discovery of the Raman effect (*1*), room-temperature Raman measurements were carried out by Robertson *et al.* (*2*) before going on to fashion the diamond classification system (*3*). The Raman technique is a widely accepted characterisation tool for all types of materials and is implemented in the study of diamond due to its capabilities of unearthing important data relative to the structural properties of the sample in question without destruction or damage.

Raman spectroscopy measurements have been implemented in the study of CH stretching on diamonds of different origins (*4*) and is key to the understanding of the growth mechanisms involved in CVD diamonds as well as being widely used as a diagnostic tool for the evaluation of the phase purity and perfection of diamond films grown by CVD (*5*). The Raman technique can be utilized in the characterisation of diamond samples such as CVDs for the purpose of application in technology. It can easily identify the diamond quality and locate for example, unwanted species such as sp^2 bonded carbon for the purpose of obtaining high quality crystals which is undoubtedly an essential aspect and vital part in the production of high quality diamond for electronic applications.

Raman scattering is seen as an important measurement technique for the characterisation of thin film diamonds. It is important to understand the mechanics in relation to the growth of the films and to establish whether the films are associated with sp^2 (graphitic – first order Raman line at $1580cm^{-1}$) or sp^3 (first order Raman line at $1332cm^{-1}$) (*6*).

An example of the effects of mixing the types of bonding within a sample on the scattered spectrum has been carried out by Shroder *et al.* whereby hexagonal boron nitride – diamond and diamond-graphite mixtures were studied. It was shown that

different concentrations and crystallite sizes had a significant effect on the ratios of Raman peak intensities in the measurements on the mixtures (*6, 7*).

Raman studies have been carried out on the diamond samples to provide information on the local chemical bonding. Raman spectroscopy is able to provide information in identifying the presence of sp^2 carbon-species in a sp^3 host material and the Raman results obtained seem to suggest the presence of these sp^2 and sp^3 bonded carbon atoms as was initially thought in some of the samples. This chapter is split into two parts; the first presents the Raman spectrum gathered for the homogeneous uniformly coloured samples of which their depth of colour is clearly visible to the naked eye, as well as being uniform throughout the sample. The second is the data gathered for the non-homogeneous variegated diamond samples, whereby the Raman mapping technique was utilized for data acquisition.

6.2.1 Uniformly Coloured Diamonds

Presented here are the Raman results for the uniformly coloured diamonds along with analysis and discussion for each individual sample. The blue and brown (small – 0473906) single crystal CVD diamond samples shall be firstly discussed as they have been jointly studied for the Raman, XEOL, NEXAFS and OD-XAS measurements throughout the course of this research.

6.2.1.1 Blue and Brown (0473906) Single Crystal CVD

The blue diamond is a CVD highly boron doped sample (~10^{16} atoms per cm^3) of which the depth of colour is a good indication of the degree of doping involved. Both blue and brown single crystal CVDs are uniform in colour and have been studied closely together during the course of this research. The reason for this was due to their differences/contrasts in colour and also their colour uniformity. The samples were used for initial experiments for Raman, XEOL, NEXAFS and OD-XAS measurements to study their chemical and local structure and find information that could lead to the discovery of the cause of the brown colour. The uniform samples were studied prior to the acquirement of the variegated samples to prove the techniques and studies successfully worked and were a feasible means of characterisation.

Figure 6-1 and 6-2 show the Raman spectrum for both the blue and brown single crystal CVD samples. It is evident that there is a significant background effect for the brown sample measurement compared to the blue sample (Figure 6-1). A study of diamond Raman spectrums carried out by Prawer *et al.* (*8*) report that when analyzing Raman data the peaks are often fitted with a combination of Gaussian and Lorentzians with sloping backgrounds and they associate the background with Photoluminescence (PL) attributed to the neutral nitrogen-vacancy complex $[N\text{-}V]^0$ (575nm) or the charged nitrogen-vacancy complex $[N\text{-}V]^-$ (638nm) optical centres, which tie in well with the XEOL studies on the brown single crystal diamond previously mentioned in chapter 5. Work carried out by Wolden *et al.* on the influence of nitrogen addition to combustion grown diamond also noticed an increase in the background as more and more nitrogen is added to the mixture (*9*).

The diamond Raman line dominates the spectrum in the results for both blue and brown CVD diamonds. It corresponds to first-order Raman scattering and can be attributed to the vibrations of the two interpenetrating cubic sublattices. The lines exist at ~1332.83cm^{-1} (Lorentzian width of ~1.64cm^{-1}) and at ~1332.77cm^{-1} (Lorentzian width of ~1.68cm^{-1}) for the blue and brown samples respectively. They are similar in location and their FWHMs agree with measurements in the literature (*8, 10*) (FWHM of 1.5 to 40cm^{-1}). Prawer and Nemanich (*8*) declare a peak at 1332cm^{-1} with a FWHM of 1.2cm^{-1} and go on to state that the 1332cm^{-1} peak on a flat background with no observable peaks in the region 1500-1550cm^{-1} can be taken as strong evidence for the production of 'pure' diamond with virtually no non-diamond components present (*5, 8*). The blue CVD diamond provides a very good Raman spectrum with high intensity along with similar trends to those stated by Prawer and Nemanich (*8*) of which are indicative of a high quality crystal diamond. No features are present in the 1400-1800cm^{-1} range.

The sharpness of the diamond line at 1332cm^{-1} allows diamond to be recognised in the presence of sp^2 bonded carbon in diamond films (*6*). A single, sharp peak at 1332cm^{-1} can be used as a signature of high crystalline quality (*11*) and the FWHM of the Raman line is often taken as a measure of the 'perfection' of the diamond crystallite, with its peak position used as an estimate of the residual stress, strain and crystal size (*8, 12, 13*). An increase in defect density for example would vary the 1332cm^{-1} peak position as well as increase the FWHM (*14*) – the peak would become broader (*15*). Haque *et al.* studied different quality arc-jet-deposited diamonds and noted that the darker the colour of the sample, the larger the nondiamond 1560cm^{-1} peak intensity and the larger the FWHM of the Raman diamond peak at 1332cm^{-1} (*16*). This agrees with some of the results mentioned later in this chapter in relation to nondiamond features at higher wavenumbers (~1560cm^{-1}) for some of the diamond samples studied during the course of this research.

A uniformly coloured brown single crystal CVD sample was also studied via Raman spectroscopy for direct comparison with the blue single crystal CVD. Peaks and features observed in the brown diamond Raman spectrum appear to reflect sp^2 bonded species within the sample and are quite possibly located either in the bulk or at grain boundaries. A band in the 1520-1580cm^{-1} range with a FWHM of 100cm^{-1} is known

in the literature as the G-peak, sp^2 amorphous carbon (*17*). Features present within the 1475 – 1564cm^{-1} range are typical signatures of disordered sp^2-bonded carbon. A feature at around 1350cm^{-1} is commonly referred to as the D-band and is also attributed to sp^2 hybridized carbon phases (*17-19*) and has the effect of broadening the 1332cm^{-1} peak at its base out towards the 1350cm^{-1} region.

There is no feature of the D or G-band present of which the latter typically composes of two bands peaking at 1470cm^{-1} and 1600cm^{-1}. There is a suggestion of a peak at ~1600cm^{-1} in the spectrum but cannot clearly be associated with the G-band. Structure seems to be present within the 1500-1600cm^{-1} region similar to those previously reported by Zhou *et al.* (*20*). The report concludes that the diamond film under study consists of both diamond (sp^3) and sp^2 non-diamond carbon.

The presence of second-order Raman peaks are clearly visible in both samples at higher wavenumbers and relate to two phonon scattering processes in diamond. They can be found with a maximum at 2467cm^{-1} along with a sharp cut-off at 2667cm^{-1} (*21, 22*). This second-order phonon band consists primarily of overtone and combination bands of phonons at high symmetry points in the Brillouin zone (*23*). The potential of using CVD diamonds for different applications where they may be subjected to high temperatures is highly significant and temperature studies of the first and second order Raman spectrum for diamond have been carried out by Solin *et al.* and Herchen *et al. (22, 24-26)*. No temperature dependence Raman measurements were undertaken during the course of this research, all samples were measured at room temperature.

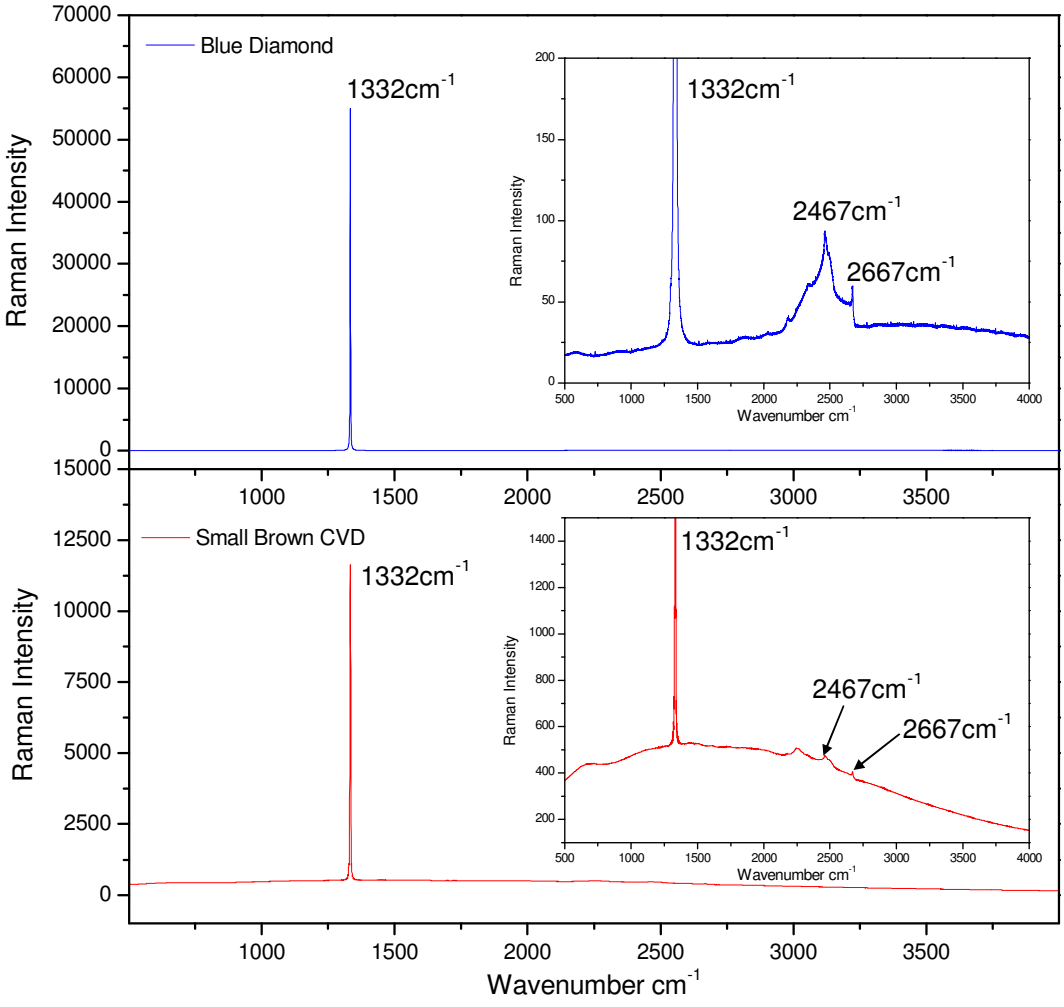

Figure 6-1: Raman spectrum for both the Blue and Brown CVD diamond samples.

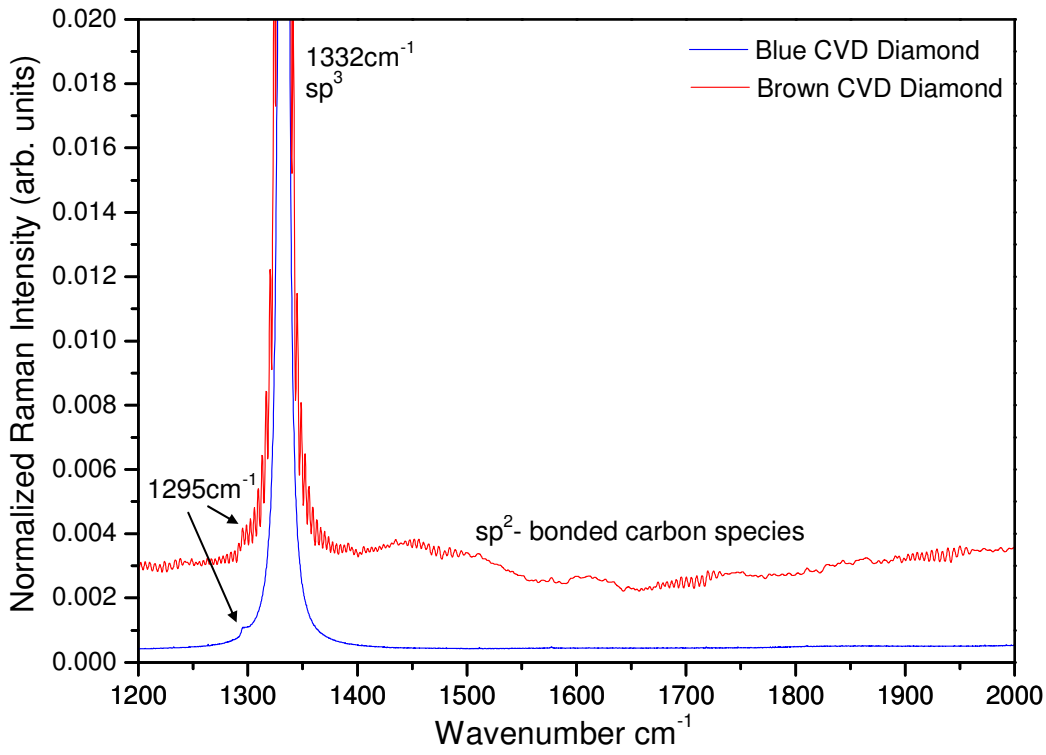

Figure 6-2: Normalized diamond peak spectrum for the Blue and Brown diamonds in the 1200-2000 cm^{-1} range. The luminescence background has also been subtracted for the brown CVD diamond. Features are clearly visible in the 1400-1800 cm^{-1} range for the brown CVD that can be attributed to sp^2 bonded-carbon features.

The Normalized Raman spectrum (figure 6-2) show features that are present in the brown CVD which are absent in the blue CVD sample. The luminescence background observed in figure 6-1 has been subtracted from the brown CVD data in figure 6-2. The spectrum obtained closely resembles the spectrum obtained by Zhou *et al.* (*20*) whereby they concluded that their film consists of both diamond (sp^3) and sp^2 non-diamond carbon. From Raman measurements, conclusions can be gathered that a significant amount of sp^2 bonded-carbon species exist in the brown CVD single crystal sample. The Raman spectrum for the blue single crystal CVD diamond suggests that it is of high quality as mentioned previously as well as the fact that no features exist indicative of sp^2 bonded-carbon species in the 1400-1700cm^{-1} region (*18*). The feature present at ~1295 cm^{-1} in both samples could be a feature related to the phonon density of states (PDOS) of diamond (*8*).

6.2.1.2 Large Brown CVD sample (0473904)

A Raman spectrum for a large brown CVD sample was also obtained to provide a comparison with measurements taken for the small brown CVD diamond (Sample No. 0473904).

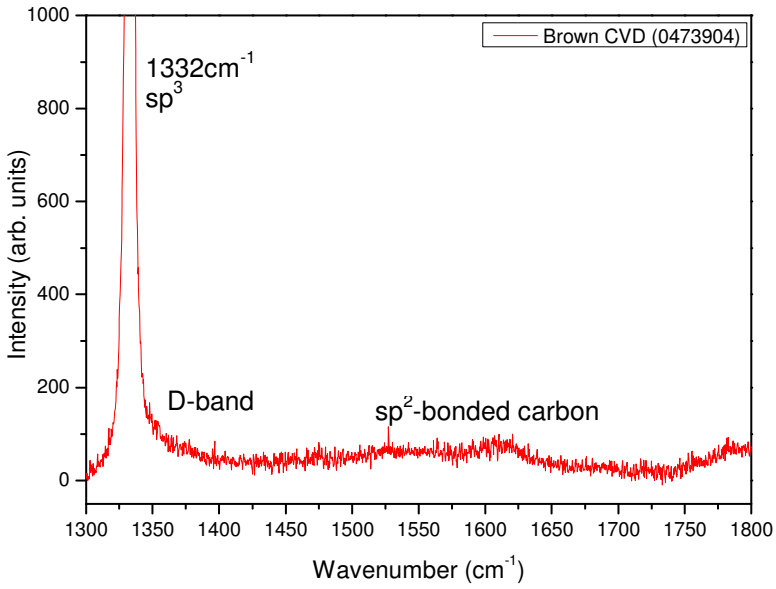

Figure 6-3: Raman spectrum for another brown CVD sample.

The spectrum for both brown CVD samples differ slightly. In the large CVD brown diamond, a broadening of the higher wavenumber side of the 1332cm^{-1} peak can be observed. This could be due to the D-band that is usually situated around 1350cm^{-1} and attributed to non-diamond phases such as sp^2 carbon species (*17*). In the small brown CVD sample, a band was present in the 1400cm^{-1} – 1500cm^{-1} region. Features in this region are not observed in the larger brown CVD, although a band is present situated at around 1600cm^{-1}. From the collated data by Zaitsev this could be attributed to amorphous carbon or microcrystalline graphite although it also states that it could be related to hydrogen bound sp^2 bonded carbon (*18*).

6.2.1.3 Untreated and HPHT treated Natural type IIa Diamonds

The three natural type IIa (brown, HPHT treated and naturally colourless) samples have also been studied with the Raman spectrometer and the results are presented here.

6.2.1.3.1 Untreated type IIa Diamond

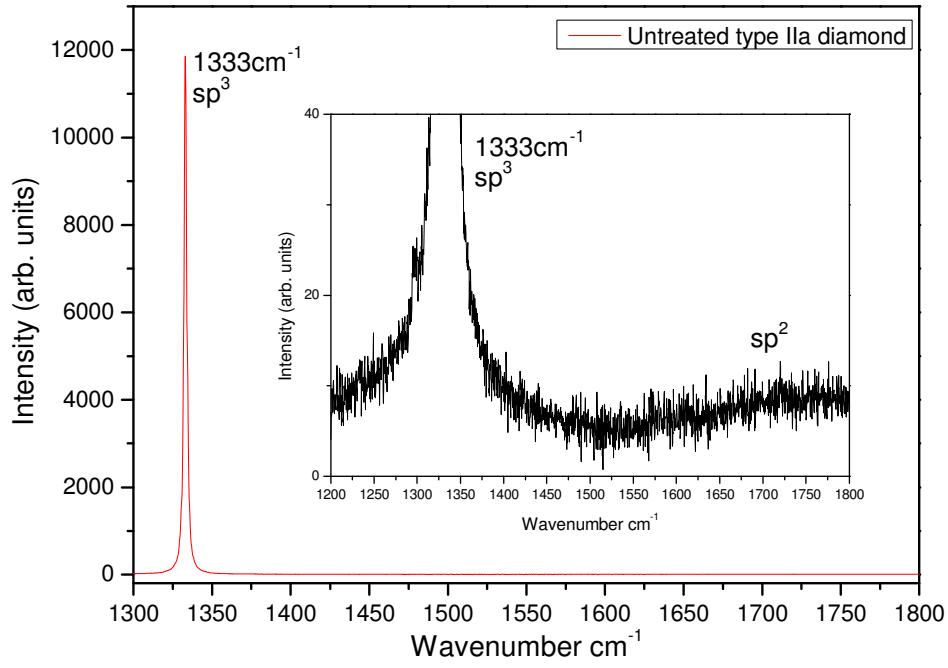

Figure 6-4: Raman spectrum for an Untreated type IIa diamond sample of uniform brown colouration.

The untreated (brown type IIa sample) (figure 6-4) has a typical Raman spectrum as would be expected for a brown diamond from previous Raman spectrum studies obtained for the brown CVD diamonds (figure 6-2 and 6-3). The diamond peak relative to C-C interactions within the lattice is well pronounced at 1333cm^{-1} with a lorentzian width of 2.05cm^{-1} and agrees with measurements mentioned found in the literature (*8, 18*). Features can also be clearly distinguished at higher wavenumbers especially in the 1500-1800cm^{-1} region when looking at the magnified spectrum in the inset (figure 6-4). These features tie in well and are in agreement with the expected sp^2 content typically observed in a brown diamond.

6.2.1.3.2 HPHT treated type IIa Diamond

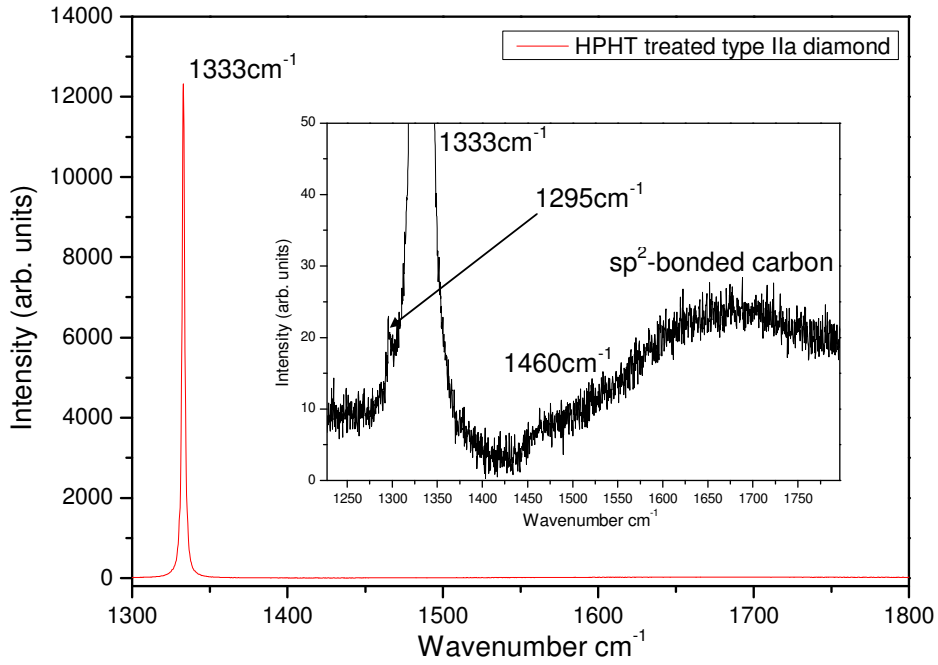

Figure 6-5: Raman spectrum gathered for a HPHT treated (therefore colourless) natural type IIa diamond.

The Raman spectrum obtained for the HPHT treated diamond is shown in figure 6-5. A narrow peak is well defined at 1333.0cm^{-1} with a lorentzian width of 1.96cm^{-1}, but there is a significant broad band that seems to peak at around 1689cm^{-1}. Another band seems to be present at around 1460cm^{-1} and this is seen in some of the variegated CVD diamonds that will be discussed in detail later in this chapter. This result when compared with the untreated brown sample suggests that there is a higher concentration of sp^2 bonded-carbon species present in the HPHT treated colourless sample than the untreated brown sample. This result is rather surprising due to the fact that the sp^2 bonded carbon species were initially thought to be responsible for the brown colouration. There could also be a slight luminescence effect on the Raman spectrum to provide a slight background effect, but nonetheless the peaks are significantly prominent. A feature is again observed here at ~1295cm^{-1} and as stated earlier could be related to the phonon density of states (PDOS) of diamond (*8*).

Work by Martineau *et al.* (*27*) state that the brown colouration is associated with plastic deformation and that they found no evidence that any of their brown CVD

synthetic samples were plastically deformed. The Raman studies undertaken by the group did find correlation with the studies presented here, that there are non-carbon species present in type IIa diamond and particularly of higher intensity in their CVD brown diamond studied. A significant statement follows this, that after HPHT treatment of their diamond samples, the non-diamond carbon is no longer present – a significant difference to the data presented here whereby an *increase* is observed in the non-diamond carbon (sp^2 bonded carbon species) in the HPHT treated sample (*27*).

A significant factor that must be considered when analysing the two natural type IIa sister diamonds is that both have originated from the same original stone with one undergone HPHT treatment. Due to both being of natural origin, it is quite possible that they could contain a wide range of impurities that are not common to both and possibly are not uniformly spread throughout the original initial stone. This would result in both i.e. having different impurity contents that would result in different results as observed in the Raman. As a means of overcoming such an occurrence for future studies, it would be best to have two sister samples of same nature but that have originated from the same synthetic stone whereby the impurity content and doping is known and has been regulated during growth.

6.2.1.3.3 Naturally Colourless type IIa diamond

For comparison a Raman spectrum was obtained for a naturally colourless type IIa diamond as shown in figure 6-6.

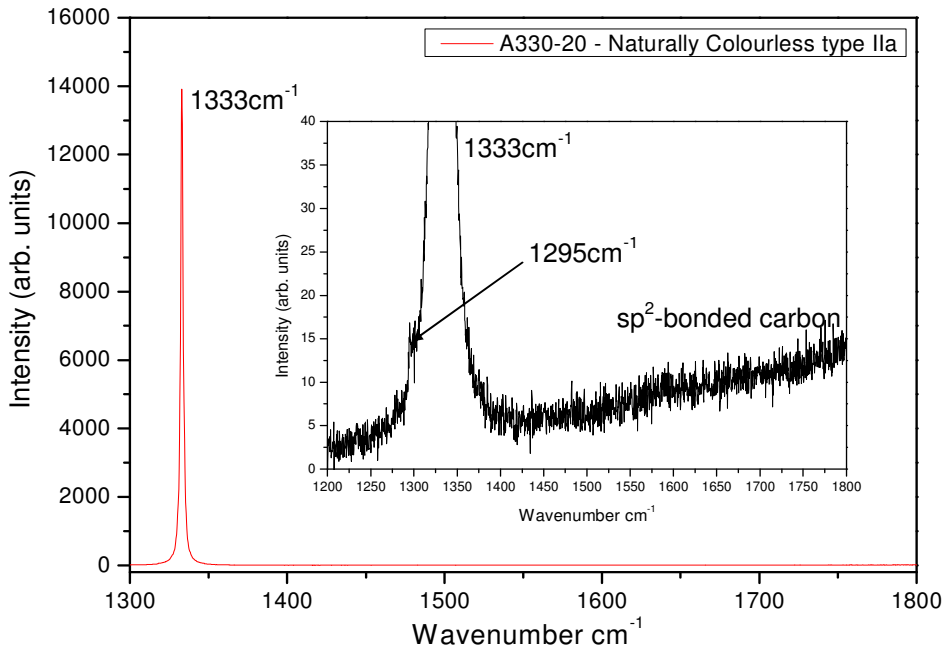

Figure 6-6: Above is the Raman spectrum for the Naturally colourless type IIa diamond for comparison with the untreated and the HPHT treated type IIa diamonds.

The naturally colourless type IIa sample shown in figure 6-6 also presents a well defined diamond peak situated at 1333.0cm^{-1} with a lorentzian width of 1.88cm^{-1}. The conclusion that can be gathered from this result is that no significant feature as predominant as that observed for the HPHT diamond has been observed at the higher wavenumbers.

It should be noted that the area under the curve does not provide any information relative to the amount of i.e. sp^2 bonded-carbon or sp^3 bonded-carbon species present. Therefore a direct comparison can not be directly made in this way. The only information that can be justifiably gathered is that sp^2 bonded-carbon species are present in the HPHT treated sample. Additional measurements with other techniques are required for further comment and discussion.

6.2.2 Variegated Diamond

On the following pages, the Raman spectrum obtained for the non-homogeneous diamond samples are presented. The results are presented alternative to the discussion for each sample.

The Raman instrument was utilized in mapping mode (red – high intensity, blue – low intensity), whereby an array of measurements were taken over a specific area. A typical area of ~500μm x ~500μm was analyzed with a Raman scan taken at 10μm steps in the 1300-1550cm^{-1} range for each sample. The photon energy for the Raman instrument was 1.96eV (632.8nm) (HeNe laser) with a magnification objective of x10.

6.2.2.1 CVD diamond (0542715)

The CVD sample shows strong lateral variations in colour and was provided by the Diamond Trading Company (DTC) and required only solvent cleaning prior to study. The sample has been polished so that the brown regions are as close as possible to the surface for study. The same brown feature has been studied in all techniques on this CVD sample.

6.2.2.1.1 Volume Integrated Raman

Prior to investigating the CVD (0542715) diamond sample in mapping mode a general Volume Integrated (over the whole sample) Raman scan was made in the 1300-1650cm^{-1} range and the results obtained are shown in figure 6-7, below.

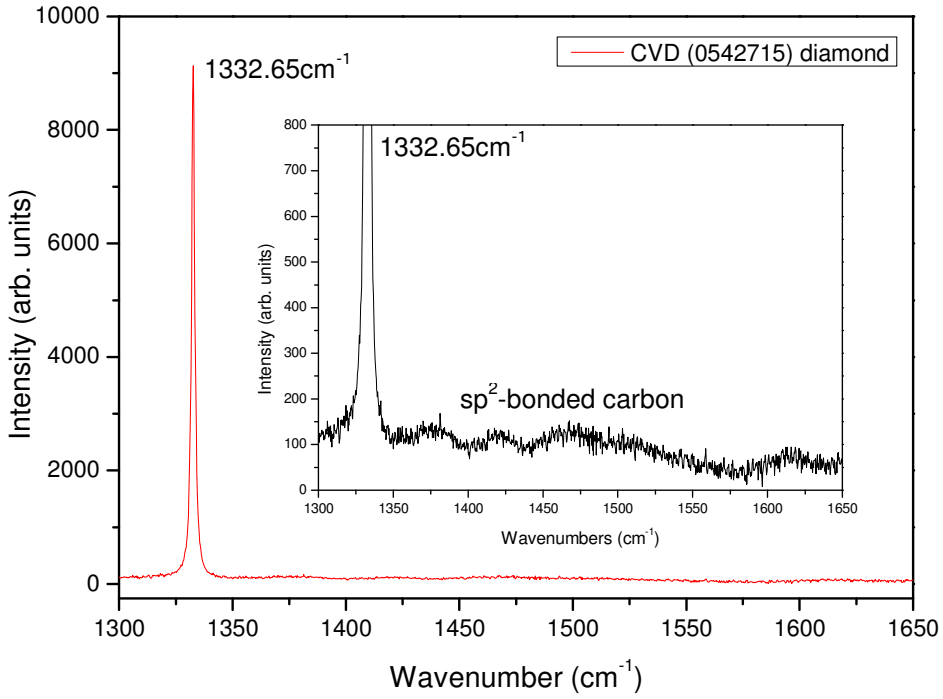

Figure 6-7: Raman spectrum over the whole of the CVD diamond in the 1300-1650cm^{-1} range.

The diamond peak situated at 1332.65cm^{-1} with a lorentzian width of 1.657cm^{-1} is of high intensity. This is a surprisingly good value for the diamond peak due to the sample being of low optical quality (*8*). Features that have already been mentioned earlier in this chapter can clearly be observed from 1350cm^{-1} to 1650cm^{-1}, ranging from the D-band at ~1350cm^{-1}, to the typical sp^2 bonded carbon features that are indicative features at these wavenumbers.

6.2.2.1.2 Raman Mapping measurements

Following the acquirement of the volume integrated spectrum for the 0542715 CVD diamond a Raman mapping spectrum was obtained as shown in figure 6-8(a-f).

BRIGHT REGION

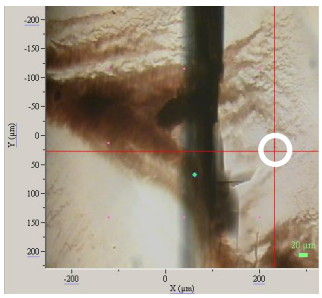

Figure 6-8a: Photograph of CVD sample

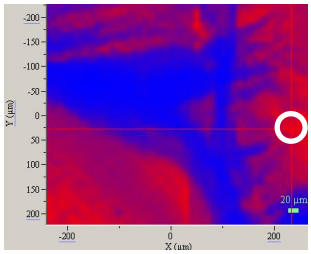

Figure 6-8b: Red intensity – high signal, relative to 1332.79cm^{-1} diamond peak

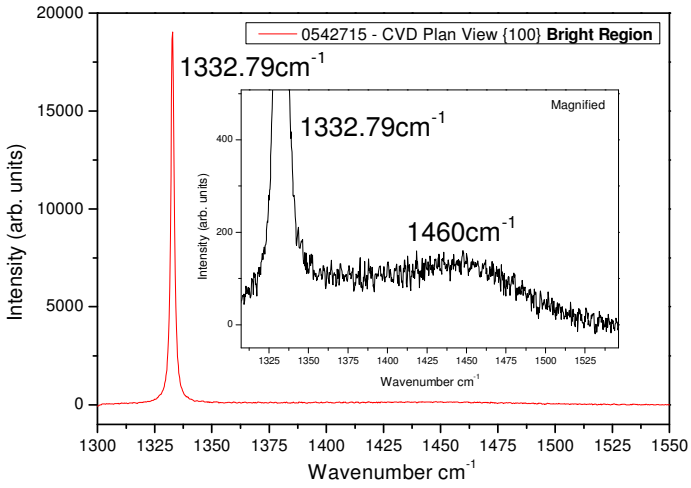

Figure 6-8c: Raman spectrum taken at a bright region. The ~1332.79cm^{-1} diamond signature line is dominant. The inset is a magnified section showing the presence of a peak at ~1460cm^{-1}.

DARK REGION

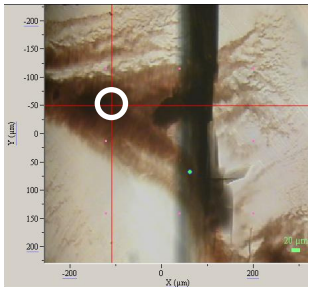

Figure 6-8d: Photograph of CVD sample

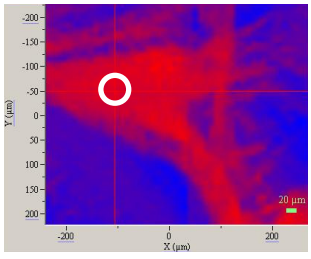

Figure 6-8e: Red intensity – high signal, relative to ~1457.75cm^{-1} diamond peak

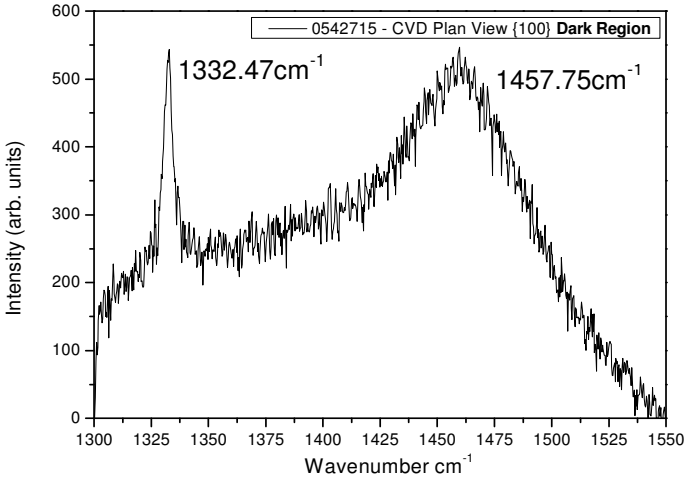

Figure 6-8f: Raman spectrum taken at a dark region clearly showing features indicative of sp^2 bonding. The ~1332.47cm^{-1} peak is present but with the addition of a large ~1457.75cm^{-1} peak with a width of 61.54cm^{-1}.

The Raman data obtained in mapping mode differs slightly from that of the Volume Integrated result shown in figure 6-7. More features were present in the Volume Integrated spectrum typically indicative of sp^2 bonded carbon.

The dark regions in the CVD diamond from the Raman mapping data are clearly defined and visible in transmitted light as shown in figure 6-8a and 6-8d. The regions are also apparent when Raman intensity mapping is used (figure 6-8b and 6-8e). The contrast is generated by the relative intensities of the diamond peak at 1332cm^{-1} (that has a lorentzian width of 1.67cm^{-1}) and the broader peak that has been observed in the brown region at ~1457.75cm^{-1} (width of 61.54cm^{-1}).

The observable features that contrast between both regions of analysis are firstly the diamond peak is significantly less intense at the darker region compared to the bright region. Although mentioned previously that a comparison of the areas under the spectrum cannot be justified in comparing different samples, but for one sample under analysis and the probing of two regions on that same sample, a conclusion can be justifiably gathered with regards to quantity. The width of the ~1332.47cm^{-1} diamond peak at the dark region is significantly broader than that at the bright region with a width of ~5.05cm^{-1} for the brown region and ~1.67cm^{-1} at the bright region. The significant difference is indicative of low quality diamond present in the dark region compared to the bright region.

The brown regions showed a higher concentration of the ~1457.75 cm^{-1} resonance with a much lower intensity 1333 cm^{-1} resonance. In fact the intensities for both features are of similar levels/values. The non-brown regions have a slight presence of the ~1457.75 cm^{-1} band along with a high concentration of the 1332.79 cm^{-1} diamond C-C resonance.

The reason for the slight presence of the ~1457 cm^{-1} peak in the brighter coloured region could be due to the fact that the bright coloured regions are not in fact perfectly colourless, but most likely to be brown or light brown and the darker regions to be *browner* – a much more intensely coloured brown.

This ~1460cm^{-1} feature has been mentioned previously in the literature but found at a slightly lower wavenumber of 1450cm^{-1} (*19*). It has generally been observed in the 1430-1470cm^{-1} range (*8*).

Interesting studies by Ferrari *et al.* on the origin of the 1150cm^{-1} Raman mode in nanocrystalline diamond mentions the presence of the 1450cm^{-1} which is always present with the 1150cm^{-1} feature. They have attributed the features to transpolyacetylene segments located at grain boundaries and surfaces (*8, 18, 19*). Ferrari *et al.* investigated the changes observed when using different Raman excitation wavelengths in order to identify the origins. They noted that the 1150cm^{-1} and 1450cm^{-1} peaks dispersed by around 50-100cm^{-1} with excitation energy. They state that this would not be possible for a density-of-states feature as it should remain fixed as the excitation energy is increased. Another factor they discovered was that the intensity of both peaks decreased compared to the 1332cm^{-1} diamond peak as the excitation energy was increased. If both of the features were due to sp^3 species, the intensity of both would increase as the excitation energy in raised. This is due to the sp^3 site having a wide, 5.5eV band gap. Teng *et al.* have also observed the 1460cm^{-1} peak and attributed it to non-diamond carbon (transpolyacetylene) located at grain boundaries (*28*).

Another factor that disregards the 1450cm^{-1} as a sp^3 bonded feature is the fact that sp^3 bonding can only give modes up to around 1350cm^{-1}, the band limit of diamond (*29*). Ferrari *et al.* have attributed the 1150cm^{-1} and 1450cm^{-1} to transpolyacetylene (trans-PA) which is an alternate chain of sp^2 carbon atoms, with a single hydrogen bonded to each C. They state that the trans-PA features are located at grain boundaries and that it must have originated from the deposition mechanism during the diamond growth. The feature is clearly connected to the presence of hydrogen and the 1450cm^{-1} feature is not seen in CVD diamond created by shock synthesis. They also state that the features are typically present in low quality CVD diamond (*19*). Zaitsev's collated Raman features data book, also mentions the trans-PA feature to be found in the 1450cm^{-1} to 1480cm^{-1} Raman region (*18*).

A conclusion can therefore be gathered that there exists a higher concentration of sp^2-bonded carbon species in the darker regions of the sample compared to the brighter coloured regions.

6.2.2.2 CVD layered (0673803)

6.2.2.2.1 Volume Integrated Raman

Prior to the Raman mapping measurements the Volume Integrated Raman spectrum was obtained for the CVD layered sample which comprised of the features shown in figure 6-9 below.

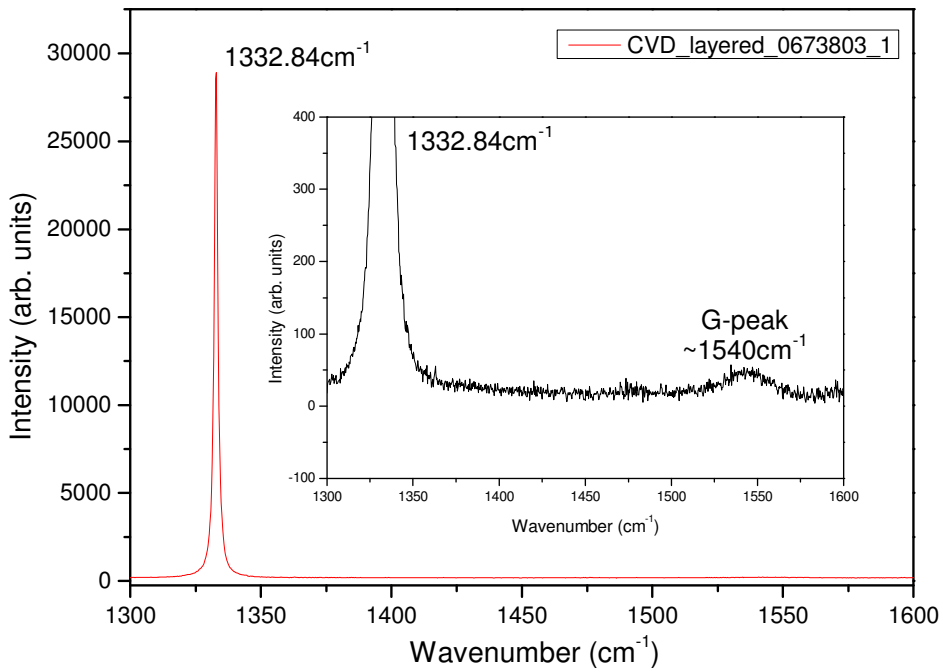

Figure 6-9: Raman spectrum for the layered CVD diamond sample over a large area.

A strong diamond peak can clearly be observed situated at ~1332.84cm^{-1} with a lorentzian width of ~1.64cm^{-1}. The reason for the high intensity diamond signal could be due to the HPHT diamond substrate the sample was grown. The only observable feature at the higher wavenumbers is the G-peak situated at ~1540cm^{-1} typically indicative of graphitic sp^2 carbon bonding.

6.2.2.2.2 Raman Mapping measurements

The Raman mapping results for this CVD layered sample can be seen in figure 6-10. New features that were not obviously present in the Volume Integrated spectrum have been observed in mapping mode.

BRIGHT REGION

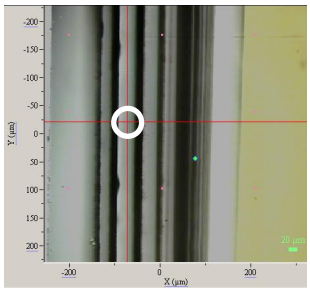

Figure 6-10a: Photograph of CVD layered sample.

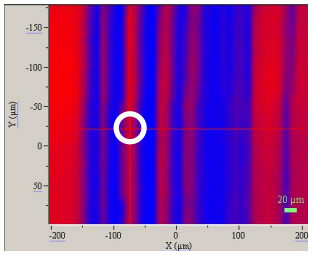

Figure 6-10b: Red intensity – high signal relative to 1332.98cm^{-1} diamond peak.

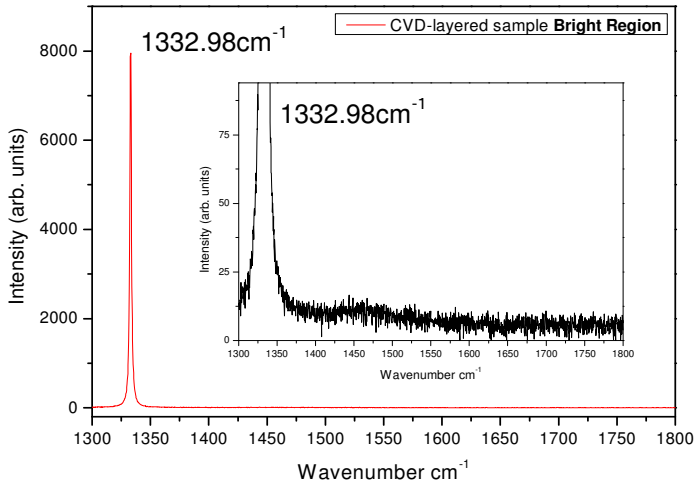

Figure 6-10c: Raman spectrum taken at a bright region. Diamond peak is located at ~1332.98cm^{-1} with a width of 1.64cm^{-1}.

DARK REGION

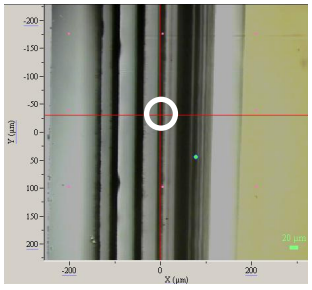

Figure 6-10d: Photograph of CVD layered sample.

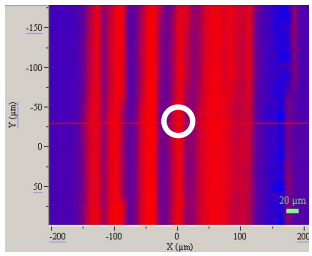

Figure 6-10e: Red intensity – high signal relative to 1456.21cm^{-1} peak.

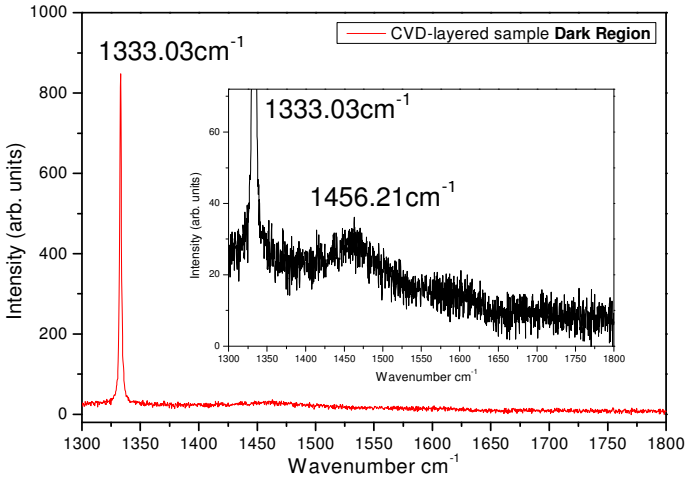

Figure 6-10f: Raman spectrum taken at a dark region clearly showing the features indicative of sp^2 bonding. Diamond peak is located at ~1333.03cm^{-1} with a width of 1.67cm^{-1} A feature is also present at ~1456.21cm^{-1} with a width of 56.25cm^{-1}.

The CVD layered sample was investigated using the Raman spectrometer in mapping mode. A faint peak was again found at ~1460 cm^{-1} as was in the previously mentioned CVD (0542715) diamond. The acquired image from the Raman measurements correlates perfectly with the location of the bands in the photograph (figure 6-10b and 6-10e).

When a comparison is made between a bright band and a dark band a significant difference observed between both. The intensity of the diamond peak (~1332cm^{-1}). In this instance the intensity is reduced by a factor of ~10 at the dark band compared to the bright band. This could be for one or two reasons. It could be due to the fact that the absorption at the darker bands is much higher and therefore less light is reflected back into the Raman spectrometer – therefore resulting in less intense diamond peak. Or it could be that the amount of sp^3 bonded Carbon (C-C) at the sampling region is much less due to the increased presence of sp^2 bonded-carbon species. i.e. the amount of sp^3 bonded-carbon is much less per unit volume in a dark region compared to a bright region.

What is apparent is the presence of a peak situated at ~1460cm^{-1} again found in a CVD diamond (as observed previously in the other CVD (0542715) diamond) which is associated with non-diamond carbon located at grain boundaries as mentioned earlier (trans-PA) (*18, 19, 28*). When this is taken into account, along with the relative intensities of the diamond peaks a clear suggestion begins to unfold that the ratios between the ~1332cm^{-1} peak and the ~1460cm^{-1} peak is the key factor in clearly comparing and getting a clear idea of the sp^3/sp^2 content present at the sampling location. The result for this CVD sample is very similar to that of the other CVD diamond (0542715) whereby the 1460cm^{-1} feature was attributed to trans-PA located at grain boundaries.

As previously mentioned, a comparison of the peak heights cannot be taken as a definitive value for the amount of sp^2 or sp^3 species within a sample, especially when comparing two different samples. Although, a comparison of two locations on the *same* sample can be justifiably made.

Again a conclusion can be gathered from the Raman mapping measurements that there is a higher concentration of sp^2 bonded carbon present in the darker coloured regions of the sample in question. This agrees with the other results obtained for the other samples. In conclusion it can be gathered that wherever dark or brown regions are present on a diamond sample, a higher concentration of sp^2 bonded carbon species is found to be present there, compared to a bright region. This does not apply for the HPHT treated sample due to the results suggesting that the HPHT process although eliminated the brown colouration has resulted in an increase in the amount of sp^2 bonded-carbon species. This does not imply that the HPHT process has *created new* sp^2 bonded carbon, but more likely has concentrated more of the sp^2 bonded carbon together, i.e. vacancy clusters initially widely distributed throughout the brown sample, then, upon HPHT treatment, the vacancy clusters gather together to create larger vacancy clusters and therefore are much more likely to result in a high Raman signal at the sp^2-bonded carbon wavenumbers (~1400-1800cm^{-1}).

6.2.2.3 Naturally Banded type IIa Diamond (A490)

6.2.2.3.1 Volume Integrated Raman

A volume integrated plot was initially obtained for the A490 type IIa natural diamond sample and is shown in figure 6-11 below.

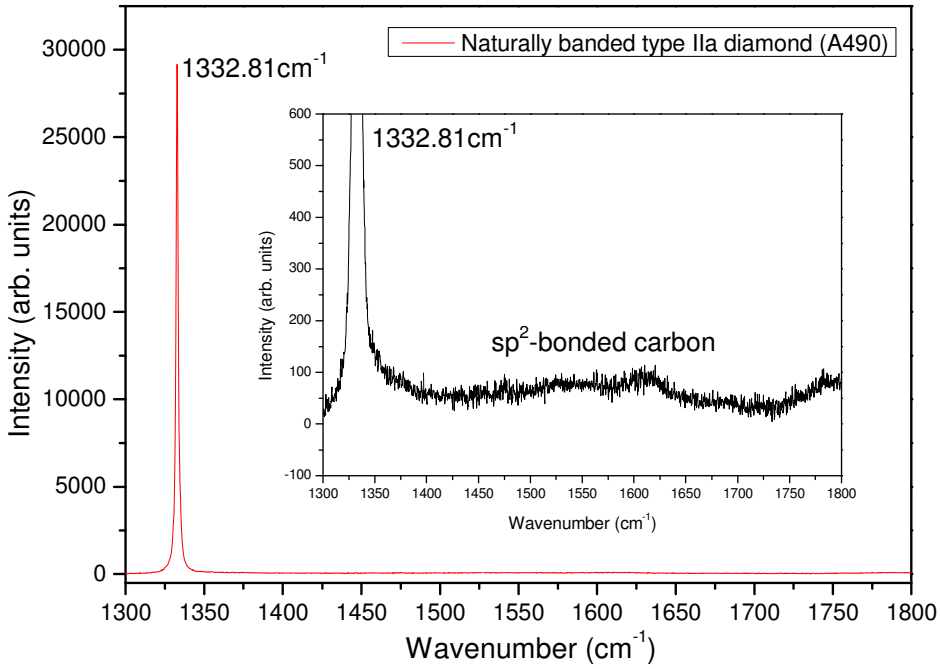

Figure 6-11: Naturally banded type IIa diamond sample. A490 Volume Integrated Raman spectrum.

The diamond peak is situated at ~1332.81cm^{-1} with a Lorentzian width of ~1.65cm^{-1}. Evidently from the spectrum shown in figure 6-11, sp^2 bonded carbon species are present within the sample. The G-peak can be observed as well as a feature that seems to peak at ~1800cm^{-1}, this has been associated with intrinsic point defects (*18*). Due to the clearly visible banding and non-uniformity of the colouration and banding that is present within this sample, Raman mapping mode measurements were carried out and are shown in figure 6-12 to provide further detail on the nature of the bonding within the bended regions of the sample.

6.2.2.3.2 Raman Mapping measurements

BRIGHT REGION

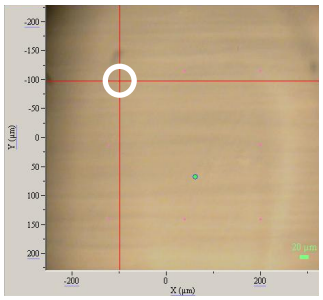

Figure 6-12a: Photograph of type IIa sample, horizontal bands are clearly visible.

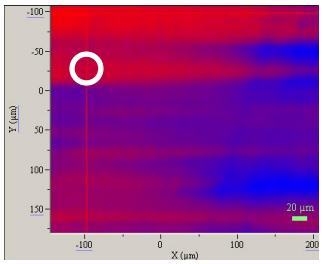

Figure 6-12b: Red intensity – high signal relative to 1334.15cm^{-1} diamond peak

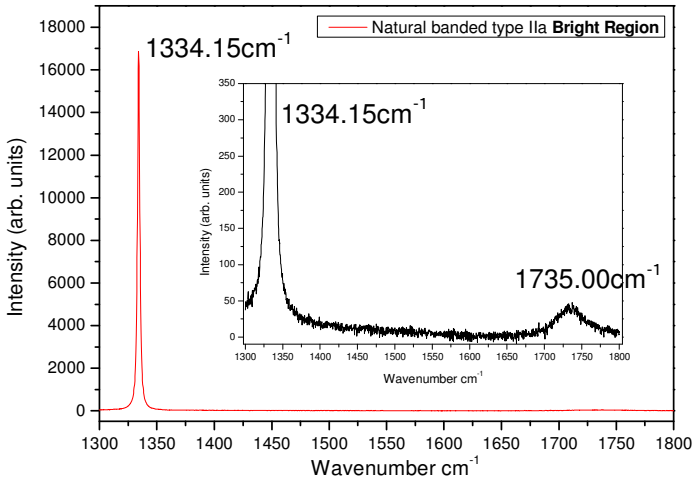

Figure 6-12c: Raman spectrum taken at a bright region with a diamond peak located at 1334.15cm^{-1} and a width of 2.19cm^{-1}. A feature is observed at 1735.00cm^{-1} with a width of 37.13cm^{-1}.

DARK REGION

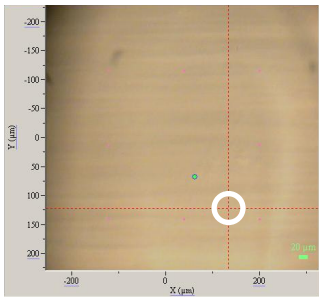

Figure 6-12d: Photograph of type IIa sample

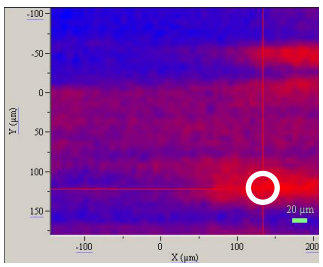

Figure 6-12e: Red intensity – high signal relative to 1334.00cm^{-1} diamond peak

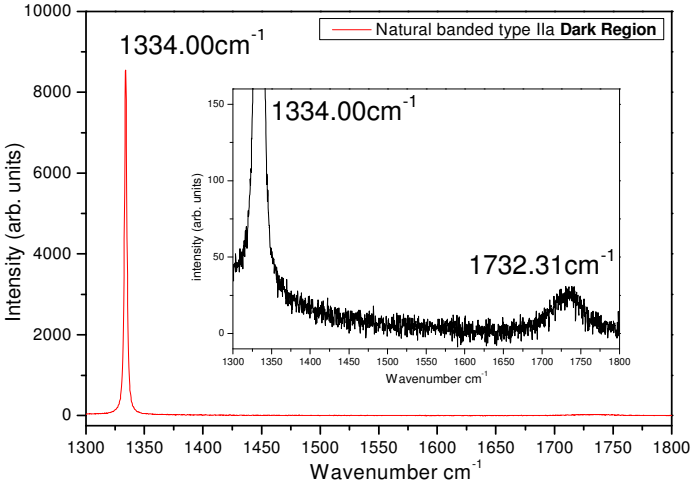

Figure 6-12f: Raman spectrum taken at a dark region showing the features indicative of sp^2 bonding. Diamond peak is located at 1334.00cm^{-1} with lorentzian width of 2.27cm^{-1}. A feature is present at 1732.31cm^{-1} with a gaussian width of 37.53cm^{-1}.

In the case of the type IIa natural diamond, banded features are clearly visible in the acquired Raman mapping images. A key factor that must be kept in mind is the fact that when bright and dark bands are mentioned it is important to remember that it is a means of differentiating between one band and the other – one could be a brown band and the other a *browner* band. A good example of this is in the case of this sample.

Observable in the Raman spectrum is once again a dominant diamond peak situated at ~1334cm^{-1} and a lorentzian width of 2.19cm^{-1}, with the intensity nearly half of what it was at the bright band compared to the dark band.

There are subtle features present at higher wavenumbers, but due to the noise levels involved they cannot be clearly observed. A peak is present at ~1732cm^{-1} with a Gaussian width of 37.53cm^{-1} in both the bright and dark regions. Zaitsev mentions that a band located at 1730cm^{-1} with a FWHM of 70cm^{-1} is attributed to C=O stretching vibrations (*18*).

6.2.2.4 Naturally Banded type Ia Diamond (A465-40-03)

6.2.2.4.1 Volume Integrated Raman

As with all the other variegated samples Volume Integrated Raman measurements were also carried out on a type Ia natural banded diamond and the Raman spectrum obtained in the 1300-1650cm^{-1} range is shown below (figure 6-13).

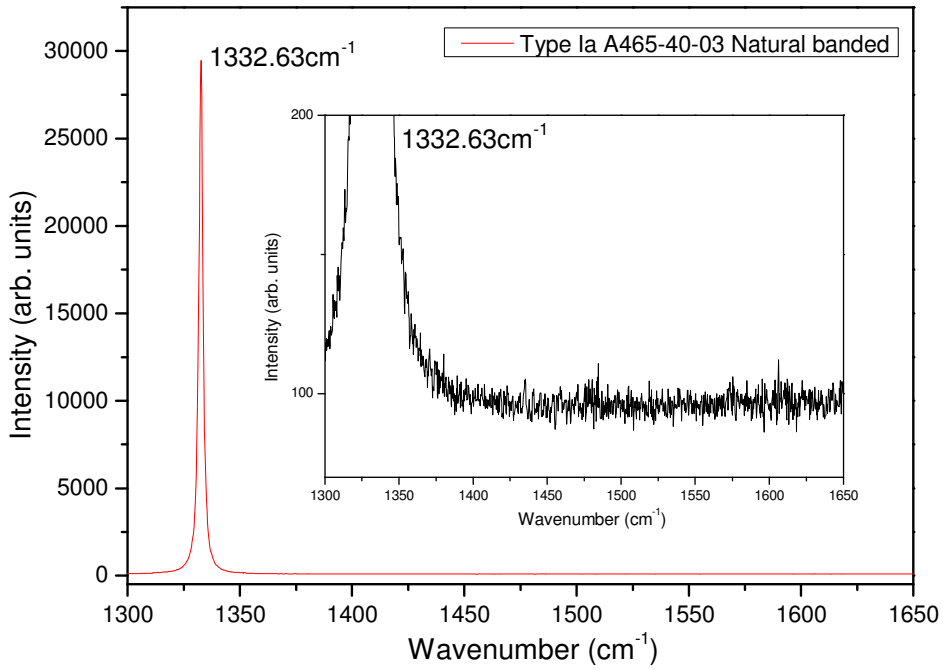

Figure 6-13: Natural type Ia banded diamond sample. Volume Integrated Raman spectrum.

The diamond peak is located at ~1332.63cm^{-1} with a lorentzian width of ~2.082cm^{-1}. No specific features can be observed from the Volume Integrated diamond spectrum for the type Ia A465-40-03 sample. There are slight features at the wavenumbers where sp^2 bonded-carbon is typically observed but it is relatively difficult to pick out any specific features.

6.2.2.4.2 Raman Mapping measurements

A Raman mapping spectrum was obtained for the same sample to see whether the mapping technique would pick up any features relative to the brown banded regions and the brighter regions on this sample. The results are shown in figure 6-14.

BRIGHT REGION

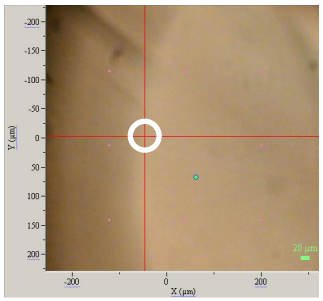

Figure 6-14a: Photograph of type Ia natural sample

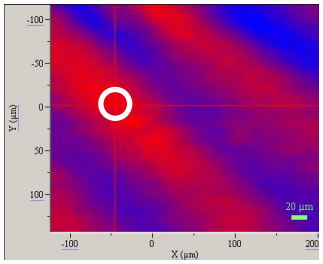

Figure 6-14b: Red intensity – high signal relative to 1333.93cm^{-1} diamond peak

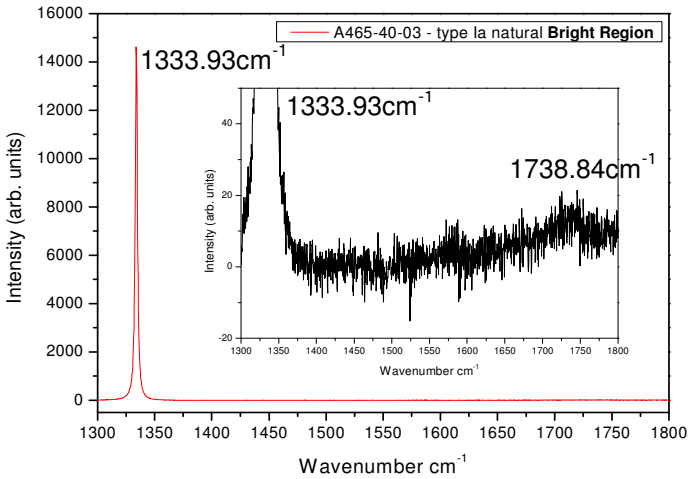

Figure 6-14c: Raman spectrum taken at a bright region with a diamond peak located at ~1333.93cm^{-1} and lorentzian width of 2.18cm^{-1}. A feature is present at ~1738.84cm^{-1} with a gaussian width of 60.68cm^{-1}.

DARK REGION

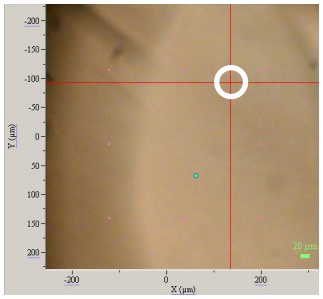

Figure 6-14d: Photograph of type Ia natural sample

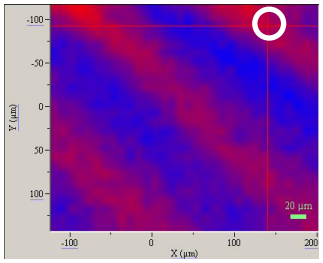

Figure 6-14e: Red intensity – high signal relative to ~1748.37cm^{-1} diamond peak

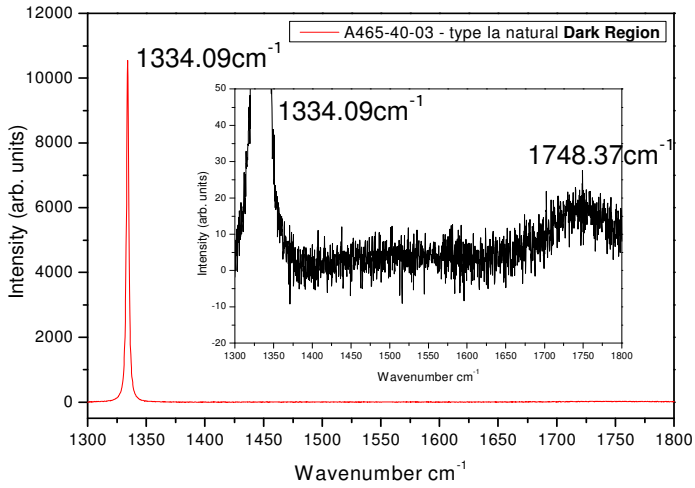

Figure 6-14f: Raman spectrum taken at a dark region clearly showing the features indicative of sp^2 bonding. The diamond peak is located at ~1334.09cm^{-1} with a lorentzian width of 2.24cm^{-1}. A feature is present at 1748.37cm^{-1} with a gausian width of 83.17cm^{-1}.

The brown bands visually seen in the type Ia diamond photograph can also be correlated with the acquired image gathered from the Raman mapping technique. Similarly to the type IIa diamond, a peak is observed at ~1730cm^{-1} but the type Ia sample has more structure in the region between the diamond 1332cm^{-1} peak and the ~1730cm^{-1} peak. These are difficult to quantify relative to position due to the Raman signal being very low as well as noise contributions present, but as stated in the literature, the ~1500-1650cm^{-1} (*17, 19*) region is typically associated with sp^2 bonded carbon. The 1730cm^{-1} peak can be attributed to C=O stretching due to the mechanochemical reactions between the diamond surface and the environment (ambient air) (*30*).

6.3 Summary

A summary of the Raman peaks and features observed from studies on the diamond samples can be found in table 6-1.

Table 6-1: A summary of the features present in the diamond samples from Raman measurements.

Sample	Type of Raman Scan	Diamond Peak Location	Other Peaks and Features
Blue Single Crystal CVD	Volume Integrated	$1332cm^{-1}$	$1295cm^{-1}$ 2^{nd} order peaks at: $2467cm^{-1}$ $2667cm^{-1}$
Brown Single Crystal CVD (0473906)	Volume Integrated	$1332cm^{-1}$	$1295cm^{-1}$ 2^{nd} order peaks at: $2467cm^{-1}$ $2667cm^{-1}$
Large Brown CVD (0473904)	Volume Integrated	$1332cm^{-1}$	D-Band ~$1350cm^{-1}$ sp^2-bonded carbon features
Untreated type IIa	Volume Integrated	$1333cm^{-1}$	Small sp^2-bonded carbon features
HPHT treated type IIa	Volume Integrated	$1333cm^{-1}$	$1285cm^{-1}$ $1460cm^{-1}$ sp^2-bonded carbon features
Naturally Colourless type IIa	Volume Integrated	$1333cm^{-1}$	$1295cm^{-1}$ sp^2-bonded carbon features
CVD (0542715)	Volume Integrated	$1332.65cm^{-1}$	Small sp^2-bonded carbon features
CVD (0542715)	Bright Region	$1332.79cm^{-1}$	Small feature at $1460cm^{-1}$
CVD (0542715)	Dark Region	$1332.47cm^{-1}$	Large feature at $1457.75cm^{-1}$

CVD layered (0673803)	Volume Integrated	1332.84cm^{-1}	G-peak at ~1540cm^{-1}
CVD layered (0673803)	Bright Region	1332.98cm^{-1}	No significant features present
CVD layered (0673803)	Dark Region	1333.03cm^{-1}	Feature present at ~1456.21cm^{-1}
Naturally Banded type IIa (A490)	Volume Integrated	1332.81cm^{-1}	Slight presence of the G-peak.
Naturally Banded type IIa (A490)	Bright Region	1334.15cm^{-1}	Peak present at ~1735cm^{-1} attributed to sp^2-bonded carbon
Naturally Banded type IIa (A490)	Dark Region	1334.00cm^{-1}	Peak present at ~1732.31cm^{-1} attributed to sp^2-bonded carbon
Naturally Banded type Ia (A465-40-03)	Volume Integrated	1332.63cm^{-1}	No significant features present
Naturally Banded type Ia (A465-40-03)	Bright Region	1333.93cm^{-1}	Slight feature present at 1758.84cm^{-1} attributed to sp^2-bonded carbon
Naturally Banded type Ia (A465-40-03)	Dark Region	1334.09cm^{-1}	Large feature present at ~1748.37cm^{-1} attributed to sp^2-bonded carbon

The Raman mapping technique has been very successful in identifying and correlating the brown regions on the diamond samples. Generally, the diamond peak was observed to be less intense at the brown regions in all of the samples studied along with an extra – or an enhancement of other peaks at higher wavenumbers.

A future approach to Raman study of diamond would be to use near-infrared excitation such as a 785nm. Work carried out by May *et al.* (*31*) discovered that when using a 1μm spot the Raman spectrum for the (polycrystalline) diamond under study provided a multitude of peaks (over 30) ranging from 400-3000cm^{-1}. They state that this excitation wavelength is extremely sensitive to sp^2 carbon.

For the brown samples containing bands (A465 and A490) (type Ia and type IIa respectively) there was no drastic difference between the Raman spectrums - this could possibly be due to the Raman being a bulk measuring process and that there is not enough contrast for the Raman instrument to pick up when looking at a brown and a *browner* region and also the possibility of overlapping bands upon measuring. This should not be the case due to resonance effects – the Raman cross-section for sp^2 clusters is far greater than those of the sp^3 bonded species. As a result scattering by the sp^2 species are the features that quite often dominate the spectrum, swamping the sp^3 bonded-carbon species' signal. This may be observed with the CVD (0542715) sample whereby the sp^3 signal is much less at the dark region compared to the brighter region, along with the added presence of an intense peak at around 1457 cm^{-1} (*32*).

The Raman measurements obtained for all samples have revealed interesting factors with regards to the concentration localities of the sp^2 bonded carbon species i.e. that they are mostly concentrated in brown or darker regions of a diamond sample with the exception of the HPHT treated diamond. More information is required still due to the fact that some of the features found especially at the higher wavenumbers in the 1400cm^{-1} to 1800cm^{-1} range not being as clear and pronounced as possible. A more sensitive approach is required in the means of synchrotron radiation stimulated measurements such as NEXAFS and OD-XAS as will be introduced in the next chapter.

Raman spectroscopy has been the primary tool for the study of sp^2 (graphitic) and sp^3 (diamond) allotropes as well as to distinguish the types of bonding that exist in combination in some cases such as those observed in the diamond samples presented in this chapter. The Raman technique, although non-destructive is limited when it comes to sensitivity. The technique is much more sensitive to graphitic inclusions in hybrid materials. The Raman cross section for graphitic features can be up to 50 times that of diamond (*33*). Coffman *et al.* go on to mention that the Raman technique is thus much more sensitive to sp^2 bonding making it impossible to distinguish materials of i.e. 96% sp^3 bonding from another with 85% sp^3 bonding. It also states that the sp^2 signal dominates the spectrum at levels of >90% sp^3 bonding. Another of the technique's downfall is the dependence on long range order parameter of the material

(*33*). The Raman incident photon wavelength is of the order of microns, which leads to strong crystal size dependence and a critical crystallite size. These limitations weaken the utility of Raman spectroscopy for studying “diamond-like carbon” (DLC) and amorphous or nanocrystalline carbon.

As a means of overcoming these difficulties, the NEXAFS or OD-XAS technique is a technique best adopted. The Raman technique is essential for initial measurements and rapid data acquisition prior to synchrotron based NEXAFS/OD-XAS, detailed measurements. Data obtained for the NEXAFS and OD-XAS measurements are presented in the next chapter.

6.4 References

1. C. V. Raman, K. S. Krishnan, *Nature* **121**, 501 (1928).
2. R. Robertson, J. J. Fox, C. Ramaswamy, *Nature* **125**, 704 (1930).
3. R. Robertson, J. J. Fox, *Philosophical Transactions of the Royal Society of London Series a, Containing Papers of a Mathematical or Physical Character* **232**, 463 (1934).
4. C. L. Cheng, C. F. Chen, W. C. Shaio, D. S. Tsai, K. H. Chen, *Diamond and Related Materials* **14**, 1455 (2005).
5. S. Prawer, K. W. Nugent, P. S. Weiser, *Applied Physics Letters* **65**, 2248 (1994).
6. J. E. Field, *The Properties of Natural and Synthetic Diamond*. (Elsevier Academic Press, 1992).
7. R. E. Shroder, R. J. Nemanich, J. T. Glass, *Physical Review B* **41**, 3738 (1990).
8. S. Prawer, R. J. Nemanich, *Philosophical Transactions of the Royal Society of London Series a-Mathematical Physical and Engineering Sciences* **362**, 2537 (2004).
9. C. A. Wolden, C. E. Draper, Z. Sitar, J. T. Prater, *Diamond and Related Materials* **7**, 1178 (1998).
10. A. M. Zaitsev, *Optical Properties of Diamond*. (Springer, 2001).
11. D. S. Knight, W. B. White, *Journal of Materials Research* **4**, 385 (1989).
12. R. Linares, P. Doering, *Diamond and Related Materials* **8**, 909 (1999).
13. T. Irifune *et al.*, *Physics of the Earth and Planetary Interiors* **143**, 593 (2004).
14. O. K. Semchinova, V. Y. Davydov, H. Neff, E. P. Smirnov, G. Holzhuter, *Carbon* **35**, 697 (1997).
15. D. Kirillov, G. J. Reynolds, *Applied Physics Letters* **65**, 1641 (1994).
16. M. S. Haque *et al.*, *Journal of Applied Physics* **83**, 4421 (1998).
17. A. C. Ferrari, *Diamond and Related Materials* **11**, 1053 (2002).
18. A. Zaitsev, *Optical Properties of Diamond A Data Handbook*. (Springer, 2001).
19. A. C. Ferrari, J. Robertson, *Physical Review B* **63**, (2001).
20. X. T. Zhou *et al.*, *Journal of the American Chemical Society* **129**, 1476 (2007).

21. R. J. Zhang, S. T. Lee, Y. W. Lam, *Diamond and Related Materials* **5**, 1288 (1996).
22. S. A. Solin, A. K. Ramdas, *Physical Review B* **1**, 1687 (1970).
23. R. W. Bormett *et al.*, *Journal of Applied Physics* **77**, 5916 (1995).
24. H. Herchen, M. A. Cappelli, *Physical Review B* **49**, 3213 (1994).
25. H. Herchen, M. A. Cappelli, *Physical Review B* **43**, 11740 (1991).
26. K. H. Chen, Y. L. Lai, L. C. Chen, J. Y. Wu, F. J. Kao, *Thin Solid Films* **270**, 143 (1995).
27. P. M. Martineau *et al.*, *Gems & Gemology* **40**, 2 (2004).
28. C. C. Teng, S. M. Song, C. M. Sung, C. T. Lin, *Journal of Nanomaterials*, (2009).
29. W. Windl *et al.*, *Physical Review B* **48**, 3164 (1993).
30. Y. G. Gogotsi, A. Kailer, K. G. Nickel, *Journal of Applied Physics* **84**, 1299 (1998).
31. A. K. Khachatryan *et al.*, *Diamond and Related Materials* **17**, 931 (2008).
32. S. Prawer *et al.*, *Chemical Physics Letters* **332**, 93 (2000).
33. F. L. Coffman *et al.*, *Applied Physics Letters* **69**, 568 (1996).

Chapter

7

7.0 X-ray Absorption Spectroscopy (XAS) Investigations on Natural and Synthetic Diamond

7.1 Introduction

Presented in this chapter are the Optically Detected X-ray Absorption Spectroscopy (OD-XAS) studies performed on diamond. The OD-XAS technique has never before been applied to the study of uniform or variegated brown diamonds.

Band-gap measurements on a type Ia diamond are firstly introduced, whereby the OD-XAS technique was implemented using low energy synchrotron radiation of UV energy excitation. The Blue and Brown single crystal CVD diamonds are then presented, on whom the first initial diamond OD-XAS measurements were undertaken to reveal the chemical structure. To follow, the naturally banded type IIa and Ia diamonds results are introduced and then the OD-XAS results obtained for the variegated CVD diamonds. The final samples presented are the three natural type IIa diamonds, which consist of an untreated (brown) diamond, a HPHT treated (colourless) diamond and a naturally colourless diamond.

As explained in the theoretical chapter (chapter 4), the incident synchrotron x-ray energy is ramped across the C K-edge and yields a sequence of images whereby the luminescence intensity is modulated by the near-edge x-ray absorption structure of the C K-edge. This structure is determined by the density of unoccupied electronic states and is a sensitive probe of the local chemical environment of the carbon atoms.

The OD-XAS technique has been applied in parallel with the XEOL technique to obtain information on the chemical structure of brown diamond. Coupled with other characterisation techniques such as Raman and PL spectroscopy, an in-depth profile has been obtained for each diamond studied.

OD-XAS experiments were carried out on beamline MPW6.1 at the SRS (Daresbury). The MoLES (*1*) spectrometer was used for the provision of OD-XAS (and XEOL) data for the homogeneous, uniformly coloured samples. For the variegated samples, containing brown inclusions, bands or brown features, the CLASSIX spectrometer (*2*) was utilized due to its imaging capabilities.

7.2 Diamond Band-gap Measurements

7.2.1 Naturally Banded type Ia Diamond

Initial band-gap measurements were performed on a type Ia naturally banded diamond sample on Beamline 3.1 (4-31eV) at the SRS, Daresbury (*3*). Using OD-XAS measurements the band-gap of luminescent materials can be identified as shown in the diagram below in figure 7-1,

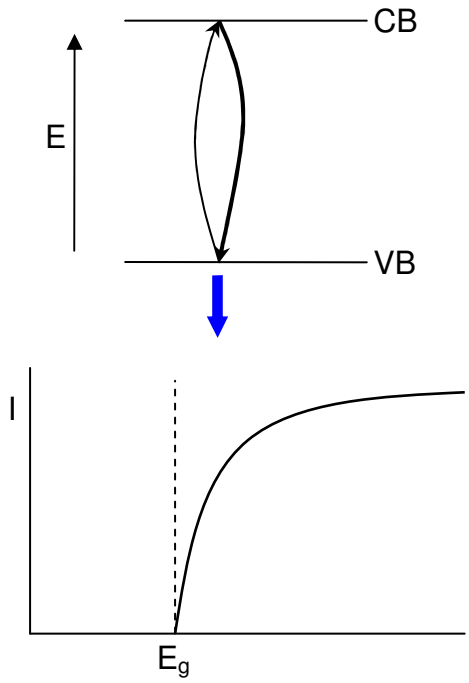

Figure 7-1: Increase of OD-XAS intensity at band-gap energy (E_g).

Figure 7-2 displays the OD-XAS results obtained for a type Ia naturally banded diamond as the incident synchrotron radiation energy is ramped from 4-8eV in steps of 0.04eV obtained in total luminescence yield (TLY – no filters) using the CLASSIX spectrometer (*2*) with the sample at a temperature of ~38K.

The results obtained clearly confirm the presence of a peak with its onset at around 5.476eV which is comparable to other measurements taken through various other techniques that are mentioned in the literature for the band-gap of diamond (*4-7*). Phonon lines are also present on the highest energy shoulder of the band which lie at

around, 5.76, 5.91, 6.08 and 6.24eV with a separation of ~0.16eV between them which corresponds to the wavevector conserving phonons of energy 163 ±1meV also known as Longitudinal Optic which cause luminescence from free excitons (*8*). The same phonons are mentioned in a paper by Dean and Male (*9*). The result proves that the OD-XAS technique is a valid and worthwhile technique for analysing the band-gap energy in luminescent materials and that information relating to the chemical and structural properties within the luminescent sample under study can be gathered from luminescent light, radiated from the sample. OD-XAS measurements have also been successfully applied to c-BN and h-BN (Boron Nitride) samples to identify where the band-gap energies lie using the luminescence that occurs as a result of irradiating with x-rays (*10*).

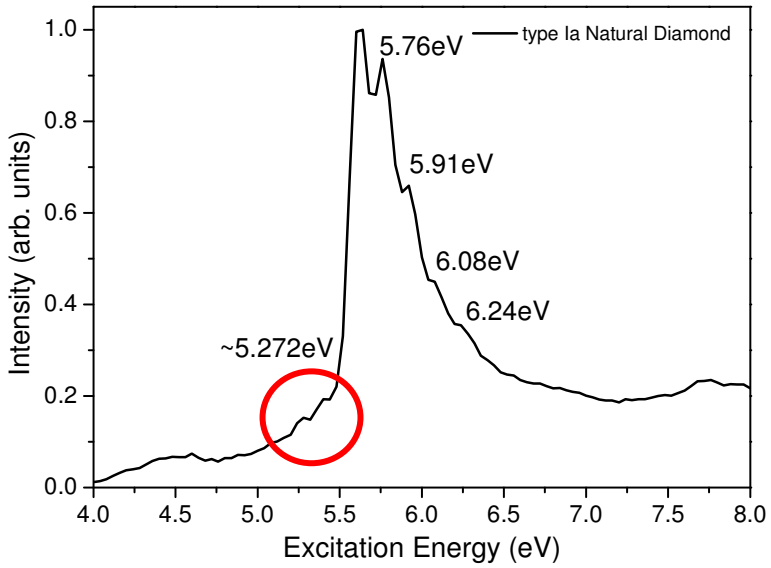

Figure 7-2: OD-XAS spectrum of a type Ia natural diamond clearly showing the band-gap at ~5.476eV. Phonons are also visible at 5.76, 5.91, 6.08 and 6.24eV.

The circled peaks (figure 7-2) have been reported in the literature as having specimen dependent strengths in every insulating diamond and correspond in energy with common ultra-violet absorption bands. They are revealed much more sensitively by the excitation technique and are not obscured by strong type I absorption. Two thresholds have been observed in the literature near 5.48 and 5.53eV that initiate a system of broader excitation bands whose strength relative to the sharp bands is specimen-dependent according to Dean and Male (*9*).

The ~5.272eV peak consists of a doublet; these pre-edge features have been related to impurities and referred to in the literature as the N9 centre (*11-13*). The 'N' refers to *naturally occurring*. It is weak in the type Ia sample. Correlation has been observed between the nitrogen content and the strength of these peaks by Wight and Dean as well as Walker (*14, 15*). There is also mention in the literature that the N9 centre is found to be present in the majority of type I diamonds although the centre is difficult to observe unless it is a thin sample (*4, 16*).

The OD-XAS technique has successfully revealed the band-gap location in type Ia diamond with the obtained value comparable to those typically found in the literature. It is therefore an accomplished technique in obtaining the wide band-gap values of semiconductors from luminescent light and can therefore be justifiably applied for further investigation into the chemical structure.

Initial studies by the materials group at Aberystwyth University had revealed that the NEXAFS and OD-XAS technique could be applied to the studies of Boron Nitride (BN) of the cubic (cBN) and hexagonal phase (hBN) (*10, 17*). It was through this technique that a detailed study into the band-gap of this material was achieved. Measurements revealed that the chemical structure can also be obtained and it was found that the hBN contained sp^2 bonded species of a similar nature to graphite, and that the cBN material had no pre-edge resonances and therefore akin to pure diamond.

For the aid of the reader, the NEXAFS spectrums for graphite and diamond are shown again below in figure 7-3.

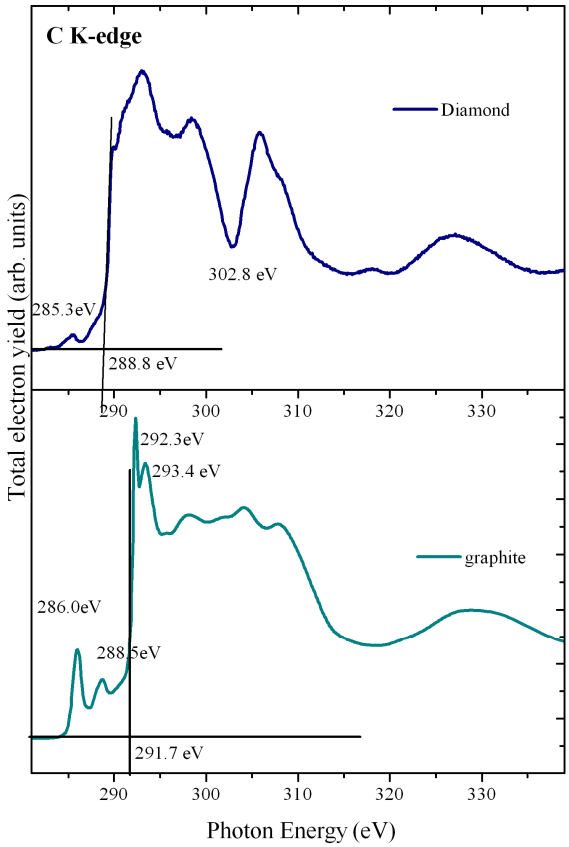

Figure 7-3: Typical NEXAFS spectrums for diamond and graphite. The pre C 1s K-edge features are typical of graphite. The pre C 1s K-edge on the diamond sample also shows a small feature – due to sp^2 bonded carbon on the surface of the material whereby the NEXAFS technique is particularly sensitive to surface anomalies (as mentioned in chapter 4). The feature at ~302.8eV in the diamond spectrum is a typical feature of diamond, the σ^* resonance indicative of diamond and sp^3 bonded-carbon.

7.3 NEXAFS and OD-XAS Measurements

Presented here are the NEXAFS and OD-XAS results obtained for the uniform and variegated diamonds along with analysis and discussion for each sample.

7.3.1 Reference Sample measurements

As mentioned in chapter 3, reference measurements were required for correction purposes due to carbon being present along the beamline on the monochromator gratings and so forth. Quartz had to be used as a reference sample (or indeed any material that would provide a luminescence OD-XAS signal that did not contain C, in some instances glass was used). This provided a correction OD-XAS spectrum that was used to correct the gathered OD-XAS spectrums for all the measurements on diamond. As a matter of principal and experimental procedure, a quartz reference sample was measured often and between sample changes, due to the synchrotron beamline fluctuating with time as its lifetime decreases prior to the next refill (SRS, Daresbury).

7.3.2 Blue and Brown (0473906) Single Crystal CVD Diamonds

A Blue highly Boron doped (~10^{16} boron atoms per cm^3) and a Brown Single Crystal CVD diamonds were obtained as initial samples for the investigation into the cause of the brown colouration in brown diamond. As mentioned in previous chapters, both were of uniform colour and with no lateral differences. The chemical bonding of these samples were analysed using the MoLES spectrometer (*1*) coupled to the synchrotron on beamline MPW6.1 at the SRS, Daresbury. NEXAFS measurements were carried out as well as OD-XAS measurements and the results are shown in figure 7-5.

Features are seen to be present in the NEXAFS pre C 1s K-edge and not in the OD-XAS. NEXAFS is very surface sensitive (1-10nm) and this feature observed at ~284.5eV is due to surface contamination of sp^2 bonded-carbon. OD-XAS is much more bulk sensitive (up to 200nm) and therefore has not picked up this surface carbon feature (figure 7-5, panel (a)).

For figure 7-5 panel (b), features are present in both the NEXAFS and OD-XAS. Its presence in the OD-XAS scans suggests that the sp^2 bonded-carbon species that are responsible for this pre C 1s K-edge resonance originate from the bulk and is therefore not likely to be surface impurities. The OD-XAS technique therefore provides a chemical map analysis of the sample's structure.

The XEOL spectrums for both samples are shown again in figure 7-4. PLY measurements were undertaken for the samples in question to further explore the nature of the bands observed in the XEOL spectrums.

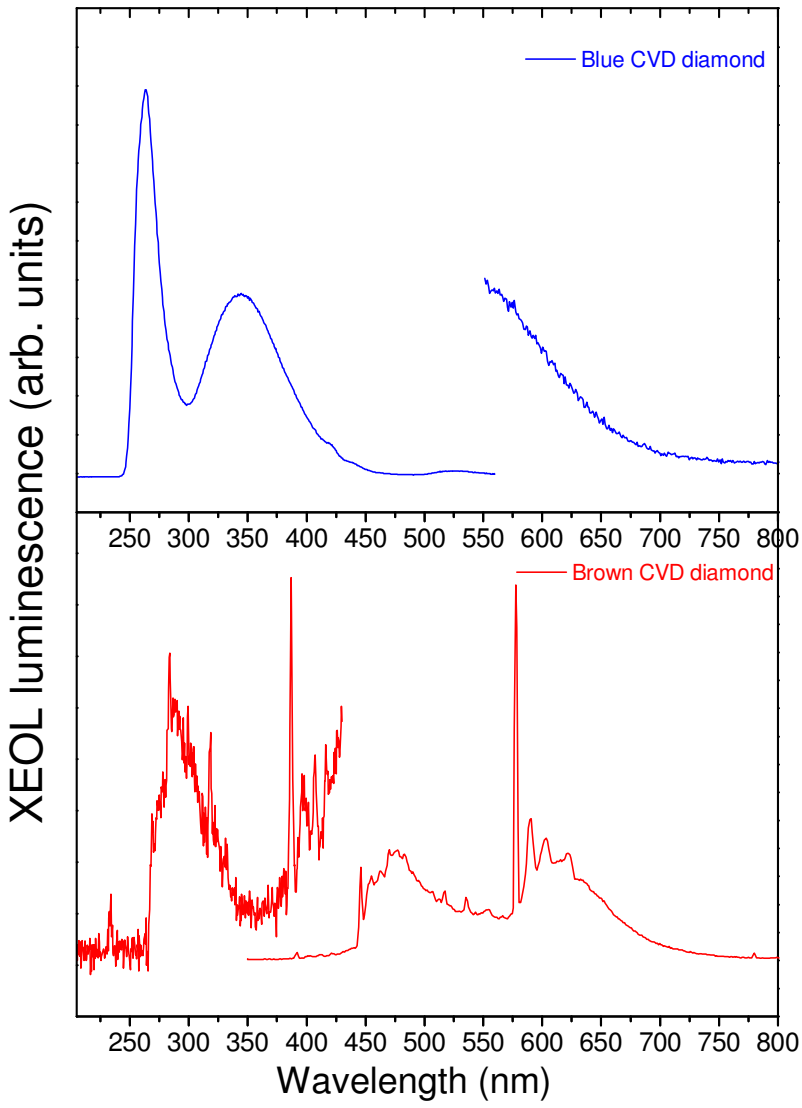

Figure 7-4: XEOL spectrums for the blue and brown single crystal CVD diamond, similar to those presented in chapter 5.

The PLY measurements were taken by measuring the luminescence intensity changes through a monochromator set at the particular wavelength (263nm, 300nm, 345nm, 435nm and 610nm in this instance) and ramping the incident photon energy from ~280-320eV.

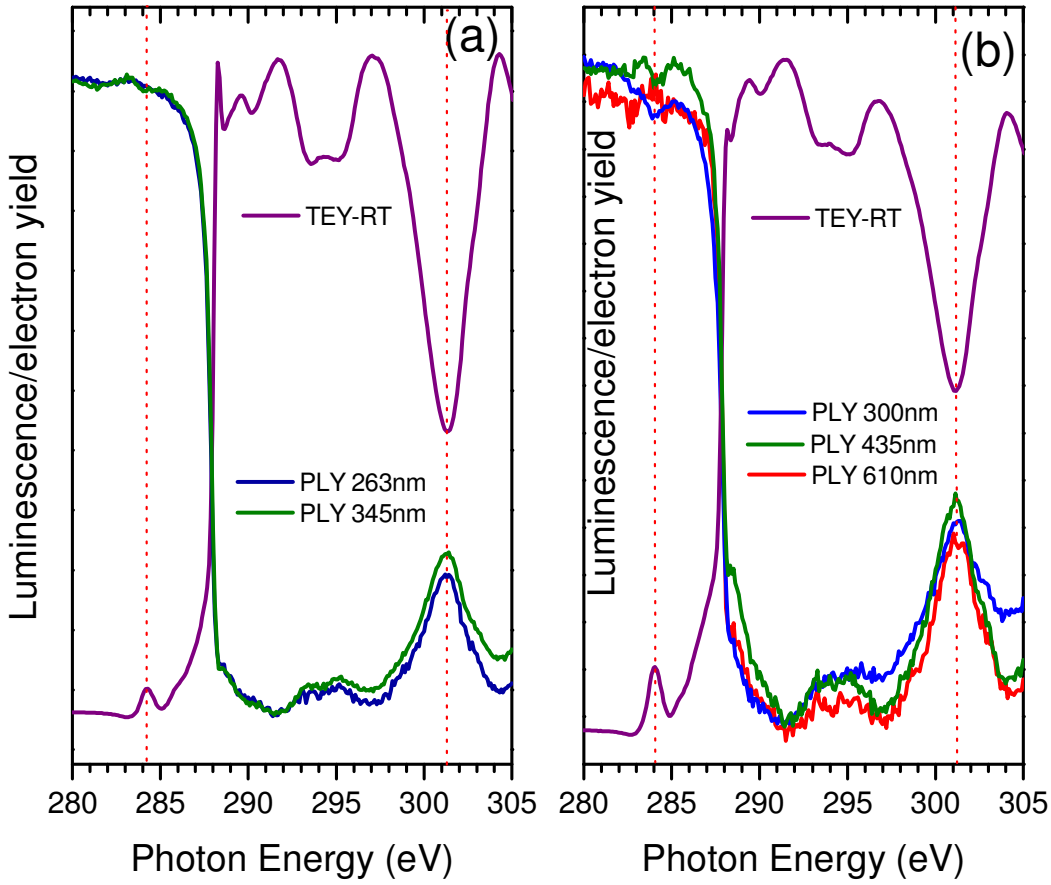

Figure 7-5: Panel (a) shows the NEXAFS (TEY) at room temperature (RT) and OD-XAS (PLY) spectrums for the blue boron doped diamond. Panel (b) shows the NEXAFS (TEY) at room temperature (RT) and OD-XAS (PLY) spectrums for the brown CVD diamond.

These initial experiments were carried out on the uniform samples to prove whether the OD-XAS technique provided the same information as NEXAFS studies. Indeed, both techniques compliment each other with the added advantage that the OD-XAS technique is more bulk sensitive (~200nm) than the NEXAFS technique which is more surface sensitive and therefore more likely to be affected by surface impurities, which as a result could affect the characterisation of the diamond features. In addition to the initial measurements the provision of the same information through the OD-

XAS technique can be directly coupled to a CCD detector rather than a PMT for imaging purposes – the CLASSIX spectrometer (*2*). The lateral differences found in some samples could be directly studied due to the pixelated format of the processed image – providing a direct XAS measurement at a particular pixel and in turn on a particular part/region of the sample under analysis (see chapter 3). Looking at figure 7-5 panel (b) it is apparent that the ~284eV feature is present in all PLY measurements except for the 610nm. This suggests that the sp^2 feature does not originate from that part of the XEOL spectrum and that it is due to the other bands.

Figure 7-6 provides the fitting for the pre-edge features observed for the brown single crystal CVD diamond.

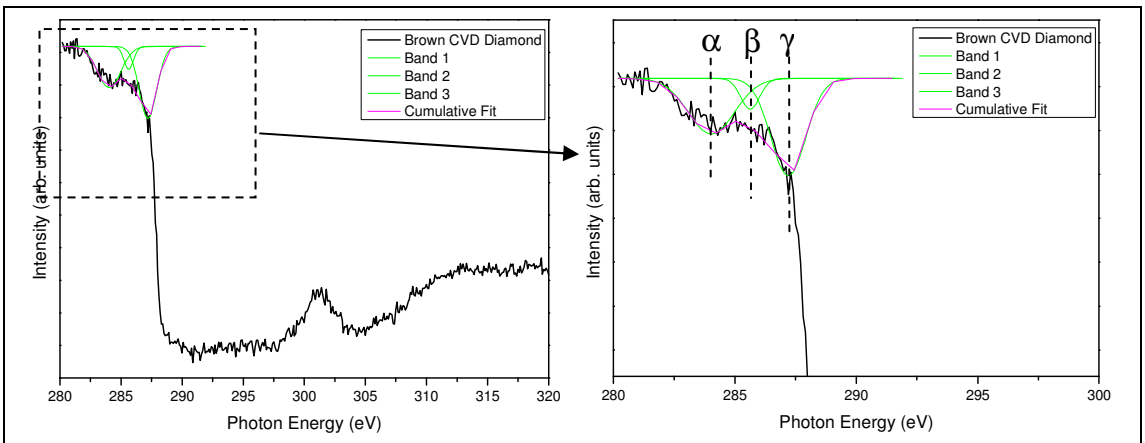

Figure 7-6: Fitted pre-edge features for the brown diamond ODXAS (PLY) 300nm spectrum. Three components are observed.

The results obtained from the fitting provide three bands that are situated pre-edge as summarized in table 7-1.

Table 7-1:

Band/feature	Peak Centre (eV)	FWHM
α	284.03	2.26
β	285.63	0.922
γ	287.20	1.70
Edge	~288.00	---
σ*	301.34	2.5715

The α band with a peak centre located at 284.03eV can be ascribed to the C = C, the π* resonance feature (*18-23*). The β band could possibly be due to the C = C bonding also, as locations for the particular bonding has been found in the range of 284-286eV (see table 7-15). C = N bonding has also been observed in the 285 to 286eV region and the band could be attributed to this (*21, 24*). The band observed at 287.20eV labelled as γ in table 7-1 is associated with the C – H* resonance which is typically found to be located at ~288 ±1eV (*20, 22, 25*). The σ* resonance feature indicative of the C – C sp^3 bonding in diamond is observed here at ~301.34eV comparable with values stated in the literature at ~303eV (*26*).

The OD-XAS technique was proved to be successful in providing the same information as the NEXAFS technique but from luminescent light. The MoLES spectrometer previously used was replaced with the CLASSIX spectrometer (*2*) due to its imaging capabilities. This CCD and filter wheel arrangement provides the capabilities of delivering the OD-XAS technique in imaging mode such as those shown in figure 7-8.

Photograph	**CLASSIX Imaging**
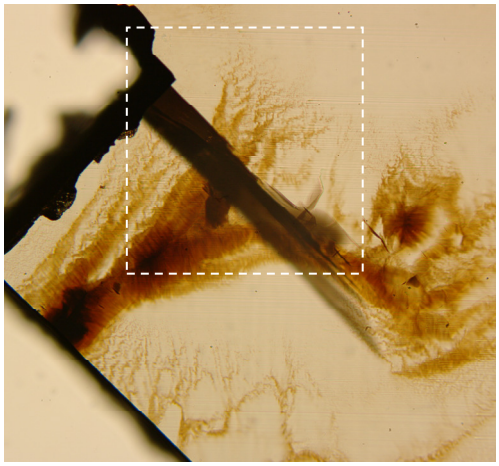	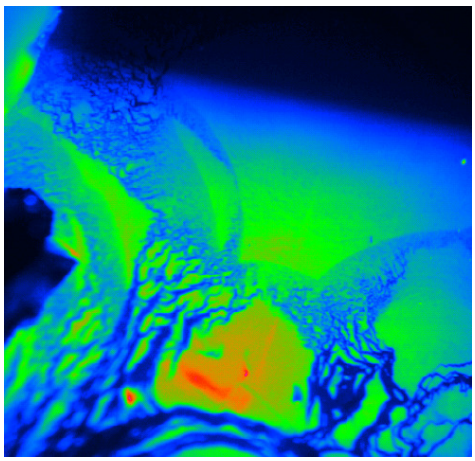
Figure 7-8a: Photograph of the CVD diamond (0542715) sample studied during the course of this research. The white boxed region corresponds to the region analysed by the CLASSIX spectrometer (figure 7-8b).	*Figure 7-8b: Luminescence image of the CVD sample taken by the CCD on the CLASSIX spectrometer. (x10 magnification).*
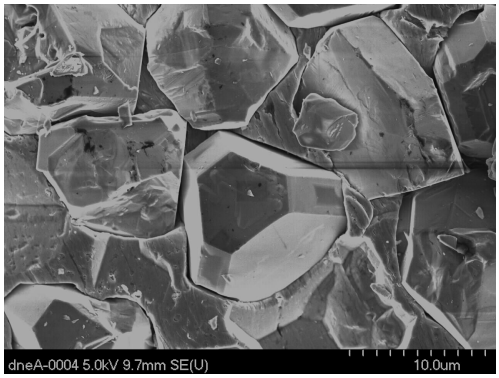	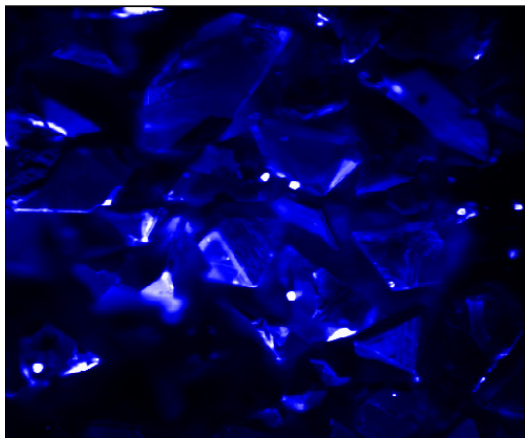
Figure 7-8c: SEM image courtesy of the Biology Laboratories at Aberystwyth University showing the 100µm cBN crystals.	*Figure 7-8d: Luminescence image taken with the CLASSIX spectrometer of the 100µm cBN crystal samples.*

Measurements such as those obtained in figure 7-8 clearly show correlation between the photo obtained from reflected light (figure 7-8a) and a luminescence gathered image (figure 7-8b). The dark features can be clearly observed in both instances. It is worthwhile to note that the colouration used in the luminescence gathered image does not resemble the luminescence light colour – it is in fact related to intensity whereby red corresponds to high intensity and blue/black – low intensity. The dark straight linear lines in figure 7-8a are due to laser cutting of the sample prior to it being obtained for study.

7.3.3 Naturally Banded type IIa diamond

7.3.3.1 TLY measurements

OD-XAS measurements were undertaken on a type IIa naturally banded diamond that showed lateral variation in transmitted light intensity and also in luminescence intensity (refer to figure 7-9a). The region of the polished diamond surface studied is shown in figure 7-9a along with an image recorded in total luminescence yield (TLY) (figure 7-9c). Within the synchrotron irradiated region (~3 mm x 1.5 mm spot), it can clearly be seen that the emission is not uniform. The luminescent image contains small dark regions of significantly reduced intensity. As the image obtained has been produced via a CCD on the CLASSIX spectrometer each pixel contains an OD-XAS spectrum (chapter 3). The spectrums obtained for these darker regions and a region of higher intensity are shown in figure 7-10. The region whereby the intensity is high (bright region) (red circle) (figure 7-9d) provides an OD-XAS spectrum with spectral features typically indicative of diamond. The lower intensity region (dark region) (yellow circle) (figure 7-9d), also provides an OD-XAS spectrum, but dominated by non-diamond carbon features, more commonly seen in graphite. There is a large C 1s – π^* resonance feature along with the complete absence of the diamond C 1s – σ^* resonance.

Using the spectrums for all pixels in the image the relative π^*-σ^* intensity can be extracted to provide a chemical state map as shown in figure 7-9d. The darker regions correspond to higher relative π^* (sp^2) intensity. Large (~100 μm) regions of non-diamond carbon have been revealed within the sampling area and have been correlated with regions of lower luminescence intensity.

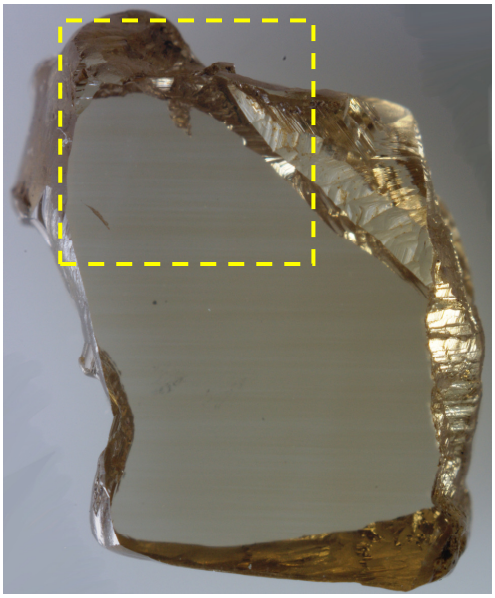

Figure 7-9a: shows a photograph of the natural type IIa diamond sample under normal light conditions displaying bands of brown colouration.

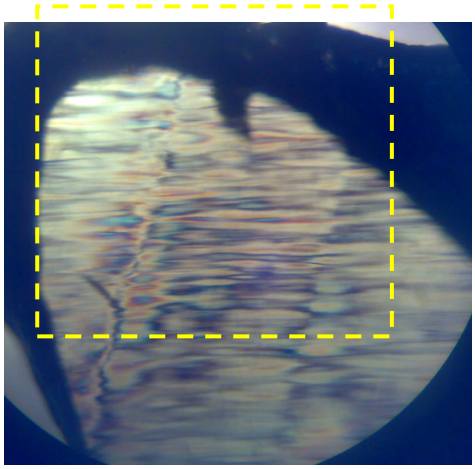

Figure 7-9b: under visible light illumination shows a Birefringence image of the same sample – clearly showing and highlighting lateral straining zones within the crystal which lie in the same direction as the brown banding.

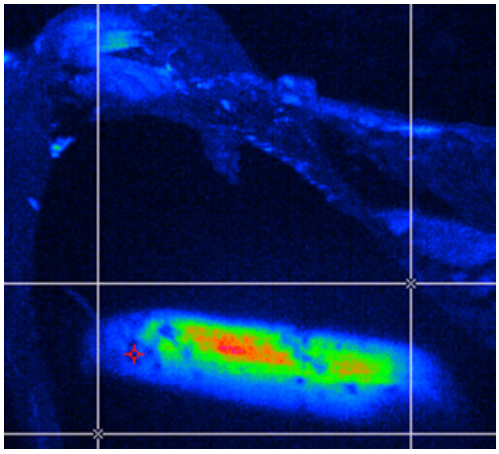

Figure 7-9c: Luminescence image for the natural IIa banded diamond recorded under irradiation by soft x-rays of energy 280 eV. The spot profile of the synchrotron beam (3 x 1.5 mm) defines the area of luminescence.

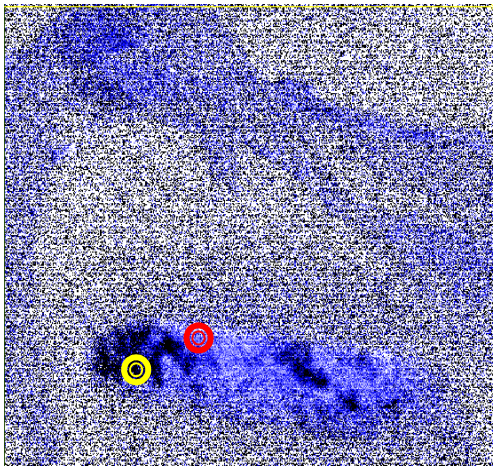

Figure 7-9d: Carbon phase map generated from ODXAS spectrums by mapping the relative sp^2 and sp^3 intensities across the sample (darker regions correspond to higher relative sp^2 concentration).

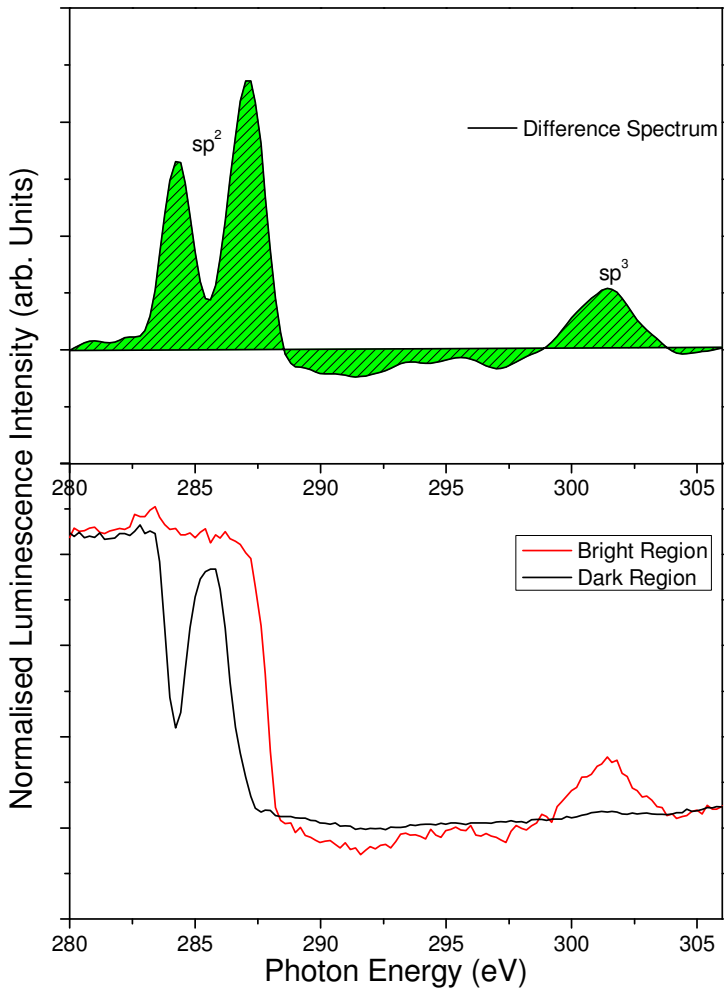

Figure 7-10: The OD-XAS spectrums obtained for the dark region and the bright region on the naturally banded type IIa diamond along with a difference spectrum showing that the sp^2-bonded carbon is situated in the dark luminescent regions of the sample due to the large π^*-resonance observed in the OD-XAS spectrum.

Curve fitting of the results obtained for the naturally banded brown type IIa diamond yields two bands as shown in figure 7-11.

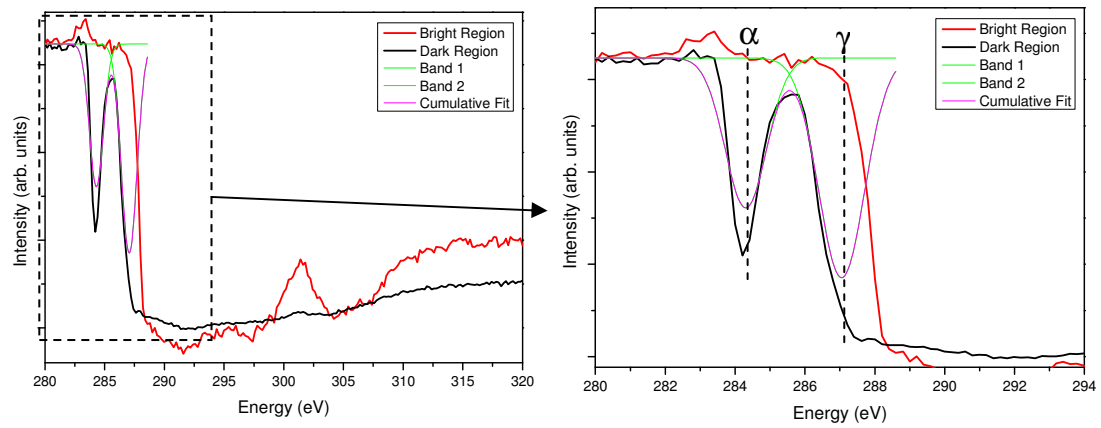

Figure 7-11: Pre-edge fitting for the A490 type IIa naturally banded diamond. The OD-XAS spectrum was taken at a dark concentrated cluster and at a bright region of the diamond. Two bands have been fitted prior to the edge.

Table 7-2:

Band/feature	Peak Centre (eV)	FWHM
α	284.31	1.396
γ	287.05	1.546
Edge	~288.39	---
σ*	301.40	2.67

The pre-edge fitting of the observed features identifies two bands, α and γ as stated in table 7-2, with peak centres located at 284.31eV and the other at ~287.05eV. The latter peak is more difficult to fit due to using the diamond edge from the bright region as a reference point to where the edge may be for the dark region. The 284.31eV feature is referred to in the literature as amorphous carbon, stated as being present at ~284.6eV therefore sp^2 bonded carbon. The π* resonance is typically found at ~285 ± 1eV which relates to the C = C π* resonance transition (*19, 21-25*). The 287.05eV feature could be related to the C – H* resonance which is typically found at around 288 ± 1eV (*22, 23, 25, 27*). No σ* resonance feature is present at all in the darker luminescence regions of the sample. The σ* feature present in the bright OD-XAS spectrum is situated at 301.40eV with a FWHM of 2.67. The bright region's diamond edge (taken at the high energy part of the spectrum edge) is found to be at ~288.39eV. The exciton feature is typically observed at ~289.3eV (*26*).

The naturally banded type IIa diamond was re-polished to eliminate the dark clustered regions previously observed and analysed again at the SRS, to try and observe whether the brown banding could itself be studied via luminescence. One of the possibilities that the banding was not previously observed could be due to the darker clustered regions observed previously affecting the relative intensities of the bands themselves, due to the dark clustered regions being at one extreme end of the intensity scale, and the bright regions at the other. The brown banding may have been washed out between these extremes due to the CCD imaging nature being intensity related and therefore could not be observed directly.

The type IIa naturally banded sample was repolished and reinvestigated with the results obtained for a second study shown in figures 7-12a to 7-12d.

Figure 7-12a shows the sample in reflected light along with the birefringence pattern in figure 7-12b which correlates with the direction of the banding. The luminescence image in figure 7-12c has been obtained by opening the exit slits fully on the beamline so that a larger synchrotron spot is incident on the sample for luminescence imaging purposes.

7.3.4 Natural Banded type IIa diamond, re-polished

7.3.4.1 TLY measurements

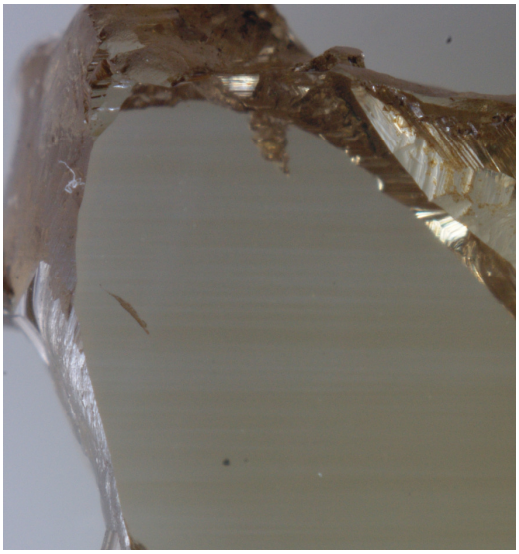

Figure 7-12a: Photograph of Type IIa natural diamond with horizontal banding.

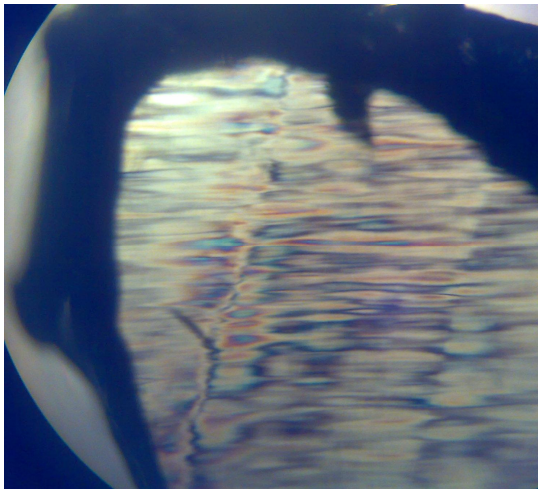

Figure 7-12b: Birefringence pattern within the sample correlating with the direction of the bands.

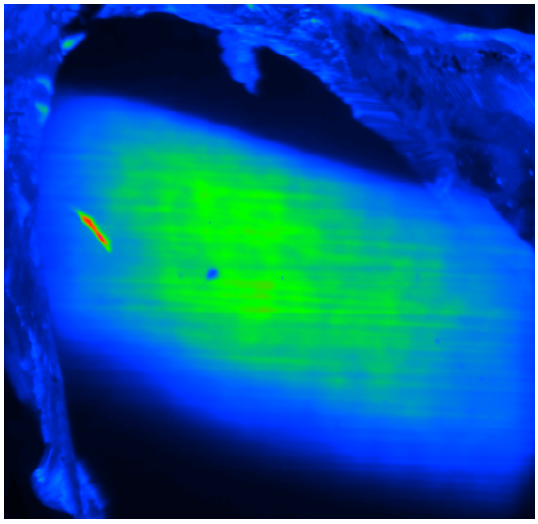

Figure 7-12c: XEOL image taken at 280eV using SR radiation. Exit slits are fully open for the image purpose. Horizontal banding is clearly visible in luminescence. Luminescence Image x2. (Synchrotron beamspot is typically around 3mm x 1.5mm in size – as shown in figure 7-9c)

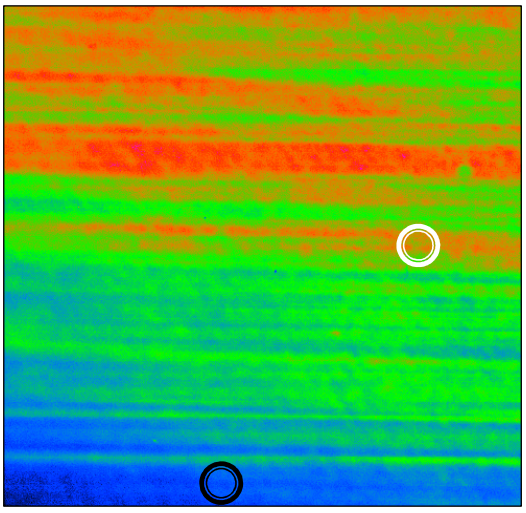

Figure 7-12d: XEOL image taken at 280eV with no filters and a magnification of x20.

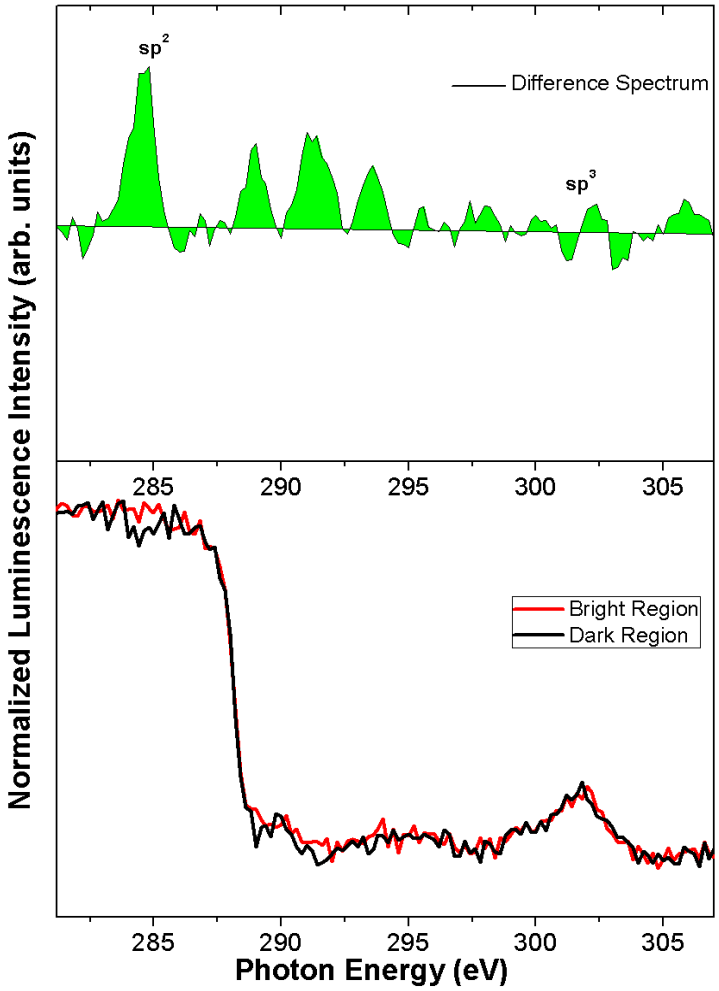

Figure 7-13: OD-XAS spectrums recorded at the two points in figure 7-12d (White circle – bright band, Black – dark band). The difference spectrum (top) shows a higher concentration of sp^2-bonded carbon in the darker banded region.

The previous measurement on this sample reveals regions of high graphitic carbon content that was identified by a particularly sharp quenching effect of the luminescence intensity at ~284.31eV (below that of the diamond absorption edge) where the x-ray energy resonates with the C 1s – π* transition in sp^2-bonded carbon. These graphitic regions can be removed by polishing and hence have been identified as being localised inclusions, distinct from the dark banding that extends throughout the thickness of the diamond. The bands are clearly observed in figure 7-12d. In figure 7-12d, two regions have been selected to illustrate variation in the relative abundance of carbon species across the sample and the corresponding OD-XAS spectrums are shown in figure 7-13. The spectrums have been normalised and aligned at the featureless regions either side of the absorption edge. At the high energy side,

the absorption feature indicative of diamond associated with the C 1s – σ* transition (sp^3 bonding) is present at both sampling regions, situated at ~301.43eV along with a pre-edge feature which is only observed in the darker banded region's OD-XAS spectrum (figure 7-13). This indicates that there is a more prominent C 1s – π* x-ray absorption channel that suggests a higher concentration of sp^2-bonded carbon species situated at the darker bands of this type IIa diamond compared with the brighter (less brown) bands.

An enhancement image or mapping image of the sp^2-bonded carbon regions could not be obtained in this instance due to the significantly less intense sp^2 feature.

Figure 7-14 provides the fitting components for the sample in question.

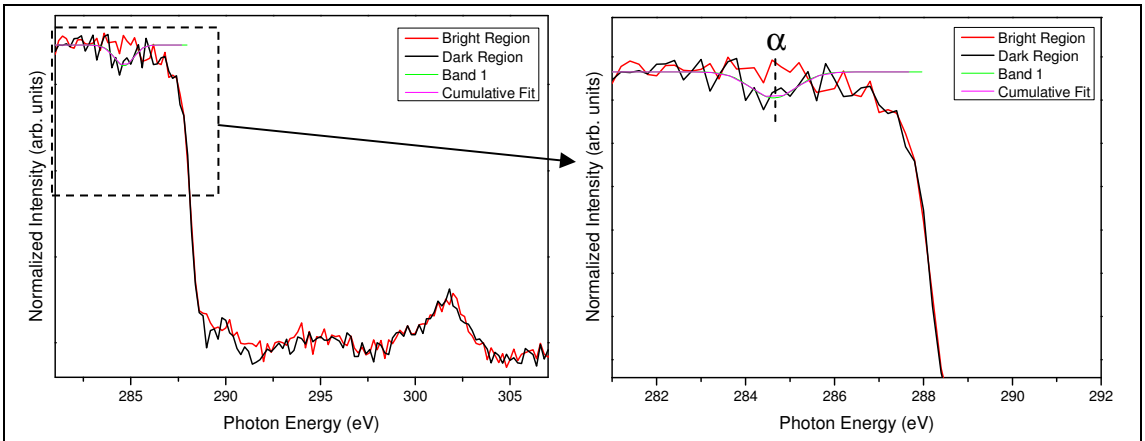

Figure 7-14: Pre-edge feature fitted with a single band for the naturally banded type IIa diamond.

Table 7-3 provides a summary of the peak centre and features location for the naturally banded type IIa diamond.

Table 7-3:

Band/Feature	Peak Centre (eV)	FWHM
α	284.63	1.21
Edge	~288.00	---
σ*	301.43	2.89

The 284.63eV band can be associated with the π* resonance as mentioned previously for this sample. The spectrums obtained after polishing is significantly different for the brown bands compared with the dark clusters previously observed prior to repolish. The brown bands are more diamond-like due to the σ* resonance feature at ~301.43eV, but still have pre-edge structure typically associated with sp^2-bonded carbon although the ~287.05eV band previously associated with C – H* resonance is no longer present.

7.3.4.2 PLY measurements

Partial Luminescence Yield (PLY) measurements were also obtained for the natural type IIa banded diamond through particular filters to observe whether the sp^2 regions are more prominent from a particular band in the XEOL (chapter 5).

The XEOL spectrum is shown again for the natural type IIa banded diamond (figure 7-15).

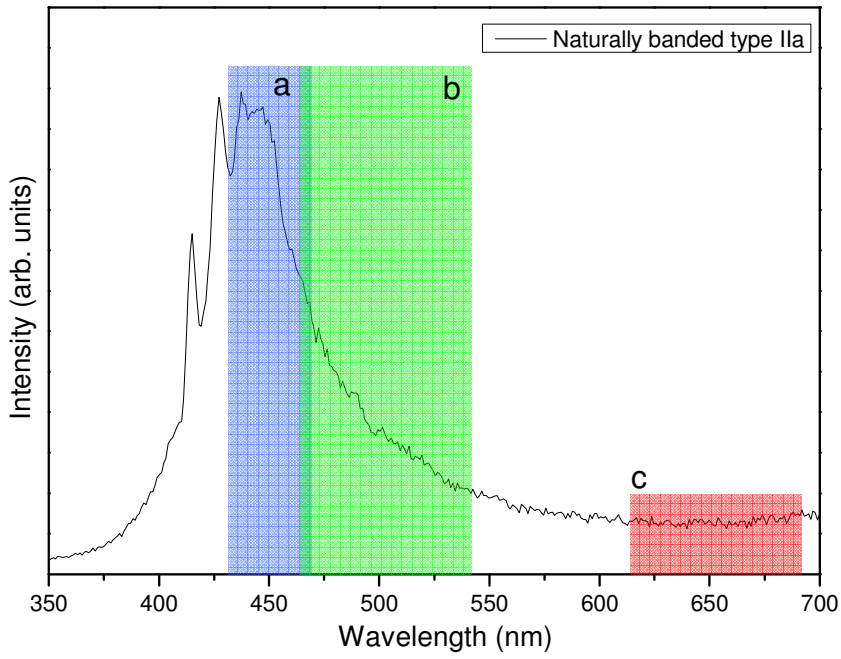

Figure 7-15: XEOL spectrum for the naturally banded type IIa diamond. The broadband filters used were the 450nm, 503nm and 652nm.

Table 7-4 provides a summary of the filters used for the PLY OD-XAS measurements.

Table 7-4:

	Broadband Filter (nm)	**Bandwidth (nm)**
a	450	40
b	503	75
c	652	72

The PLY OD-XAS spectrums obtained for the dark bands on the naturally banded type IIa diamond are shown for comparison in figure 7-16. Pre-edge features are clearly visible in all three but the ~285eV feature is not as apparent in the 652nm PLY OD-XAS spectrum. This suggests that the 285eV feature does not originate from the 652nm part of the XEOL spectrum (figure 7-15). Its presence in the other spectrums could suggest that its origin lies at those luminescence bands, from those particular defects.

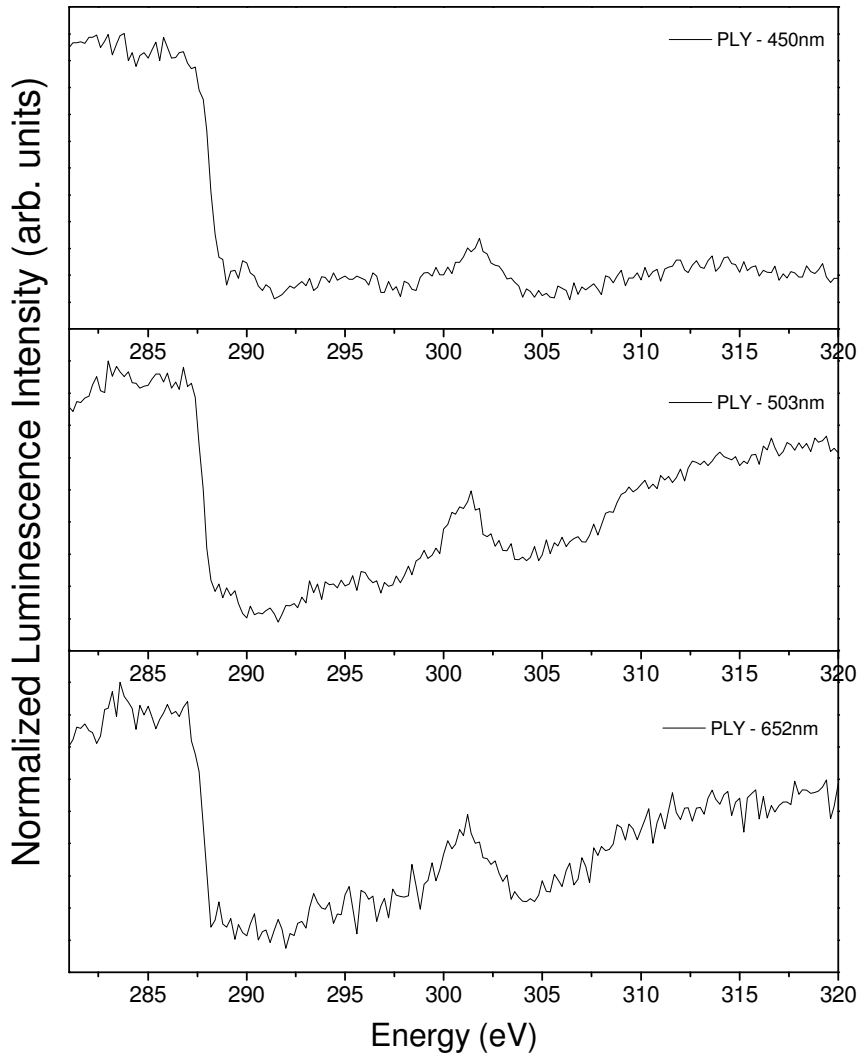

Figure 7-16: PLY – OD-XAS spectrums for the naturally banded type IIa diamond.

7.3.5 Naturally Banded type Ia diamond

7.3.5.1 TLY measurements

Figure 7-17a: Photograph of Type Ia natural diamond with diagonal banding taken in reflected light.

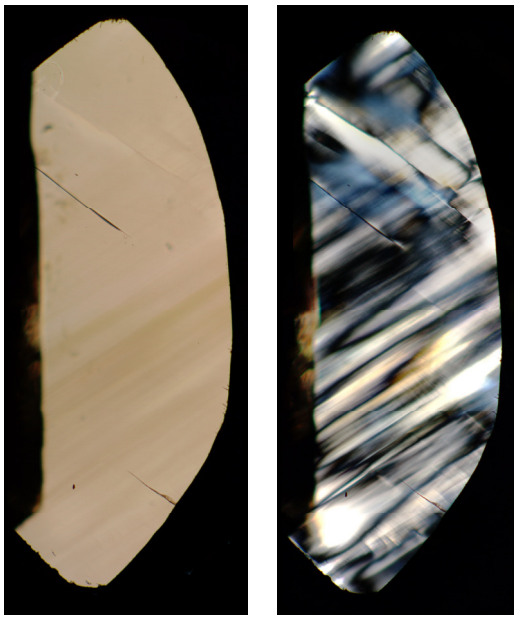

Figure 7-17b: Photograph of brown banding taken in transmitted light (left image). Birefringence pattern within the sample correlating with the direction of the bands (right image).

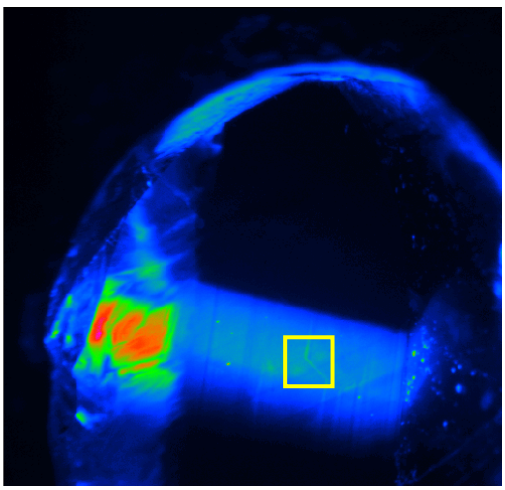

Figure 7-17c: XEOL image taken at 280eV using SR radiation. Diagonal banding is clearly visible in luminescence. Yellow square corresponds to the x20 region (Figure 7-17d). Luminescence image x2.

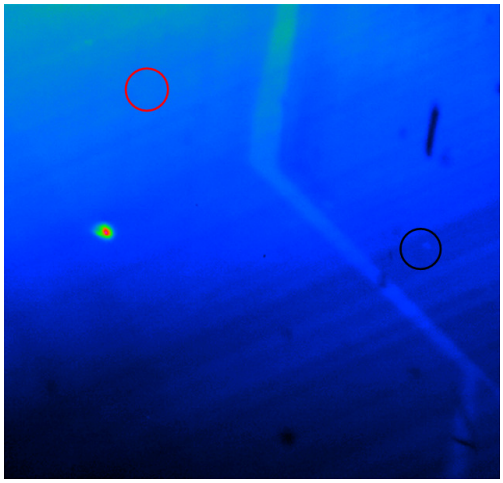

Figure 7-17d: XEOL image taken at 280eV and no filters with magnification of x20. (Yellow squared region in figure 7-17c).

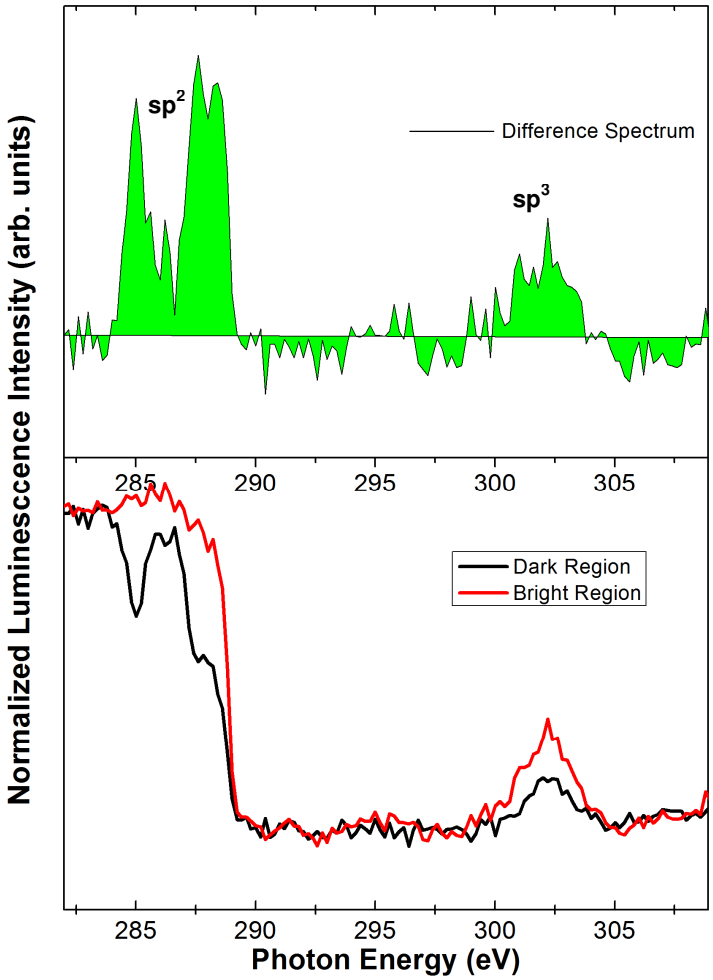

Figure 7-18: OD-XAS spectrums recorded at the two points in figure 7-17c (Red circle – bright band, Black – dark band). The difference spectrum (top) shows a higher concentration of sp^2-bonded carbon in the darker banded region.

The type Ia banded diamond was also studied with the OD-XAS technique. Similar dark clustered regions were also observed for this sample, but of a significantly less amount compared to the numbers found in the type IIa naturally banded sample prior to its more recent polish. The darker regions of this type Ia diamond also show a higher concentration of sp^2-bonded carbon.

The striking banding present in this sample can be observed in reflected light as well as in transmitted light (figures 7-17a and 7-17b). The birefringence image is also shown in figure 7-17b and correlates with the direction of the banding. Luminescence images taken at ~280eV (figures 7-17c and 7-17d) also reveal the banding as is the case for all the samples studied. The x20 magnification image provides a better

resolution of the banding under study for the provision of the OD-XAS spectrums in figure 7-17d for a bright band and a dark band. The OD-XAS spectrums for both regions provide a feature at ~302.27eV which as mentioned previously is related to the σ* resonance, a typical indicative feature of diamond which relates to the tetrahedral nature of the bonding involved in diamond (sp^3). It is of relatively less intensity in the spectrum obtained form the dark region and could be due to the significant pre-edge features that are clearly observed and related to sp^2 bonded carbon. The decrease in intensity is due to the sp^2 bonded carbon features that are observed in the region of analysis, the amount of sp^3 bonded carbon is less as a result. The σ* resonance is typically found in diamond at ~303eV (*26*).

The type Ia diamond sample studied (figure 7-17) has an interesting OD-XAS spectrum (figure 7-18) and contains a significant feature present as a shoulder just before the edge. There is mention in the literature that this feature is associated with C 1s – π* (C – H) transition (*18, 21-27*).

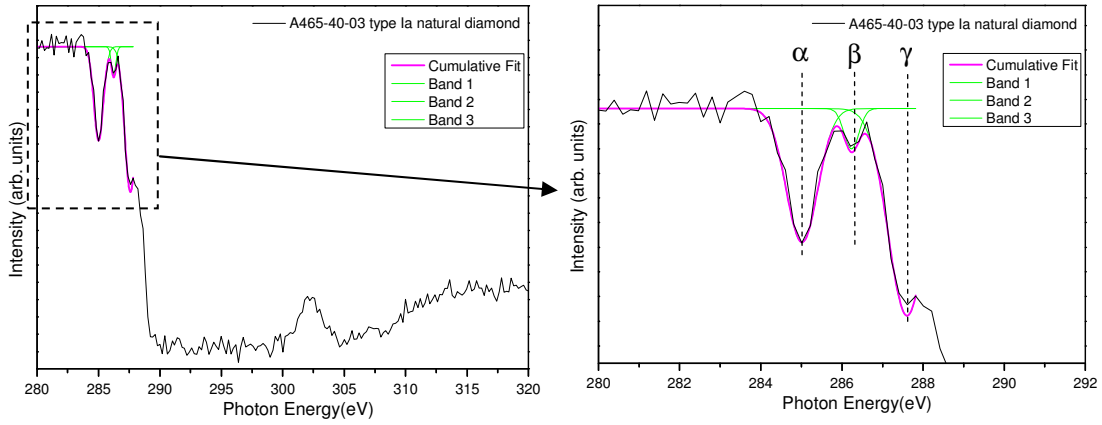

Figure 7-19: Fitted features on the type Ia naturally banded diamond.

A summary of the fitting parameters are provided in table 7-5.

Table 7-5:

Band	Peak Centre (eV)	FWHM
α	285.02	0.91347
β	286.24	0.25943
γ	287.61	0.55310
Edge	~288.00	---
σ*	302.27	2.09

The fitting of the OD-XAS spectrum obtained at the dark region of the type Ia diamond sample is shown in figure 7-19. Table 7-5 shows the fitted peak centres along with their FWHM. The pre C K-edge features have previously been identified. The α band (285.02eV) has been identified in previous samples as the C = C (C 1s – π* transition) that typically lies at ~285.4eV (*18, 19, 21-26, 28-30*). The β band situated at ~286.24eV could be related to the C = O, whereby a C 1s – π* transition is induced by the presence of oxygen (*21, 22, 24, 29*). Although there is also mention in the literature that the ~286.24eV band centre could be related to the C 1s – π* resonances involving C = N bonds which could be possible, due to the sample being a type Ia sample and therefore containing N (*21, 22, 31, 32*). The third band, labelled as the γ band for this sample is located at ~287.61eV and is responsible for the shoulder that is observed in the OD-XAS spectrum for the dark region (band) in this sample. This has been attributed to C – H* resonance which is typically observed at around 287.5eV and therefore in good agreement with the results obtained (*18, 21-27, 33*). In conclusion the higher concentration of sp^2-bonded carbon species is again typically found in the darker regions of the diamond sample.

7.3.5.2 PLY measurements

PLY OD-XAS measurements were also undertaken on the type Ia diamond with the CLASSIX spectrometer (*2*).

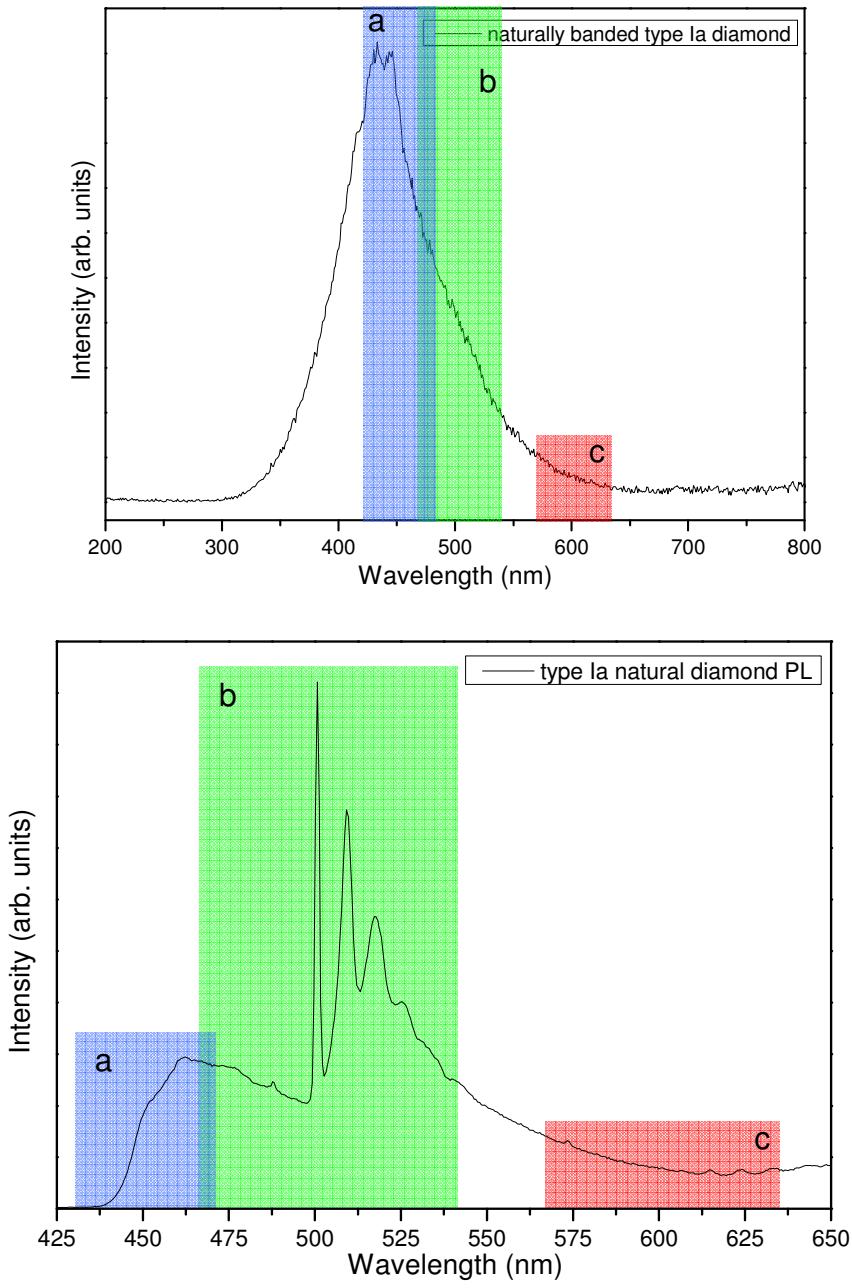

Figure 7-20: XEOL (top) and PL (bottom) spectrums for the type Ia banded diamond obtained using a 404nm laser on MoLES. Both spectrums are shown for comparison of the luminescence band studied in PLY.

The broadband filters in figure 7-20 are summarised in table 7-6.

Table 7-6:

	Broadband Filter (nm)	**Bandwidth (nm)**
a	450	40
b	503	75
c	600	68

Figures 7-21a to 7-21f show the PLY OD-XAS spectrums obtained for the type Ia sample. The bright regions have also been included in the analysis for this particular sample and the pre-edge features are relatively unaffected by the filtering. The most prominent differences are observed in the OD-XAS spectrums that originate from the dark regions.

PLY OD-XAS spectrum – Broadband Filter (450nm)

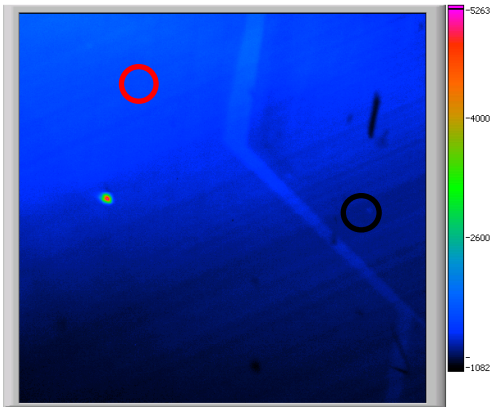

Figure 7-21a: XEOL image taken at 280eV with a 450nm broadband filter.

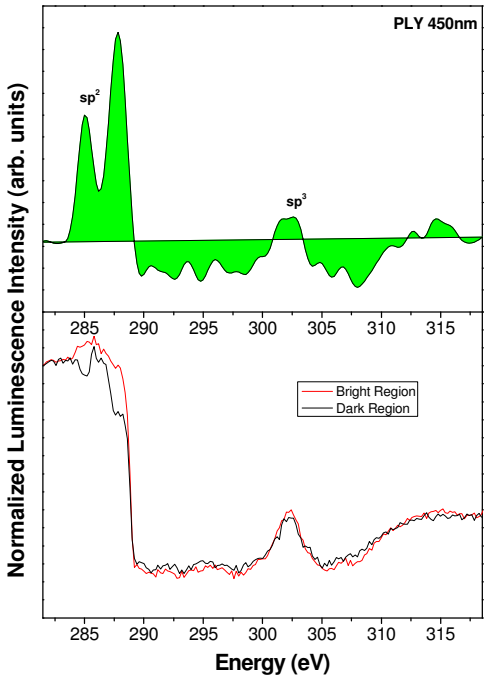

Figure 7-21b: PLY OD-XAS spectrum taken with the 450nm broadband filter.

PLY OD-XAS spectrum – Broadband Filter (503nm)

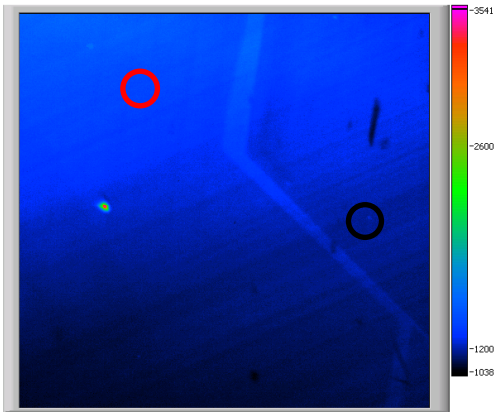

Figure 7-21c: XEOL image taken at 280eV with a 503nm broadband filter.

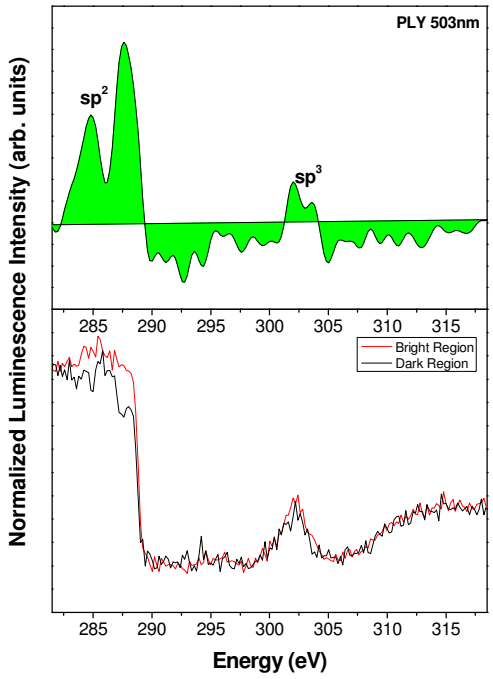

Figure 7-21d: PLY OD-XAS spectrum taken with the 503nm broadband filter.

PLY – OD-XAS spectrum – Broadband filter (600nm)

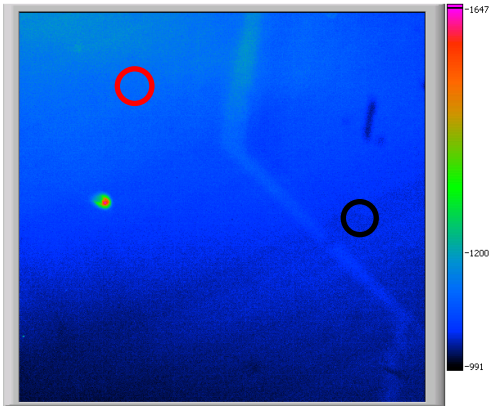

Figure 7-21e: XEOL image taken at 280eV with a 600nm broadband filter.

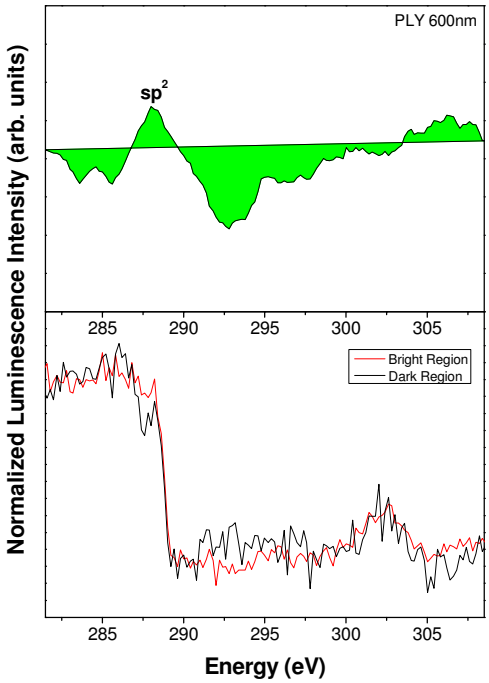

Figure 7-21f: PLY OD-XAS spectrum taken with the 600nm broadband filter.

The PLY measurements for the type Ia diamond do not show significant differences in the features that have been observed in TLY. The only apparent difference observed is that the typical sp^2 feature often found at ~285.5eV is not as apparent in the PLY-600nm OD-XAS spectrum as has been observed with the previous samples. This could be due to the fact that the feature does not originate from that part of the luminescence (refer to the XEOL and PL figure 7-20). It should also be noted that the signal is affected by noise in this instance due to the weaker luminescence signal and therefore could also affect the features prior to the edge, but they are relatively small in comparison with the typical size of the feature (285eV). This is a similar conclusion to that observed in the type IIa naturally banded sample. The OD-XAS spectrums originating from the brighter regions of the sample are relatively unaffected in PLY. The C – H* resonance is present in all PLY OD-XAS spectrums.

7.3.6 CVD Diamond (0542715)

7.3.6.1 TLY measurements

The CVD diamond inclusive of brown features was also studied via OD-XAS. A striking luminescence image can be obtained with the CLASSIX spectrometer that again, as with all the previously mentioned samples, provides a correlation with the diamond photograph in transmitted and reflected light. The darker bands are clearly seen with dark features that extend into the bright regions, which the naked eye, in transmitted light, cannot observe.

Zhou *et al.* have previously reported that the sp^2-bonded regions in CVD diamond are not luminescent (*34*). They state that all the luminescence originate from defects within the sp^3-bonded bulk. The CVD sample studied here, as stated previously, is a sample that contains strong lateral variations in colour (figure 7-22a). Figure 7-22c is a photograph of the region studied via synchrotron irradiation (white rectangle). The image recorded in TLY at incident photon energy of 280eV is shown in figure 7-22d. Correlation can clearly be observed between the TLY and the dark colouration in the diamond.

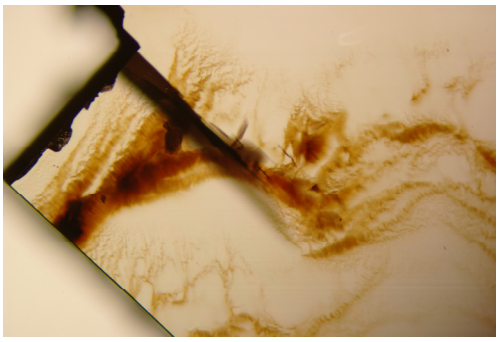

Figure 7-22a: Photograph of a CVD diamond with brown regions.

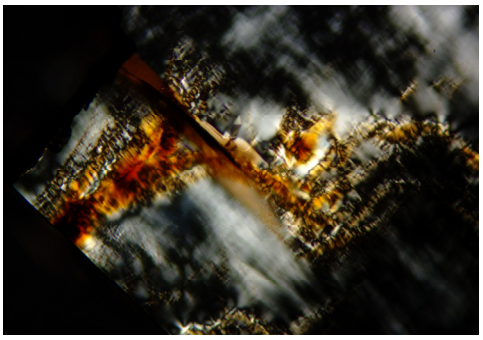

Figure 7-22b: Birefringence pattern of the CVD sample. Brown regions are still clearly visible.

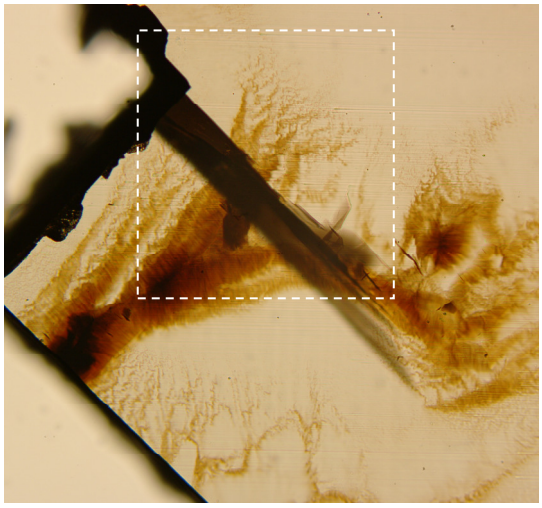

Figure 7-22c: Photograph of the CVD sample showing the region (white rectangle) of imaging relative to figure 7-22d.

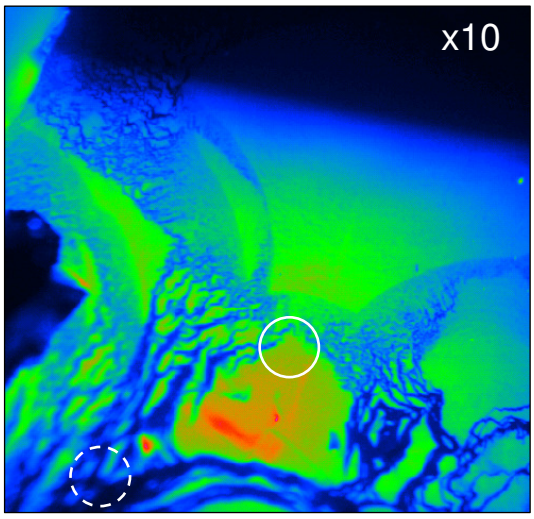

Figure 7-22d: Luminescence image taken at 280eV using SR radiation and no filters – TLY with a magnification of x10. Luminescence image correlates with the photograph (figure 7-22c, white rectangle) with the brown regions clearly visible here too.

OD-XAS spectrums for this sample were obtained and the results are shown in figure 7-23. The two spectrums shown in figure 7-23 originate from a dark and bright region of the sample (figure 7-22d). The spectrums have been normalized to the incident flux and also normalized to each other to obtain a difference spectrum in the top panel (figure 7-23). Differences can clearly be observed between both regions when comparing the relative sp^2 and sp^3 carbon-bonded species within the two sampling regions. A higher fraction of sp^2-bonded carbon is found present in the dark area compared to the bright area.

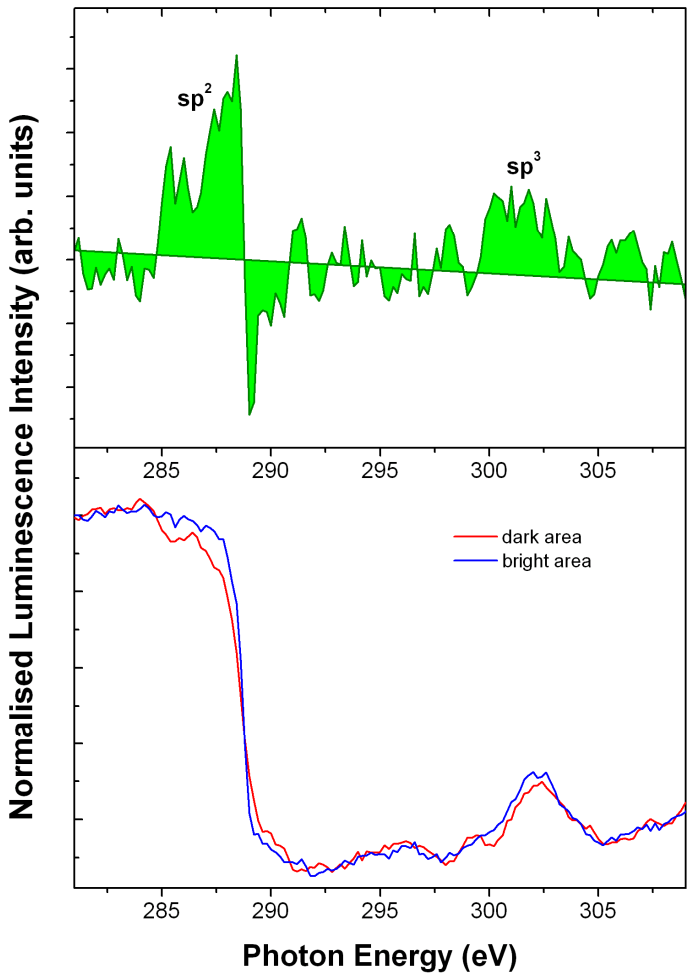

Figure 7-23: OD-XAS spectrums recorded at the two points in figure 7-22d (White solid circle – bright region, dashed white circle – dark region). The difference spectrum (top) shows a higher concentration of sp^2-bonded carbon in the darker region.

Figure 7-24 shows the fitting for the CVD diamond for the brown region of the sample.

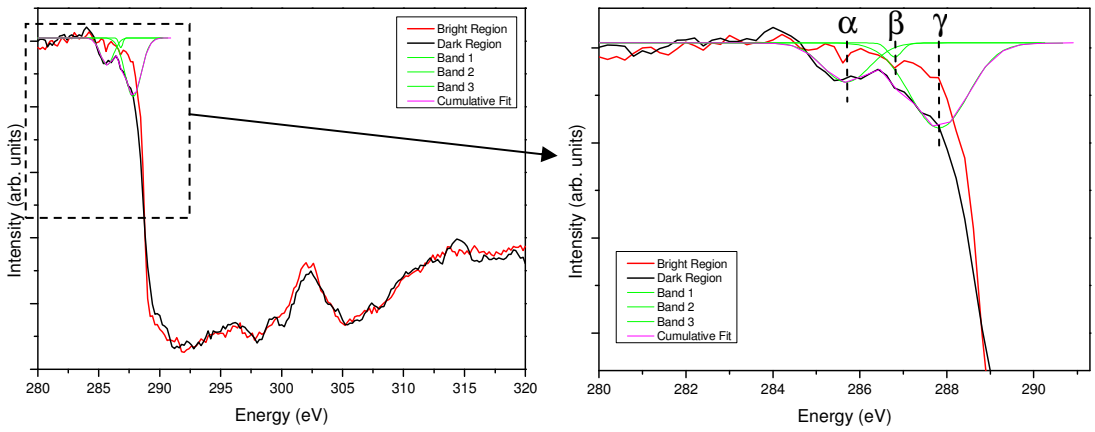

Figure 7-24: Pre-edge features fitted with three bands for the CVD sample.

The pre-edge resonance features have been fitted and are summarised in table 7-7.

Table 7-7:

Band	Peak (eV)	FWHM
α	285.69	1.26
β	286.80	0.39
γ	287.82	1.58
Edge	~288.70	---
σ*	302.21	3.05

Three bands have been identified prior to the edge located at 285.69eV, 286.80 and 287.82eV. The exciton peak for the bright region is present at ~289.2eV comparable to that found in the literature at 289.3eV (*26*).

The 285.69eV peak can be ascribed to the typical sp^2-bonded carbon peak C 1s – π* transition that is related to C = C bonding and graphitic in nature (*18, 19, 21-26, 28-30*). The 286.80eV band is typically associated with C = O bonding (*22, 29*). There is also mention in the literature that π* resonance associated with acetylene can be found at around 285.9eV (*29*). This may be associated with the significant sp^2-bonded

carbon species observed in the Raman (chapter 6) for this sample that was attributed to transpolyacetylene. The 287.82eV band could possibly be associated with either C – H bond or the C = N bond which are located at around this region (*18, 22, 25, 26, 31, 32*) (see summary table of relative C 1s – π^* resonance locations in table 7-15). Typically observed at around 303eV is the diamond sp^3-bonded carbon σ^* peak (*26*) whereby for this sample, found to be at ~302.21eV.

7.3.6.2 PLY measurements

OD-XAS PLY measurements were also undertaken for this sample at different wavelengths and magnifications but the transmission was relatively poor for any significant analysis to be performed with regards to the presence of any of the pre-edge features. The spectrums were all affected considerably by noise due to the poor filter transmission in this instance and therefore Volume Integrated plots of the PLY spectrums were taken, with the region selected over a large dark region of the sample (see figure 7-26a and 7-26b).

Figure 7-25 is the PL spectrum obtained for the CVD diamond. The coloured regions correspond to the broadband filters used for the PLY measurements. A summary of the filters used can be found in table 7-8.

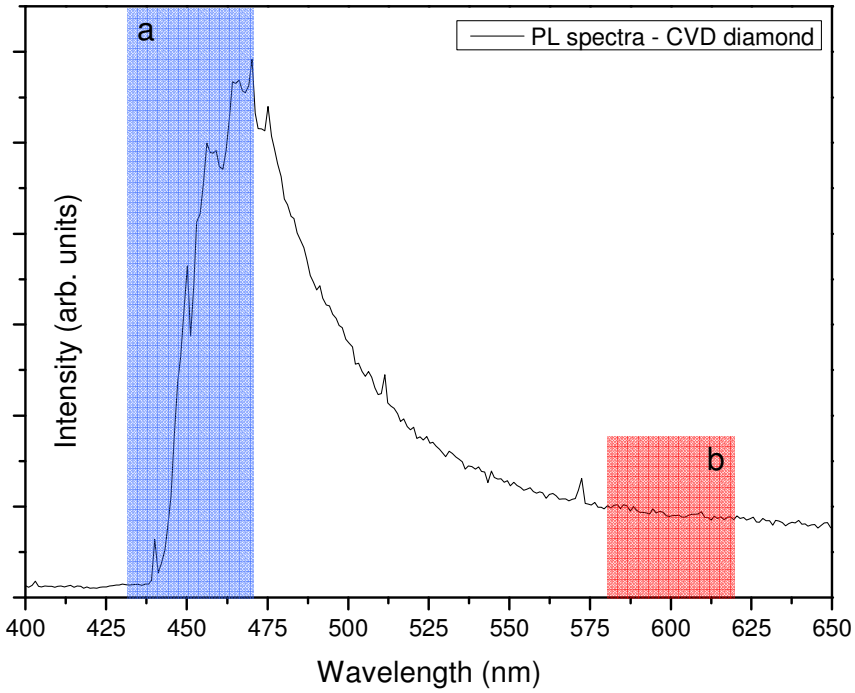

Figure 7-25: PL spectrum for the CVD diamond showing the regions studied via PLY at 450nm and 600nm.

Table 7-8:

	Broadband Filter (nm)	**Bandwidth (nm)**
a	450	40
b	600	68

Figure 7-26 shows the PLY OD-XAS spectrums obtained for this sample. The features observed pre-edge are similar to those obtained from TLY measurements.

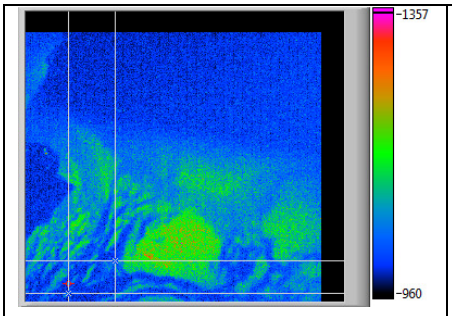

Figure 7-26a: XEOL image taken at ~280eV with a 450nm broadband filter.

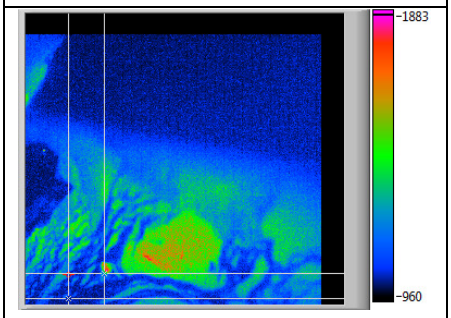

Figure 7-26b: XEOL image taken at ~280eV with a 600 broadband filter.

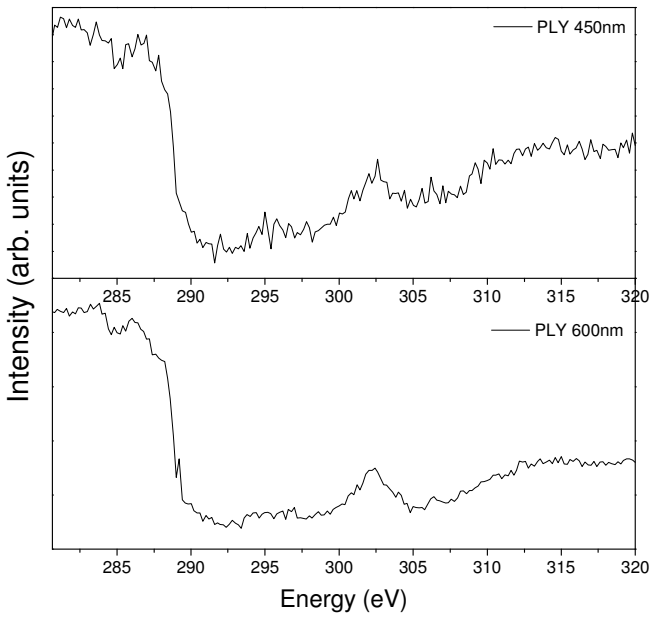

Figure 7-26c: Volume integrated PLY OD-XAS spectrums for the CVD diamond taken from the rectangular regions (dark) in figures 7-26a and 7-26b.

Figure 7-26c provides the PLY OD-XAS spectrums for the CVD sample. Pre-edge features are observed in both cases. The ~285eV feature is visible at 600nm in this instance.

7.3.7 CVD layered diamond (0673803)

7.3.7.1 TLY measurements

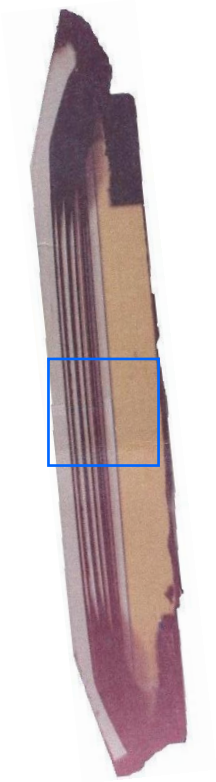

Figure 7-27a: Photograph of a CVD diamond with brown lines purposely grown. Large 'yellow' section is the HPHT substrate.

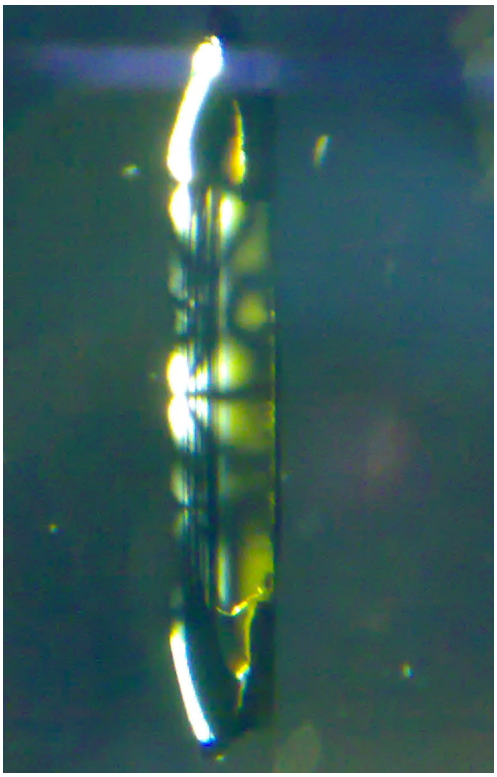

Figure 7-27b: Birefringence pattern of the CVD sample. Brown lines are still clearly visible, along with the growth pattern.

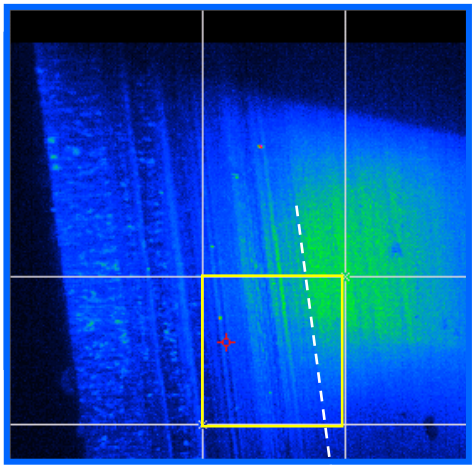

Figure 7-27c: Luminescence image taken at 280eV using SR radiation. Bands are clearly visible in luminescence. Magnification, x10.

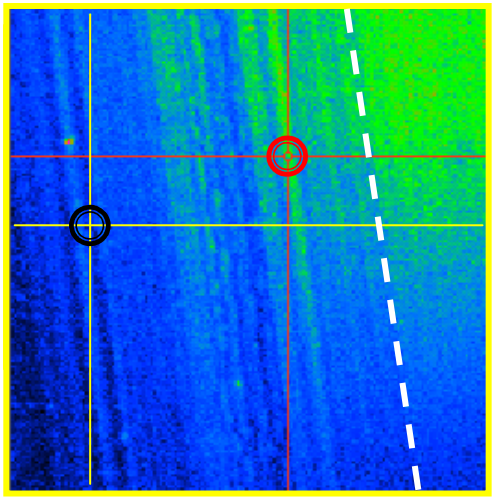

Figure 7-27d: Magnified Luminescence image of Figure 7-27c.

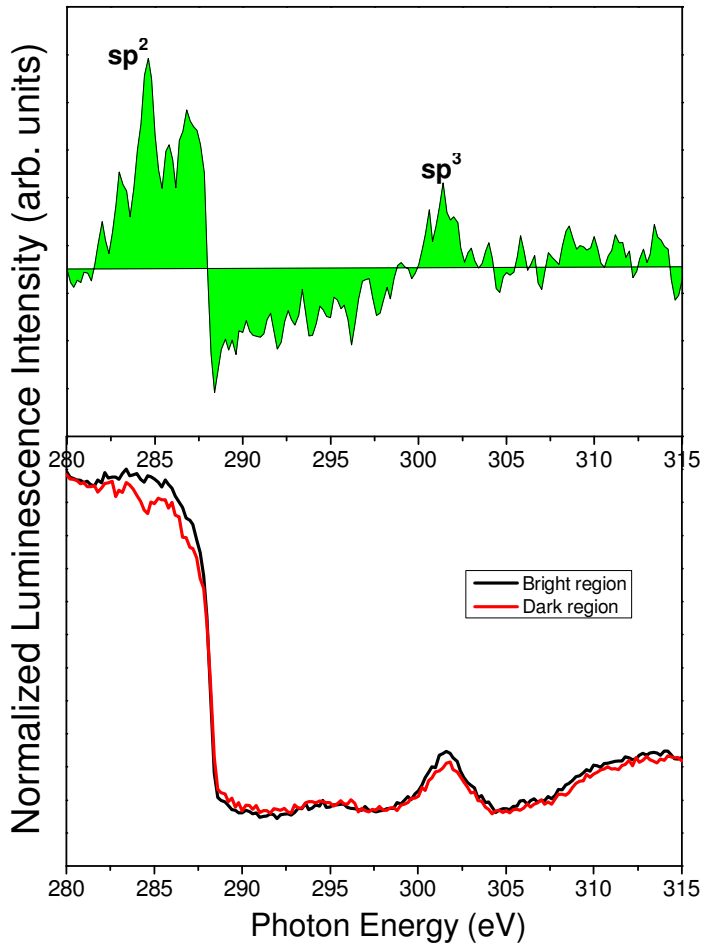

Figure 7-28: OD-XAS spectrums recorded at the two points in figure 7-27d (Red circle – bright band, Black – dark band). The difference spectrum (top) shows a higher concentration of sp^2-bonded carbon in the darker banded region.

Figure 7-27c is a luminescence image of the multilayered CVD-grown diamond (figure 7-27a) recorded in TLY with an incident photon energy of 280eV. The layered structure of the sample is evident in the luminescence image and the luminescence intensity varies across the sample surface with an enhancement at the transparent (bright) regions compared to the darker bands. OD-XAS spectrums have been recorded at a dark band and at a brighter band (figure 7-27d) and are shown along with a difference spectrum in figure 7-28. Both spectrums are indicative of diamond, with a well-defined C K-edge absorption and the characteristic C 1s – σ* resonance feature at ~301.57eV. However, the bright region has very little structure prior to the main absorption edge, while the OD-XAS spectrum obtained at the darker band shows structure similar to those previously observed in the other diamonds studied

during the course of this research which are indicative of sp^2-bonded carbon. There appears to be a higher concentration of sp^2-bonded carbon species at the dark bands in this sample compared with the brighter bands and these measurements agree with those gathered in similar instances on other diamond samples.

Figure 7-29 shows the fitting for the pre-edge features observed for this multilayered CVD diamond sample.

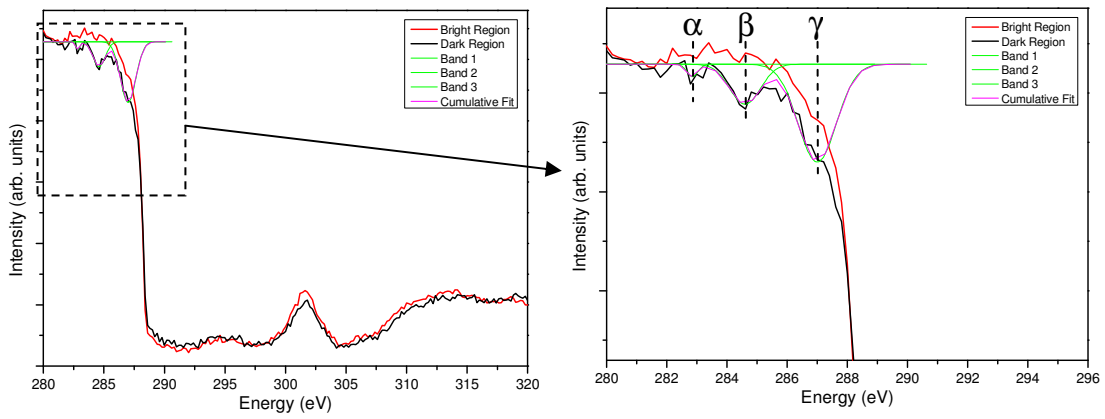

Figure 7-29: Fitted pre-edge features for the CVD layered sample consisting of three bands.

Table 7-9 provides a summary of the peak centres relative to the fitted bands in figure 7-29.

Table 7-9:

Band	Peak Centre (eV)	FWHM
α	282.85	0.43
β	284.60	1.21
γ	287.00	1.50
Edge	~288.30	---
σ*	301.57	2.56

The 282.85eV band could be attributed to the feature that has been reported at a slightly higher energy at 283.5eV and is suggested that it is related to amorphous sp^2 bonded carbon but it is not fully understood (*35*) or to the graphitic feature as suggested in (*36*). The second, 284.60eV band as has been previously observed for the

other diamond samples, can be attributed to the C 1s – π* resonance due to the C = C bond (*18, 19, 21-26, 28-30*). At 287.00eV the band can be tentatively attributed to either C = N (*21, 22, 24, 31, 32*) or C = H (*18, 21-27, 33*). It could also possibly be also related to the band observed at 285.9eV which has been attributed to acetylene (*29*), whereby a significant feature was also observed for this sample in the Raman measurements which was attributed to transpolyacetylene as well as in the studies for the other CVD diamond (0542715). It is more likely that the C = H bonds are being measured here since H is highly significant in the production of diamond from CVD synthesis (see chapter 1).

7.3.7.2 PLY measurements

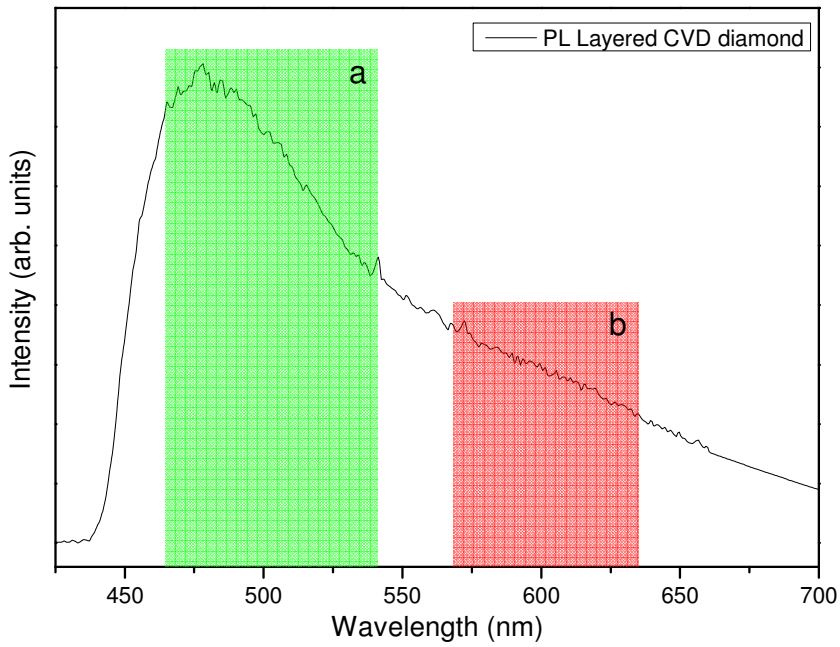

Figure 7-30: PL spectrum for the layered CVD diamond showing the broadband filter regions used for PLY OD-XAS measurements.

Table 7-10 shows a summary of the filters used for the PLY OD-XAS measurements.

Table 7-10:

	Broadband Filter (nm)	**Bandwidth (nm)**
a	503	75
b	600	68

Figure 7-31 shows the PLY OD-XAS spectrums obtained for the layered CVD diamond.

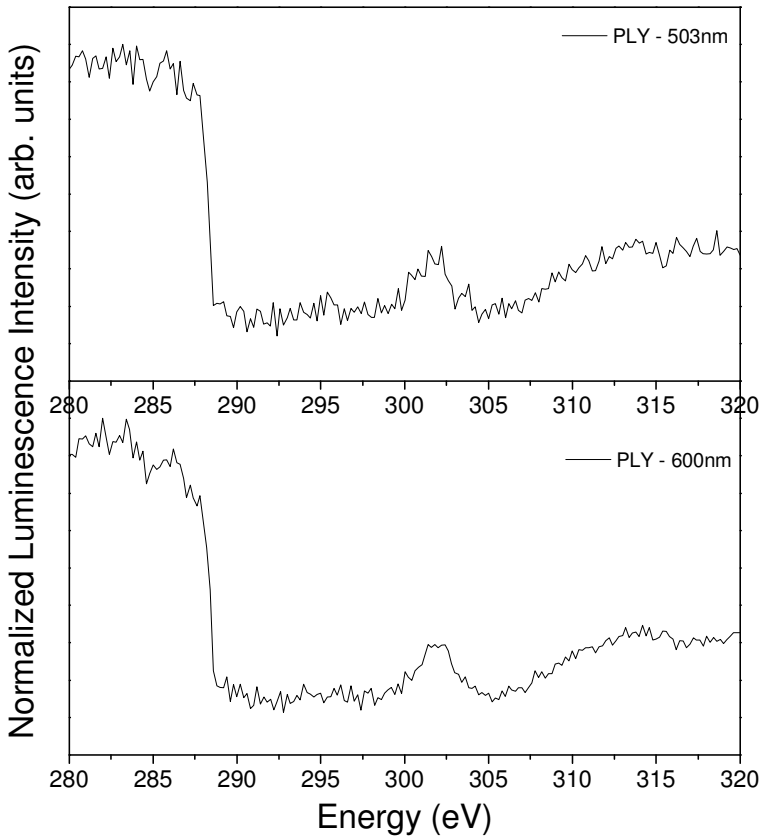

Figure 7-31: The PLY OD-XAS measurements obtained for the layered CVD diamond sample at 503nm and 600nm.

The pre-edge features can clearly be seen in the PLY OD-XAS measurements as well as in the TLY measurements obtained for this sample. These sp^2-bonded carbon species are more concentrated in the brown regions of the sample.

7.3.8 Untreated and HPHT treated type IIa diamond samples

7.3.8.1 TLY and PLY measurements

The two natural type IIa sister samples were also studied via the OD-XAS technique. Both were measured side-by-side using the CLASSIX spectrometer with the synchrotron beam overlapping both samples as shown in figure 7-32. This allowed only the requirement of one (quartz) reference sample for correction and provided results that could be directly and accurately compared between each other.

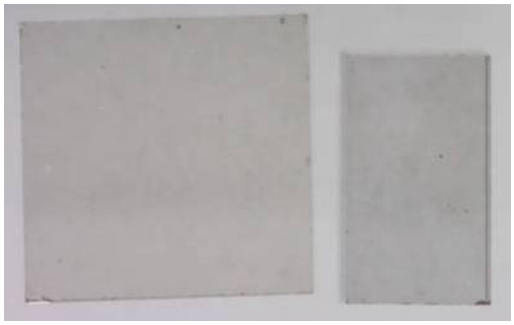

Figure 7-32a: Photograph of the two sister type IIa diamond samples, untreated (left) and HPHT treated (right).

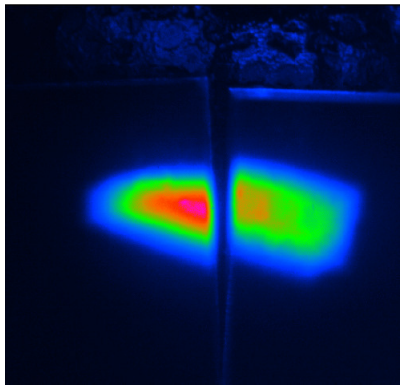

Figure 7-32b: x2 magnification luminescence image taken together at 280eV with synchrotron spot overlapping both samples, untreated sample (left), HPHT (right).

The XEOL spectrums for both samples are provided again along with the relative broad band filters used for the PLY measurements in figure 7-33.

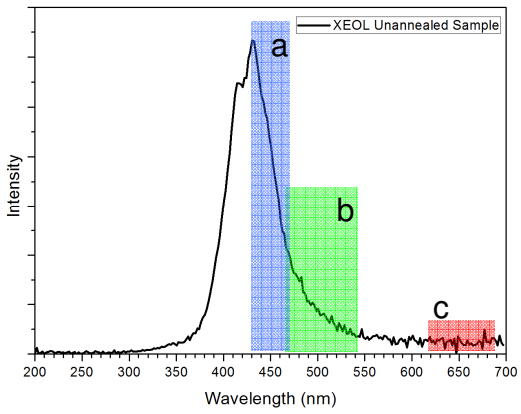

Figure 7-33a: XEOL spectrum for the untreated type IIa diamond (brown). Broadband filters used were, 450, 503 and 652nm.

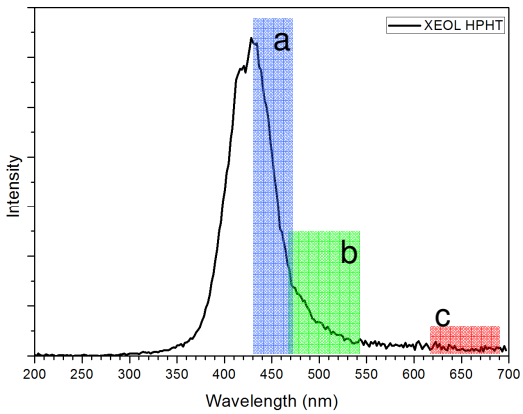

Figure 7-33b: XEOL spectrum for the HPHT treated type IIa diamond. Broadband filters used were, 450, 503 and 652nm.

Table 7-11 provides a summary of broadband filters used.

Table 7-11:

	Broadband Filter (nm)	**Bandwidth (nm)**
a	450	40
b	503	75
c	652	72

The TLY and PLY OD-XAS measurements for the untreated and HPHT type IIa diamond samples are provided in figures 7-34 and 7-35 respectively.

7.3.8.1.1 Untreated type IIa

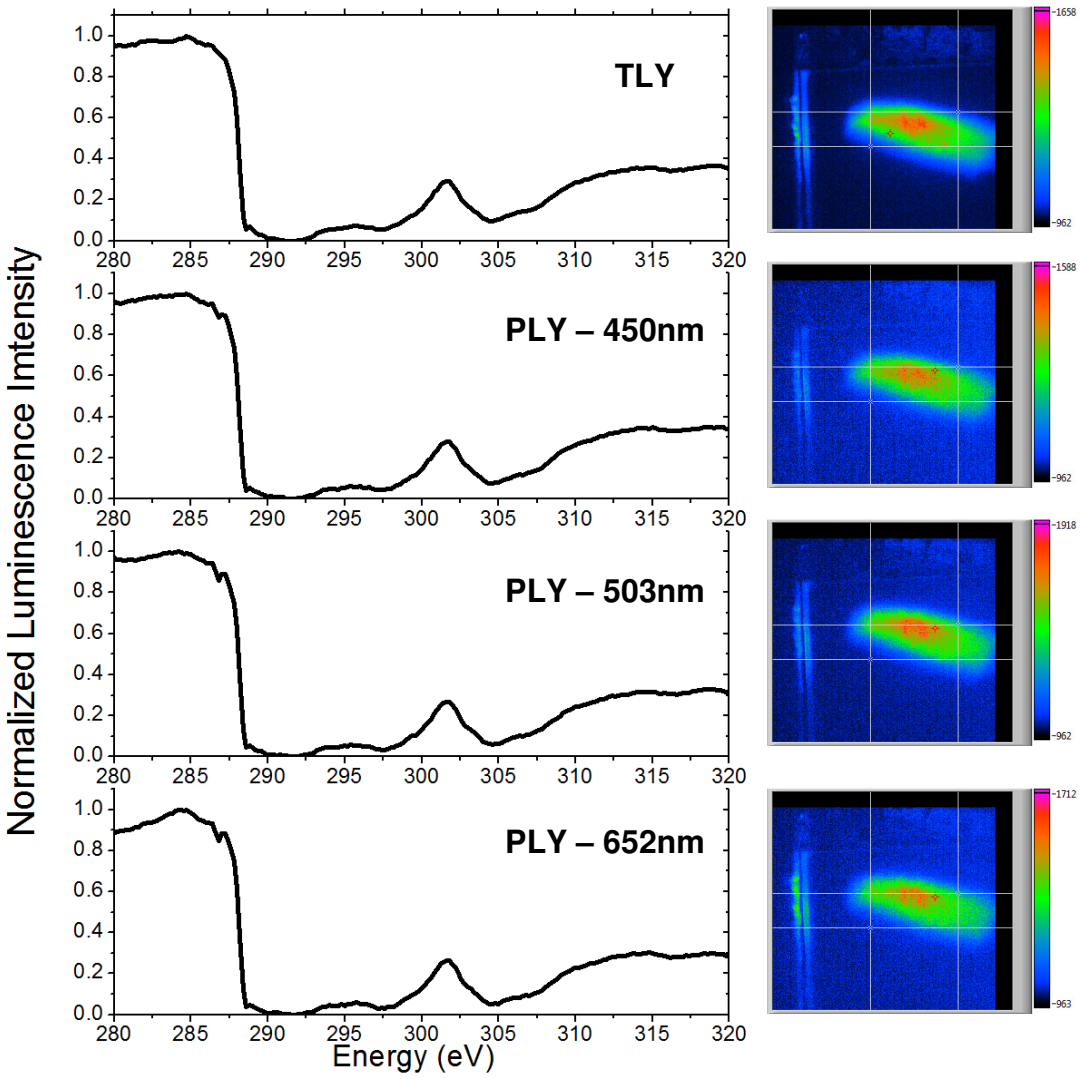

Figure 7-34: TLY and PLY OD-XAS spectrums obtained for the untreated type IIa diamond sample along with the corresponding XEOL image (taken at 280eV) for that particular filter. Images were taken at 285eV.

The OD-XAS spectrum obtained for the untreated type IIa diamond sample of which its colour is brown in nature is relatively featureless prior to the edge, except for a significant feature located at ~286.8eV which is present in all the PLY OD-XAS spectrums. The 286.8eV feature could be related to the C 1s – π* resonance with the C = O bond (*29*). No bands could be sensibly fitted to the pre-edge features.

Table 7-12 provides a summary of the fitted peaks for the natural untreated type IIa diamond.

Table 7-12:

Band/Feature	**Peak Centre (eV)**	**FWHM**
γ	286.80	---
Edge	~288.10	---
σ*	301.60	2.53

7.3.8.1.2 HPHT treated type IIa

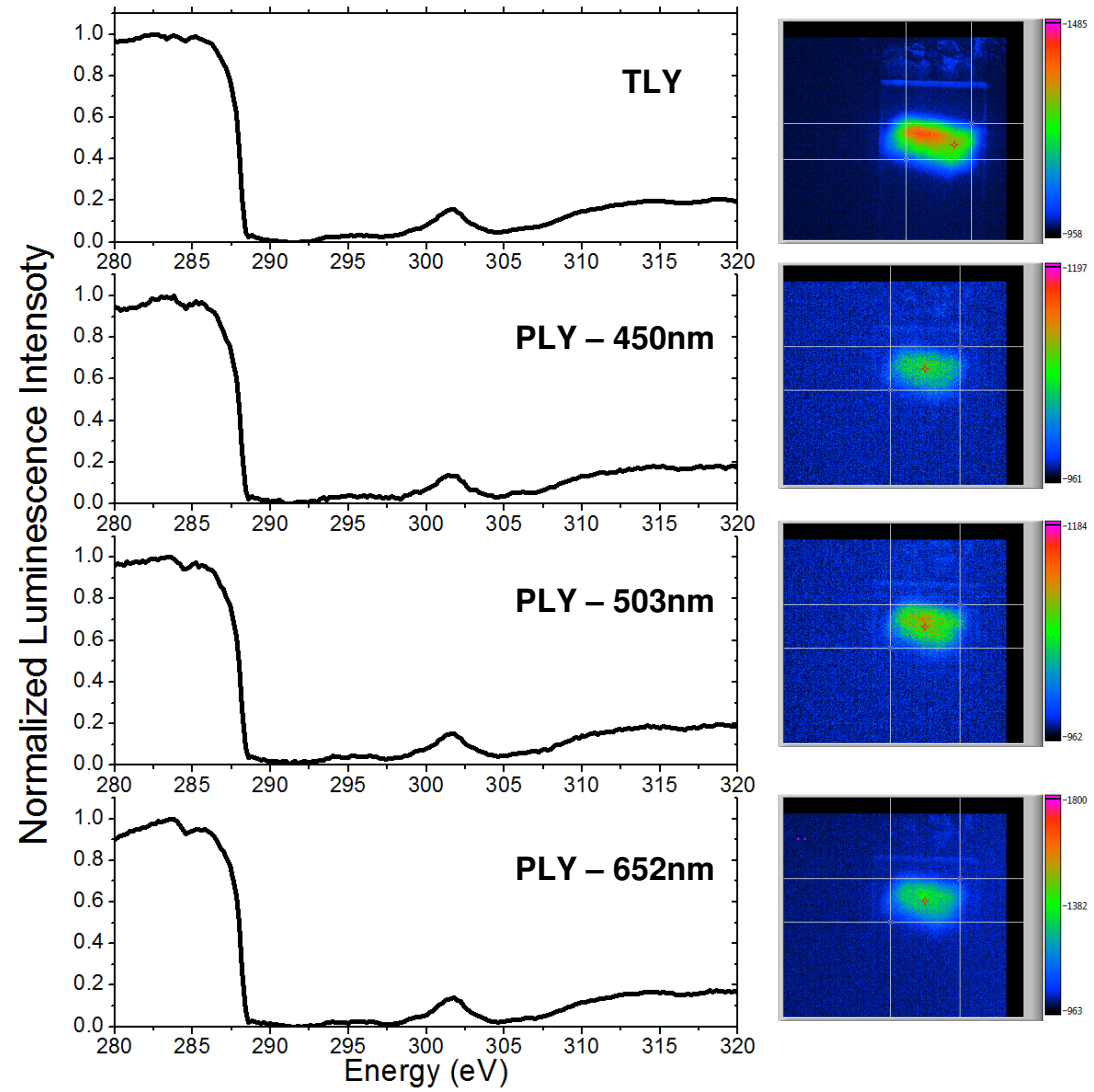

Figure 7-35: TLY and PLY OD-XAS spectrums obtained for the HPHT treated type IIa diamond sample along with the corresponding XEOL image (taken at 280eV) for that particular filter. Images were taken at 285eV.

There are more features present in the HPHT treated sample prior to the edge. This would suggest that there is an increase in the amount of sp^2-bonded carbon species that are present in this sample compared to the untreated type IIa diamond. This does not correlate with the trend observed when analysing the bright and dark regions of the other samples, as the highest concentration of sp^2-bonded carbon is typically found in the darker regions of the sample compared to the bright regions.

Figure 7-36 provides the fittings for the pre-edge features observed for the HPHT treated type IIa diamond.

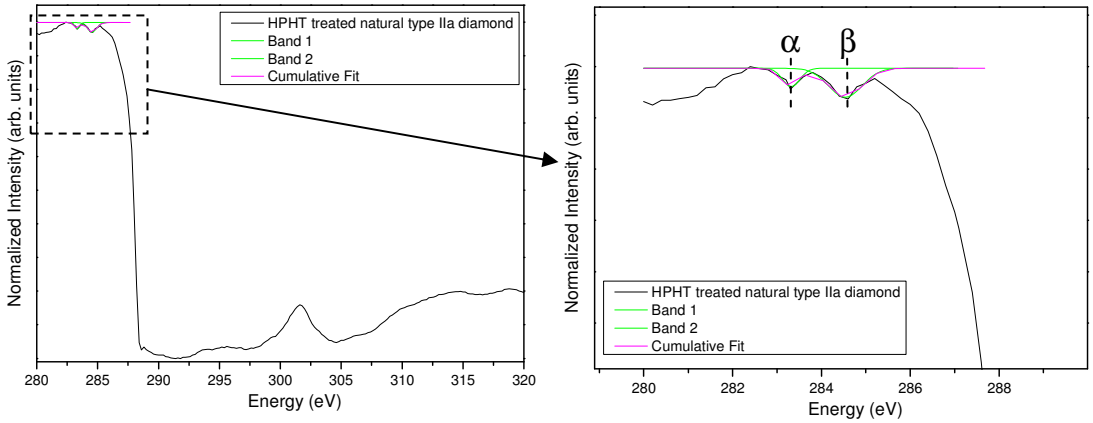

Figure 7-36: Fitting for the pre-edge features observed in the HPHT treated type IIa sample.

Table 7-13 provides a summary of the fitting parameters used in figure 7-36.

Table 7-13:

Band/Feature	Peak Centre (eV)	FWHM
α	283.32	0.46
β	284.54	0.9
Edge	287.89	---
σ*	301.57	2.54

The 284.54eV centred band can be attributed as with the other samples studied to the C 1s – π* resonance feature due to the C = C bonding. The lower energy band situated at ~283.32eV could also be related to the graphitic feature as is suggested in (*36*) whereby EELS measurements reveal that a feature characteristic of graphite, but not amorphous-Carbon, is a sharp peak at the onset of the π* band.

The HPHT treatment may have contributed to this increase in the sp^2-bonded carbon species present by changing the sample in some way. The OD-XAS results obtained here does confirm and support the Raman findings. The HPHT treated type IIa diamond did reveal a significant feature at wavenumbers above that of the diamond

peak at 1332cm^{-1} (chapter 6). The same feature was significantly less in the untreated sample. Both techniques compliment each other and support each other's findings. It is difficult to tell whether the elimination of the H3 centre (observed in the XEOL for the untreated sample and not in the HPHT treated sample) is related to any of the features witnessed here.

The σ* peak is significantly less prominent in the HPHT treated sample compared with the untreated type IIa sample.

A possible explanation for the increase in the sp^2 carbon bonding observed in the HPHT treated sample could be that the HPHT treatment has caused vacancy clusters (of which are sp^2 in nature) to migrate and combine with other sp^2 clusters to create larger clusters. This would increase the probability of detection via luminescence and therefore provide a larger pre-edge sp^2 feature in the OD-XAS spectrum. Bangert *et al.* have observed similar features in their diamond samples where small scale features were observed and attributed to collections of vacancy-clusters (*37*). Other studies by the same group do not agree with the measurements obtained here whereby they observe significantly less near-band edge features via the EELS technique in their treated samples studied (*38*), whereas here during the course of this study an enhancement of pre-edge features are observed in the HPHT treated diamond.

The PL measurements obtained in chapter 5 for both the untreated and HPHT treated sample show significant differences. The H3 centre has been eliminated due to the HPHT process and as a result, an increase is observed in the sp^2-bonded carbon signal in the OD-XAS spectrums obtained for the HPHT treated sample. The disappearance of the H3 centre could as a result have left dangling bonds or the treatment to cause a migration of small vacancy clusters to create larger ones, which contribute to the increase in the sp^2-bonded carbon signal measured via OD-XAS.

Similar observations have been made via other techniques such as positron annihilation. Positron annihilation spectroscopy is an efficient tool for studying crystallographic defects in materials of which consist of an open volume, such as vacancies. Mäki *et al.* (*39*) have carried out such measurements on brown type IIa

diamond and have suggested a relation between the presence of vacancy clusters and brown colour. They have noticed that the vacancy clusters disappear during HPHT treatment in good correlation with the decrease or loss in brown colour. They suggest that the clusters disappear, but it could be that the small clusters do not disappear and instead combine with other smaller clusters to create larger ones, the positron annihilation technique would not pick these up in measurements as the clusters are too large and the positron would die down, therefore suggesting that the clusters have disappeared (*40*). Similar work has been carried out by Bangert *et al.* on the imaging of vacancy defects in natural diamond using aberration corrected STEM and have also observed similar pre-edge features to those presented here.

7.3.9 Three natural type IIa uniformly coloured diamond samples

A third type IIa diamond of which is naturally colourless has been measured via OD-XAS for direct comparison with the HPHT treated (colourless) type IIa diamond as well as with the untreated type IIa for completeness (figure 7-37).

Untreated	HPHT treated	Naturally Colourless
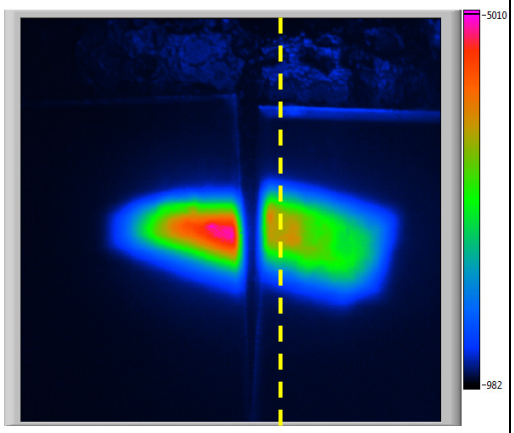		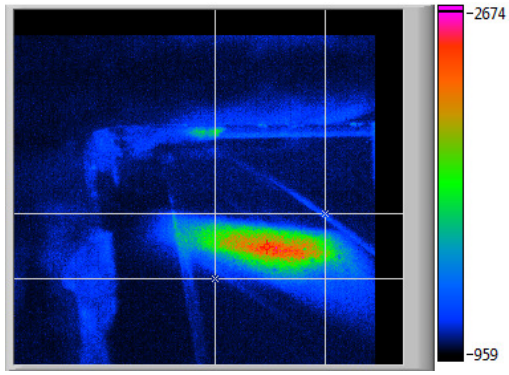
Figure 7-37a: (Shown again) Synchrotron beam incident on both untreated and HPHT treated sample. (Dotted yellow line is the region of separation between the two samples)		*Figure 7-37b: The naturally colourless sample was also mounted in the CLASSIX spectrometer and an OD-XAS measurement was taken.*
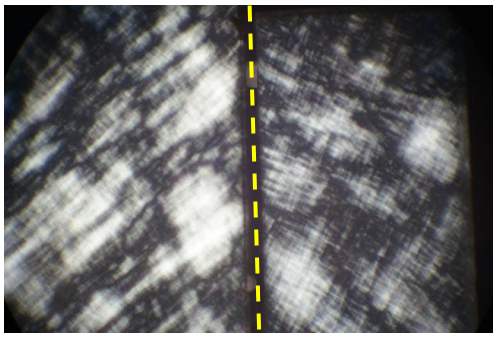		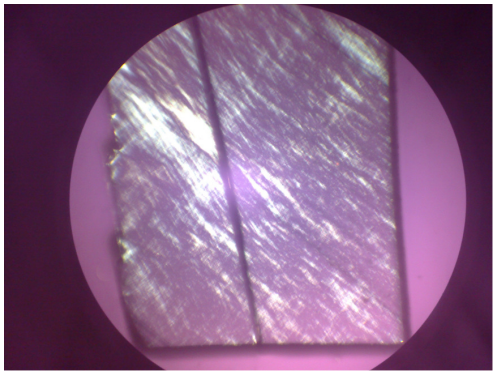
Figure 7-37c: Birefringence pattern for the untreated (left) and HPHT treated (right) samples.		*Figure 7-37d: Birefringence pattern for the naturally colourless type IIa diamond sample. (Black line down centre of diamond is a fracture).*

Birefringence images have been obtained for all three samples and differences have been observed in the direction of the stress patterns, particularly in the HPHT treated

type IIa diamond. The untreated and naturally colourless type IIa diamonds seem to have a birefringence pattern that is well ordered and in one particular direction, whereby the HPHT treated sample's birefringence pattern is much more dispersed and disordered with no particular direction. Another important factor to note is that the luminescence intensity for the HPHT treated diamond is significantly less than that of the untreated sample (figure 7-37a). This could be related to the far more dispersed birefringence pattern observed for the HPHT treated sample.

Only TLY measurements are available for the naturally colourless type IIa diamond and therefore only the TLY measurements for all three will be directly compared (figure 7-38).

7.3.9.1 Three natural type IIa samples TLY comparison

Untreated

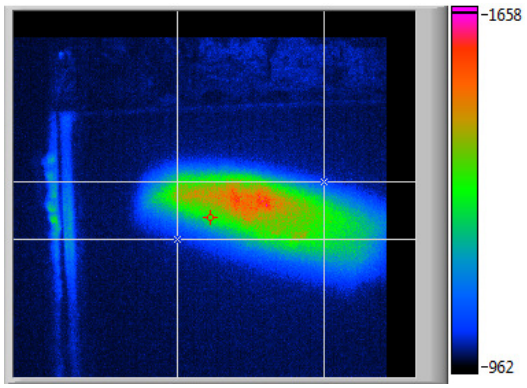

Figure 7-38a: Luminescence image taken at 280eV of the untreated type IIa diamond sample.

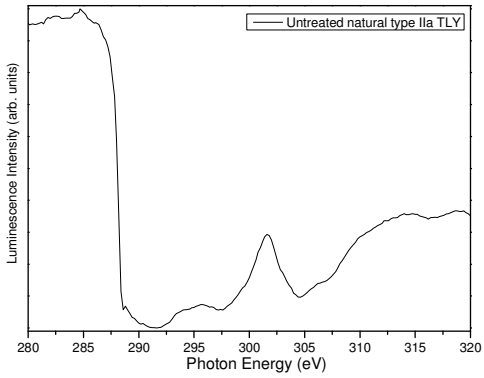

Figure 7-38b: TLY, OD-XAS spectrum for the untreated type IIa diamond sample.

HPHT treated

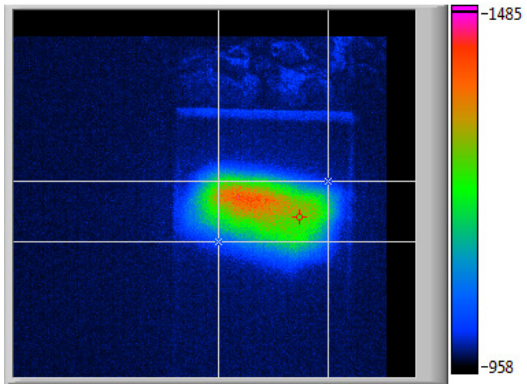

Figure 7-38c: Luminescence image taken at 280eV of the HPHT treated type IIa diamond sample.

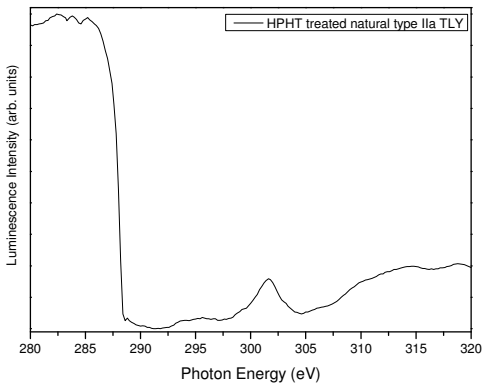

Figure 7-38d: TLY, OD-XAS spectrum for the HPHT treated type IIa diamond sample.

Naturally Colourless

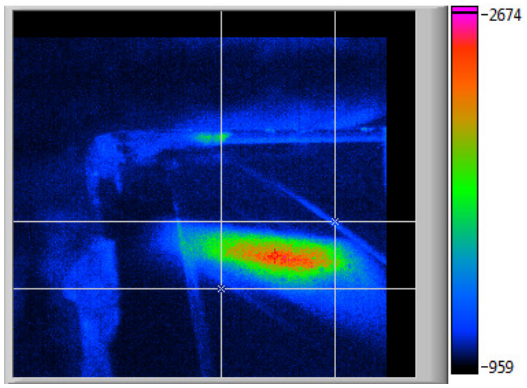

Figure 7-38e: Luminescence image taken at 280eV of the naturally colourless type IIa diamond sample.

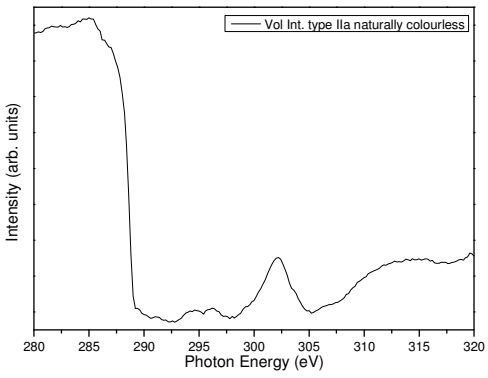

Figure 7-38f: TLY, OD-XAS spectrum for the naturally colourless type IIa diamond sample.

A clearly visible feature is present pre-Carbon edge at around 285eV in the HPHT treated sample. This colourless HPHT treated diamond can be directly compared with the naturally colourless type IIa diamond. The pre-edge features when comparing both are significantly different – with the HPHT treated sample containing a strong resonance feature at ~285eV as well as ones at a lower energy.

The untreated (brown) sample has no features that are particularly strong and that can compare with the variegated samples which have previously shown strong sp^2-bonded species highly concentrated in the brown, dark regions. The spectrum is a Volume Integrated plot, and therefore gathers all of the luminescence light. The sp^2 bonded-carbon species could be much more dispersed within the sample, and thus would not create such a strong sp^2 feature in the OD-XAS spectrum. In the HPHT treated sample, it is possible that the HPHT treatment has caused these sp^2 bonded carbon sites – such as vacancy clusters (as mentioned previously) to become mobile within the lattice formation and gather together causing a much stronger sp^2 resonance feature at ~285eV. These larger clusters evidently do not contribute to creating a brown colour within the diamond, whereas the smaller vacancy-clusters possibly do.

7.3.9.2 Naturally Colourless type IIa diamond

The Volume Integrated plot was used for comparison with the untreated and HPHT treated diamonds due to the samples being of uniform colour, and that the Volume Integrated plot would therefore provide a general OD-XAS spectrum for that particular sample. The volume integrated plot is shown again in figure 7-39b.

On closer inspection, the naturally colourless sample contains dark regions similar to those initially observed for the naturally banded type IIa (A490) diamond. The images obtained are shown in figures 7-39c and 7-39d. Dark regions are observed and as before OD-XAS spectrums can be obtained for the bright and dark regions (figure 7-40).

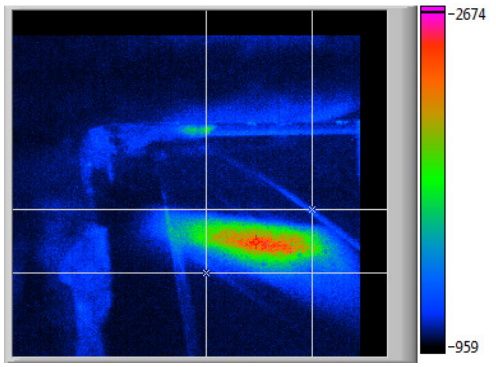

Figure 7-39a: Volume Integrated region on naturally colourless type IIa diamond.

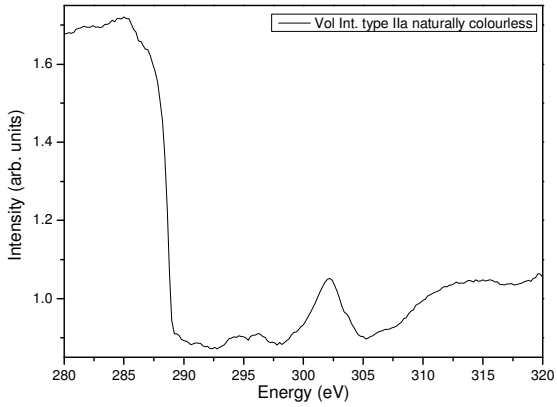

Figure 7-39b: (Shown again) Volume Integrated plot shown again for comparison with Bright and Dark regions below (figures 7-39c and 7-39d).

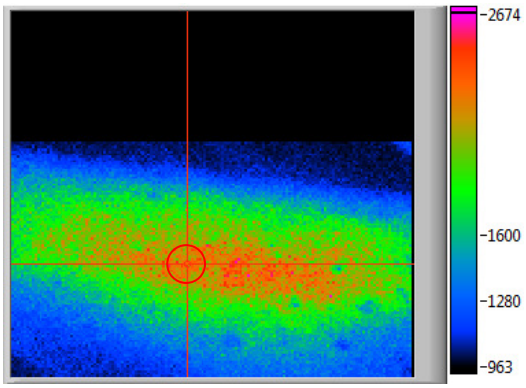

Figure 7-39c: Bright Region on naturally colourless type IIa diamond.

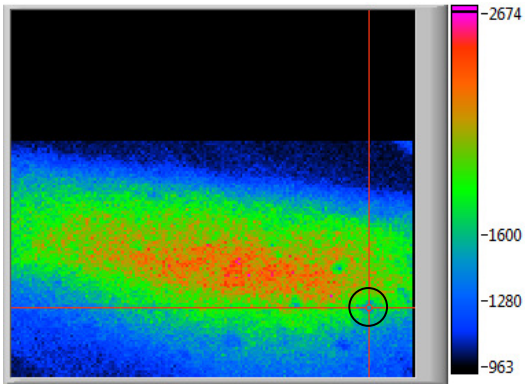

Figure 7-39d: Dark Region on naturally colourless type IIa diamond.

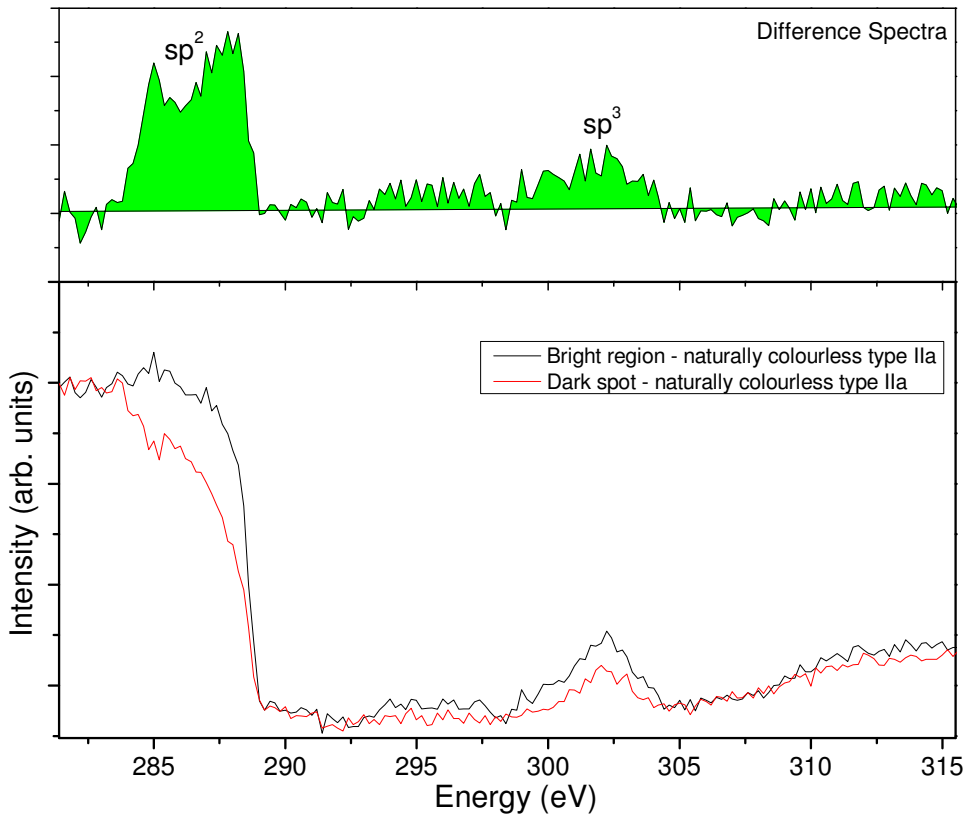

Figure 7-40: OD-XAS spectrums for the Bright (red circle figure 7-39c) and Dark regions (black circle figure 7-39d) on the naturally colourless type IIa diamond.

The fittings for the naturally colourless sample's dark region is shown in figure 7-41 along with a table summarising the features found (table 7-14).

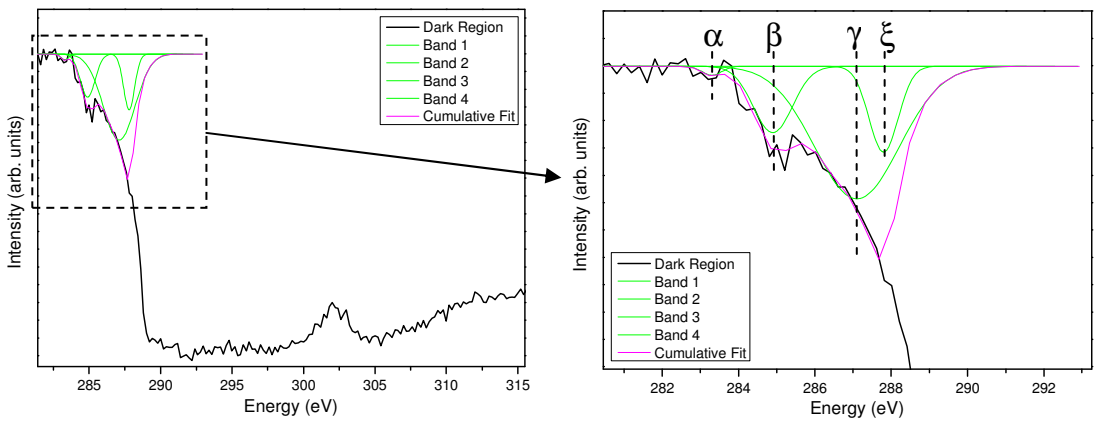

Figure 7-41: Fitting for the pre-edge features observed in the OD-XAS spectrum obtained at the dark region of the naturally colourless type IIa diamond.

Table 7-14:

Band/Feature	Peak Centre (eV)	FWHM
α	283.30	0.60
β	284.90	1.21
γ	287.10	2.62
ξ	287.80	0.90
Edge	~288.50	---
σ*	302.07	2.51

Four bands were fitted for the pre-edge features observed for the dark region on the naturally colourless type IIa diamond. The 283.30eV as mentioned previously for the naturally banded type IIa diamond is mentioned in the literature at around 283.5eV and its origin is not well understood (*35*). The 284.90eV band is associated with the C 1s – π* transition related to the C = C bonding (sp^2-bonded carbon) as found in graphite (*19*), it has also been found at slightly higher energies ranging from 284 – 286eV (*18, 21-26, 28-30*). The 287.10eV and 287.80 bands are ones that have been previously observed for the diamond samples studied during the course of this research and could be associated with C = N and/or C = H respectively (*18, 22, 25-27, 31-33*).

7.4 Summary Table of C 1s – π* resonances:

Table 7-15 provides a summary of the peak locations and sp^2-bonded carbon features found in the literature that correlate with the types of π* resonances that have been observed in this study, along with the particular bonding involved. Amorphous carbon consists of localized π electrons, the bond lengths and distances are inconsistent with other allotropes of carbon and the sp^2 peak obtained via NEXAFS or OD-XAS is usually broader due to the dispersal of energy levels than for the graphitic π-bonding case. As stated in work carried out by Grierson *et al.* the C 1s – π* transition for graphite (ordered sp^2 bonding) is typically located at ~285.5eV and the C 1s – π* transition in disordered carbon is ~285eV, typical features of amorphous-carbon structures (*41-43*). Broadening effects are observed prior to the edge in some of the diamond samples studied as can also be observed in studies on amorphous sp^2-bonded carbon which are found in the literature to be attributed to an increase in bond length distribution (*41*).

Table 7-15:

Bond	Peak Location (eV)	Reference
C = C	284.00	(*18*)
	284.60	(*18*)
	284.80	(*19*)
	285.00	(*18, 24, 29, 30*)
	285.30	(*22*)
	285.38	(*28*)
	285.50	(*23, 25, 26*)
	285.50 – 286.00	(*21*)
C = N	285.00	(*24*)
	285.50 – 286.00	(*21*)
	287.20	(*22*)
	287.30	(*31*)
	288.00	(*32*)
C = O	286.50	(*22*)
	286.60	(*29*)
	289.00	(*31*)
	289.30	(*21*)
	289.50	(*24*)
C = H	287.00	(*18*)
	287.50	(*18, 25*)
	287.80	(*22*)
	288.00	(*26, 33*)
	288.00 ± 1.00	(*27*)
	288.80	(*22*)
	289.30	(*21*)
	289.50	(*24*)
	~290.00	(*23*)

7.5 Summary of OD-XAS results obtained for Diamond samples

A summary of the NEXAFS and OD-XAS features obtained for the diamond samples during the course of this study can be found in tables 7-16 and 7-17. The pre-edge features' energy locations are provided along with the relative energy separation between the σ* and the pre-edge features. The values obtained for the energy separations are similar and comparable between the different samples. This suggests that the pre-edge features related to sp^2-bonded carbon are the same and present in the other diamond samples studied. These pre-edge features are found to be common in the majority of the diamonds and could suggest a generic picture for the pre-edge structures observed via OD-XAS studies.

Table 7-16:

Sample	α	π*	Edge	σ*	σ*-Edge	σ*-α
Diamond	285.30	-	288.80	302.80	14.00	17.50
Graphite	286.00	288.50	291.70	-	-	-

The results obtained can be compared with the results obtained from the literature (table 7-15) and the location of the features observed relative to other features common in all diamond studies i.e. sp^3-bonded carbon (σ*).

Table 7-17:

Sample	α (eV)	β (eV)	γ (eV)	ξ (eV)	Edge (eV)	σ* (eV)	σ*-Edge (eV)	σ*-α (eV)	σ*-β (eV)	σ*-γ (eV)	σ*-ξ (eV)
Brown CVD Diamond	284.03	285.60	287.20	-	288.00	301.34	13.34	17.31	15.74	14.14	-
Type IIa (Graphitic Incl) (A490)	284.31	-	287.05	-	288.39	301.40	13.01	17.09	-	14.35	-
Type IIa bands (re-polished) (A490)	284.63	-	-	-	288.00	301.40	13.40	16.77	-	-	-
Type Ia banded	285.02	286.24	287.61	-	288.00	302.27	14.27	17.25	16.03	14.67	-
CVD_plan (0542715)	285.69	286.80	287.82	-	288.70	302.21	13.51	16.52	15.41	14.39	-
CVD_layered (0673803)	282.85	284.60	287.00	-	288.30	301.57	13.27	18.72	16.97	14.57	-
Untreated brown type IIa	-	-	286.80	-	288.10	301.60	13.50	-	-	14.80	-
HPHT treated type IIa	283.32	284.54	-	-	287.89	301.57	13.68	18.25	17.03	-	-
Naturally Colourless type IIa	283.30	284.90	287.10	287.80	288.50	302.07	13.57	18.77	17.17	14.97	14.27

7.6 Summary

A comprehensive study of all the diamond samples has been presented in this chapter via the OD-XAS technique. The technique has been successfully implemented in the study of natural and synthetic brown diamonds. It has proved successful in providing information on the local chemical structures of the diamonds situated at the non-brown and brown regions. Differences in the pre-edge features have been observed between the non-brown and brown locations and have been attributed to sp^2-bonded carbon species of which the type of bonding is particularly highly concentrated in the brown regions compared to the brighter regions of the diamond in question.

The Raman and OD-XAS measurements support each other's findings in relation to the discovery of sp^2-bonded carbon species. The presence of the 1400 cm^{-1} to 1800 cm^{-1} features in the Raman measurements (chapter 6) tie with the presence of features pre C K-edge via the OD-XAS technique of which confirm the peak to be sp^2-carbon bonded related – due to the π-resonance signature in the OD-XAS spectrum.

CVD brown diamonds are different to naturally brown diamonds when HPHT treated. The brown colouration disappears at lower temperatures in CVD compared to natural diamond suggesting a less stable defect. As well as this, positron annihilation experiments have found different lifetimes than those found in natural diamonds (*44*). Jones *et al.* also mention that the brown centres in natural diamonds are multivacancy clusters of globular nature in agreement with TEM studies (*38, 44*).

For the studies carried out on the untreated and HPHT treated type IIa diamond samples it was found via Raman and OD-XAS measurements that the sp^2-bonded carbon was significantly more prominent in the non-brown (HPHT treated) sample. This results suggests that the HPHT treatment has contributed to an increase in the sp^2-bonded carbon detection via Raman and OD-XAS measurements whereby the treatment may have affected the lattice structure in some respect. A possible explanation for this could be due to sp^2-bonded carbon clusters widely dispersed in the untreated sample and responsible for the brown colouration become mobile under the HPHT conditions and combine together to create larger clusters, which are far

more likely to be detected via the techniques implemented during the course of this research.

Further measurements with a wider range of samples at different stages during their HPHT treatment are required with the study being focussed on the changes observed in the Raman spectrum (such as an increase in the sp^2-bonded features as the treatment progresses) as well as OD-XAS concentrating on the pre-edge features which also could become more significant as the HPHT process progresses.

This chapter has provided a thorough investigation into the chemical structure of the diamond samples studied. Key differences have been observed between bright coloured regions and brown regions of diamond samples and it has been conclusively gathered that there exists a higher concentration of sp^2-bonded carbon species at these brown locations compared to the brighter coloured (non-brown) regions of the diamond.

7.7 References

1. F. Quinn *et al.*, *Journal of Synchrotron Radiation* **10**, 461 (2003).
2. N. R. J. Poolton, B. M. Towlson, B. Hamilton, D. A. Evans, *Nuclear Instruments & Methods in Physics Research Section B-Beam Interactions with Materials and Atoms* **246**, 445 (2006).
3. C. R. Howle, S. Ali, R. P. Tuckett, D. A. Shaw, J. B. West, *Nuclear Instruments and Methods in Physics Research Section B: Beam Interactions with Materials and Atoms* **237**, 656 (2005).
4. P. Denham, E. C. Lightowlers, P. J. Dean, *Physical Review* **161**, 762 (1967).
5. J. E. Field, *The Properties of Natural and Synthetic Diamond*. (Elsevier Academic Press, 1992).
6. J. Ristein, *Applied Physics a-Materials Science & Processing* **82**, 377 (2006).
7. R. Kalish, *Journal of Physics D-Applied Physics* **40**, 6467 (2007).
8. S. J. Sharp, A. T. Collins, G. Davies, G. S. Joyce, *Journal of Physics-Condensed Matter* **9**, L451 (1997).
9. P. J. Dean, J. C. Male, *Proceedings of the Royal Society of London Series a-Mathematical and Physical Sciences* **277**, 330 (1964).
10. D. A. Evans *et al.*, *Journal of Physics-Condensed Matter* **20**, (2008).
11. L. Landt *et al.*, *Physical Review Letters* **103**, 047402 (2009).
12. A. Zaitsev, *Optical Properties of Diamond A Data Handbook*. (Springer, 2001).
13. K. Iakoubovskii, G. J. Adriaenssens, *Physical Review B* **61**, 10174 (2000).
14. D. R. Wight, P. J. Dean, *Physical Review* **154**, 689 (1966).
15. J. Walker, *Reports on Progress in Physics* **42**, 1605 (1979).
16. F. A. Raal, *Proceedings of the Physical Society of London* **24**, 649 (1959).
17. D. A. Evans, A. R. Vearey-Roberts, N. R. J. Poolton, *Applied Physics Letters* **89**, (2006).
18. S. Ohmagari *et al.*, *Journal of Nanomaterials* **2009**, 876561 (2009).
19. B. Bouchet-Fabre *et al.*, *Diamond & Related Materials* **14**, 881 (2005).
20. J. Stohr, *NEXAFS Spectroscopy*. (Springer, 1996).
21. R. McCann *et al.*, *Thin Solid Films* **482**, 34 (2005).
22. C. Lenardi *et al.*, *Surface and Coatings Technology* **125**, 317 (2000).
23. F. L. Coffman *et al.*, *Applied Physics Letters* **69**, 568 (1996).

24. S. S. Roy, R. McCann, P. Papakonstantinou, P. Maguire, J. A. McLaughlin, *Thin Solid Films* **482**, 145 (2005).
25. R. McCann *et al.*, *Diamond & Related Materials* **14**, 1057 (2005).
26. S. Yang, Q. Yang, Z. Sun, *Nanotechnology* **18**, 065703 (2007).
27. T. Schedel-Niedrig *et al.*, *Europhysics Letters* **31**, 461 (1995).
28. P. E. Batson, *Physical Review B* **48**, 2608 (1993).
29. L. Ravagnan *et al.*, *Carbon* **44**, 1518 (2006).
30. N. Mubumbila *et al.*, *Diamond & Related Materials* **13**, 1433 (2004).
31. M. Ramm, M. Ata, K.-W. Brzezinka, T. Gross, W. Unger, *Thin Solid Films* **354**, 106 (1999).
32. S. Bhattacharyya, M. Lubbe, P. R. Bressler, D. R. T. Zahn, F. Richter, *Diamond & Related Materials* **11**, 8 (2002).
33. R. Gago, I. Jimenez, J. M. Albella, *Surface Science* **482-485**, 530 (2001).
34. X. T. Zhou *et al.*, *Journal of the American Chemical Society* **129**, 1476 (2007).
35. A. Laikhtman, I. Gouzman, A. Hoffman, *Diamond and Related Materials* **9**, 1026 (2000).
36. D. A. Muller, Y. Tzou, R. Raj, J. Silcox, *Nature* **366**, 725 (1993).
37. R. Barnes, U. Bangert, P. Martineau, *Physica Status Solidi a-Applications and Materials Science* **203**, 3081 (2006).
38. U. Bangert *et al.*, *Philosophical Magazine* **86**, 4757 (2006).
39. J. M. Maki, F. Tuomisto, C. J. Kelly, D. Fisher, P. M. Martineau, *Journal of Physics-Condensed Matter* **21**, 364216 (2009).
40. J. M. Maki. (Personal Communication, 2010).
41. D. S. Grierson *et al.*, *Journal of Applied Physics* **107**, (2010).
42. G. Comelli, J. Stohr, C. J. Robinson, W. Jark, *Physical Review B* **38**, 7511 (1988).
43. S. Anders, J. Diaz, J. W. Ager, R. Y. Lo, D. B. Bogy, *Applied Physics Letters* **71**, 3367 (1997).
44. R. Jones, *Diamond and Related Materials* **18**, 820 (2009).

Chapter

8

8.0 Summary, conclusions and further work

Presented in this chapter is a summary of the work carried out during the course of this research.

The OD-XAS technique has never before been implemented in the study of brown diamonds and presented here are new discoveries relating to the bonding in uniform brown and variegated diamond.

Natural and synthetic diamond samples have been synthesized and characterized via a range of techniques. XEOL and PL measurements have revealed the defects present within the band-gap of the materials studied and a comprehensive analysis of the defects present has been achieved (chapter 5).

Uniformly brown and variegated brown samples have been studied using a Raman System which has been utilized in regular mode for the uniform samples and in image mapping-mode for the variegated samples. Lateral differences are found to be visually apparent and are confirmed and supported by the Raman measurements. Higher concentrations of sp^2-bonded carbon species have been exposed at the brown sites, compared to non-brown regions, or where the brown colour is less intense (chapter 6).

The Raman measurements were supported with NEXAFS and OD-XAS studies on the same samples. Both synchrotron-based techniques provided information on features that were present pre C K-edge, which are of a graphitic nature (sp^2-bonded carbon) and located in the brown regions of the diamond samples. OD-XAS measurements utilized in imaging mode for the variegated samples, also confirmed these discoveries (chapter 7).

A higher concentration of sp^2-bonded carbon was discovered present in a HPHT treated type IIa colourless diamond compared to a brown type IIa sample of which both were cut from the same original stone. This was observed in the Raman (chapter 6) and in the OD-XAS (chapter 7) measurements. This suggests that the HPHT treatment has affected the sample in some way by possibly moving defects or vacancies. Previous work supports the suggestion that the brown colouration in diamonds is related to vacancy clusters as has already been mentioned in this thesis. The measurements obtained in this study suggest that the HPHT treatment may have caused the vacancies to become mobile within the lattice and combine to form larger vacancies which could explain the higher concentration of sp^2-bonding observed compared to the untreated brown.

Future measurements on the study of diamond would significantly benefit from acquiring the new CLASSIX spectrometer once completed, CLASSIX 2. The filter wheel is to be replaced by a liquid crystal filter arrangement which would drastically improve the resolution and aid in the identification of the bands and features in the XEOL, as well as pin-pointing the origin of the spectra relative to the sample surface in imaging mode i.e. brown band.

Spin resonance measurements would also be beneficial for the untreated and HPHT treated samples in clearly identifying the nature of the defects discovered. Multi-wavelength Raman measurements may also be useful in providing a further insight into the samples studied as well as Pump-probe measurements to provide information on the trapping dynamics of the defects.

Appendix

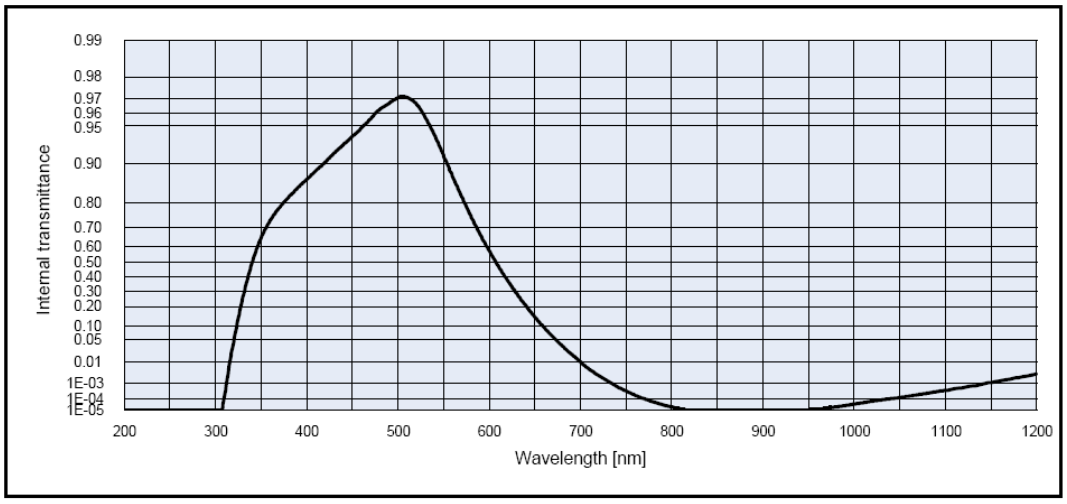

BG39 schott filter specifications.